UNIVERSITÀ
DEGLI STUDI
DI PADOVA

Sede Amministrativa: Università degli Studi di Padova
Dipartimento di Biologia

SCUOLA DI DOTTORATO DI RICERCA IN BIOSCIENZE E BIOTECNOLOGIE

INDIRIZZO DI NEUROBIOLOGIA

CICLO 28°

The role of GABAergic interneurons and astrocytes in the mechanism of seizure generation and propagation

Direttore della Scuola: Ch.mo Prof. Paolo Bernardi

Coordinatore d'indirizzo: Ch.ma Prof.ssa Daniela Pietrobon

Supervisore: Dott. Giorgio Carmignoto

Dottorando: Iacopo Marcon

SUMMARY

Within the brain, inhibitory signals originating from different GABAergic interneurons play crucial roles in establishing proper neural circuit operations. GABAergic interneurons are also directly involved in multiple neurological disorders, including epilepsy. The inhibitory signal from these cells can, indeed, counteract seizures and pharmacological agents that strengthen GABAergic transmission represent powerful anticonvulsant drugs extensively used by epileptic patients. Among the diverse classes of interneurons, Parvalbumin-expressing (Pv) interneurons have been proposed to play a central role in seizure control. In both experimental epilepsy models and patients these interneurons have been observed to generate a feedforward inhibition that effectively opposes seizure spread. When Pv interneurons were artificially activated *in vivo* with optogenetic techniques, ongoing seizures were interrupted. However, studies in different experimental epilepsy models revealed that Pv interneurons may, under certain conditions, favor seizure generation. It is therefore highly debated whether an intense activity of Pv interneurons can ultimately result in a pro- or in an anti-convulsant action. In my Doctorate thesis, I used a mouse brain slice model of focal epilepsy in which the epileptogenic focus can be identified and the role of Pv interneurons in the generation and in the propagation of seizure-like events accurately analyzed by a combination of optogenetic, electrophysiological and imaging techniques. I observed that a selective rhythmic activation of Pv interneurons at the focus failed to prevent seizure generation, and it rather contributed to prolong seizure duration by synchronizing the afterdischarges of the clonic phase. Moreover, this pattern of Pv interneuron activation induced in pyramidal neurons a post-inhibitory rebound spiking that enhances neuronal synchrony and promotes seizure generation. In contrast, a selective activation of Pv interneurons distant from the focus blocked seizure propagation and shortened seizure duration at the focus. I then revealed that the reduced seizure duration at the focus was a direct consequence of the propagation block which probably prevented newly generated afterdischarges to travel backwards to the original focus of seizure initiation. The functional dichotomy of Pv interneurons described in the thesis opens new perspectives to our understanding of how local inhibitory circuits govern generation and spread of focal epileptiform activities. Given the wealth of evidence pointing at Pv interneurons as key players in epilepsy, their disfunction might also be

at the basis of genetic epilepsies such as the severe myoclonic epilepsy of infancy (SMEI or Dravet syndrome), a rare epileptic encephalopathy characterized by an elevated mortality rate, early onset and seizures associated with elevated body temperature. SMEI is associated with a loss of function of the Na_V 1.1 isoform of the sodium channel α–subunit. Recently, a mouse model of SMEI was generated by specific deletion of the SCN1A gene that codes for Na_V 1.1. Importantly, in this model GABAergic interneurons, and in particular Pv interneurons, have been proposed to be specifically affected by the Na_V 1.1 deletion, resulting in a reduced excitability of these cells that might leads to network disinhibition and possibly seizures. Therefore, in the framework of a broad characterization of synaptic and network activities in *in vitro* and *in vivo* models from Na_V 1.1 heterozygous KO mice, I report here evidence that the propagation of focal epileptiform events in brain slices from Na_V 1.1 KO mice is faster than in WT mice, hinting at a weakening of feedforward inhibition that restrains seizure spread, most likely deriving from Pv interneuron impaired excitability. Finally, as accumulating evidence supports a novel view of brain function where neurons intensively cooperate with astrocytes, I decided to investigate if a specific communication between GABAergic interneurons and astrocytes may exist. Indeed, neurotransmitters can elicit in astrocytes Ca^{2+} elevations that, in turn, trigger the release of neuroactive molecules, commonly known as gliotransmitters. However, whether and how GABA, the main inhibitory neurotransmitter, can evoke similar Ca^{2+} elevations in astrocytes and what is the functional outcome of these GABA-activated astrocytes are questions poorly addressed. These questions are particularly relevant in epilepsy, where we observe a massive GABAergic activity during seizure generation and propagation. To this aim, I found that in somatosensory and temporal cortex slices loaded with the Ca^{2+} indicator Fluo-4 AM, a large number of astrocytes in the layer 5 exhibited somatic Ca^{2+} rises in response to GABA or Baclofen (a specific $GABA_B$ receptor agonist). Patch-clamp recordings in the presence of TTX also revealed that $GABA_B$ activation triggered N-methyl-D-aspartate receptor-mediated slow inward currents (SICs) in principal neurons, suggesting that astrocytes in local circuits can convert an intense inhibitory input into a delayed excitatory output. These data support the presence of a dynamic, bidirectional signaling between GABAergic interneurons and astrocytes, which opens new perspectives for our understanding of the role of these different cell types in brain physiopathology.

RIASSUNTO

I segnali inibitori generati da una grande varietà di interneuroni GABAergici hanno un ruolo cruciale nell'assicurare il corretto funzionamento dei circuiti neuronali nel cervello. Gli interneuroni GABAergici sono anche direttamente coinvolti in numerose patologie neurologiche, compresa l'epilessia. L'azione inibitoria di questi interneuroni è in grado di contrastare le crisi epilettiche, e, infatti, gli agenti farmacologici che rafforzano la trasmissione sinaptica GABAergica sono utilizzati come farmaci anticonvulsivanti per i pazienti epilettici. Tra le numerose classi di interneuroni GABAergici, gli interneuroni esprimenti Parvalbumina (Pv) sembrano giocare un ruolo fondamentale nel controllo delle crisi epilettiche. In modelli sperimentali di epilessia ed in pazienti umani è stato dimostrato che queste cellule generano un'inibizione a *feedforward*, che si oppone efficacemente alla propagazione delle crisi epilettiche. Quando gli interneuroni Pv sono stati attivati artificialmente *in vivo* con tecniche optogenetiche, le crisi in corso sono state rapidamente interrotte. Ciò nonostante, altri studi hanno dimostrato che gli interneuroni Pv possono, in determinate circostanze, favorire la generazione delle crisi epilettiche. Non è quindi chiaro se l'intensa attività di questo sottogruppo di interneuroni abbia un effetto pro - o anti - epilettico.

Nella mia tesi di dottorato ho usato un innovativo modello di epilessia focale in fettine cerebrali di topo, dove il sito di generazione delle scariche epilettiche (focus) può essere precisamente identificato, per studiare il ruolo degli interneuroni Pv nella generazione e nella propagazione delle scariche epilettiche attraverso tecniche di elettrofisiologia, optogenetica e imaging. Innanzitutto ho osservato che l'attivazione ritmica degli interneuroni Pv nella zona focale non è in grado di prevenire la generazione di una scarica epilettica, mentre ha invece contribuito a prolungare la durata della crisi attraverso la sincronizzazione degli afterdischarges, picchi di attività tipici della fase clonica. Inoltre, questo pattern di attivazione degli interneuroni Pv ha indotto nei neuroni piramidali un *rebound spiking* post – inibitorio che ha intensificato la sincronia della rete neuronale, facilitando così la generazione della crisi. Al contrario, l'attivazione degli interneuroni Pv nelle aree distanti dal focus ha bloccato con successo la propagazione della scarica epilettica e ha ridotto la durata della crisi nel focus. Ho poi dimostrato che la ridotta durata della crisi nell'area focale è una conseguenza diretta del blocco della propagazione che ha probabilmente impedito ai

nuovi afterdischarges di viaggiare a ritroso verso il focus per mantenere l'attività epilettica. La dicotomia funzionale degli interneuroni Pv descritta in questa tesi apre nuove prospettive per comprendere come i circuiti inibitori locali governano la generazione e la propagazione dell'attività epilettica focale. Vista la grande mole di dati esistenti che indicano gli interneuroni Pv come protagonisti centrali nell'epilessia, è possibile ipotizzare che disfunzioni a loro carico contribuiscano alla patogenesi di forme genetiche come l'epilessia mioclonica severa dell'infanzia (SMEI, detta anche sindrome di Dravet). Questa grave patologia neurologica è una rara forma di encefalopatia epilettica caratterizzata da esordio precoce, crisi epilettiche associate ad elevata temperatura corporea ed elevato tasso di mortalità. La SMEI è associata ad una mutazione che causa l'inattivazione di uno dei due alleli codificanti la subunità alfa del canale del sodio voltaggio-dipendente Na_V 1.1. Recentemente, è stato generato un modello murino di SMEI che riproduce abbastanza bene il fenotipo umano della malattia. In questo modello, gli interneuroni Pv sembrano essere selettivamente affetti dalla delezione dei canali Na_V 1.1, provocando in queste cellule una riduzione di eccitabilità che può portare alla disinibizione della rete neuronale e, eventualmente, alle crisi epilettiche. Alla luce di queste premesse, nell'ambito di un'estesa caratterizzazione dell'attività sinaptica e di network in modelli *in vitro* ed *in vivo* da topi eterozigoti per la delezione dei canali Na_V 1.1, ho osservato che le scariche epilettiche si propagano più velocemente nelle fettine cerebrali provenienti da topi eterozigoti per la delezione rispetto ai topi selvatici di controllo. Questa evidenza suggerisce un indebolimento dell'inibizione a *feedforward* derivante probabilmente dalla ridotta eccitabilità degli interneuroni Pv. Infine, dato che negli ultimi anni si sta facendo strada con forza una visione del funzionamento del cervello dove i neuroni collaborano strettamente con gli astrociti, ho voluto capire se esiste una interazione specifica tra interneuroni GABAergici ed astrociti, e quali conseguenze questa interazione ha sull'attività neuronale. Infatti, i neurotrasmettitori sono in grado di stimolare risposte Ca2+ negli astrociti le quali, a loro volta, possono provocare il rilascio di molecole neuroattive, comunemente note come gliotrasmettitori. Tuttavia, mentre la comunicazione tra astrociti e neuroni eccitatori è ben caratterizzata, l'interazione con gli interneuroni inibitori è ancora largamente inesplorata. In particolare, questa interazione può essere molto rilevante nell'epilessia, dove osserviamo una massiccia attività GABAergica durante la generazione e la propagazione della scarica epilettica. A questo proposito, ho

osservato che nelle fettine di corteccia somatosensoriale e temporale caricate con l'indicatore Ca^{2+} Fluo-4 AM, la maggior parte degli astrociti nello strato 5 ha mostrato aumenti di Ca^{2+} in risposta all'applicazione di GABA o di Baclofen (un agonista specifico del recettore metabotropico $GABA_B$). Per verificare se gli astrociti attivati dal GABA possano rilasciare glutammato, ho effettuato registrazioni di patch-clamp da neuroni piramidali grazie alle quali ho potuto verificare che l'attivazione del recettore $GABA_B$ negli astrociti provocava correnti depolarizzanti lente (SIC) nei neuroni mediate da recettore NMDA. I risultati di questi esperimenti suggeriscono che gli astrociti possono convertire nei circuiti locali un forte input inibitorio in un output eccitatorio ritardato, e che evidentemente esiste una comunicazione bidirezionale tra astrociti e interneuroni GABAergici che apre nuove prospettive sul ruolo di queste cellule nella fisiopatologia cerebrale.

TABLE OF CONTENTS

1. INTRODUCTION

1.1 Organization of the cortex

Neurons in the neocortex, i.e., the phylogenetically most recent part of the brain, are organized in six horizontal layers from the outer edge of the cortex to the basal white matter [1]. The relative extent of each layer can be different at functionally different cortices. Of the six layers, layer 1 (molecular layer) has the lowest density of cells being essentially composed of inhibitory interneurons and astrocytes. Layer 1 is also occupied by axon projections generated from neurons of extracortical regions and dendrites from neurons of deep cortical layers. Layer 2 (external granule cells layer) is characterized by round-shaped cells and in the mouse cortex is fused with the layer 3 (external pyramidal layer) which contains several types of neurons, mainly pyramidal neurons. Layer 4 is the internal granule cell layer populated by excitatory spiny neurons, which are the principal recipient layer for thalamocortical inputs. The thalamocortical inputs are in turn transmitted from granule cells to layers 2, 3, 5 and 6 [8]. Layer 5 (which can be divided in layer 5a and 5b) is the internal pyramidal layer characterized by the presence of pyramidal cells, bigger than layer 2/3 pyramidal cells. Layer 5 pyramidal neurons project their axons to subcortical regions and constitute the principal cortical output that innervates other cortical areas. Layer 6 is a polymorphic or multiform layer because it is occupied by several types of neurons. Together with the layer 5, layer 6 neurons project back to the thalamus regulating thalamocortical interactions [8]. Cortical neurons are also organized in vertical columns that contains all of the six cortical layers. In rodents, a neocortical column of about 0.3 mm in diameter contains roughly 7,500 neurons. The neuronal network within a cortical column performs basic processing of inputs; for example cortical columns of primary somatosensory cortex process the

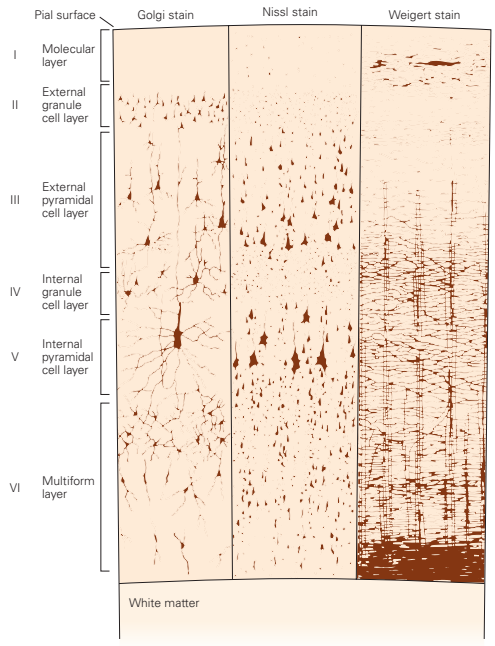

Figure 1 The neurons of the neocortex are arranged in distinctive layers. The appearance of the neocortex depends on what is used to stain it. The Golgi stain reveals a subset of neuronal cell bodies, axons, and dendritic trees. The Nissl method shows cell bodies and proximal dendrites. A Weigert stain reveals the pattern of myelinated fibers. From [1].

information from mouse vibrissae. Each functional column is defined by discrete and well-defined structure in layer 4 known as barrel. Layer 4 barrels are arranged somatotopically in an almost identical fashion to the layout of the whiskers in the snout [9]. Most neocortical neurons (70-80%) are excitatory pyramidal neurons, which have relatively stereotyped anatomical, physiological, molecular and synaptic characteristics, while the remaining 20-30% of neocortical neurons are inhibitory interneurons. Cortical transmission between these cells is largely mediated by ionotropic neurotransmitter receptors that produce fast (<10 ms) synaptic conductances. For instance, pyramidal neurons release the excitatory neurotransmitter glutamate onto other neurons, eliciting fast excitation via activation of cation permeable AMPA (α-amino-3-hydroxy-5-methyl-4-isoxazolepropionic acid) and NMDA (N-methyl-D-aspartate) receptor-mediated conductances, possibly generating a positive excitatory feedback.

1.2 Inhibitory circuits in the cortex

Within the brain, inhibitory signals originating from different GABAergic interneurons play crucial roles in establishing proper functional operations of neural circuits, such as the maintainance of a correct equilibrium between excitation and inhibition which prevents network over-excitation, and the regulation of both spontaneous and sensory-driven activities [10]. Interneurons are able to exert these actions by releasing onto pyramidal neurons the inhibitory neurotransmitter γ-aminobutyric acid (GABA), that evokes fast inhibition via anion (Cl^- and HCO_3^-) permeable $GABA_A$ receptor-mediated conductances. Changes in the ratio between synaptic excitation and inhibition can cause in neurons membrane potential variations toward any arbitrary value in-between the reversal potential of synaptic excitation (~ 0 mV for AMPA and NMDA receptors) and synaptic inhibition (typically around - 70 to - 80 mV for $GABA_A$ receptors). Importantly, because the impact on membrane potential of any currents flowing through the membrane is affected in a divisive manner by the conductance of the membrane (Ohm's law), the activation of $GABA_A$ receptors, simply by increasing the conductance, can significantly reduce the excitability of a neuron, an effect referred to as "shunting inhibition". This might represent the major inhibitory effect of $GABA_A$ receptor activation in those specific cases in which the resting membrane potential is equal to or more negative than the reversal potential of

$GABA_A$ receptor-mediated currents. Membrane pumps, by setting intracellular Cl^- concentration, play a critical role in regulating the reversal potential of $GABA_A$-mediated synaptic currents [11]. In addition to fast $GABA_A$ receptor mediated conductances, GABA activates G protein-coupled $GABA_B$ receptors that cause a slow (100-500 ms) postsynaptic inhibition by opening inwardly rectifying K^+ (GIRK) channels [12]. It has been suggested that synaptically released GABA from a large number of coactive interneurons must be pooled or accumulated to activate $GABA_B$ receptors ([13]). $GABA_B$ receptors are present on both glutamatergic and GABAergic nerve terminals where their activation causes presynaptic inhibition of transmitter release. In contrast to their counterpart, the pyramidal cells, GABAergic interneurons do not form, with a few exceptions, long-range axonal projections, hence, the name local circuit interneurons. The interactions between GABAergic interneurons and glutamatergic principal cells are reciprocal: interneurons inhibit principal cells and are excited by them. In fact, the connectivity between these two neuronal classes is quite high: individual interneurons can inhibit >50% of principal cells located within ~ 100 μm and receive excitatory input from a large fraction of them [14],[15]. Thus, not only are GABAergic interneurons excited in proportion to the activity of excitatory pyramidal neurons, but they directly influence local network excitability through their inhibitory feedback. This simple connectivity pattern is ubiquitous in the cortex and forms the basis for the so-called feedback or recurrent inhibition (Fig. 2, [16],[14]). Feedback inhibition implements a “winner-takes-all” mechanism: once the principal cells with the strongest input fire, action potential initiation in the remaining cells is inhibited (Fig. 2). This computation could be particularly important in the dentate gyrus, where it may contribute to sparsification of activity, pattern separation and grid-to-place code conversion [17]. Of course, not all cortical excitation received by

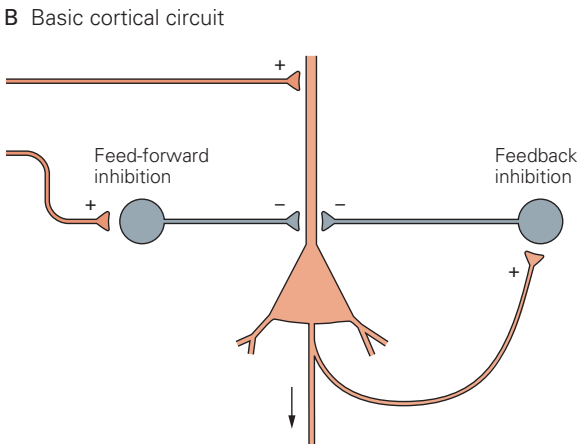

Figure 2. Feedback and feedforward inhibition A simplified version of the inputs to a cortical pyramidal neuron. The orange terminals are excitatory, whereas the gray terminals are inhibitory. Recurrent axon branches activate inhibitory neurons, causing feedback inhibition of the pyramidal neuron. Extrinsic excitatory inputs can also activate feed-forward inhibition. Adapted from [1].

inhibitory interneurons is locally generated. Cortical cells receive excitatory inputs via long-range axons originating from subcortical nuclei, as well as from different cortical regions and different cortical layers. These excitatory afferent inputs diverge onto both principal cells and interneurons, generating feedforward inhibitory circuits (Fig 2,[18]). In these feedforward circuits, the onset of excitation recorded in principal neurons will precede the onset of inhibition by a monosynaptic delay (that can be as brief as one ms) [19]. Together, these two simple inhibitory circuits, feedback and feedforward, represent fundamental building blocks of the functional cortical architecture [10]. The recruitment of interneurons via feedforward and/or feedback excitatory projections generates inhibition that is somehow proportional to local and/or incoming excitation [20]. Acute experimental manipulations selectively decreasing either inhibition or excitation shift cortical activity to a hyperexcitable (epileptiform) or silent (comatose) state [21].

1.3 Interneurons diversity in the cortex

GABAergic inhibitory interneurons of the cerebral cortex are a heterogeneous population of cells, and their classification is a topic of intense debate in the scientific community. Their diversity is manifested in every aspect of their phenotype, as evidenced by their different morphological, physiological and molecular properties. The large amount of data available on these cells and the many parameters used to describe interneurons have rendered difficult the adoption of a standardized nomenclature. However, a large group of scientists converged to a unitary terminology for the classification of interneurons based on morphological, electrophysiological and molecular features [22]. Inhibitory interneurons vary greatly in their somatic, dendritic and axonal morphologies, but the axonal arborization is the principal morphological feature used to reveal the anatomical identity of an interneuron. This is possible because interneurons seem to be particularly specialized in targeting different domains of principal neurons, such as the soma and the proximal dendrites, the distal dendrites and the axon initial segment (AIS) (Fig. 3). This subdivision of the postsynaptic targeting region is strongly correlated with their synaptic physiology and ultimately with their function inside the cortical network. An additional layer of specificity in determining the identity of an interneuron is given by the expression of molecular markers. These can be transcription factors,

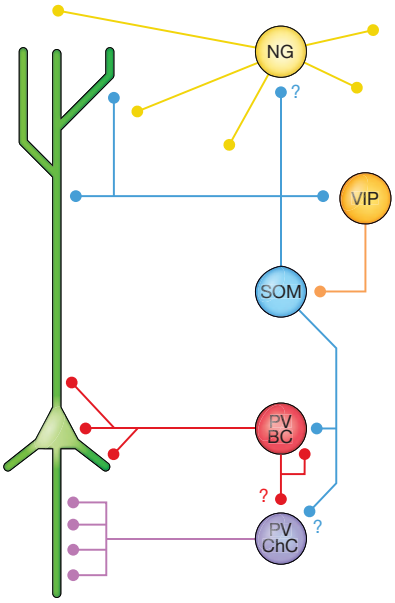

Figure 3. Classes of inhibitory interneurons. The cortex contains three major families of interneurons, each of which divides into multiple subclasses. The figure shows a current understanding of the synaptic targets of five classes of cortical interneurons (PV ChC, Parvalbumin Chandelier Cell; PV BC Parvalbumin Basket Cell; SOM, Somatostatin interneuron; VIP, Vasointestinal Peptide Interneuron; NG, Neurogliaform Cell), while the green neuron is a pyramidal cell. From [5])

neurotransmitter or their synthetizing enzymes, neuropeptides (somatostatin, vasointestinal peptide), calcium binding proteins (parvalbumine, calretinin…), ionotropic and metabotropic receptors and structural proteins. Finally, the electrophysiological characteristics of a neuronal population are important in determining what part those cells play in circuit activity and computation. The four main electrophysiological features are: the passive and subthreshold properties (such as resting membrane potential and input resistance), the action potential (AP) properties (threshold voltage for spike triggering, spike amplitude at half-width…), the firing patterns and the postsynaptic responses [22]. Three major groups of neurons, those expressing the calcium-binding protein parvalbumin (Pv), those expressing the neuropeptide somatostatin (Som) and those expressing ionotropic serotonin receptor 5HT3a (5HT3aR) account for nearly 100% of neocortical GABAergic interneurons [23]. Pv-expressing neurons represent ~40 % of the total GABAergic population, while Som-expressing and 5HT3aR-expressing neurons account for ~30% each. These major interneuronal classes comprise several subclasses that differ in a number of the aforementioned physiological, morphological and molecular properties (Fig. 3). The large diversity of GABAergic interneurons that have arisen through evolution has provided the means by which the cerebral cortex can perform complex operations. Indeed, the ability of each interneuronal subclass to target distinct compartments of pyramidal neurons, coupled to their specific electrophysiological properties, allows them to precisely control different spatiotemporal aspects of principal neurons activity and, as a consequence, the information flow in the cortex. GABAergic interneurons are believed to control the timing of pyramidal cell firing, the synchronization of network activity, and the generation of cortical rhythms. They also seem to be important in increasing the dynamic range of cortical circuits, controlling sensory receptive fields and plasticity,

and maintaining the excitatory and inhibitory balance necessary for the transfer of information while preventing runaway excitation [23],[24],[19]. Moreover, interneuron malfunction has been implicated in a number of diseases ranging from epilepsy to schizophrenia, anxiety disorders and autism [23].

1.3.1 5HT3aR interneurons

5HT3aR-positive interneurons represent ~30% of GABAergic neurons in somatosensory cortex. This group of interneurons is heterogeneous and remains to be fully characterized. There are two main subclasses of 5HT3aR-expressing neurons which either express (~ 40%) or do not express (~ 60%) the neuropeptide VIP [23]. VIP interneurons are particularly enriched in the superficial layers of the cortex and include bitufted and multipolar neurons expressing different markers and exhibiting different electrophysiological properties. The bitufted VIP neurons present a descending axon that reaches deep layers. These neurons have an irregular firing pattern and for this reason are often referred to as irregular-spiking. Multipolar VIP neurons have an axon that forms branches both locally and towards deep layers, showing a fast-adapting firing pattern. In general, VIP neurons are among the interneurons with the highest input resistance, and are therefore among the most excitable [25]. These cells form synapses preferentially with the dendrites, but in some cases they target the soma of pyramidal cells [26]. In addition, some VIP interneurons have been shown to target mainly somatostatin interneurons [27]. Non-VIP cells include the neurogliaform cells. These cells, originally described by Ramon y Cajal, have a typical morphology characterized by a small round soma from which multiple dendrites spread radially in all directions. Neurogliaform cells are quite unique among all interneurons, because they form electrical synapses not only with each other but also with other interneuronal types. Another peculiarity of these neurons is that they seems to inhibit target neurons by volume release of GABA. For these reasons, they were suggested to play a central role in generating and regulating synchronized activity of neuronal circuits [23].

1.3.2 Somatostatin interneurons

Somatostatin-positive (Som) interneurons have been typically identified with Martinotti GABAergic interneurons that target preferentially the apical and basal

dendrites of pyramidal neurons, as well as the dendrites of other interneurons, such as Parvalbumin interneurons [27], [28]. Martinotti cells are more abundant in layer 5 but are present throughout the layers. Their morphology is characterized by bitufted or multipolar dendrites, an ovoidal soma and an ascending axon that arborizes in layer 1 horizontally reaching neighbouring columns and making synapses on the dendritic tufts of pyramidal neurons [14]. These interneurons display a regular adapting firing pattern and in some cases, especially in layer 5, they also fire bursts of two or more spikes on slow depolarizing humps when repolarized from hyperpolarized potentials (for this reason, these cells have also been called low-threshold spike (LTS), burst spiking non-pyramidal or intrinsic bursting interneurons). Martinotti cells can be recruited by repetitive firing of a single pyramidal neuron as a result of strong facilitating excitatory inputs, and hence mediate a strong feedback inhibition on neighbouring pyramidal neurons [14, 15]. The unique anatomical and synaptic properties of martinotti interneurons make them particularly suited to control dendritic integration of excitatory inputs to pyramidal neurons. Indeed, these interneurons spontaneously provide tonic inhibition to distal dendrites of pyramidal neurons during quite wakefulness. Conversely, during cortical processing after an external sensory stimulation, inhibition of martinotti SOM cells enhances distal dendritic excitability, which might be important for top-down computation and sensorimotor integration [29]. Other subtypes of Som interneurons have been also discovered, that differ from martinotti cells in a number of electrophysiological properties and axonal distribution [23].

1.3.3 Parvalbumin interneurons

Parvalbumin-expressing (Pv) interneurons account for about 30% of all neocortical GABAergic interneurons and are all characterized by a fast-spiking firing pattern, [22]. There are two main subtypes of Pv neurons: basket cells that make synapses at the soma and proximal dendrites of pyramidal neurons and have multipolar morphology, and chandelier cells that target the axon initial segment of pyramidal cells [30]. These fast-spiking neurons are able to sustain high-frequency trains of brief action potentials with large and fast after-hyperpolarization (AHP) and little spike frequency adaptation. Near threshold, they fire abrupt episodes of nonadapting repetitive discharges. They have the lowest input resistance and the fastest

membrane time constant of all interneurons, characteristics that ensure fast synaptic responses [31],[30],[32],[33], [22],[17]. Although both Pv-expressing basket cells and chandelier cells are fast-spiking, their electrophysiological properties are not identical. Fast-spiking, Pv-positive basket cells receive strong albeit depressing thalamocortical (in layer 4) and intracortical excitatory inputs (Rudy 2010), as well as inhibitory inputs from other Pv cells. These interneurons mediate a fast, precise and powerful somatic inhibition of target neurons. These properties allow them, among other functions, to mediate a feedforward inhibition of several cortical circuits, which is important for creating a strict window for temporal summation of excitatory inputs and spike generation by principal cells [19]. Feed-forward inhibition by Pv-interneurons also expands the dynamic range of activity in large principal neuron ensembles. For both these functions, the fast signaling of these interneurons in response to excitatory afferents is crucial, because it can drive a substantial inhibitory signal onto principal neurons before action potential generation.in these cells. Pv interneurons are also involved in feedback (recurrent and lateral) inhibition, and have a prominent role in the establishment and maintenance of fast (gamma frequency) and slow (theta frequency) cortical rhythms [34], [35]. Finally, Pv-interneurons are involved in the regulation of plasticity and learning, as it was demonstrated in the case of associative fear learning [36]. Most importantly, defects in their behavior can be at the basis of different neurological disorders such as schizophrenia and epilepsy.

1.4 Epilepsy: a general overview

The term “epilepsy” encompasses a number of different syndromes whose cardinal feature is a predisposition to recurrent and unprovoked seizures. Seizures are temporary disruption of brain function resulting from abnormal and excessive neuronal activity. For centuries understanding the neurological origin of seizure was confounded by the dramatic behavior associated with seizures. Epilepsy was, in fact, associated with possession by evil spirits and the seizure was thought to reflect oracular, prescient or special creative power. The World Health Organization (WHO) reports that approximately 50 million people worldwide have epilepsy, making it one of the most common neurological diseases. In many parts of the world, people with epilepsy and their families still suffer from stigma and discrimination [37]. Although

specific seizures can be classified according to their clinical features, epilepsy syndromes can also be classified according to the type of seizure, the presence or absence of neurological or developmental abnormalities, and electroencephalographic (EEG) signatures. Indeed, epilepsies can be classified conceptually into two broad categories: focal (or partial) and generalized. In generalized epileptic syndromes, the predominant type of seizure begin simultaneously in both cerebral hemispheres and can be further divided into convulsive or nonconvulsive types depending on whether the seizure is associated with tonic or clonic movements [1, 38]. The prototypic nonconvulsive generalized seizure is the absence seizure in children: these events begin abruptly, usually last than 10 seconds and are associated with cessation of all motor activity, resulting in loss of consciousness. The mechanism that generates absence seizures is believed to involve an alteration in the circuitry between the thalamus and the cerebral cortex, which normally produces a physiologic state of rhythmic cortical activation during non-REM sleep [39]. The overriding concept that emerges from these findings and that extends also to many forms of epilepsy, is that a dysfunction in physiological neuronal circuits can lead to abnormal paroxysmal episodes, such as the seizures. Seizures quite literally hijack the normal functions of the brain.

The most common convulsive generalized form of epilepsy is the tonic-clonic seizure. This type of seizures begin abruptly, often with a grunt or cry, as a tonic contraction of the diaphragm and thorax forces expiration. During the tonic phase, the patient may fall to the ground in a rigid posture. The tonic phase typically last 30 seconds before evolving into clonic jerking of the extremities, which lasts 1 to 2 minutes. This active phase is followed by a postictal phase during which the patient is sleepy.

The second main category of seizures is the focal (or partial) seizure. This event originates in a small group of neurons (the seizure focus) exhibiting an enhanced excitability which eventually spreads to neighboring regions, ultimately involving the entire brain with the aforementioned tonic-clonic pattern. In this case, the focal seizure has secondarily generalized. Most partial epilepsies are believed to be the result of one or more central nervous system insults, but in many cases the nature of the insult remains unknown. The development of a focal seizure can be arbitrarily divided into four phases: (1) the interictal period between seizures followed by (2) synchronization of activity within the seizure focus, (3) seizure spread, and finally (4)

secondary generalization. Phases 2 to 4 represent the ictal phase of the seizure, and different factors contribute to each phase [1], [40].

1.5 Epilepsy: the causing factors

Our understanding of the factors that contribute to epilepsy susceptibility is still rudimentary. Some forms of epilepsies are caused by genetic predisposition, and recent studies have provided a wealth of new information concerning the molecular genetics of epilepsy: at present, more than 70 genes have been linked to an epileptic phenotype. The affected proteins include ion channels, proteins involved in synaptic transmission, such as transporters, vesicle proteins, synaptic receptors, and molecules involved in Ca^{2+} signaling. Most genetic epilepsy syndromes in humans have complex rather than simple (Mendelian) inheritance patterns, suggesting the involvement of many rather than single genes. Nevertheless, a number of monogenic epilepsies have been identified, and we now know that mutations in ion channel genes (channelopaties) are the major cause of these epilepsies (Fig. 4). In the early days of research on epilepsy genes, it was widely expected that gene mutations would underlie generalized epilepsies, based on the idea that a gene mutation (e.g., for an ion channel) would be expected to affect large neuronal populations. However, the first autosomal dominant epilepsy gene discovered by Steinlein and colleagues causes focal and not generalized seizures [41]. In voltage-gated channels, mutations largely affect the main pore-forming subunit(s), but there are also examples of epilepsy causing mutations in regulatory subunits. When examined in vitro, the mutant channel proteins are most commonly associated with either reductions in the

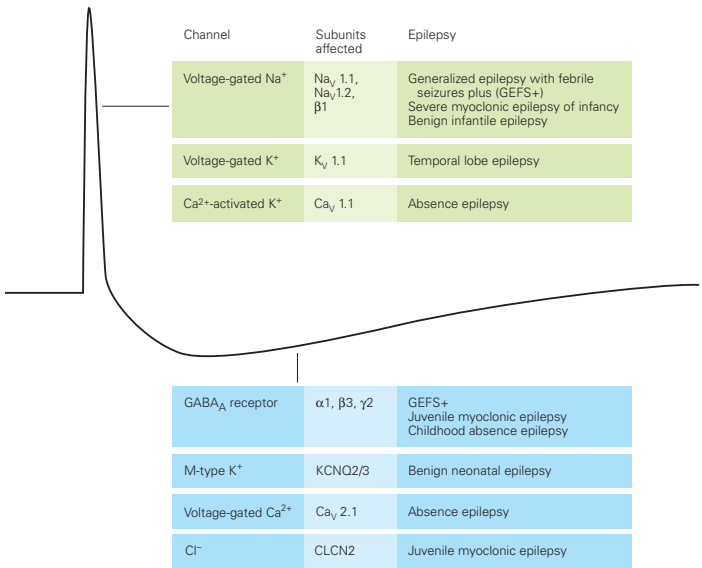

Figure 4 Gene mutations that affect ion channel function are a major cause of monogenic human epilepsies. The human epilepsy genes discovered in the past 10 years can affect multiple phases of neuronal excitability, from the shape of the action potential to the afterpotentials and synaptic events that follow. In the figure the mutations listed near the spike affect the repolarization of the action potential; those listed below affect either the afterhyperpolarization, synaptic conductances, or interspike interval. From [1].

expression of the channel on the surface of the plasma membrane (caused by reduced targeting to the membrane or premature degradation) or altered kinetics of the channels, leading to neuronal hyperexcitability ([1], [40],[38]. For example, the genes most frequently associated with epilepsy encode for voltage-gated sodium channels. Screening of human patients with inherited epilepsy first led to the identification of missense mutations of $Na_V1.1$ channels in two large families with the autosomal dominant epilepsy disorder GEFS+ (Generalized Epilepsy with Febrile Seizures Plus, OMIM 604233) [42]. These missense mutations have been found in the α and β subunits of Na_V 1.1 channels and cause both loss-of-function and gain-of-function effects, caused by the alteration of multiple biophysical properties and of the trafficking (and/or folding) of $Na_V1.1$ channels [43], [44], [45]. Conversely, heterozygous non-sense mutations of the *Scn1a* gene, coding for the α subunit of the channel, lead to the haploinsufficiency of Na_V 1.1, causing the severe myoclonic epilepsy of infancy (SMEI or Dravet syndrome, OMIM 607208), a rare and pharmacoresistant epileptic encephalopathy characterized by an elevated mortality rate and an early onset [46]. The convulsive and generalized seizures in SMEI are often associated with elevated body temperature, and SMEI patients develop comorbidities such as ataxia and cognitive impairments. Insights from a SMEI animal model in which one of the two *Scn1a* alleles has been disrupted, revealed that the heterozygous loss of function of the channel leads to a decreased excitability of GABAergic inhibitory interneurons - where Na_V 1.1 channels seem to be selectively expressed [47] - but not of pyramidal neurons. The overall effect is an imbalance of the excitation/inhibition ratio in the network that is likely at the basis of seizure development [48],[49]. Similarly, sodium currents and action potential firing are impaired in the GABAergic Purkinje neurons in the cerebellum, most likely contributing to ataxia [50].

On the other hand, epilepsies involving repeated focal seizures often develop following a discrete cortical injury, such as a penetrating head wound. This injury serves as the nidus for a seizure focus, leading at some later points to seizures. The most prevalent of the focal (partial) epileptic syndromes is the temporal lobe epilepsy (TLE), an acquired form of epilepsy featuring seizures that arises in mesial temporal structures such as hippocampus, amygdala and adjacent parahippocampal cortex, often stemming from focal lesions such as head trauma, strokes and tumors. Acquired epilepsy, such as TLE, seems to have a progressive development that

starts from a latent period, i.e., the time between the brain insult and the first clinical seizure, after which seizures appear with increasing frequency until a plateau is reached. TLE (and in general acquired epilepsy after brain injury) is commonly associated with hippocampal sclerosis, a well-described histopathological profile whose cause remains elusive. In hippocampal sclerosis, there is selective loss of neurons in the dentate hilus and the hippocampal pyramidal cell layer. The dense gliosis that accompanies the loss of neurons causes shrinkage and hardening of the tissue. Detailed studies of the morphological and functional rearrangement in hippocampal sclerosis led to the idea that during the silent period that follows brain insults, some maladaptive changes occur. One of the best described change is the sprouting of mossy-fiber axons from dentate granule cells due to the loss of post-synaptic neuronal targets, which leads to the formation of new recurrent excitatory circuits and an overall increase of hippocampal network excitability. Another change, possibly associated with hippocampal sclerosis, is the selective loss of GABAergic interneurons which again leads to an overall increase in network excitability due to decreased inhibitory signals [40], [38],[1].

1.6 Interictal and ictal events: the cellular correlates of focal epilepsy

Much of our knowledge about the electrophysiological events that occur during seizures comes from studies of focal epilepsy in animal models. Indeed, information gained from human patients suffering of epilepsy are often limited due to obvious ethical, technical, statistical and economic constraints. Seizures are induced in animals by focal electrical stimulation or by acute or systemic injection of a convulsant agent, that can model either acute and chronic seizures. Among commonly used convulsant drugs, it is worth to remember: i) kainic acid (KA), an agonist of AMPA receptors; ii) pilocarpine, a potent cholinergic agonist and iii) pentylentetrazol (PTZ), a $GABA_A$ receptor antagonist. As an example, intrahippocampal injections of KA can reproduce most of the features observed in human TLE. Moreover, the development of *in vitro* brain slice preparations offered a variety of options for studying the cellular and molecular mechanisms underlying the generation, spread and termination of seizures using methods that are difficult to employ under *in vivo* conditions [51]. In vitro acute models of epileptogenesis are based on alteration in the excitation/inhibition balance through a variety of

pharmacological approaches. Examples include: the reduction of GABAergic transmission efficiency through application of $GABA_A$ receptor antagonists (Bicuculline, Picrotoxin, Strychnine, Penicillin); the increase in neuronal excitability and the reduction of hyperpolarizing conductances by raising the extracellular K^+ concentration; the enhancement of synaptic transmission by reducing some K^+ currents with the application of 4-aminopyridine (4-AP), barium and cesium (K^+ channels blockers). Additional methods, such as the modification of synaptic strength through repetitive electrical stimulation (e.g. kindling) and the enhancement of excitatory synaptic transmission through NMDA receptors due to the removal (or reduction) of extracellular Mg^{2+} (0 Mg^{2+} model) [52] also induce epileptiform activity [53].

Both in vivo and *in vitro* models allowed to unveil the cellular correlates of the two characteristic electrographic (EEG) hallmarks of an established seizure, namely the interictal spike and the full ictal event or seizure [54]. The interictal (between seizures) spike is the simplest identifiable unit of epileptiform activities in the brain. These events are brief (80-200 ms), large sharp spikes in the EEG that occur in isolation on a background of otherwise normal activity. Interictal spikes may serve to localize the epileptogenic focus, but they are not always easily detected from the primary focus of seizure initiation. The intracellular correlate of the interictal spike is

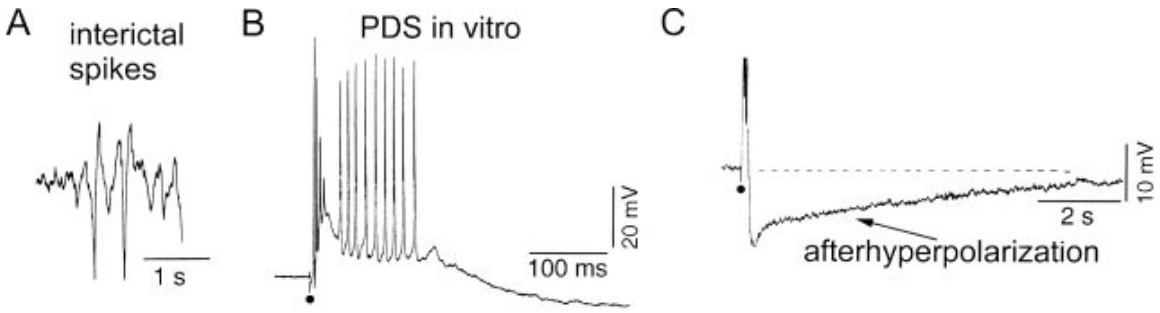

Figure 5. Interictal spike generation in hippocampus and cortex. (*A*) Example of two interictal spikes in the human EEG. Interictal spikes are brief (0.1 s) events typically localized to a particular region of the forebrain. (*B*) Intracellular recording in a human cortical pyramidal cell maintained in a cortical slice *in vitro* during the generation of a epileptiform burst similar to that underlying the generation of interictal spikes. The depo- larization underlying the epileptiform activity is termed a paroxysmal depolarization shift (PDS) and results in the initiation of a high-frequency burst of action potentials. (*C*). The PDS in the human cortical neuron is followed by a prolonged after-hyperpolarization that is generated by the activation of various potassium currents. Adapted from [6].

an overt depolarization, called the paroxysmal depolarizing shift (PDS), that lasts tens of milliseconds, results in the initiation of a high-frequency burst of action potentials and can be so large that leads to sodium channels inactivation at the end (Fig. 5, [6],[55]). It is noteworthy that PDSs are commonly observed in acute *in vitro*

models of epileptogenesis in which $GABA_A$ receptor mediated inhibition is impaired [56], as well as in models with preserved inhibition, such as the 0 Mg^{2+} [52] and the 4-AP [57] models.

The PDS and the subsequent afterhyperpolariziation are shaped by a massive enhancement of a ubiquitous microcircuit of neocortical and hippocampal networks: the disynaptic inhibition [14]. Indeed, the principal cell response to incoming excitatory inputs usually consists of an initial excitation followed by the activation of inhibitory post-synaptic conductances. The GABA-mediated afterhyperpolarization limits the duration of the PDS, and its gradual disappearance plays an important role in the focal seizure onset, as it will be discussed below. The mechanisms that synchronize PDSs within a population of neurons large enough to generate an interictal spike rely on the enhancement of recurrent excitatory connections between pyramidal neurons. Indeed, the bursting activity of a single neuron in the hippocampus has been demonstrated to be sufficient, in a condition of partial disinhibition, to initiate a synchronized discharge in a large neuronal population [58]. According to this model, the activation of primary intrinsic bursts in a small number of neurons induces a synaptic entrainment of neighboring neurons, which, in turn, causes a feedback recurrent synaptic excitation that prolongs membrane potential depolarization and promotes a secondary bursting associated with late PDSs [59],[60]). Although all the layers of the cerebral cortex and the different hippocampal regions have the potential of generating epileptiform activities, the cells that seem to discharge first during the PDS generation are layer 5 pyramidal neurons in the cortex [61] and CA3 pyramidal neurons in the hippocampus. This propensity relies not only on the excitatory

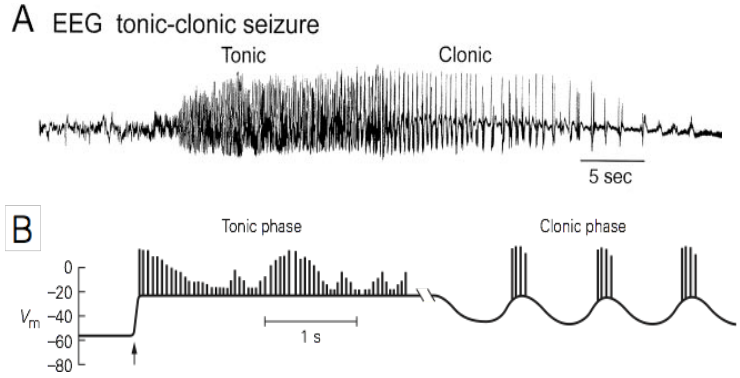

Figure 6 Tonic-clonic seizures. (A) Single EEG trace from a curare-treated patient undergoing a tonic-clonic seizure. Note that the tonic portion of the seizure is associated with high-frequency discharge in cortical networks and that this high-frequency discharge gradually gives way to the lower-frequency synchronized discharges of the clonic portion of the seizure. From McCormick and Contreras, 2001.
(B) Schematic of an intracellular recording of a seizure. At the onset (arrow), neurons in the focus depolarize as in the first part of the PDS. However, unlike the interictal period, the depolarization persists for seconds or minutes. This activity corresponds to the tonic phase of a secondarily-generalized tonic-clonic seizure. In this initial phase GABA inhibition is impaired, while as soon as it returns the neurons enter in the clonic phase, a period of oscillation. Adapted from [1].

interconnectivity of pyramidal neurons, but also on the presence of intrinsically burst-generating cells [62],[63].

In addition to interictal spikes, epileptic activity can also appear as the generation of full tonic-clonic seizures [54]. The typical EEG pattern observed during tonic-clonic seizures is an initial high-frequency activity (tonic phase), which then may evolve into large-amplitude, rhythmic discharges (clonic phase) that secondarly diffuse to adjacent cortical areas [54]. The transition from the generation of single PDSs during interictal spikes by a discrete ensemble of neurons to a full seizure is associated, from the intracellular point of view, with the maintained or tonic depolarization of the membrane potential and superimposed action potential firing at few to tens of Hz. This period of tonic activity is often followed by a period of irregular and periodic bursts of action potentials highly synchronous between all the neuronal elements involved, with relatively little synaptic and action potential activity in between bursts. These rhythmic cycles of depolarization and repolarization are also called afterdischarges and correspond to the clonic phase of the seizure. The high degree of neuronal coherence and synchrony during the clonic phase generates the large amplitude of EEG signals observed in this phase. The seizure is often followed by a period of decreased electrical activity, the postictal period (Fig. 6, [6], [1]).

Some lines of evidence suggest that the interictal spikes may not play a role in the ictal generation and they may rather prevent or diminish the occurrence of ictal events [55]. Moreover, a high degree of heterogeneity in neuronal spiking at seizure onset was recently observed in human patients, arguing against homogeneous runaway excitation or widespread paroxysmal depolarization as the primary mechanism of seizure generation [64]. On the other hand, an even more recent human study suggested that the failure in recording hypersynchronous activity at seizure onset might be due to the fact that genuine ictal recruitment occurs in far smaller territories than previously suspected as a result of an inhibitory restraint surrounding the seizure focus [65]. This crucial aspect in the cellular mechanisms at the basis of focal seizure propagation will be later discussed.

The cellular and network events that lead to epileptiform synchronization have been extensively studied in *in vitro* brain models. We know now that various synaptic and non-synaptic factors contribute to form a hyperactive network that, in turn, promotes seizure generation and favours seizure propagation [66], [67], [68], [69], [70]. Among

the synaptic factors, I will now focus my attention on GABAergic inhibition and on its role in the generation and the propagation of epileptic activity.

1.7 The role of GABAergic inhibition in focal epilepsy

1.7.1 Ictal generation

Because blocking GABAergic neurotransmission in control tissue generates seizures and because GABA boosters control epilepsy in many patients (as I will discuss later), studies on epilepsies have been dominated by the axiom that seizures are generated by a failure of GABA-mediated inhibition. However, GABAergic interneurons have many roles that goes far beyond the general and straightforward concept of “inhibition of target”. Operation of such a diversified system cannot be ascribed to a single mechanism. In epileptic tissue, GABAergic networks undergo complex rewiring at the anatomical, physiological and functional levels; GABAergic synapses are still operative but show unique features, including excitatory effects [71]. Several electrophysiological data support the view that a transient enhancement of interneuron network activity is associated with, and could be causally linked to, seizure initiation. Indeed, studies in the 4-AP [72] and in the 0 Mg^{2+} [73] slice model of focal epilepsy indicate that ictal discharges can originate from a synchronous event dependent on $GABA_A$ receptor activation. This mechanism might rely on the $GABA_A$ receptor-dependent increase in extracellular K^+ that can cause positive shifts of both $GABA_A$ and $GABA_B$ receptor-mediated postsynaptic inhibition, can depolarize neighboring neurons and can disinhibit excitatory postsynaptic interactions [74], [75]. Thus, the ictogenic role of GABAergic inhibition might rely on the increase of extracellular potassium associated with interneuronal activity [76]. Noteworthy is, however, a recently emerging, more intriguing hypothesis on the action of perisomatically targeting Pv interneurons (see chapter 1.3.3) that can synchronize large neuronal ensembles by inducing in pyramidal neurons a rebound-spiking immediately after the recovery from an intense inhibitory episode [77]. This rebound excitation, that is mainly mediated by hyperpolarization-activated, cyclic nucleotide-gated (HCN) ion channels, can shape the rhythmicity of the network by resetting the firing activity of pyramidal neurons [35], [78], [79], [80]. Such an effect might lead the

network to a hyperexcitability state that possibly favours seizure generation. In fact, studies in *in vitro* models of epileptiform activity revealed that optogenetic activation of GABAergic interneurons can trigger seizures [81], [82]. Among other possible links between GABAergic inhibition and seizure generation, it is worth to remember $GABA_A$ receptor function alterations in TLE, such as the modification in subunit composition and the positive shift in the reversal potential of $GABA_A$-mediated currents. This shift is caused by intracellular Cl^- accumulations that may reflect a downregulation of KCC2, i.e., the transporter responsible for extruding Cl^- ions from neurons. KCC2 dowregulation has been observed both in TLE and after an intense seizure activity induced in healthy tissue. The consequent shift in $GABA_A$ reversal potential results in a decreased efficacy of inhibition or even in a depolarizing and excitatory effect of GABAergic transmission on pyramidal neurons. Moreover, since KCC2 co-transport Cl^- and K^+ ions outside neurons, an increased activity of this transporter may lead to an increased extracellular K^+, which in turn causes a further depolarization of neurons, thus progressively impairing the KCC2 function. Such a positive feedback loop could be a major pro-convulsant mechanism [83], [71].

1.7.2 Ictal propagation

Focal seizures arise at restricted brain sites of abnormally active neuronal ensembles and secondarily involve adjacent regions, eventually spreading to distant areas [84]; [60]. As long as the abnormal electrophysiological activity is restricted to a small group of neurons, there are no clinical manifestations. The paroxysmal activity is confined to the focus by inhibitory effects of the excited region on surrounding tissue. This inhibitory surround is particularly dependent on feed-forward and feedback inhibition by GABAergic interneurons (Fig. 7, [85], [86], [70], [87]). When this inhibitory surround is overcome, the afterhyperpolarization in neurons at the original focus gradually disappears and the focal seizure begins to spread.

In the guinea pig isolated brain preparation, as well as in acute slice mouse models, it was observed that the low-voltage, high frequency (beta-gamma range) activity that is observed ahead of seizures in patients [88], correlates with a sustained firing in interneurons and with rhythmic inhibitory post-synaptic potentials (IPSPs) in principal neurons. These inhibitory events progressively decreased in amplitude during the development of a slow depolarization associated with an increase in extracellular K^+. In this way, the phase of robust inhibitory network activation

gradually shifts into a phase during which principal cell firing resumes, thus progressing into a pattern of recurrent population discharges as those seen during an electrographic seizure [89], [90], [91], [92], [75]. Moreover, other studies in hippocampal slice models (low Mg^{2+} and 4-AP) suggested that the transition to ictal events is marked by a shift from dominant phasic inhibition to dominant phasic excitation. During this period, interneurons increase their activity during the pre-ictal period (*i.e.* the period prior to the arrival of the ictal wave of excitation at the recorded area) when the pyramidal neurons receive strong inhibitory inputs and then they undergo long-lasting periods of depolarization block (with suppression of action potential generation) during the ictal event [93], [94]. The involvement of interneurons as the source of the feed-forward inhibitory restraint that locally oppose seizure propagation was further confirmed by the observation that applications of $GABA_A$ receptor antagonists allow the spread of epileptiform activity into the tissue at much higher speed than in the 0 Mg^{2+} model, where inhibition is broadly preserved [70], [95]. In this regard, models where inhibition is preserved appear to reflect better the classic description of neocortical epileptic propagation *in vivo* [96]. Indeed, it was demonstrated that in the 0 Mg^{2+} model ictal propagation is slow because it requires the stepwise recruitment of cortical modules, and the timing of pyramidal neurons recruitment into the propagating epileptic event is determined primarily by the efficacy of a powerful inhibitory restraint. These inhibitory barrages occlude a very large excitatory drive that pyramidal neurons experience, and only after inhibition collapses pyramidal neurons are recruited into the propagating ictal discharge [97], [4]. Moreover, it was observed that these inhibitory barrages that cause the ictal

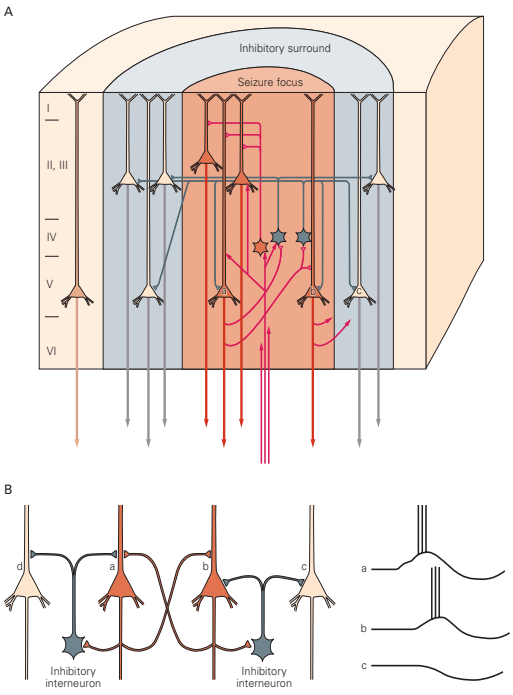

Figure 7 Surround inhibition. In this hypothetical seizure focus, the red pyramidal cells shows the abnormal activity typical of neurons in the focus, the PDS. This activity is reinforced by recurrent excitatory circuits between focal neurons, but these cells also activates GABAergic inhibitory interneurons (gray). These interneurons can reduce the activity of cells *a* and *b* through feedback inhibition, thus limiting the seizure focus temporally, as well as prevent the firing of cells outside the focus, represented here by cell *c*. This latter phenomenon creates an *inhibitory surround* that contains the seizure focus spatially. Adapted from [1].

wavefront to stall, corresponds to excitatory volleys of already recruited pyramidal neuron of a distal area, upstream of the propagation direction. The delay in the recruitment of downstream pyramidal neuron modules is directly correlated with the number of these pre-ictal inhibitory barrages and inversely correlated with the number of epileptic events that the network has experienced. Indeed, early ictal events show a large number of pre-ictal inhibitory barrages and a slow, modular propagation, while late ictal events exhibit a reduced number of inhibitory barrages and their propagation is rapid and generalized, with no evidence of modular recruitment [98]. Studies using slices from enthorinal cortex suggest that failure of feedforward inhibition coincides with an increased resistance to common antiepileptics [99]. How feedforward inhibition fails with successive ictal events is undefined and may be linked to an impairment of the inhibitory transmission to pyramidal neurons, possibly due to presynaptic depletion of GABA-containing vesicles [100], reduction in $GABA_A$ conductance [101], increased threshold for activation of interneurons, changes in the metabolic processing of GABA after intense neuronal activation [102], internalization of $GABA_A$ receptors [103], or even interneuron death induced by the extreme activity during ictal events [104]. An additional possibility is that such a sustained activation of $GABA_A$ receptor coupled to a downregulation of KCC2 transporters might overload pyramidal neurons of Cl^- ions, thus causing a positive shift in the $GABA_A$ reversal potential [105]. Therefore, in these conditions, GABA released during the preictal phase of late ictal events could be less inhibitory or even excitatory.

In order to better identify the type of interneurons involved in the generation of the feed-forward inhibition ahead of ictal event propagation, our laboratory recently developed a novel model of focal epileptiform activity, in which we can precisely control the site and the timing of ictal discharge generation. In this slice model from the temporal or the entorhinal cortex, a double pressure pulse applied to an NMDA-containing glass pipette positioned at cortical layer 5/6 while bath-applying 4-AP and 0.5 Mg^{2+}, induce full propagating ictal discharges [106]. These events closely mimic seizures recorded in vivo, including the activation of feedforward inhibition, rapid propagation across the cortex, transitions from tonic to clonic phase, and interictal events. This model allows precisely controlled experiments that cannot be performed in the currently available in vivo models, where the epileptogenic site is not identifiable in advance.

Using this model, we recently identified Pv interneurons as the major source of the feedforward inhibitory activity that locally restrains focal ictal discharge propagation. Indeed, in this study it was demonstrated that the pre-ictal inhibitory barrages that temporarily oppose the spreading of epileptiform activity are generated by local Pv interneurons, and also that a functional impairment (i.e. a depolarization block) in these interneurons contributes to the collapse of local inhibition that allows focal ictal discharges to further propagate across the cortex (Fig. 8, [4]). Consistently with this evidence, a reduced excitability of Pv interneurons caused by a defective expression of Na_V 1.1 channels is at the basis of Dravet syndrome, a severe genetic form of epilepsy [107], [47] (see also section 1.5). Pv interneurons were also demonstrated to maintain the clonic phase of the seizure by synchronizing afterdischarges through GABAergic synaptic transmission that becomes excitatory as a result of a transient collapse in the chloride (Cl^-) reversal potential [108].

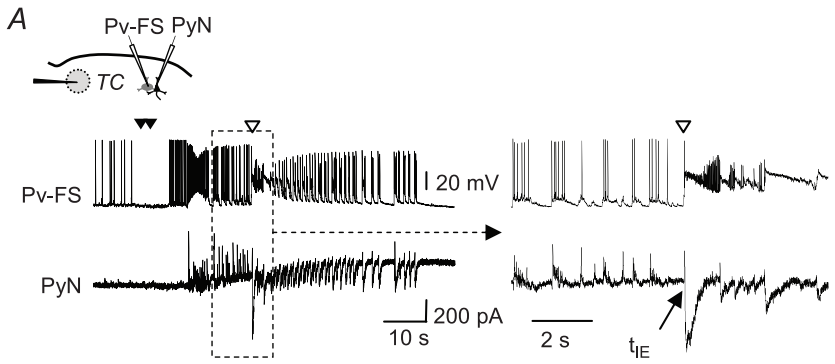

Figure 8 Hyperactivity and block in Pv interneurons precedes the transition to an ictal event. Dual current-clamp recordings from a Pv interneurons and voltage-clamp recording from a neighboring pyramidal neuron during an NMDA-evoked ictal event. Note in the enlargement that Pv interneurons firing is highly correlated with the inhibitory barrages recorded in the pyramidal neuron prior to ictal onset. When the Pv interneuron enter into a depolarization block (marked by the arrow), the pyramidal neuron is recruited into the seizure (tIE). From [4].

Thus, when the ictal wavefront generates such a prominent feedforward excitation, a rapid feedforward inhibition provides a powerful restraint, meaning that the cortical territories ahead of the ictal wavefront experience large amplitude excitatory and inhibitory conductances, but with little or no postsynaptic recruitment. A recent study in human patients suffering of chronic and pharmacoresistant focal epilepsy revealed that this inhibitory restraint exists also in the human brain, and that it is highly relevant for our ability to map seizure foci. By using multi-electrode array (MEA) recordings, these authors showed that, as observed in animal studies, there is a sharp delineation between areas with intense, hypersynchronous firing indicative of recruitment into the seizure, and adjacent territories where only a low level, unstructured firing is observed [65]. This latter has been also termed “ictal

penumbra", because of the contrast between the large amplitude EEG signals (reflecting the strong afferent excitatory and inhibitory synaptic activity) and the low-level of post-synaptic firing there. This finding calls for a careful reconsideration on how we interpret the low-frequency patterns in EEG recordings used to locate seizure focus. Indeed these EEG recordings are likely to be misleading, as they convey also postsynaptic activity not linked to a real recruitment into the seizure.
In contrast to the propagation of ictal wavefronts, the propagation of individual afterdischarges of the clonic phase seems to be governed by different principles. Indeed, the source of afterdischarges is different from that of the ictal event itself, and these individual bursts of the clonic phase propagate without stalling, since they are not influenced by the inhibitory restraint that limit ictal wavefront propagation. The reason of this is that afterdischarges emerge from recruited territories, where the inhibitory veto has already failed. Moreover, afterdischarges seem to switch their direction of propagation in coincidence with the peak excitatory drive, corresponding to the ictal wavefront [109]. This means that the ictal wavefront must be the source of all activity, driving the recruitment of new territories ahead of the wavefront and also seeding afterdischarges that then propagate in the opposite direction, possibly sustaining ictal activity.

1.8 Epilepsy treatment

The treatment of epilepsy is currently based on two main approaches: pharmacological and surgical. Recent studies have shown that up to 70% of children and adults with epilepsy can be successfully treated with anti-epileptic drugs (AEDs) [37]. Indeed, AEDs have the remarkable ability to protect against seizures while permitting normal functioning of the nervous system. AEDs act on diverse molecular targets to selectively modify the excitability of neurons so that seizure-related firing is blocked without disturbing non-epileptic activity. These targets include ion channels, neurotransmitter transporters and neurotransmitter metabolic enzymes. Some of the most used compounds act on voltage-gated sodium and calcium channels (Phenytoin, Carbamazepine, Lamotrigine, Valproate), by promoting GABA receptors-mediated inhibition (Benzodiazepines) or by increasing GABA turnover (Gabapentin) [110]. Furthermore, after 2 to 5 years of successful treatment and being seizure-free, drugs can be withdrawn in about 70% of children and 60% of adults. However, in

some patients the pharmacological treatment fails to control focal seizures (so-called intractable), and the only option is the surgical resection of the brain region from which the seizure originates (the focus). It is evident that the surgical outcome is directly related to the adequacy of the resection, and for this reason a precise localization of the seizure focus is essential. Electrical mapping of seizure foci originally relied on the surface EEGs, which however suffer of a bias toward particular sets of neurons in the cortex immediately adjacent to the skull. The development of magnetic resonance imaging (MRI), positron emission tomography (PET) and of single-photon emission computed tomography (SPECT) has markedly improved the noninvasive anatomical and functional mapping of seizure foci [111]. These techniques are based on the focal coupling of alterations in blood flow and metabolism with neuronal activity, as well as on the localization of peculiar anatomical changes in epileptic patients such as the hippocampal atrophy. However, these imaging techniques lack the temporal resolution necessary to resolve brief epileptiform events and to differentiate ictal onsets from areas of early spreads. For these reasons, optical imaging of intrinsic brain signals was proposed as an alternative for mapping epileptic foci [86]. This technique is based on the changes in light absorption of active neural tissue, and can be used to study and map at high resolution spontaneous epileptic events *in vivo*.

Many patients, however, are not suitable candidates for brain surgery. Therefore, direct electrical brain stimulation may provide a nondestructive treatment option for people with medically intractable partial seizures. For this purpose, it has been successfully proven the efficacy of deep brain stimulation (DBS) already used for Parkinson disease and essential tremor [112], as well as of direct cortical stimulation of the seizure focus in response to epileptiform electrographic events [113].

1.9 An optogenetic approach for treating epilepsy

As extensively reviewed in this introduction, different subtypes of GABAergic inhibitory interneurons have different and highly specialized functions in establishing proper operations in neural circuits. This is true also for epilepsy, where seizures are generated and propagated by the same cortical microcircuits involved in normal brain function [114]. Thus, specific subtypes of GABAergic interneurons likely have different roles in epilepsy, with some subtypes more involved than others. Indeed, Pv

interneurons were demonstrated to be key players in limiting the spread of seizures, and they may be also involved in the events underlying seizure generation [4], [81]. This prominent role of PV interneurons in epilepsy is probably linked to their particular morphological and physiological characteristics, such as their ability to tightly regulate the spiking output of pyramidal neurons by forming strong inhibitory synapses onto the soma of these cells. Therefore, an approach that allows to specifically modulate the activity of GABAergic interneurons, and possibly Pv interneurons, might represent a strategy to effectively control seizures. The optogenetic technique, i.e., a combination of genetic and optical tools, which provides a fast and cell specific control of neuronal spiking in intact tissue, is an ideal candidate to achieve such a challenging task [115]. This approach has grown exponentially in the last ten years, allowing elucidation of the neural circuitry underlying adaptive and maladaptive behaviors. Optogenetics is based on three core features: (i) the use of microbial opsins, light-sensitive ion channels that can be activated with sub-millisecond temporal precision upon the illumination with light of specific wavelengths, (ii) general methods for targeting sufficiently strong and specific opsin gene expression to well-defined cellular elements in the brain, and (iii) general methods for guiding sufficiently strong and precisely timed light to specific brain regions, cells or parts of cells [116].

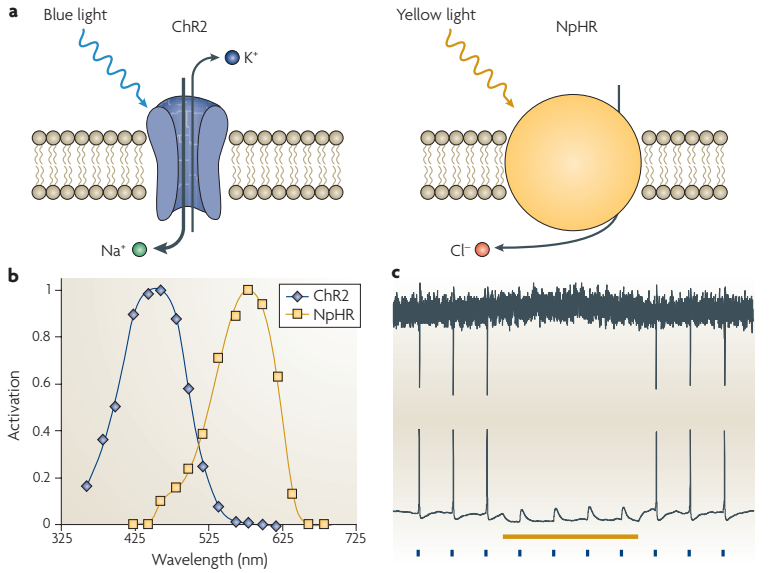

Figure 9 Optogenetic tools: ChR2 and NpHR. (a) Schematic of channelrhodopsin-2 (ChR2) and the halorhodopsin (NpHR) pump. Following illumination with blue light (activation maximum ~470 nm), ChR2 allows the entry of cations (mostly sodium and very low levels of calcium) into the cell. NpHR is activated by yellow light illumination (activation maximum ~580 nm) and allows the entry of chlodide anions. (b) Activation spectra for ChR2 and NpHR. The excitation maxima for ChR2 and NpHR are separated by ~100 nm, making it possible to activate each opsin independently with light.
(c) Cell-attached (top) and whole-cell current-clamp (bottom) traces from hippocampal neurons showing all-optical neural activation and inhibition. Blue pulses represent the blue light flashes used to drive ChR2-mediated activation and the yellow bar denotes NpHR-mediated inactivation. Adapted from [7].

The optogenetic toolbox includes a wide array of available opsin variants that allows cell specific excitation, inhibition, and activation of intracellular signaling cascades. More

specifically, the microbial light sensitive protein Channelrhodopsin-2 (ChR2) from *Chlamydomonas reinhardtii* is a monovalent cation channel that allows Na^+ to enter the cell following exposure to ~ 470 nm blue light, eliciting in neurons action potentials time-locked with light pulses. On the other hand, the halorhodopsin from *Natronomonas pharaonis* (NpHR) is a chloride pump that activates upon illumination with ~ 580 nm yellow light. As the activation maxima of these two proteins are over 100 nm apart, they can be controlled independently to either drive action potential firing or suppress neural activity, bidirectionally turning neurons on and off with high temporal precision and with high cellular specificity (Fig. 9, [117], [7]). One of the most widely used approach to express these proteins inside neurons in the living brain is the viral gene delivery. Viral vectors carrying the gene for ChR2 and/or NpHR can be delivered stereotactically into discrete brain regions [118]. Recombinant lentiviral and adeno-associated viral (AAV) vectors have been and are popular choices for gene transfer in animal models, especially in rodents [119], ensuring a stable expression over time. These vectors can be also rendered cell-type specific by the choice of promoter, viral receptor (serotype) or spatial targeting strategies. Moreover, these vectors can be floxed, thus being dependent for their expression on the presence in the cell of Cre-recombinase. This approach has broadened even more the cell types that can be targeted, given the great abundance of Cre mouse lines existing. For this reason, transgenic mice containing the floxed sequence of some opsins have been developed, allowing to induce cell-specific expression of these proteins by crossing mice expressing Cre recombinase under specific promoters and opsin-floxed mice.

Studies in rodent brain slices revealed that optogenetics is, indeed, a powerful tool to investigate the role of GABAergic interneurons in acute epilpeptiform activity. For example, Ledri and colleagues demonstrated that the global optogenetic activation of a mixed interneuron population (Som, Pv, NPY, CCK) can suppress ongoing epileptiform activity, and that this approach is more effective than the

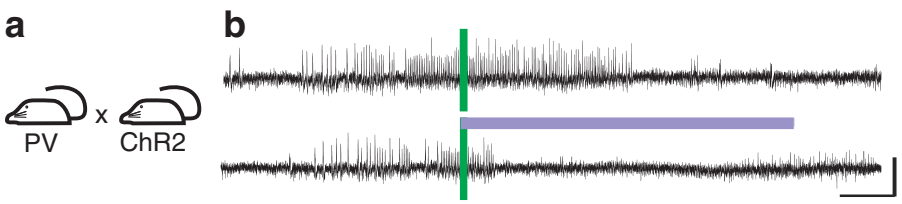

Figure 10 On demand, *in-vivo* optogenetic seizures control in Pv-ChR2 mice. The closed loop system was able to automatically detect the onset of the spontaneuos seizure (green bar) and, as a consequence, to initiate the optogenetic stimulation of Pv cells with an optical fiber inserted into the hippocampus (violet bar). This shortened seizure duration of about 40%. Adapted from [2].

activation of just one single population of interneurons [120]. The potential of a selective stimulation of GABAergic interneurons, and in particular of Pv interneurons, as a strategy to limit seizures, was further proven by Krook-Magnuson and colleagues in an *in vivo* mouse model of temporal lobe epilepsy. Indeed, these authors have developed an on-demand system capable of detecting the onset of a seizure (recorded by intra-hippocampal EEG electrodes) and, as a consequence, to automatically initiate the light stimulation of Pv interneurons in the hippocampus by means of an optical fiber. When Pv interneurons were stimulated, the seizures were rapidly suppressed (Fig. 10, [2]). Similar results were obtained by another group through a closed-loop optogenetic stimulation of thalamocortical neurons. These authors revealed that seizures that develop after a cortical injury are maintained also by the thalamus, and that by reducing in real-time the activity of this nucleus with optogenetic silencing (NpHR), electrographic and behavioral seizures were immediately interrupted [121].

However, several groups recently reported an excitatory, proconvulsant effect of optogenetic stimulation of GABAergic interneurons, and in particular of Pv interneurons, in both the generation and in the mainteinance of epileptiform activity in brain slices [81], [82], [108]. Therefore, there is a discrepancy between these two conflicting views that calls for reconciliation.

1.10 Astroglia in the epileptic brain

Astrocytes are the major class of glial cells in the brain and play essential roles in brain homeostasis and metabolism. They are coupled in a syncytium through gap junctions and exert a homeostatic control of the extracellular space by regulating the pH, the water content and the extracellular concentration of different neurotransmitters and ions. In addition, astrocytes supply neurons with nutrients, trophic factors, cytokines and neuromodulators [122], contributing to the neurovascular coupling mechanism [123] and to the defensive reaction to tissue insult. Only recently the role of astrocytes has been extended to functions that were once considered an exclusive domain of neurons, such as short- and long-term modulation of synaptic transmission. This has led to the concept of the tripartite synapse in which the astrocytic finest processes, together with the pre- and post-synaptic neuronal elements, actively participate in the regulation of information

transfer and integrative processes [124], [125]. Indeed, astrocytes express a wide variety of receptors for neurotransmitters, neuromodulators, cytokines and trophic factors that are used by these cells to sense the synaptic activity as well as other extracellular signals [126]. In response to these signals, astrocytes can release molecules that regulate fundamental events in brain function by acting on neurons, glia, and vascular cells. Molecules such as glutamate, ATP, D-serine, cytokines and GABA have been collectively termed gliotransmitters, and they target similar receptors to those activated by neurotransmitters. Gliotransmitters have been shown to exert distinct modulatory actions on synaptic activity and network excitability through different mechanisms [126], [127]. Evidence for a Ca^{2+}-dependent exocytotic release mechanism has been provided for these gliotransmitters, but Ca^{2+}-independent mechanisms have also been identified [128], [129].

The discovery that astrocytes modulate neuronal communication and are involved in the control of brain network activities suggest that astrocytes have the potential to be involved in a number of brain disorders, from acute brain injury to chronic diseases including Alzheimer's disease, Parkinson disease, amyotrophic lateral sclerosis, and epilepsy [130], [131], [132]. Early in the development of many brain disorders, astrocytes exhibit significant morphological and functional changes, a condition termed reactive gliosis [133]. Gliosis is frequent in the human epileptic brain and seizures have been shown to frequently initiate within or very near gliotic brain tissues [134]. Although the significance of this alteration is poorly understood, recent findings suggest the hypothesis that astrocyte disfunction contributes or even plays a central role in epileptogenesis. The involvement of astrocytes in epilepsy is linked with at least three important functions that they exert inside the brain: i) the K^+ homeostasis, ii) the glutamate homeostasis and iii) gliotransmission (for a review see [3]).

1.10.1 K^+ homeostasis

Neuronal activity produces transient increases in the extracellular K^+ concentration ($[K^+]_o$), which, if uncorrected, would cause network hyperactivity and, possibly, epileptiform events. Clearance of K^+ from the extracellular space is considered to be an important function of astrocytes. Indeed, glial cells possess high and rapid permeability to K^+ ions, and are able to spatially redistribute through gap junctions a

local excess of K^+ to neighboring regions or into blood vessels [135]. According to this peculiar ability, astrocytes are thought to play a key role in the uptake of K^+ ions which accumulate in the extracellular space during an intense action potential firing in large neuronal ensemble such as that characterizing seizures. The inwardly rectifying K^+ channels (K_{ir}) are the principal mediators of the huge K^+ permeability observed in astrocytes. The most studied K_{ir} channels is the K_{ir} 4.1, that is abundantly expressed in astrocytes throughout the brain [136], [137]. These channels are characterized by a high open probability at resting potential and by a conductance that is proportional to $[K^+]_o$ [138]. These features allows K_{ir} 4.1 channels to be effectively activated by large increases in $[K^+]_o$ and to mediate a large K^+ influx at hyperpolarized potential and a small K^+ efflux at depolarized potentials. A reduction of K_{ir} 4.1 expression has been observed in tissues from TLE patients as well as in experimental epilepsy models [139], [140]. This reduction, along with a possible functional impairment of these channels due to neuronal injury, might increase network activity leading to a higher susceptibility to proconvulsant stimuli or to spontaneous seizures. However, it is still unclear whether these dysfunctions in K_{ir} 4.1 channels are directly involved in epileptogenesis or if these changes are a reaction of the tissue to the aberrant epileptic activity.

1.10.2 Glutamate homeostasis

Astrocytes have a prominent role also in the regulation of extracellular levels of the excitatory neurotransmitter glutamate, which is internalized by these cells through an efficient reuptake system that includes five different excitatory amino acid transporters (EAAT1-5). Among these, EAAT1 and EAAT2 (GLAST and GLT-1 in rodents, respectively) are exclusively expressed in astrocytes [141]. However, while high extracellular glutamate levels have been reported in human epileptic tissue [142], there are controversial results on astrocytic EAAT expression levels in tissue from TLE patients. Indeed, while some studies revealed a down regulation of astrocytic glutamate transporters [143], others failed to observe similar alterations [144]. Nevertheless, the potential of astrocytic EAAT transporters to participate in seizure generation was demonstrated in a transgenic mouse model in which the deletion of EAAT2 in astrocytes resulted in epileptiform activities [141].

1.10.3 Gliotransmission

The local hypersynchronous and excessive activity that characterize epileptogenesis are classically thought to arise from abnormalities intrinsic to neurons. In the generation of epileptic activity, however, non-neuronal mechanisms may also be involved. The aforementioned observations on a Ca^{2+}-dependent release of glutamate by astrocytes is of particular relevance in this context. Indeed, astrocytes represent an extrasynaptic source of glutamate that triggers a synchronous response in neuronal ensembles. Indeed, the release of astrocytic glutamate – in response to Ca^{2+} elevations evoked by different agents – induced in two neighboring neurons NMDA receptor- mediated highly synchronous slow inward currents (SICs) [145], [146]. Accordingly, Ca^{2+} imaging experiments revealed that astrocyte Ca^{2+} elevations could be followed by episodes of simultaneous Ca^{2+} elevations in small groups of adjacent neurons, a response that our group termed a "domain response" [145].

These observations support the hypothesis that an abnormal activation of these "domains" might, under certain conditions, hypersynchronize neurons and predispose them to seizures. This view was supported by a controversial study which reported that a large fraction of paraoxysmal depolarizing shifts (PDSs) were insensitive to tetrodotoxin (TTX) suggesting, according to the authors, that SICs coincide with PDSs and that seizure activity may have an astrocytic basis [147]. This conclusion, however, was in striking contrast with other observations reporting an efficient block of PDSs by TTX and with a wealth of data supporting the view that PDSs

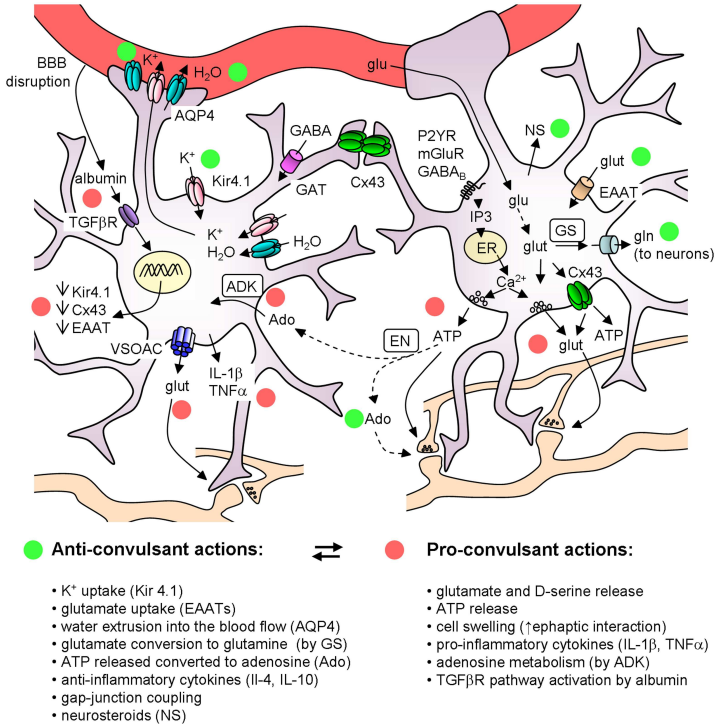

Figure 11 Schematic of the main astrocyte actions that can affect epileptiform activities. The colored circles mark the anticonvulsant (green) and the proconvulsant (red) actions of astrocytes. ADK, adenosine kinase; Ado, adenosine; AQP4, aquaporin 4; BBB, blood brain barrier; Cx43, connexin 43; EAAT, excitatory amino acid transporters; EN, ectonucleotidase; ER, endoplasmatic reticulum; GAT, GABA transporters; glu, glucose; glut, glutamate; gln, glutamine; GS, glutamine syntethase; NS, neurosteroids; VSOACs, volume-sensitive organic anion channels. From [3].

and SICs are different cellular events [148]. Despite these contradictory evidence on a causal role for astrocytes in epileptogenesis, the possibility that astrocytic glutamate contributes to seizures development cannot be ruled out. Indeed, by using the aforementioned slice model of focal seizures, our group demonstrated that neuronal hyperactivation arising at a restrict cortical site is accompanied by early Ca^{2+} elevations in a large number of neighboring astrocytes, that in turn, by releasing glutamate, contributes to drive neurons towards the threshold of seizure generation [149]. This study highlights also that astrocytes are not an absolute requirement for this process, but they can provide an important and even, under certain circumstances, crucial contribution to seizure generation.

1.10.4 GABAergic inhibition and astrocytes

As highlighted in the previous chapters, GABAergic inhibitory interneurons are massively activated during both the generation and the propagation of epileptic activity. Therefore, the hypothesis that GABA released by these interneurons may elicits Ca^{2+} elevations similar to those observed for glutamate can be reasonably advanced. Importantly, GABA – activated astrocytes may release gliotransmitters that can differently impact on the delicate balance of inhibition and excitation that characterizes the boundary between the seizure focus and the inhibitory surround as well as the propagating regions.

Astrocytes are, indeed, responsive to GABA signals, as they express both $GABA_A$ and $GABA_B$ receptors similar to those expressed by neurons [150], [151]. The activation of astrocytic $GABA_A$ receptors results in a depolarizing current, as opposed to neurons, due to a high intracellular content of Cl^- [152]. The role for this Cl^- efflux from astrocytes is still unclear, but it was proposed that it may serve to restore the Cl^- extracellular levels after intense activation of GABAergic interneurons, thus preserving the inhibitory driving force of Cl^- ions in neurons [153]. GABA can also evoke Ca^{2+} events in astrocytes by acting on $GABA_A$ receptor that, by depolarizing the membrane potential, activate voltage-sensitive Ca^{2+} channels [150]. But the main mediator of GABA – evoked Ca^{2+} events in astrocytes seems to be $GABA_B$ receptors [151], [154]. The mechanism of $GABA_B$ – mediated Ca^{2+} events was shown to involve G proteins and Ca^{2+} release from intracellular store, but it is still unclear exactly which G protein is responsible for these events. Although the Ca^{2+}-dependent

release of gliotransmitter by astrocytes upon $GABA_B$ activation is not conclusively proved, a few studies hint at this possibility by demonstrating that: i) synaptically released GABA mediates Ca^{2+} oscillations in astrocytes that, in turn, result in the modulation of inhibitory synaptic inputs to hippocampal neurons [151], and ii) that GABA – activated astrocytes modulate heterosynaptic depression by releasing ATP in a Ca^{2+} - dependent manner, which is rapidly converted in the extracellular space to adenosine, inhibiting presynaptic release of glutamate through A1 receptor activation [154]. Given that Ca^{2+} elevations represent, as previously described, a form of excitability in astrocytes, it follows that in the neuron – astrocyte network an inhibitory GABA input has also the potential to be translated into an excitatory output by astrocytes. This hypothesis has, of course, important implications in epilepsy.

2. AIM OF THE THESIS

The successful implementation of closed-loop optogenetic stimulation of GABAergic interneurons, and in particular of Pv interneurons, as a tool to stop seizures in animal models demonstrated that this could be a promising approach to oppose those epileptic events that typically arise from restricted focal sites, such as TLE. Indeed, increasing inhibition at this site by Pv interneuron optogenetic activation may be technically feasible and represent a potential alternative to resective surgery commonly used in untreatable temporal lobe epilepsy forms. Most importantly, it has the potential not only to interrupt ongoing seizures, but also to suppress the abnormal activity that precedes seizures preventing the generation of a full epileptic event. To test this hypothesis, light has to be delivered at the epileptogenic focus. However, the unpredictable nature of focal seizures renders the identification of the epileptogenic focus in the intact brain a daunting challenge. We thus developed a focal epilepsy model in temporal cortex (TCx) slices that gives the unique opportunity to identify the precise site of seizure initiation and to generate an epileptic event at any given time. The hallmark of this *in vitro* model is that it allows precisely controlled experiments that cannot be accomplished in currently available *in vivo* models, where the seizure initiation site is not identifiable in advance. The fact that in our model we know where and when the seizure will be generated allowed us to investigate whether and how Pv interneurons differentially control initiation and propagation of focal epileptiform activities. We addressed two main questions that will clarify the role of these cells in epileptiform activities. First, does Pv interneuron activation suppress the ictogenic activity that, at the epileptogenic focus, contributes to ictal event generation? Second, does Pv interneuron activation out of the focus (i.e., the ictal propagating region) oppose ictal event spread? To answer these questions, we combined single/dual cell patch-clamp and local field potential recordings with optogenetics and Ca^{2+} imaging in cortical slice preparations.

Moreover, we have investigated the role of Pv interneurons in a genetic form of epilepsy, the severe myoclonic epilepsy of infancy (SMEI or Dravet syndrome). As I thoroughly reported in the introduction, GABAergic interneurons and in particular Pv interneurons are deeply involved in the pathogenesis of this severe epileptic encephalopathy. Therefore, we decided to use our focal model of ictal discharges to study seizure propagation in cortical brain slices from mice lacking one of the two

Scn1a alleles, a mouse model that recapitulates several deficits observed in SMEI patients.

As regards the potential activation of a $GABA_B$ receptor – dependent Ca^{2+} signaling in astrocytes during the strong activation of GABAergic interneurons triggered by epileptic activity, we have initially characterized the astrocyte Ca^{2+} response to exogenous bath application with either GABA or the selective $GABA_B$ receptor agonist baclofen in brain slices of young (P15-P20) and adult mice. We have also investigated whether and how these GABA – activated astrocytes may signal back to neurons.

3. RESULTS

Journal of Neuroscience Methods xxx (2015) xxx–xxx

Contents lists available at ScienceDirect

Journal of Neuroscience Methods

journal homepage: www.elsevier.com/locate/jneumeth

Basic neuroscience

A brain slice experimental model to study the generation and the propagation of focally-induced epileptiform activity

Gabriele Losi*, Iacopo Marcon, Letizia Mariotti, Michele Sessolo, Angela Chiavegato, Giorgio Carmignoto*

Neuroscience Institute, National Research Council (CNR) and Department of Biomedical Sciences, University of Padova, via U. Bassi 58/b, 35121 Padova, Italy

HIGHLIGHTS

- We propose a model of seizure-like events in temporal cortex slices from young mice.
- In the model local NMDA stimulations induce multiple seizure-like events.
- Electrophysiological, Ca^{2+} imaging and optogenetics are combined in the model.
- Seizures generation and propagation are separately studied.
- The role of specific cell population on these events can be accurately analyzed.

ARTICLE INFO

Article history:
Received 12 February 2015
Received in revised form 1 April 2015
Accepted 2 April 2015
Available online xxx

Keywords:
Focal seizures
Temporal cortex
GABAergic interneurons
Astrocytes

ABSTRACT

The early cellular events that in a brain network lead to seizure generation and govern seizure propagation are probably based on different cellular mechanisms. Experimental models in which these events can be separately studied would contribute to improve our understanding of epilepsy. We recently described an in vitro model in entorhinal cortex slices from young rats in which focal seizure-like discharges (SLDs) can be induced in spatially defined regions and at predictable times by local NMDA applications performed in the presence of 4-amimopyridine (4-AP) and low extracellular Mg^{2+}. Through the use of single-dual cell patch-clamp and field potential recordings, and Ca^{2+} imaging from large ensembles of neurons, interneurons and astrocytes, we here extend this model to entorhinal and temporal cortex slices of rat and mouse brain, providing evidence that multiple SLDs exhibiting the typical tonic–clonic discharge pattern can be also evoked in these cortical regions by successive NMDA applications. Importantly, the temporal cortex is more accessible to viral vector injections than the entorhinal cortex: this makes it feasible in the former region the selective expression in inhibitory interneurons or principal neurons of genetically encoded Ca^{2+} indicators (GECI) or light-gated opsins. In this model, an optogenetic approach allows to activate specific neuronal types at spatially defined locations, i.e., the focus or the propagating region, and at precise time, i.e., before or during SLD. The NMDA/4-AP model can, therefore, represent a valuable tool to gain insights into the role of specific cell populations in seizure generation, propagation and cessation.

1. Introduction

Epilepsy is a severe neurological disorder characterized by recurrent convulsive or non-convulsive episodes reflecting massive neuronal discharges. Medial temporal lobe epilepsy (MTLE) is one of the most frequent and severe form of epilepsy in adulthood with seizures originating in hippocampal and para-hippocampal regions. As nearly one third of TLE patients are unresponsive to currently available antiepileptic drugs, the need for novel therapeutic tools, possibly with lower side effects, is impelling. The development of new therapeutic strategies relies on our knowledge of the cellular, molecular and network events that lead to seizure maturation, for which experimental animal models are of crucial importance. The most common animal models of epilepsy make use of chemoconvulsants such as pilocarpine and kainic acid (for review see Curia et al., 2008; Levesque and Avoli, 2013). Both toxins are used in rodents to induce status epilepticus which is followed by spontaneous recurring seizures after a latent period recapitulating

* Corresponding authors. Tel.: +39 0498276075.
E-mail addresses: gabriele.losi@bio.unipd.it, gabrielelosi@hotmail.com (G. Losi).

http://dx.doi.org/10.1016/j.jneumeth.2015.04.001

in many aspects human TLE. As the epileptic phenotype develops in vivo, these models are considered valuable to study epileptogenesis (for a recent review on animal models see Kandratavicius et al., 2014).

A different approach uses acute slice preparations from non epileptic brain tissue that can, under certain conditions, develop seizures-like events. For example, slice perfusion with reduced extracellular Ca^{2+}, Mg^{2+}-free solutions (Jefferys and Haas, 1982; Jefferys, 1995; Trevelyan et al., 2006), increased extracellular K^+ (Bear and Lothman, 1993) or the addition of compounds like pentylenetetrazol (PTZ), *N*-methyl-D,L-aspartate (NMDA), tetanus toxin or GABA receptors antagonists, including penicillin, picrotoxin or bicuculline, all cause a dramatic increase in neural network excitability that leads to the generation of epileptiform activity (Pinto et al., 2005; Pitkänen et al., 2006). It is noteworthy that these experimental conditions represent models of acute seizures generation (i.e., ictogenesis) rather than models of epileptogenesis. An additional diffused model of ictogenesis makes use of the K^+ channel blocker 4-aminopyridine (4-AP) that induces epileptiform activity in brain slices in vitro (Voskuyl and Albus, 1985; Perreault and Avoli, 1991, 1992; Avoli et al., 1996; Ziburkus et al., 2006; Uva et al., 2009) and in vivo (Mihaly et al., 1990; Levesque and Avoli, 2013). In this model, after prolonged perfusion of the drug, seizure-like ictal discharges arise spontaneously at unpredictable time and locations (Avoli et al., 1996), but mainly in deep cortical layers (Avoli et al., 2002; Uva et al., 2009).

To study the abnormal activity that at the level of local circuits precedes the generation of focal seizures, as well as the dynamics of the cellular and network events that govern seizure propagation, it is necessary to identify the site of seizure initiation. However, the unpredictable nature of seizures renders the identification of this focal site a daunting challenge, especially in the intact brain. We describe here an experimental model in slice preparations from the entorhinal or temporal cortex of young rats and mice in which seizure-like discharges (SLDs) can be focally induced by challenging small groups of neurons with local NMDA applications. We will provide the experimental procedures in detail and discuss the applicability of the model in specific brain areas. As we show here, NMDA-evoked focal SLDs are indistinguishable from spontaneous events and their site of origin and propagation can be analyzed with unprecedented spatial and temporal accuracy. In the model, single and dual cell patch-clamp recordings, local field potential recordings, Ca^{2+} imaging and optogenetic techniques can be combined to provide insights into the cellular events that govern initiation and spread of SLDs. Explicative experiments are reported.

2. Methods

2.1. Animals

All experiments are carried out in strict accordance with the guidelines established by the European Communities Council Directive and approved by the National Council on Animal Care of the Italian Ministry of Health. All efforts are done to reduce the number of animals used. Brain slices (see Section 2.2) were obtained from Wistar rats, C57BL6J mice, G42 mice (Chattopadhyaya et al., 2004) (kindly donated by Alberto Bacci), and from GCaMP3::Pv-Cre mice obtained by crossing GCaMP3 mice (B6;129S-Gt(ROSA)26Sortm38(CAG-GCaMP3)Hze/J) with B6.Cg-Pvalbtm1.1(cre)Aibs/J mice (id #012358; Jackson Laboratory).

2.2. Brain slice preparations and Ca^{2+} dye loading

Coronal slices are prepared from postnatal day 14–20 animals as previously described (Cammarota et al., 2013). Briefly, rats and mice are deeply anaesthetized with intraperitoneally injected Zoletil (40 mg/kg) and decapitated; the brain is quickly removed and transferred to ice-cold standard ACSF, sACSF (in mM 125 NaCl, 2.5 KCl, 2 $CaCl_2$, 1 $MgCl_2$, 25 glucose, pH 7.4 with 5% CO_2/95% O_2). After brain dissection on the coronal plane, 350 μm-thick slices are cut with a vibratome (VT1000S, Leica Microsystems, GmbH, Wetzlar, Germany). Cutting solution for rat and mice brain are described in Cammarota et al. (2013) and in Dugue et al. (2005), respectively. Slices from mice are transferred for 1 min in a 95% O_2 and 5% CO_2 saturated solution containing (in mM) 225 D-mannitol, 2.5 KCl, 1.25 NaH_2PO_4, 26 $NaHCO_3$, 25 glucose, 0.8 $CaCl_2$, 8 $MgCl_2$, 2 kynurenic acid with 5% CO_2/95% O_2. Slices from both rats and mice are finally transferred in sACSF at 30 °C for 20 min and then maintained at room temperature. Slices are kept in ACSF with Sulforhodamine 101 (SR-101) (0.2 μM, Sigma Aldrich, Milano) at 30 °C for 15 min to selectively stain astrocytes. Loading with the fluorescence Ca^{2+} indicator Oregon Green BAPTA1-AM (10 μM; Life Technologies, Monza) is performed at 30 °C for 50–60 min in the sACSF solution containing pluronic (0.12%, Sigma Aldrich, Milano, Italy) and kynurenic acid (1 mM, Sigma Aldrich, Milano, Italy). After loading, slices are recovered and kept at room temperature.

2.3. Ca^{2+} imaging

Images are acquired with a single-photon upright laser-scanning microscope (TCS-SP5-RS, Leica Microsystems, GmbH, Wetzlar, Germany) with an acquisition time frame of 491 ms (seven line averaging). Oregon Green and GCaMP3 are excited at 488 nm, SR-101 at 543 nm. The microscope is also equipped with a CCD camera for differential interference contrast (DIC) image acquisition.

2.4. Electrophysiology and induction of focal SLDs

Brain slices are continuously perfused in a submerged chamber (Warner Instruments, Hamden, USA) at a rate of 3–4 ml min^{-1} with (in mM): NaCl, 120; KCl, 3.2; KH_2PO4, 1; $NaHCO_3$, 26; $MgCl_2$, 0.5; $CaCl_2$, 2; glucose, 10; at pH 7.4 (with 5% CO_2/95% O_2). Single and dual cell recordings are performed in current-clamp and voltage-clamp configuration using a multiclamp-700B amplifier (Molecular Devices, Foster City, CA, USA). Signals are filtered at 1 kHz and sampled at 10 kHz with a Digidata 1440s interface and pClamp10 software (Molecular Devices, Foster City, CA, USA). Typical pipette resistance was 3–4 MΩ. Access resistance is monitored throughout the recordings and was typically <25 MΩ. Whole-cell intracellular pipette solution is (in mM): K-gluconate, 145; $MgCl_2$, 5; EGTA, 0.5; Na_2ATP, 2; Na_2GTP, 0.2; HEPES, 10; to pH 7.2 with KOH, osmolarity, 280–300 mOsm (calculated liquid junction potential: −14 mV). All patched neurons are from cortical layer V–VI; pyramidal neurons are voltage-clamped at −50 mV (Vh) or current clamped at resting potential as with Pv-FS interneurons. Induction of focal SLDs is performed in the presence of 4-AP (100 μM) and bath temperature maintained at 30–32 °C by an inline solution heater and temperature controller (TC-324B, Warner Instruments, Hamden, USA). A pressure ejection unit (PDES, NPI Electronics, Tamm, Germany) is used to apply a single or double pulse to NMDA (1 mM, Sigma Aldrich, Milano, Italy)-containing pipettes with a 3 s interval, a pressure of 4–10 psi, and a duration of 300–600 ms. In some experiments, the NMDA glass pipette includes an $AgCl_2$ electrode for extracellular local field potential recordings. Field potential signals are filtered at 1 kHz, amplified by an AM-amplifier (AM-systems, Carlsborg, WA, USA) and sampled at 10 kHz.

2.5. Data analysis

In voltage-clamp recordings, the recruitment of principal neurons into propagating ictal events is marked by the transition from

the predominant inhibitory to the predominant excitatory phase (t_{IE}), which is calculated as described in Cammarota et al. (2013). Ictal event duration in voltage-clamp recordings is calculated from the t_{IE} to the end of the last afterdischarge recorded with an instant frequency higher than 0.1 Hz. Spectrogram of local field potential recording are performed with an algorithm written in Matlab using logarithmic wavelet windows. The Ca^{2+} signal is reported as $\Delta F/F_0$, where F_0 is the baseline fluorescence. Significant Ca^{2+} events are considered when exceeding three folds SD of baseline. Data analysis was performed with Clampfit 10 (Molecular Devices, Foster City, CA, USA), Origin 8.0 (Microcal Software), Leica Application Suite (Leica Microsystems, GmbH, Wetzlar, Germany), Microsoft Office and MATLAB 7.6.0 R2008A (Mathworks, Natick, MA, USA).

3. Results

3.1. Focal ictal discharges in rat temporal and entorhinal cortex

Whole-cell patch-clamp recordings from single or dual neurons and simultaneous Ca^{2+} imaging from different neuronal cells and glia in layer V of entorhinal or temporal cortex slices from young rats (PN 15-P19) can provide useful indications on the generation and spread of epileptic seizure-like discharge (SLD) at the level of both individual neurons and network provided that the site and the time of SLD initiation can be predicted. This is achievable in cortical slice preparations perfused with 4-AP (50–100 μM) and reduced Mg^{2+} (0.5 mM). After 10 min of slice perfusion, largely before spontaneous epileptiform activity could emerge, brief pressure pulses (4–10 psi; 300–600 ms) are applied to a NMDA containing glass pipette (NMDA: 1 mM; typical tip resistance, 2 MΩ), located in layer V in proximity to the rhinal fissure, 20–30 μm below the slice surface (Fig. 1A), every 4–5 min. Single NMDA pulses evoke only a transient (10–20 s) membrane depolarization and action potential firing in a current-clamped pyramidal neuron located at ~150 μm from the NMDA-pipette tip and simultaneous Ca^{2+} elevations in other neighboring neurons. With respect to single NMDA pulses, double NMDA pulses cause a larger membrane depolarization and a more intense firing in the patched neuron as well as Ca^{2+} elevations in a larger number of neurons. The direct neuronal response to double NMDA pulse defines a region of about 200 μm in radius, that we named focal area (gray circles in this and the other figures). Most importantly, the response to double NMDA pulses is followed by a SLD typically characterized by a tonic phase of sustained depolarization followed by a clonic phase of rhythmic bursting events, i.e., the afterdischarges, that according to the accompanied Ca^{2+} signal occur in the neuronal network with a high degree of synchrony (Fig. 1A). Notably, neurons located immediately outside the focal region (a corona between 200 and 300 μm from the NMDA-pipette tip that we termed peri-focal region), exhibit Ca^{2+} elevations (lower blue traces) that match those of neurons in the focal region (upper blue traces), with the only exception of the initial Ca^{2+} increase induced directly by NMDA (Fig. 1A–C). The Ca^{2+} elevation directly activated by NMDA in neurons located at the focus often hampers the possibility to identify from these neurons the timing for SLD onset (see upper Ca^{2+} traces in Fig. 1B and C) which can be more clearly and precisely evaluated from the response of neurons in the peri-focal region (Fig. 1A–C). After double NMDA pulses, SLDs are generated with a delay that marks the transition from a focal hyperexcitable network to a fully propagating epileptiform event. Depending on the strength of local circuit inhibition (see below), this delay can be as brief as a few seconds. In general, it corresponds to about 10 s (mean, 10 ± 1 s with respect to the first of the two NMDA pulses, range 5–18 s; $n = 127$ SLDs, 18 rats). A double NMDA pulse (3 s apart) successfully evokes an ictal discharge in 82% of the trials ($n = 162$ SLDs out of 198 trials, 18 rats). In contrast, a single NMDA pulse (Fig. 1A) is successful in only 15% of the trials ($n = 5$ SLDs out of 32 trials, 18 rats).

The SLD initiation can be studied by Ca^{2+} imaging from the focal and peri-focal regions while the lateral propagation of SLDs across layer V temporal cortex can be monitored by recording from a pyramidal neuron located in the propagating region, i.e., 800–1000 μm from the NMDA-pipette tip. As shown in Fig. 1C, NMDA-evoked SDLs propagated to the distant neuron with a mean delay of 21 ± 1 s ($n = 28$ SLDs from 11 experiments, 8 rats). In particular, SLD propagation was characterized by a series of hyperpolarizations that preceded the full recruitment of the distant pyramidal neuron (Trevelyan et al., 2006, 2007; Cammarota et al., 2013). Notably, the SLDs recorded in pyramidal neurons from the peri-focal or from the propagating region are undistinguishable from spontaneous events. These events are only occasionally observed in these experiments probably because eliciting multiple SLDs by repetitive NMDA applications prevents the occurrence of further spontaneous SLDs. Spontaneous events can reliably be observed to arise from unknown foci in specifically designed experiments in which NMDA stimuli were not applied.

The dynamics of NMDA-evoked SLDs can be also monitored by extracellular local field potentials (LFP) recorded through glass pipettes that can be differently positioned with respect to the focus. In LFP recordings, SLDs are characterized by initial high frequency, low voltage signals followed by large amplitude low frequency events that parallel the clonic phase of the afterdischarges. In Fig. 1E we report an example of two LFPs from peri-focal (LFP-1) and distant region (LFP-2) which illustrates the generation and the delayed propagation of SLDs. By outlining the typical pattern of epileptiform events commonly observed in different in vitro and in vivo models of epilepsy, LFP recordings further validate our experimental model of focal SLDs.

3.2. Focal seizure-like discharges in the mouse entorhinal and temporal cortex

Over the last two decades transgenic and gene targeting techniques combined with optogenetics resulted in a large number of genetically modified mouse strains that have been used to define the role of distinct neuronal populations in brain functions. Furthermore, these techniques have been proved to be extremely useful for improving our understanding of the pathological mechanisms at the basis of brain disorders including epilepsy. It is, therefore, important to further characterize our model of focal epilepsy in the mouse brain and extend it to other brain regions, such as the temporal cortex. We here reveal that in slices from the temporal cortex of young C57BL6J mice (PN 16-22), a single NMDA pulse applied in the presence of 4-AP and low extracellular Mg^{2+} (0.5 mM) is poorly successful in evoking a SLD (only 15% successes; 9 of 61 trials; 24 mice) with respect to double NMDA pulses (92% successes, 117 of 127 trials; 24 mice). Successive double NMDA pulses evoke SLDs with reproducible pattern and duration (Fig. 2A; mean duration in the entorhinal cortex, 77 ± 7 s, $n = 24$ SLDs from 10 experiments, 4 mice; mean duration in the temporal cortex, 69 ± 4 s, $n = 43$ SLDs from 6 experiments, 5 mice), provided that an interval of at least 4–5 min is used to allow the recovery from post-seizure refractory periods. Notably, the same NMDA-containing pipette which delivers NMDA can be used as an extracellular electrode to monitor at the focus the generation of evoked SLDs (see Section 2; Fig. 2A). NMDA-evoked SLDs propagate to distant pyramidal neurons after a series of hyperpolarizing events (Fig. 2A, insets). In voltage-clamp recordings at −50 mV, these events correspond to large outward inhibitory currents generated by GABAergic interneurons that delay the progression of SLDs (Trevelyan et al., 2006, 2007) (Fig. 2B). As we reported (Cammarota et al., 2013), the recruitment process occurs subsequently to the collapse of the

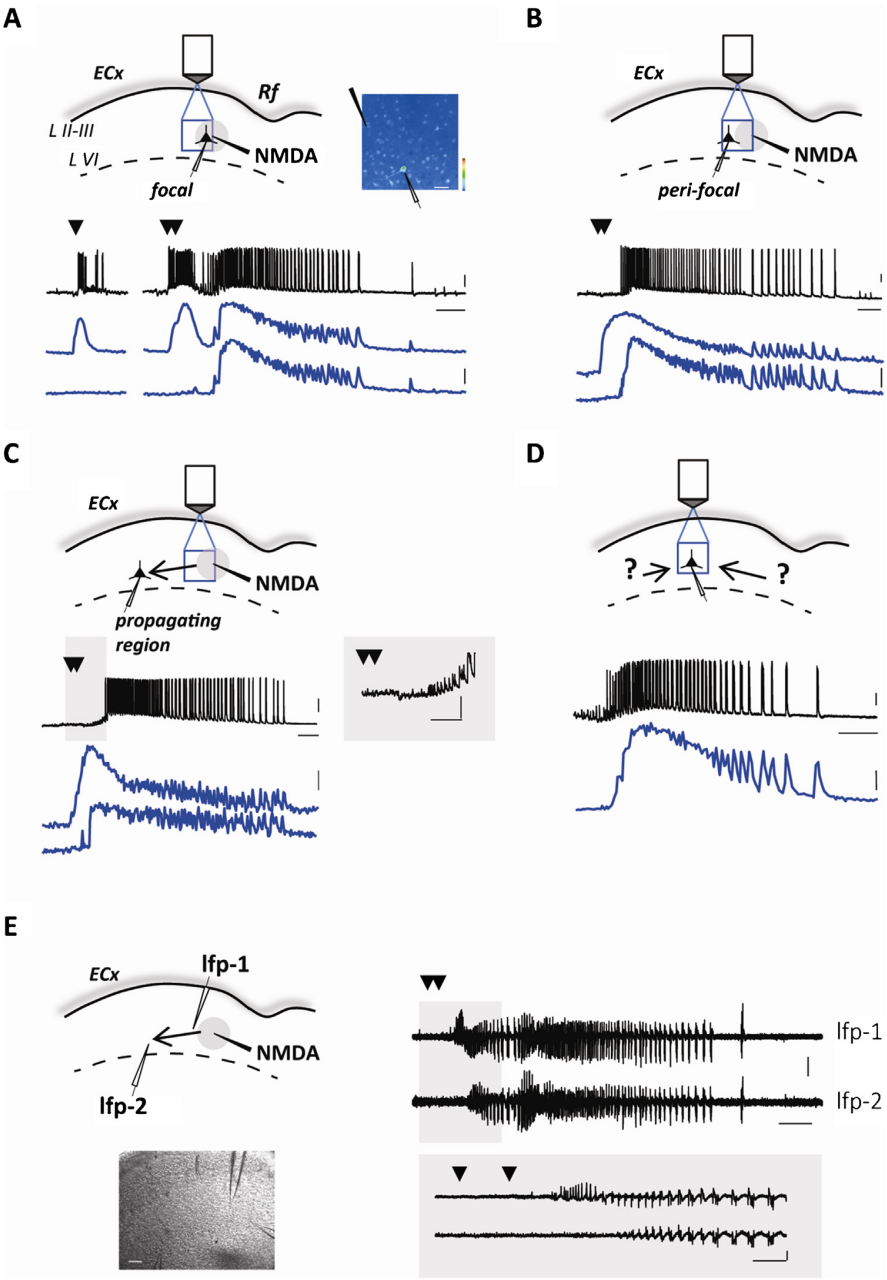

Fig. 1. Focally induced SLDs in entorhinal cortex slice preparations from young rats. (A–C). Upper panels, schematic of the experiments with the NMDA pipette (black), the focal area (gray circle), the patched pyramidal neuron and the area of Ca^{2+} imaging (blue square) in rat entorhinal cortex. Lower traces, membrane potential of the pyramidal neuron (black traces) and simultaneous average Ca^{2+} signal from 4 putative pyramidal neurons located in the focal (upper blue traces) and peri-focal (lower blue traces) area. In A, right panel reports the Oregon-Green BAPTA-1 fluorescence with indication of the NMDA and the patch pipette (black and white, respectively). (D) Schematic of the experiment with patch recording from a pyramidal neuron and simultaneous average Ca^{2+} signal from 3 putative pyramidal neurons located in the same region during a spontaneous SLD. Scale bars: 20 mV; 20% $\Delta F/F_0$; 10 s (5 s for inset in (C)). Black arrowheads in this and other figures mark the NMDA pulses. E. Left panel, schematic of the experiment with two electrodes for local field potential (lfp) recording, one in the peri-focal region (250 μm) and the other distant 550 μm form the NMDA-pipette tip, and DIC image (scale bar 100 μm) of the rat brain slice during the experiment. Right traces, LFP recordings during the evoked SLD. Scale bars, 0.1 mV; 10 s. (For interpretation of the references to color in this figure legend, the reader is referred to the web version of this article.)

feedforward inhibition and it is marked by both the transition from inhibition to excitation in the voltage-clamp recordings from pyramidal neurons and the intracellular Ca^{2+} elevations in these cells. Pyramidal neurons in the peri-focal region are recruited into the propagating SLD with a mean delay of 11 ± 1 s ($n = 33$ SLDs,) after the double NMDA pulse. At 1 mm from the NMDA-pipette this delay increases to 21 ± 1 s in the entorhinal cortex ($n = 24$ SLDs, 10 experiments, 4 mice) and 21 ± 2 s in the temporal cortex ($n = 12$ SLDs, 6 experiments, 4 mice). The use of dual patch-clamp recordings in the NMDA/4-AP model allows to study how the activity of a specific

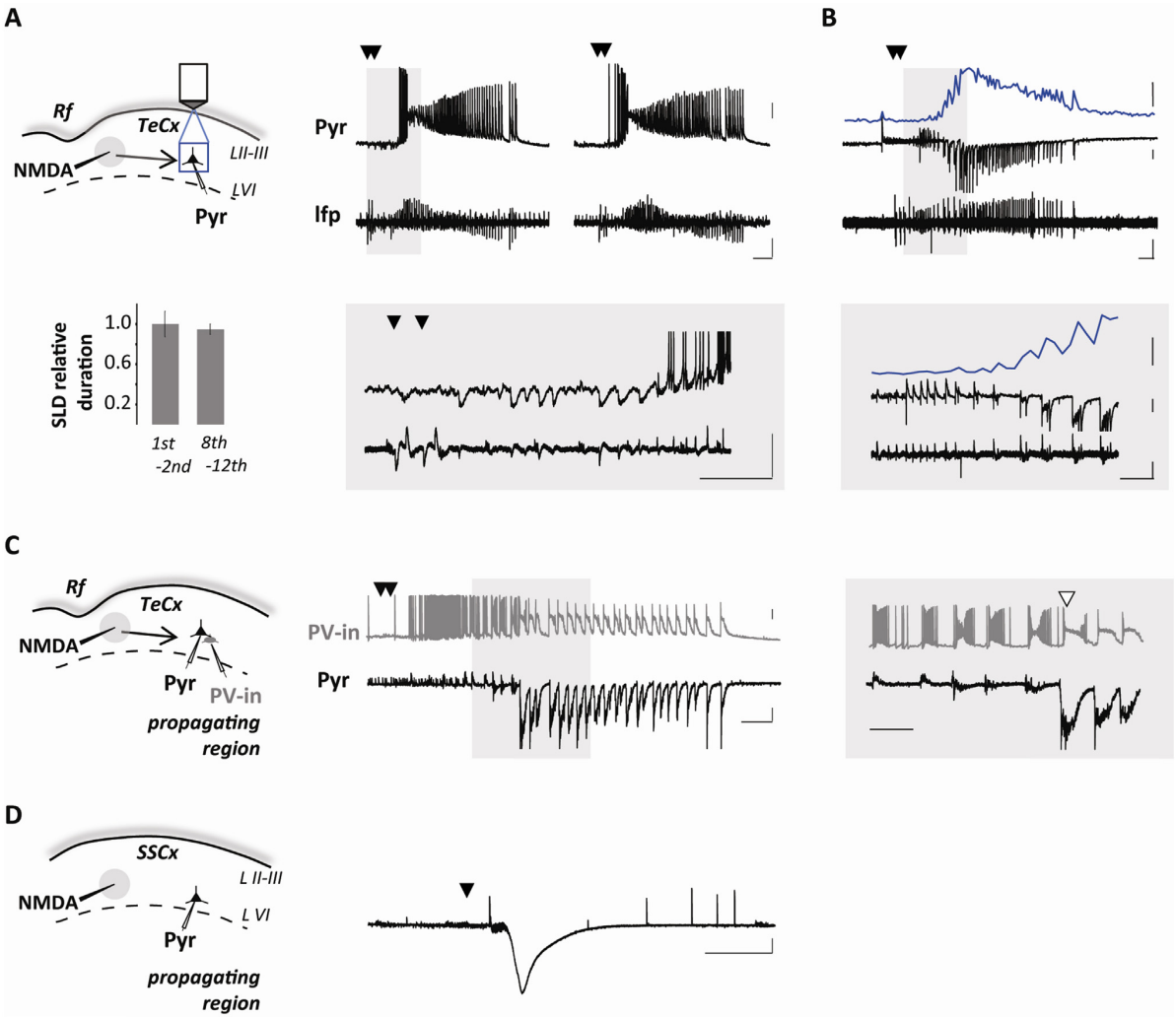

Fig. 2. Focally induced SLDs in temporal cortex slice preparations from young mice. (A, C and D) Left panels, schematic of the experiments in mouse temporal cortex (in somatosensory cortex for (D)) with the NMDA pipette (black), also used for lfp recording in A, the focal area (gray circle), the patched pyramidal neuron (and a Pv-interneuron, (C)) in the propagating region located 1000 μm from the focal area and the region of Ca^{2+} imaging (blue square). (A) Right traces, membrane potential of the pyramidal neuron and lfp recording during 2◦ and 8◦ evoked SLDs and histogram showing the relative duration of successive NMDA evoked SLDs (average of the 1st and 2nd event vs average of 8th to 12th events). (B) Whole-cell current of the pyramidal neuron (middle black trace, Vh = −50 mV), lfp recording (lower black trace) and average Ca^{2+} signal from 3 putative pyramidal neurons (blue traces) located in the same propagating region as in (A) Scale bars, 20 mV; 0.1 mV; 200 pA; 20% $\Delta F/F_0$; 10 s; for lower insets, 5 s. (C) Right traces, membrane potential of the PV-interneuron (PV-in; gray trace) and simultaneous whole-cell current of the pyramidal neuron (Vh −50 mV, black trace) in slice from a G42 mouse. White arrowhead in inset marks depolarization block in the PV-interneuron and full excitatory input in the pyramidal neuron. Scale bars, 20 mV, 200 pA, 5 s; for right inset 2 s. (D) Right trace, whole-cell current of the pyramidal neuron (Vh −50 mV) showing a cortical spreading depression like event. Scale bars, 500 pA, 2 min. (For interpretation of the references to color in this figure legend, the reader is referred to the web version of this article.)

interneuron class can affect SLD propagation. As an example, dual recordings from a parvalbumin-expressing GABAergic interneuron and a neighboring pyramidal neuron in slices from G42 mice show that inhibitory barrages preceding SLD in the pyramidal neuron are temporally correlated with the firing activity in the parvalbumin interneuron. These interneurons have been shown to represent a main source of feedforward inhibition and only after their firing discharge suddenly enter into a depolarization block are the neighboring pyramidal neurons fully recruited into the propagating SLD (Cammarota et al., 2013) (Fig. 2C).

In contrast to entorhinal and temporal cortex from rats, both entorhinal and temporal cortex from C57BL6J mice showed to be less prone to seizure generation. In particular, we found that 20% ($n = 3$ out of 15 slices; 10 animals) and 27% of mouse brain slices (15 out of 55 slices; 28 animals) were completely refractory to seizure generation in entorhinal and temporal cortex, respectively, with respect to only 8% of rat ($n = 15$ out of 199 slices; entorhinal and temporal cortices pooled data; 110 animals).

The somatosensory cortex (SCx) from C57BL6J mouse appears fully refractory to NMDA-induced SDLs. In SCx slices obtained from PN16-18 mice, upon recordings from layer V pyramidal neurons (5 experiments, 3 animals) we failed to observe focal SLDs after performing 30 double NMDA pulse stimulations. Following 4 of these trials we observed instead a prolonged and sustained depolarization in the pyramidal neurons that closely resembles a typical cortical spreading depression (CSD) (Fig. 2D).

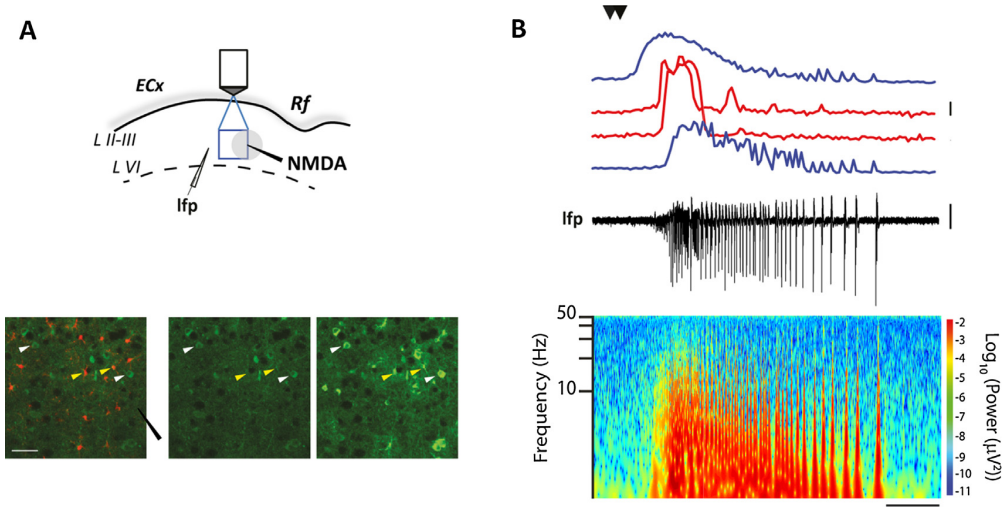

Fig. 3. Astrocyte and neuron activity during SLD generation. Left panel, schematic of the experiment in a mouse entorhinal cortex slice with the NMDA pipette (black), the focal area (gray circle), the LFP electrode positioned 300 μm from the NMDA pipette and the area of Ca^{2+} imaging (focal and peri-focal region, blue square). Left lower panels, images of the GCaMP3 and SR-101 fluorescence (green and red, respectively) at basal (left and middle panels) and during the NMDA-evoked SLD (right panel). Scale bar, 50 μm. Right, simultaneous lfp recording (black trace) and Ca^{2+} signal from neurons in the focal (upper blue trace) and perifocal area (lower blue trace) and from astrocytes from the focal region (red traces). Lower panel, spectrogram of the recorded lfp. Scale bars, 0.01 mV, 50% $\Delta F/F_0$; 10 s. (For interpretation of the references to color in this figure legend, the reader is referred to the web version of this article.)

3.3. Cellular players during focal ictal discharge generation: Neurons and astrocytes

Knowing where a SLD will be generated provides the unique opportunity to study the abnormal activity that at the level of local circuits precedes SLD generation. To this aim, Ca^{2+} imaging from different neurons and glia can provide important information on network activities at the focus. As an explicative example, we illustrate in Fig. 3 the use of GCaMP3, a genetically encoded calcium indicator (GECI) (Tian et al., 2009). Although GECI can be selectively expressed in specific cell populations with the Cre recombinase system, due to an unspecific Cre recombinase expression in this mouse line, GCaMP3 results to be present in a number of interneurons, pyramidal neurons and astrocytes (see Section 2, Fig. 3A). In Fig. 3B, a typical NMDA-evoked SLD from the entorhinal cortex of these mice is reported by simultaneous LFP and Ca^{2+} signal recordings from different cell types. The spectrogram shows the typical pattern of an epileptiform event with rhythmic activity in the beta-gamma frequencies. Astrocytes, that are selectively marked with sulforhodamine 101, show large Ca^{2+} transients that differ substantially from neuronal ones. In the focal region, a group of astrocytes exhibit large amplitude Ca^{2+} elevations (red traces) immediately after the direct activation of neurons by NMDA (upper blue trace) and before the SLD initiation that is revealed from the Ca^{2+} signal changes in the peri-focal neurons (lower blue trace). As we previously reported (Gomez-Gonzalo et al., 2010), these early activated astrocytes contribute to lower the threshold of NMDA-evoked SLDs probably through the release of gliotransmitters promoting neuronal synchrony.

4. Discussion

We here describe an experimental model of focal epileptiform activity in cortical slices from young rats and mice. In this model, a focal SLD is generated after a transition phase that follows an episode of intense activity induced in a group of layer V neurons by a local NMDA application in the presence of 4-AP and low Mg^{2+}. With the use of different combinations of single-dual cell patch-clamp recordings with local field potential and Ca^{2+} imaging techniques, we here extend to the temporal cortex of rats and mice the model that was originally developed in the rat entorhinal cortex.

Although a different susceptibility to epileptiform activity is observed in rats and mice, with slices obtained from mice being less prone to SLD generation with respect to slices from rats, both species can be used with this model that represents a powerful tool to study with high accuracy the spatial and temporal features of seizure generation and propagation. Indeed, as we already described in the rat entorhinal cortex (Gomez-Gonzalo et al., 2010; Losi et al., 2010), also in mouse entorhinal and temporal cortex multiple SLDs can be evoked by repetitive NMDA challenges and the evoked SLDs exhibit similar pattern and duration. As discussed below, the use of mice has the great advantage, with respect to rats, to exploit different transgenic lines for identification and selective stimulation of specific cell populations.

We also show that as opposed to entorhinal and temporal cortex, NMDA local applications in a different cortical area, such as the somatosensory cortex, fail to induce SLDs, and occasionally evoke cortical spreading depression-like events.

The NMDA/4-AP model can be used to gain insights into the cellular events at the basis of SLD generation and propagation. We can study how the activity of specific cell populations, from either the focus or the propagating region, evolves during the different phases of a SLD, including the transition phase, the development of tonic/clonic discharges and the cessation. Because multiple SLDs initiating from the same focal site can be induced, we can also analyze whether and how these distinct activities can eventually change upon the recurrent impact of the successive SLDs. Furthermore, using optogenetic tools, a specific class of neurons or interneurons can be selectively activated or inhibited by non-invasive light pulses delivered to a spatially defined location, i.e., the focus or the propagating region, and at a precise time, i.e., before or during the different SLD phases. For example, we can modify the response of the neural network to NMDA, possibly lowering or increasing the threshold of SLD generation. Changes in SLD threshold can be, indeed, evaluated in the model given that two successive NMDA pulses, as opposed to a single NMDA pulse at the same intensity and duration, are needed to successfully evoke a SLD. In the model, single and double NMDA

pulses can represent, therefore, sub- and supra-threshold stimuli, respectively, which can be used to study different conditions or drug treatments that favor or oppose SLD generation. It is note worth that the threshold of SLD generation appears to slightly decrease along with prolonged 4-AP perfusion. This should be taken into account in studies aimed to evaluate the conditions that eventually favor SLD generation. One obvious way to overcome this caveat is to perform as control two sub-threshold NMDA stimulations, one before and the other *after* the experimental conditions that lower SLD threshold. Using this model, we could reveal that activation of astrocytes at the focus favors SLD generation by lowering SLD threshold, while the inhibition of Ca^{2+} elevations in these cells increases SLD threshold (Gomez-Gonzalo et al., 2010). Recently, using the NMDA/4-AP model we could reveal a functional dichotomy of Parvalbumin-positive (Pv) inhibitory interneurons in epileptiform activity. We found that an optogenetic activation at the focus of Pv interneuron expressing the light-gated cation channel channelrhodopsin-2 (Zhang et al., 2010) enhances the generation of SLDs, while a similar activation restricted to Pv interneurons distant from the focus blocked SLD propagation (Sessolo, Marcon et al., J Neurosci, in press).

An important advance in optogenetic techniques is the use of patterned illumination through light phase modulation that allows the selective activation/inhibition of a few cells as opposed to classical illumination methods (Dal Maschio et al., 2010; Bovetti and Fellin, 2015). In the NMDA/4-AP model this approach would allow to functionally test, for instance, whether activation or inhibition of a defined number of cells in the focal region is sufficient to favor or oppose SLD generation.

In conclusion, as we move forward in our attempts to understand the mechanism(s) of epilepsy, it is important to identify models of focal epileptiform activity in vitro and in vivo that combined with modern optogenetics (Zhang et al., 2010; Tye and Deisseroth, 2012; Kokaia et al., 2013; Packer et al., 2013) and GECI have the potential to provide fundamental insights into the different role played by specific cell populations in seizure generation, propagation and cessation.

Acknowledgements

We thank Alberto Bacci for the gift of G42 mice. The original work described in this manuscript was supported by Telethon, Italy, grants GGP10138 and GGP12265; Consiglio Nazionale delle Ricerche, Italy, Aging Project; Cariparo Foundation, Italy; Ministero dell'Istruzione Università e Ricerca, Italy, FIRB project RBAP11X42L.

References

Avoli M, Barbarosie M, Lucke A, Nagao T, Lopantsev V, Kohling R. Synchronous GABA-mediated potentials and epileptiform discharges in the rat limbic system in vitro. J Neurosci 1996;16:3912–24.

Avoli M, D'Antuono M, Louvel J, Kohling R, Biagini G, Pumain R, et al. Network and pharmacological mechanisms leading to epileptiform synchronization in the limbic system in vitro. Prog Neurobiol 2002;68:167–207.

Bear J, Lothman EW. An in vitro study of focal epileptogenesis in combined hippocampal-parahippocampal slices. Epilepsy Res 1993;14(3):183–93.

Bovetti S, Fellin T. Optical dissection of brain circuits with patterned illumination through the phase modulation of light. J Neurosci Methods 2015;241:66–77.

Cammarota M, Losi G, Chiavegato A, Zonta M, Carmignoto G. Fast spiking interneuron control of seizure propagation in a cortical slice model of focal epilepsy. J Physiol 2013;591:807–22.

Chattopadhyaya B, Di Cristo G, Higashiyama H, Knott GW, Kuhlman SJ, Welker E, et al. Experience and activity-dependent maturation of perisomatic GABAergic innervation in primary visual cortex during a postnatal critical period. J Neurosci 2004;24:9598–611.

Curia G, Longo D, Biagini G, Jones RS, Avoli M. The pilocarpine model of temporal lobe epilepsy. J Neurosci Methods 2008;172:143–57.

Dal Maschio M, Difato F, Beltramo R, Blau A, Benfenati F, Fellin T. Simultaneous two-photon imaging and photo-stimulation with structured light illumination. Opt Express 2010;18:18720–31.

Dugue GP, Dumoulin A, Triller A, Dieudonne S. Target-dependent use of co-released inhibitory transmitters at central synapses. J Neurosci 2005;25:6490–8.

Gomez-Gonzalo M, Losi G, Chiavegato A, Zonta M, Cammarota M, Brondi M, et al. An excitatory loop with astrocytes contributes to drive neurons to seizure threshold. PLoS Biol 2010;8:e1000352.

Jefferys JG. Nonsynaptic modulation of neuronal activity in the brain: electric currents and extracellular ions. Physiol Rev 1995;75:689–723.

Jefferys JG, Haas HL. Synchronized bursting of CA1 hippocampal pyramidal cells in the absence of synaptic transmission. Nature 1982;300:448–50.

Kandratavicius L, Balista PA, Lopes-Aguiar C, Ruggiero RN, Umeoka EH, Garcia-Cairasco N, et al. Animal models of epilepsy: use and limitations. Neuropsychiatric Dis Treat 2014;10:1693–705.

Kokaia M, Andersson M, Ledri M. An optogenetic approach in epilepsy. Neuropharmacology 2013;69:89–95.

Levesque M, Avoli M. The kainic acid model of temporal lobe epilepsy. Neurosci Biobehav Rev 2013;37:2887–99.

Losi G, Cammarota M, Chiavegato A, Gomez-Gonzalo M, Carmignoto G. A new experimental model of focal seizures in the entorhinal cortex. Epilepsia 2010;51:1493–502.

Mihaly A, Bencsik K, Solymosi T. Naltrexone potentiates 4-aminopyridine seizures in the rat. J Neural Transm Gen Sect 1990;79:59–67.

Packer AM, Roska B, Hausser M. Targeting neurons and photons for optogenetics. Nat Neurosci 2013;16:805–15.

Perreault P, Avoli M. Physiology and pharmacology of epileptiform activity induced by 4-aminopyridine in rat hippocampal slices. J Neurophysiol 1991;65:771–85.

Perreault P, Avoli M. 4-aminopyridine-induced epileptiform activity and a GABA-mediated long-lasting depolarization in the rat hippocampus. J Neurosci 1992;12:104–15.

Pinto DJ, Patrick SL, Huang WC, Connors BW. Initiation, propagation, and termination of epileptiform activity in rodent neocortex in vitro involve distinct mechanisms. J Neurosci 2005;25:8131–40.

Pitkänen A, Schwartzkroin PA, Moshé SL. Models of seizures and epilepsy. Amsterdam: Elsevier; 2006.

Tian L, Hires SA, Mao T, Huber D, Chiappe ME, Chalasani SH, et al. Imaging neural activity in worms, flies and mice with improved GCaMP calcium indicators. Nat Methods 2009;6:875–81.

Trevelyan AJ, Sussillo D, Watson BO, Yuste R. Modular propagation of epileptiform activity: evidence for an inhibitory veto in neocortex. J Neurosci 2006;26:12447–55.

Trevelyan AJ, Sussillo D, Yuste R. Feedforward inhibition contributes to the control of epileptiform propagation speed. J Neurosci 2007;27:3383–7.

Tye KM, Deisseroth K. Optogenetic investigation of neural circuits underlying brain disease in animal models. Nat Rev Neurosci 2012;13:251–66.

Uva L, Avoli M, de Curtis M. Synchronous $GABA_A$-receptor-dependent potentials in limbic areas of the *in-vitro* isolated adult guinea pig brain. Eur J Neurosci 2009;29:911–20.

Voskuyl RA, Albus H. Spontaneous epileptiform discharges in hippocampal slices induced by 4-aminopyridine. Brain Res 1985;342:54–66.

Zhang F, Gradinaru V, Adamantidis AR, Durand R, Airan RD, de Lecea L, et al. Optogenetic interrogation of neural circuits: technology for probing mammalian brain structures. Nat Protoc 2010;5:439–56.

Ziburkus J, Cressman JR, Barreto E, Schiff SJ. Interneuron and pyramidal cell interplay during in vitro seizure-like events. J Neurophysiol 2006;95:3948–54.

Systems/Circuits

Parvalbumin-Positive Inhibitory Interneurons Oppose Propagation But Favor Generation of Focal Epileptiform Activity

Michele Sessolo,[1]* Iacopo Marcon,[1]* Serena Bovetti,[2] Gabriele Losi,[1] Mario Cammarota,[1] Gian Michele Ratto,[3] Tommaso Fellin,[2] and Giorgio Carmignoto[1]

[1]Neuroscience Institute, National Research Council and Department of Biomedical Sciences, University of Padova, 35121 Padova, Italy, [2]Department of Neuroscience and Brain Technologies, Istituto Italiano di Tecnologia, 16163 Genova, Italy, and [3]NEST, Istituto Nanoscienze-National Research Council, 56127 Pisa, Italy

Parvalbumin (Pv)-positive inhibitory interneurons effectively control network excitability, and their optogenetic activation has been reported to block epileptic seizures. An intense activity in GABAergic interneurons, including Pv interneurons, before seizures has been described in different experimental models of epilepsy, raising the hypothesis that an increased GABAergic inhibitory signal may, under certain conditions, initiate seizures. It is therefore unclear whether the activity of Pv interneurons enhances or opposes epileptiform activities. Here we use a mouse cortical slice model of focal epilepsy in which the epileptogenic focus can be identified and the role of Pv interneurons in the generation and propagation of seizure-like ictal events is accurately analyzed by a combination of optogenetic, electrophysiological, and imaging techniques. We found that a selective activation of Pv interneurons at the focus failed to block ictal generation and induced postinhibitory rebound spiking in pyramidal neurons, enhancing neuronal synchrony and promoting ictal generation. In contrast, a selective activation of Pv interneurons distant from the focus blocked ictal propagation and shortened ictal duration at the focus. We revealed that the reduced ictal duration was a direct consequence of the ictal propagation block, probably by preventing newly generated afterdischarges to travel backwards to the original focus of ictal initiation. Similar results were obtained upon individual Pv interneuron activation by intracellular depolarizing current pulses. The functional dichotomy of Pv interneurons here described opens new perspectives to our understanding of how local inhibitory circuits govern generation and spread of focal epileptiform activities.

Key words: **channelrhodopsin-2; cortex; epileptiform activity; optogenetics; parvalbumin; rebound spiking**

Introduction

Within the brain, inhibitory signals that originate from different GABAergic interneurons play fundamental roles in establishing proper operation of neural circuits (Markram et al., 2004; Monyer and Markram, 2004; Kepecs and Fishell, 2014). GABA-mediated inhibition shapes the response of principal neurons to synaptic inputs, controls local circuit excitability, and generates network oscillations by synchronizing the firing in large neuronal ensembles (Bartos et al., 2007; Buzsáki and Wang, 2012). GABAergic interneurons are also involved in the pathophysiology of brain disorders, including epilepsy, where they may, under certain conditions, favor seizure initiation (Avoli and de Curtis, 2011; Jiruska et al., 2013). However, GABA antagonists are ictogenic (Gutnick et al., 1982; Miles and Wong, 1983; Connors, 1984), and inhibition is commonly thought to counteract seizures. Indeed, GABAergic interneurons, and in particular parvalbumin (Pv)-expressing interneurons, can generate a feedforward inhibition that opposes seizure spread in both experimental models (Trevelyan et al., 2006; Cammarota et al., 2013) and patients (Schevon et al., 2012). Moreover, whereas studies in brain slices suggest that optogenetic activation of GABAergic interneurons can enhance epileptiform activity (Shiri et al., 2014; Yekhlef et al., 2014), optogenetic *in vivo* studies reveal that Pv interneuron activation interrupts spontaneous ongoing seizures (Krook-Magnuson et al., 2013; Paz et al., 2013). Optogenetics was thus proposed as a promising approach for those epilepsies, such as temporal lobe epilepsy, that have typical activity arising from restricted epileptogenic sites. Increasing inhibition at this site by Pv interneuron optogenetic

Received Dec. 16, 2014; revised Jan. 29, 2015; accepted Feb. 22, 2015.

Author contributions: M.S., I.M., G.L., T.F., and G.C. designed research; M.S., I.M., S.B., G.L., and M.C. performed research; M.S., I.M., G.L., M.C., and G.M.R. analyzed data; T.F. and G.C. wrote the paper.

This work was supported by Telethon Italy Grant GGP10138/GGP12265, Cariparo Foundation, National Research Council Aging Project, and Fondo per gli Investimenti della Ricerca di Base Grant RBAP11X42L to G.C. and San Paolo Programma in Neuroscienze, Ministero dell'Istruzione, dell'Università e della Ricerca Fondo per Gli Investimenti Della Ricerca di Base Grant RBAP11X42L, Telethon-Italy Grant GGP10138, and a FP7 DESIRE project to T.F. We thank Alberto Bacci for critical reading of a previous version of the manuscript; and Karl Deisseroth for AAV2/1.EF1.dflox.hChR2(H134R)-mCherry.WPRE.hGH.

The authors declare no competing financial interests.

*M.S. and I.M. contributed equally to this work.

Correspondence should be addressed to either of the following: Dr. Giorgio Carmignoto, Neuroscience Institute, National Research Council and Department of Biomedical Sciences, University of Padova, via U.Bassi 58/b, 35121 Padova, Italy, E-mail: giorgio.carmignoto@bio.unipd.it; or Dr. Tommaso Fellin, Department of Neuroscience and Brain Technologies, Istituto Italiano di Tecnologia, via Morego 30, 16163 Genova, Italy. E-mail: Tommaso.Fellin@iit.it.

DOI:10.1523/JNEUROSCI.5117-14.2015

 0270-6474/15/359544-14$15.00/0

activation may be technically feasible and represent a potential alternative to resective surgery commonly used in untreatable temporal lobe epilepsy forms. Most importantly, it has the potential not only to interrupt ongoing seizures, but also to suppress the abnormal activity that precedes seizures preventing seizure generation. To test this hypothesis, light has to be delivered at the epileptogenic focus. However, the unpredictable nature of focal seizures renders the identification of the epileptogenic focus in the intact brain a daunting challenge. We thus used a focal epilepsy model in temporal cortex (TCx) slices (Losi et al., 2010) that gives the unique opportunity to identify the precise site of seizure initiation and to generate an epileptic event at any given time. The hallmark of this *in vitro* model is that it allows precisely controlled experiments that cannot be accomplished in currently available *in vivo* models, where the seizure initiation site is not identifiable in advance. The fact that in our model we know where and when the seizure will be generated allowed us to investigate whether and how Pv interneurons differentially control initiation and propagation of focal epileptiform activities. We addressed two main questions that will clarify the role of these cells in epileptiform activities. First, does Pv interneuron activation suppress the ictogenic activity that, at the epileptogenic focus, contributes to ictal event generation? Second, does Pv interneuron activation out of the focus (i.e., the ictal propagating region) oppose ictal event spread? To answer these questions, we combined single/dual cell patch-clamp and local field potential recordings with optogenetics and Ca^{2+} imaging in cortical slice preparations.

Materials and Methods

Animals. All experiments involving animals were performed in strict accordance with the guidelines established by the European Communities Council Directive and approved by the National Council on Animal Care of the Italian Ministry of Health. The PV-IRES-Cre (parvalbumin internal ribosomal entry site (IRES) Cre-recombinase) mouse strain (B6; 129P2-*Pvalb*$^{tm1(cre)Arbr/J}$, id #017320) was purchased from The Jackson Laboratory. The G42 mouse strain (Chattopadhyaya et al., 2004) was donated by Alberto Bacci (ICM- Institut du Cerveau et de la Moelle épinière, Paris, France). Control slices were obtained from littermates mice of the corresponding mouse strain.

Viral injections. Stereotaxic injections were performed on postnatal day 0–2 (P0-P2) PV-IRES-Cre mice. Pups were deeply anesthetized by hypothermia and placed on a custom neonatal stereotaxic apparatus maintained at 4°C during surgery; 100–200 nl of AAV2/1.EF1.dflox.hChR2(H134R)-mCherry.WPRE.hGH (Addgene 20297) or AAV1.EF1a.DIO.hChR2(H134R)-eYFP.WPRE.hGH (Addgene 20298, University of Pennsylvania Viral Vector Core) was injected at stereotaxic coordinates of 0.85 mm anterior from the λsuture, 2.5 mm lateral from midline, and 0.15 mm depth, by means of a glass micropipette. After injections, the skin was sutured and pups were revitalized under a heat lamp and returned to the dam.

Slice preparations and Ca^{2+} dye loading. Coronal slices were prepared from G42 mice, and Pv-Cre mice of either sex injected with saline solution or with AAV between postnatal day 15 and 23. Briefly, mice were deeply anesthetized with intraperitoneal injected Zoletil (40 mg/kg) and decapitated; the brain was quickly removed and transferred to ice-cold standard ACSF, sACSF (in mM as follows: 125 NaCl, 2.5 KCl, 2 $CaCl_2$, 1 $MgCl_2$, 25 glucose, pH 7.4, with 5% CO_2/95% O_2). After brain dissection on the coronal plane, 350-μm-thick slices were cut with a vibratome (VT1000S, Leica Microsystems) in the solution described previously (Dugué et al., 2005). Slices were transferred for 1 min in a 95% O_2 and 5% CO_2 saturated solution containing (in mM) the following: 225 D-mannitol, 2.5 KCl, 1.25 NaH_2PO_4, 26 $NaHCO_3$, 25 glucose, 0.8 $CaCl_2$, 8 $MgCl_2$, 2 kynurenic acid with 5% CO_2/95% O_2. Slices were finally transferred in sACSF at 30°C for 20 min and then maintained at room temperature.

Slice loading with the fluorescence Ca^{2+} indicator Rhod-2 AM (10 μM; Invitrogen) was performed for 50–60 min at 30°C. Although Rhod-2 is known to accumulate in mitochondria (Kovács et al., 2005), with this loading protocol, it was highly present in the cytosol. Dye loading was performed in the sACSF solution containing sulfinpyrazone (200 μM, Sigma-Aldrich), pluronic (0.12%, Sigma-Aldrich), and kynurenic acid (1 mM, Sigma-Aldrich). After loading, slices were recovered and kept at room temperature.

Ca^{2+} imaging. Images were acquired with a single-photon upright laser-scanning microscope (TCS-SP5-RS, Leica Microsystems) with an acquisition time frame from 351 to 491 ms (five to seven line averaging). Rhod-2 AM was excited at 543 nm. The microscope was also equipped with a CCD camera for differential interference contrast image acquisition.

Electrophysiology and induction of focal ictal discharges. Brain slices were continuously perfused in a submerged chamber (Warner Instruments) at a rate of 3–4 ml/min with (in mM) the following: 120 NaCl, 3.2 KCl, 1 KH_2PO_4, 26 $NaHCO_3$, 0.5 $MgCl_2$, 2 $CaCl_2$, 10 glucose, pH 7.4 (with 5% CO_2/95% O_2). Single- and dual-cell recordings were performed in current-clamp and voltage-clamp configuration using a multiclamp-700B amplifier (Molecular Devices). Signals were filtered at 1 kHz and sampled at 10 kHz with a Digidata 1440s interface and pClamp10 software (Molecular Devices). Typical pipette resistance was 3–4 MΩ. Access resistance was monitored throughout the recordings and was typically <25 MΩ. Whole-cell intracellular pipette solution was (in mM) as follows: 145 K-gluconate, 2 $MgCl_2$, 0.5 EGTA, 2 Na_2ATP, 0.2 Na_2GTP, 10 HEPES, pH 7.2, with KOH, osmolarity, 305–315 mOsm (calculated liquid junction potential: −14 mV). Data were not corrected for the liquid junction potential.

Pyramidal cells were identified on the basis of their distinct morphology characterized by the triangular shape of the soma, a main apical dendrite pointing toward the pia and the absence of a main dendrite in the opposite direction. Their biophysical identity was confirmed by their response to hyperpolarizing and depolarizing 750 ms current steps. In particular, regular spiking pyramidal neurons showed a firing discharge with no spike amplitude accommodation (except for the second action potential in some cells), small afterhyperpolarization, and low steady-state frequency (15–23 Hz with 200 pA current injection). ChR2-positive Pv-fast spiking (FS) cells were identified by fluorescence and their biophysical identity was confirmed by high steady-state firing frequency (50 – 90 Hz with 400 pA current injection), no spike amplitude accommodation or frequency adaptation and large afterhyperpolarization. The following parameters were measured to characterize passive membrane properties: resting membrane potential (V_{rest}) was recorded immediately after the rupture of the neuronal membrane; input resistance (R_{in}) was determined by measuring the voltage change in response to a small hyperpolarizing and depolarizing current pulses (±50 pA, 750 ms) at resting potential.

All patched neurons were from cortical layer V-VI. All pyramidal neurons were voltage-clamped at −50 mV. In Pv-FS interneurons, we performed whole-cell current-clamp recordings at resting potential or juxtasomal recordings without rupture of the membrane patch using pipettes filled with the bath perfusing solution. Ictal event induction experiments were performed in the presence of 4-aminopyridine (4-AP, 50–100 μM) and bath temperature was maintained at 30–32°C by an inline solution heater and temperature controller (TC-324B, Warner Instruments). A pressure ejection unit (PDES, NPI Electronics) was used to apply a single or double pulse to NMDA (1 mM, Sigma-Aldrich)-containing pipettes with a 3 s interval, a pressure of 4–10 psi, and a duration of 200–600 ms. The NMDA pipette was positioned in vicinity of the rhinal fissure. The epileptogenic focus is defined as the region up to 300 μm from the pipette tip where neurons are directly activated by NMDA (Gómez-Gonzalo et al., 2010), whereas the ictal propagating region is the region distant at least 400 μm from the NMDA pipette tip. In most experiments, the NMDA glass pipette included an $AgCl_2$ electrode for extracellular local field potential recordings. Field potential signals were filtered at 1 kHz, amplified by an AM-amplifier (AM Systems), and sampled at 10 kHz.

Optical stimulation. Photostimulation was performed with a 473 nm continuous wave, solid-state laser source (Cobolt). The laser was directly

controlled by a command voltage with a TTL signal. Light was delivered to brain slices via an optical fiber (ThorLabs) with 50 or 300 μm diameter positioned close to the surface of the slice. Blue light intensity was adjusted with neutral density filters (ThorLabs) to obtain a power between 1 and 3 mW (measured at the fiber tip). The photostimulated area for the 300 μm and for the 50 μm diameter fiber positioned at ~300 μm from the slice surface was evaluated to be ~0.9 mm^2 and 0.048 mm^2, respectively.

Data analysis. Data analysis was performed with Clampfit 10, Origin 8.0 (Microcal Software), Microsoft Office and MATLAB 7.6.0 R2008A (MathWorks).

Ictal events analysis. In voltage-clamp recordings, the recruitment of principal neurons into propagating ictal events was marked by the transition from the predominant inhibitory to the predominant excitatory phase (t_{IE}), which is defined as the timing in which the ratio between the inhibition and the excitation index is for the first time <0.1. Inhibition and excitation indices were calculated, respectively, as the part of the positive and the negative component of the time derivative of the trace that exceeded 5× the mean standard deviation (SD) evaluated during the baseline (Cammarota et al., 2013). Ictal event duration in voltage-clamp recordings was calculated from the t_{IE} to the end of the last afterdischarge (see Afterdischarge analysis, below) recorded with an instant frequency >0.1 Hz.

Local field potential recordings were filtered with low-pass Gaussian filter. The ictal discharge onset at the focus was considered as the first detectable event in the field potential recordings larger than 4× the mean SD. The end of the ictal discharge at the focus was determined as the last epileptic event detectable in the field potential recordings. Action potentials in juxtasomal recordings from Pv interneurons were identified as spikes in voltage-clamp at 0 mV that exceeded 5× the mean SD evaluated during the baseline.

Afterdischarge analysis. The afterdischarges typically characterize the clonic activity that follows the tonic phase of long-lasting ictal events and were identified in voltage-clamp recordings as large excitatory bursts of <3 s duration. Afterdischarge onsets were set by the amplitude of the event that exceeded 3× the mean SD evaluated during the baseline. To evaluate the delay between excitatory bursts in voltage-clamp recordings from two pyramidal neurons located at different distances from the epileptogenic focus, we calculated the cross-correlation between the time derivative of both signals, in time bins of 1000 ms separated by 30 ms. We finally represented the pseudo-colors plot of the cross-correlation. We measured the lag corresponding to the maximal value of the cross-correlation before and after the change in direction of the afterdischarge.

Synchrony of pyramidal neurons. Spikes were recorded in current-clamp mode and the spike timing was obtained by thresholding the traces in Clampfit. Files holding the spike timing were analyzed by custom software to compute the nearest neighbor (NN) distance of each spike. The distance was always computed from the spikes recorded in the cell that had a lower frequency of firing. A simulated spike train was obtained by randomly placing spikes on a 2 s time window respecting the basic statistics of the original data: the randomized data had the same spike density and similar distribution of distance from the preceding spike. The simulation of the experiments that included optogenetic activation included a refractory window, determined for each simulated cell, in which spike density was zero.

Ca^{2+} imaging experiments. The Ca^{2+} signal is reported as $\Delta F/F_0$, where F_0 is the baseline fluorescence. Significant Ca^{2+} events were considered when exceeding 3× SD of baseline. No background subtraction or other manipulations were applied to digitized Ca^{2+} signal images that are reported as raw data. Ca^{2+} signals from neurons were obtained using Leica Applicaction Suite (Leica Microsystems).

Statistical analysis. Data are shown as mean ± SEM. Quantitative results were analyzed using *t* test and paired *t* test setting the statistical significance at $p < 0.05$. Wilcoxon signed-rank test was used to evaluate the statistical significance of the firing rate change in pyramidal neurons (see Fig. 5). Cumulative probability distributions of Figure 6 were compared using Kolmogorov–Smirnov test.

Tissue processing and immunohistochemical procedures. Postnatal day 21 (P21) mice were deeply anesthetized with an intraperitoneal injection of Zoletil (40 mg/kg) and perfused transcardially with 0.9% saline, followed by 4% PFA in 0.1 M phosphate buffer (PB), pH 7.4. Brains were removed from the skull, postfixed for 6 h in the same solution, cryoprotected in a 30% sucrose solution in 0.1 M PB, pH 7.4, frozen, and cryostat sectioned (Leica Microsystems). Free-floating coronal serial sections (30 μm) were collected in multiwell dishes. For immunofluorescence, sections were incubated overnight at 4°C in primary antibody diluted in 0.01 M PBS, pH 7.4, 0.5% Triton X-100, and 1% normal serum of the same species of the secondary antibody, and then incubated for 1 h at room temperature in the appropriate secondary antibody. Sections were mounted and coverslipped with a DABCO [1,4-diazobicyclo-(2,2,2)octane]-based antifade mounting medium. The following primary antibodies were used: anti-GABA (1:1000 rabbit, Sigma, A2052) and anti-paravalbumin (PV) (1:1000; mouse; Sigma, P3088). Secondary antibodies were as follows: goat anti-rabbit Alexa-488 (1:800, Invitrogen, A11034) and goat anti-mouse Alexa-488 (1:800, Invitrogen, A11029).

Confocal single image and *z*-stacks (1 μm optical steps) were acquired with a Leica SP5 inverted confocal microscope (Leica Microsystems). The percentage of mCherry-positive cells in temporal cortex (3 slices for each animal, range −2.92 to −4.04 mm from bregma) expressing either GABA or paravalbumin was evaluated on confocal *z*-stacks captured through the thickness of the slice using ImageJ/Fiji software. Data are mean ± SEM.

Results

The expression of the light-gated cation channel channelrhodopsin-2 (ChR2) in Pv interneurons was induced by injecting AAV vectors carrying the doublefloxed ChR2 sequence in Pv-Cre mouse pups (ChR2 Pv mice). ChR2 was tagged with the red fluorescent reporter mCherry. Immunohistological experiments in TCx slice preparations obtained from postnatal day 18–23 ChR2 Pv mice showed that a large fraction of ChR2-positive cells stained for GABA (96.7 ± 0.97%, $n = 319$ cells, 3 mice; Fig. 1*A*a_2–a_5) and for Pv (96.8 ± 1.00%, $n = 1006$ cells, 6 mice; Fig. 1*A*a_6–a_9). By using Pv-Cre mice crossed with a red fluorescence reporter line (floxed td-Tomato) and injected with AAV carrying the ChR2 sequence tagged with the enhanced yellow fluorescent protein (eYFP), we quantified that 61.3 ± 5.80% ($n = 1456$ cells, 6 mice) of PV cells expressed ChR2. All recorded ChR2-positive cells displayed a fast-spiking discharge pattern compatible with those of Pv-positive fast spiking interneurons (Levy and Reyes, 2012; Schiff and Reyes, 2012). Single-cell patch-clamp recordings from ChR2-positive cells revealed that blue light illumination ($\lambda = 473$ nm) reliably lead to membrane depolarization and action potential firing (Fig. 1*B*). The rate of action potential induced by light could be reliably mimicked by applying intracellular current pulses of different amplitudes (mean current injection, 320 ± 33.3 pA, ChR2-mediated mean firing rate, 73 ± 2.8 Hz; $n = 8$ cells, 6 mice; Fig. 1*B*). In the presence of the proconvulsant agent 4-AP, the firing rate evoked by light pulses was similar to control conditions ($p = 0.26$; $n = 5$, 5 mice, paired *t* test; Fig. 1*C*). Light-induced action potential exhibited unchanged mean amplitude and half-width, and a reduced threshold (amplitude, 69.3 ± 2.46 vs 68.6 ± 4.14 mV, $p = 0.84$; half-width, 1.07 ± 0.081 vs 0.95 ± 0.101 ms, $p = 0.41$; threshold, −59.7 ± 0.40 mV vs −56.7 ± 1.08, $p = 0.03$; $n = 5$ cells, 5 mice, paired *t* test).

In our focal epilepsy model using TCx slice preparations, a seizure-like ictal discharge could be generated by a double application of NMDA (100–500 ms of duration) delivered to layer V-VI neurons, in the presence of 50–100 μM 4-AP and 0.5 mM Mg^{2+} (Losi et al., 2010) (Fig. 1*D*). The NMDA application represents an experimental tool that we used to drive normal networks to seizure-like ictal discharges. However, the seizure-like ictal discharges evoked in brain slice preparations closely mimic

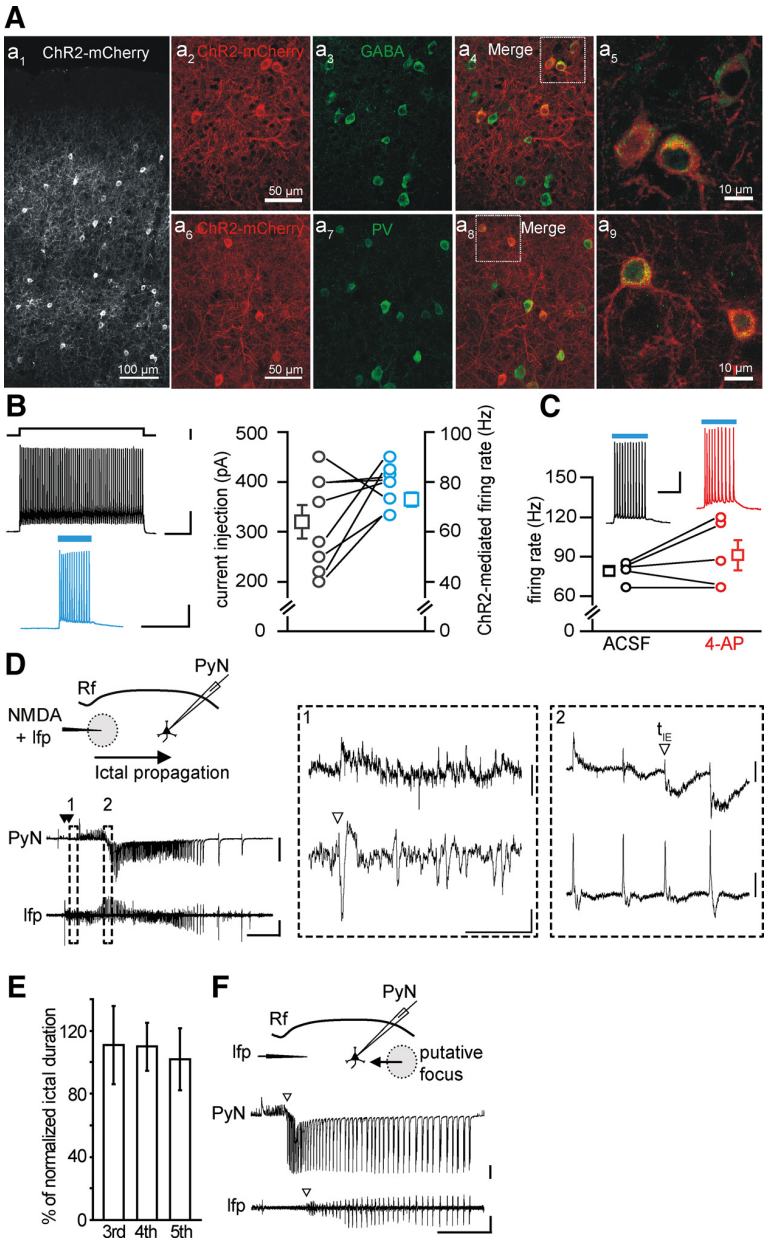

Figure 1. Characterization of ChR2-expressing neurons in Pv-Cre injected mice. ***A***, Immunohistological characterization of ChR2-expressing neurons. ***Aa*$_1$**, Confocal image of a cortical section from Pv-Cre mice injected with AAV-transducing ChR2-mCherry. ***Aa*$_2$–*a*$_5$**, A large fraction of ChR2-mCherry-positive cells (***a*$_2$**) stains for GABA (***a*$_3$**, $n = 325$ cells, 3 mice). The ChR2-mCherry and GABA fluorescence signals are shown merged in ***a*$_4$** (multiconfocal stack). A higher-magnification image of two ChR2-mCherry and Pv-positive cells is shown in ***a*$_5$** (single confocal image). ***Aa*$_6$–*a*$_9$**, Same as in ***a*$_2$–*a*$_5$** for cortical sections that were stained against PV ($n = 319$ cells, 3 mice). The large majority of cells expressing ChR2-mCherry also stain for GABA and Pv, confirming that transgenes are expressed selectively in inhibitory neurons expressing parvalbumin. Scale bars in ***a*$_2$** and ***a*$_6$** apply to ***a*$_3$**, ***a*$_4$**, ***a*$_7$**, and ***a*$_8$**. ***B***, Representative traces of the action potential firing in a ChR2-expressing Pv interneuron in response to an intracellular depolarizing current pulse (top left) and to a 473 nm light stimulation of 150 ms duration (bottom left). Right, Amount of injected current required to evoke a firing rate (in the first 150 ms, black circles) similar to that elicited by light stimulation (cyan circles, $n = 8$ cells, 6 mice). Calibration: top, 200 ms, 500 pA, 20 mV; bottom, 200 ms, 20 mV. ***C***, Action potential firing rate in response to 473 nm light stimulation of ChR2-expressing Pv interneurons in the absence (black, ACSF) and in the presence of 100 μM 4-AP and Mg^{2+} 0.5 mM (red, $n = 5$, 5 mice). Calibration: 100 ms, 20 mV. ***D***, Schematic of the experiment performed in a TCx slice from a Pv-Cre mouse injected with AAV-transducing ChR2, and representative traces of voltage-clamp recordings ($V_h = -50$ mV) from a pyramidal neuron located 1 mm from the NMDA application site (PyN, top) and of local field potentials (lfp, bottom) recorded from the focus. A double NMDA pulse (closed arrowheads) evoked an ictal event that propagated from the focal site of NMDA application to the distant pyramidal neuron. Calibration: 40 s, 500 pA, 0.01 mV. Rf, Rhinal fissure. Insets illustrate at expanded time scales the ictal event onsets (open arrowheads) at the focal area (1) and at the propagating region (2), as revealed by lfp change and voltage-clamp recording from a pyramidal neuron (see Materials and Methods). Calibration: 2 s; inset 1, 40 pA, 0.002 mV; inset 2, 100 pA, 0.004 mV. ***E***, Mean duration of the third, fourth, and fifth ictals normalized to the averaged duration of the first and second ictal ($n = 30$ ictals, 5 mice, $p = 0.97$ between third and fourth, $p = 0.62$ between third and fifth, paired t test). ***F***, Spontaneous ictal event arising from an unpredictable focus. As revealed by the different ictal onset in the PyN and the field potential recordings (open arrowheads), the epileptiform activity propagated first to the pyramidal neuron and second to the site of field potential recording. Calibration: 40 s, 500 pA, 0.01 mV. In this and the other figures, traces may report unclamped action potentials, closed arrowheads indicate NMDA pulses, and cyan bars represent 473 nm light pulses. Empty squares represent mean values. Error bars indicate SEM.

in vivo recorded seizures, including activation of feedforward inhibition, rapid propagation across the cortex, transitions from tonic to clonic phase, and interictal discharges (Prince and Wilder, 1967; Anderson et al., 1986; Trevelyan et al., 2006, 2007a, b). Indeed, the epileptic discharge escaped from the epileptogenic focus and propagated to distant regions where it evoked a series of outward inhibitory currents reflecting the feedforward inhibition activated by focal seizure events, followed by inward currents in pyramidal neurons (Trevelyan et al., 2006; Cammarota et al., 2013) (Fig. 1*D*). In no circumstances were NMDA-evoked ictal events observed to cross the rhinal fissure. Successive NMDA stimulations triggered repetitive ictal events of comparable duration ($n = 30$ ictal events, 5 mice; Fig. 1*E*) provided that a time interval of at least 5 min was applied to overcome the postictal refractory period. Spontaneous ictal events did not occur between successive NMDA applications. Only in specifically designed experiments, in which no NMDA challenges were applied, were ictal events observed to arise spontaneously from unpredictable foci, and they were similar to NMDA-evoked ictal events (Fig. 1*F*). These important control experiments demonstrate that ChR2 expression in Pv interneurons does not, per se, impair the potential of the neural network to generate epileptiform activities.

Optogenetic activation of Pv interneurons at the epileptogenic focus fails to block the generation and prolongs the duration of ictal events

Previous *in vivo* studies showed that spontaneous ongoing seizures can be aborted by optogenetic activation of Pv interneurons (Krook-Magnuson et al., 2013; Paz et al., 2013). We hypothesized that optogenetic activation of Pv interneurons, which in our model can be performed before ic-

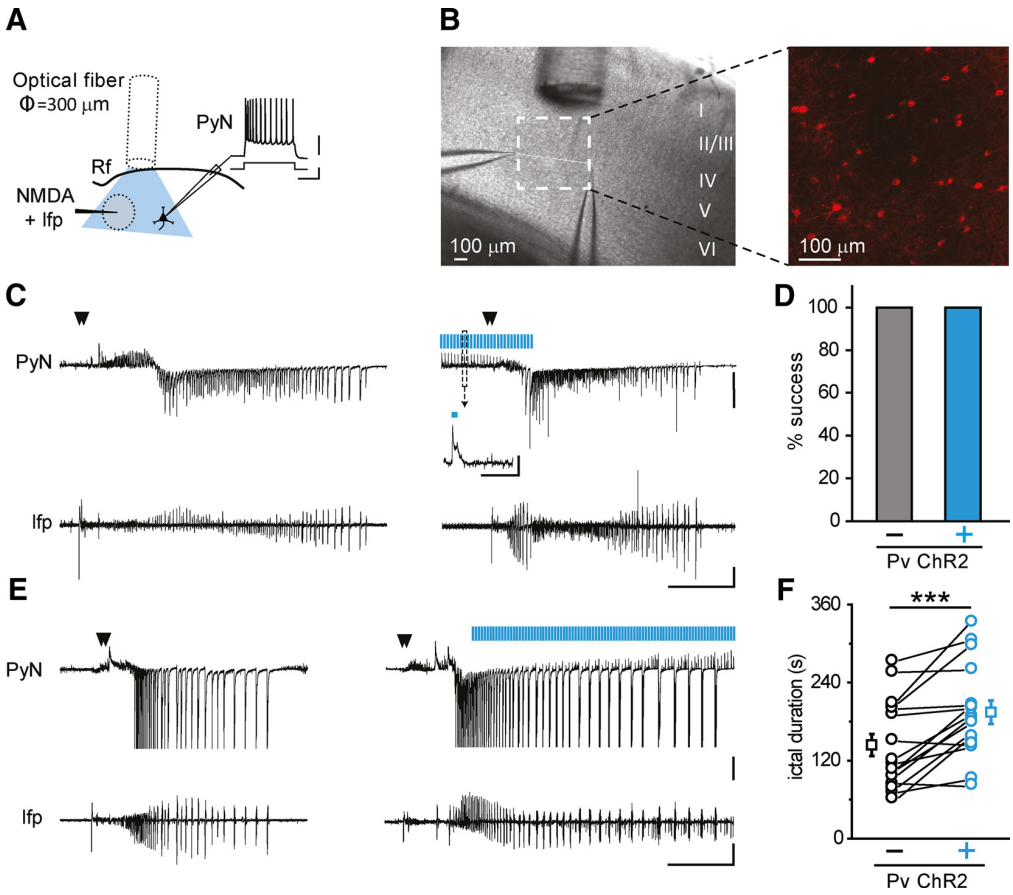

Figure 2. Optogenetic activation of Pv interneurons does not prevent ictal event generation. ***A***, Schematic of the experimental configuration also showing the typical firing of patched pyramidal neurons. Calibration: 0.2 s, 30 mV, 200 pA. ***B***, Differential interference contrast image of the cortical region showing the NMDA-containing pipette that is used to both apply NMDA pulses and record extracellular local field potentials, the optical fiber used to activate ChR2 Pv interneurons, and the patch pipette onto a pyramidal neuron located at ~400 μm from the ictal initiation site. A confocal *z*-stack maximal projection showing fluorescent ChR2-mCherry expressing Pv interneurons from the same region is also reported. ***C***, Representative voltage-clamp recordings ($V_h = -50$ mV) from a pyramidal neuron and simultaneous local field potential recordings of ictal events in the absence (left) and in the presence (right) of pulsed light stimulation. A light-evoked IPSC is reported at enlarged scale. Calibration: 40 s, 500 pA, 0.01 mV; inset, 1 s, 100 pA. ***D***, Percentage of ictal events evoked by double NMDA pulses in the presence and in the absence of pulsed stimulation applied at 0.5 Hz ($n = 16$, 10 mice), 2 Hz and 4 Hz ($n = 8$, 4 mice). ***E***, Representative voltage-clamp recordings from a pyramidal neuron and simultaneous field potential recordings of ictal events in the absence (left) and in the presence (right) of a pulsed light stimulation at 0.5 Hz ($n = 30$ ictals, 13 mice) or 2 Hz ($n = 5$ ictals, 3 mice) that initiated after ictal onset. Calibration: 40 s, 0.01 mV, 500 pA. ***F***, Ictal duration distribution in the absence (black) and in the presence (cyan) of pulsed light stimulation ($n = 16$, 10 mice). ***$p < 0.001$.

tal event onset, could prevent seizure generation. We delivered light pulses at 0.5 Hz or higher frequency (2 and 4 Hz; pulse duration, 150 ms) at the site where NMDA will be subsequently applied (called from here on, focus) by using a large fiber optic (diameter, 300 μm) positioned between the focus and the patched pyramidal neuron (located at ~400 μm from the focus; Fig. 2*A*,*B*). We found that a light pulse activation of ChR2-expressing Pv interneurons initiated 30 s before the ictogenic double NMDA pulse failed to inhibit ictal event generation in all experiments ($n = 24$ ictal events, 11 mice; Fig. 2*C*,*D*).

We next asked whether an optogenetic activation of Pv interneurons, which started 5–15 s after the initiation of an ictal event, could interrupt the epileptic discharge, as it was reported for spontaneously occurring ongoing seizures in the living brain (Krook-Magnuson et al., 2013; Paz et al., 2013; Ledri et al., 2014). Surprisingly, we found that optogenetic stimulation at 0.5 or 2 Hz invariably failed to stop both ictal events evoked by the NMDA challenge ($n = 35$, 16 mice; Fig. 2*E*) and those occurring spontaneously ($n = 9$, 5 mice, data not shown). In contrast, upon a continuous light pulse activation of Pv cells (150 ms at 0.5 Hz), the majority of ictal events (9 of 16) showed an increased duration. As a mean, ictal event duration ($n = 16$) was significantly increased with respect to controls (from 144 ± 17.0 s to 194 ± 18.1 s, $n = 16$ ictal events, 10 mice, $p = 0.00031$, paired *t* test; Fig. 2*E*,*F*).

Activation of Pv interneurons at the epileptogenic focus facilitates ictal event generation

The prolongation of ictal event duration by optogenetic light stimulation suggests that activation of Pv interneurons might have a pro- rather than an anti-epileptic action. We thus tested the hypothesis that Pv interneuron activity can lower focal ictal event threshold. To this aim, we used slices from ChR2 Pv mice and a single NMDA pulse, which has been reported to be a subthreshold stimulus for ictal event generation (Gómez-Gonzalo et al., 2010; Losi et al., 2010). In each experiment, we first controlled the efficacy of NMDA stimulation and the slice integrity by applying a double NMDA pulse that reliably evoked an ictal event. We then applied a single NMDA pulse and found that, as previously reported (Gómez-Gonzalo et al., 2010; Losi et al., 2010), it induced a short-lasting change in the local field potential and no response in pyramidal neurons distant from the focus in 31 of 33

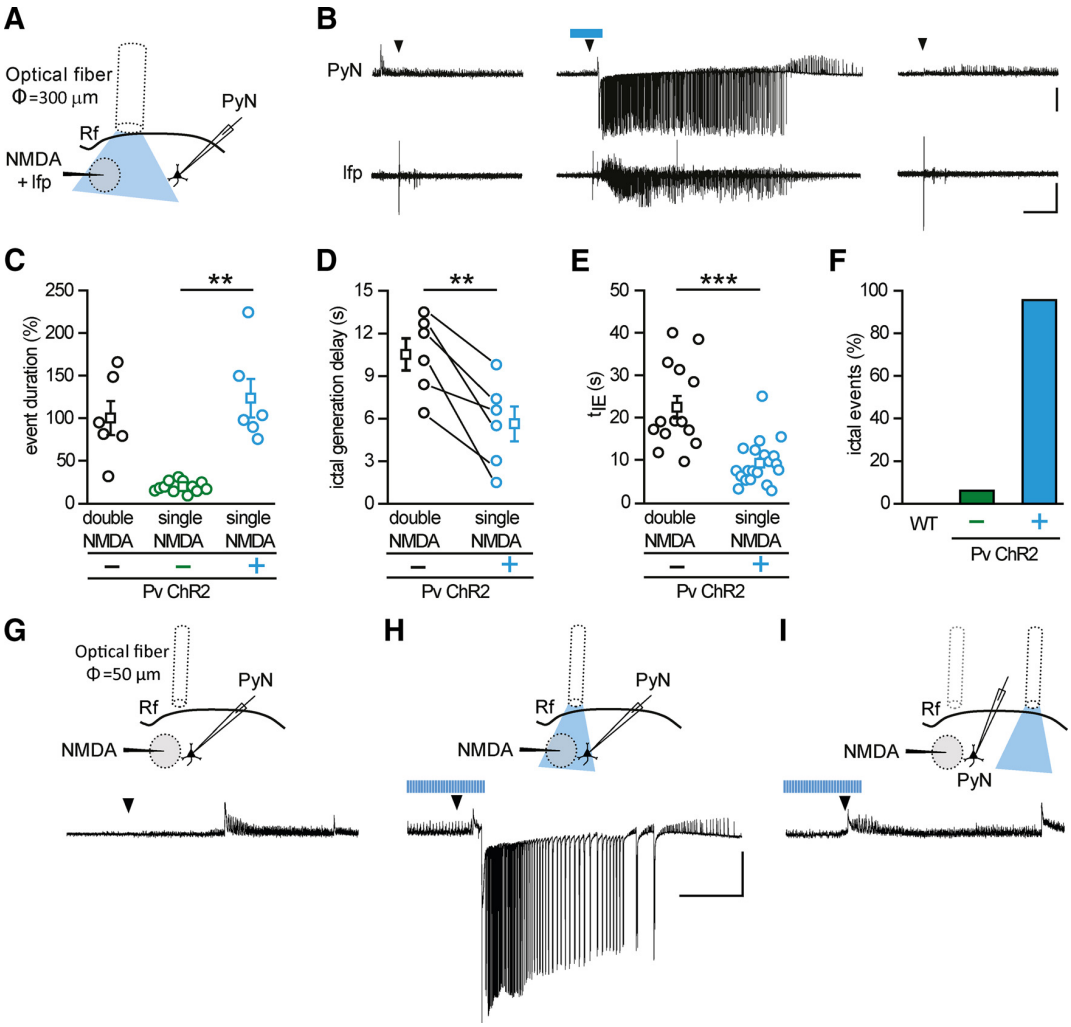

Figure 3. Optogenetic activation of Pv interneurons at the epileptogenic focus promotes ictal event generation. ***A***, Schematic of the experiment and (***B***) representative voltage-clamp recording ($V_h = -50$ mV) from a pyramidal neuron 700 μm from the focus and simultaneous local field potential recording in response to a single NMDA pulse in the absence (left, right) and in the presence (middle) of light stimulation at 0.5 Hz, which was initiated 30 s before the NMDA challenge. Note the ictal response evoked by a single NMDA pulse in the presence of optogenetic stimulation. Calibration: 40 s, 0.01 mV, 500 pA. ***C***, Distribution of normalized event duration in double NMDA pulses (black circles, $n = 6$, 4 mice) and single NMDA pulse experiments in the absence (green circles, $n = 12$, 4 mice) and in the presence (cyan, $n = 6$, 4 mice) of light stimulation. As in the representative experiment reported in ***B***, in the six experiments the effect of a single NMDA pulse was checked twice, both before and after the ictal event evoked by the single NMDA pulse coupled with light stimulation. All data points are normalized to the mean duration of double NMDA-evoked events. ***D***, Paired distribution of the delay in ictal onset measured from local field potentials recorded at the focus in a subset of the experiments ($n = 6$ ictals, 4 mice) that are reported in ***E***. ***E***, Distribution of the delay between the first NMDA pulse and the recruitment of the pyramidal neuron, as measured by t_{IE} (see Materials and Methods), in ictal events evoked by double NMDA pulses in the absence of light stimulation (black, $n = 14$, 7 mice), and single NMDA pulses in the presence of light stimulation (cyan, $n = 20$, 7 mice). ***F***, Bar histogram of the percentage of ictal events evoked by a single NMDA pulse in slices from Pv-Cre mice injected with saline solution ($n = 9$ trials, 3 mice) and from ChR2 Pv mice in the absence (−, green bar, $n = 33$ trials, 9 mice) and in the presence (+, cyan, $n = 23$ trials, 9 mice) of pulsed light stimulation. ***G–I***, Schematic of the experiment (top) and representative voltage-clamp ($V_h = -50$ mV) recordings (bottom) of the response to a single NMDA pulse in a pyramidal neuron located 250 μm from the focus in the absence of light stimulation (***G***), in the presence of light stimulation at the focus (***H***), and in the presence of light stimulation in distant regions 1 mm from the focus (***I***) ($n = 3$ ictal events, 2 mice). $^{**}p < 0.01$. $^{***}p < 0.001$.

single NMDA pulses (Fig. 3*B*, left, right, Fig. 3*F*; $n = 33$, 9 mice). Surprisingly, when single NMDA pulses were coupled with light stimulation at 0.5 Hz, they reliably evoked an ictal event (Fig. 3*B*, middle), which escaped from the focus and rapidly recruited distal pyramidal neurons in 22 of 23 single NMDA pulses ($n = 23$, 9 mice; Fig. 3*F*). As a further control, we tested whether, in slices from Pv-Cre mice injected with saline solution, light pulse stimulation at the focus could affect per se seizure threshold. Under these conditions, a single NMDA pulse remained ineffective (WT, $n = 9$ single NMDA pulses, 3 mice; Fig. 3*F*). The duration of ictal events evoked by single NMDA pulses in the presence of light stimulation ($n = 6$ ictals, 4 mice) was comparable with that of ictal events evoked by double NMDA pulses ($n = 6$ ictals, 4 mice, $p = 0.46$, *t* test; Fig. 3*C*), and it was significantly longer than the response evoked by single NMDA pulses in the absence of light stimulation, as measured by field potential changes ($n = 12$ single NMDA pulses, 4 mice, $p = 0.0058$, *t* test). Furthermore, the latency of ictal event onset after single NMDA pulses in the presence of light, as measured by field potential recordings at the focus, was also significantly shorter than that of the events generated by double NMDA pulses ($n = 6$ ictals, 4 mice, $p = 0.0054$, paired *t* test; Fig. 3*D*). Consistent with these results, in additional experiments we found that the recruitment of pyramidal neurons distant from the focus into the ictal event evoked by a single

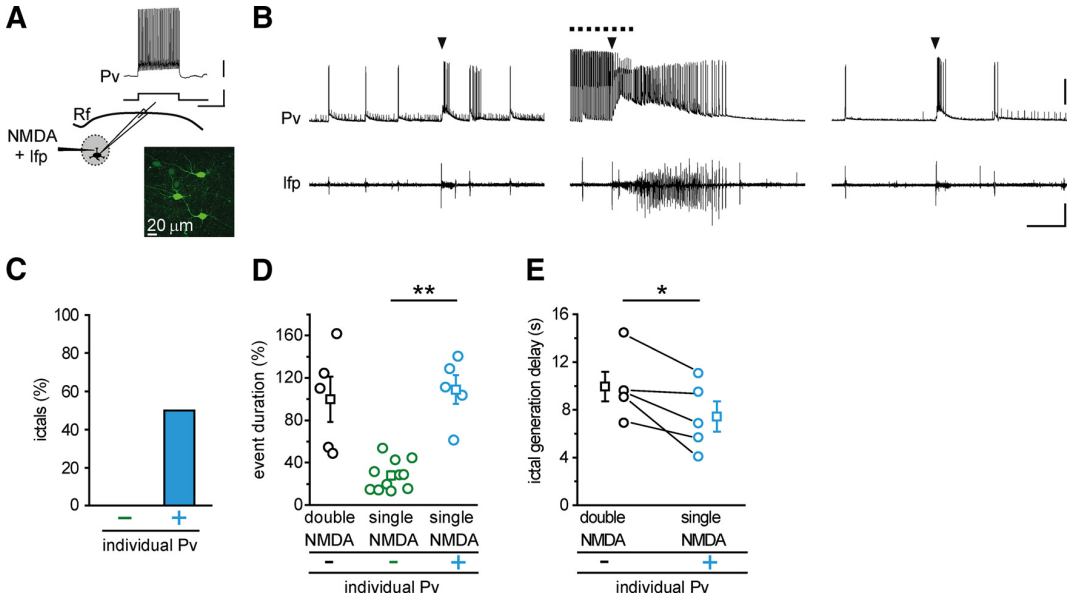

Figure 4. Individual Pv interneuron activation at the epileptogenic focus promotes ictal event generation. ***A***, Schematic of the experiment also showing the typical firing discharge of an FS interneuron expressing GFP in a TCx slice from a G42 mouse. Calibration: 0.5 s, 20 mV, 500 pA. ***B***, Representative current-clamp recordings at resting potential from a Pv interneuron located at the focus and simultaneous local field potential recordings in response to a single NMDA pulse in the absence (left, right) and in the presence (middle) of 1 s intracellular current pulses at 0.5 Hz (dashed line). The intense firing activity in the interneuron facilitates the generation of a full ictal event (middle). Calibration: 40 s, 30 mV, 0.01 mV. ***C***, Percentage of ictal events successfully evoked by a single NMDA pulse in the absence (−, $n = 11$, 3 mice) and in the presence (+, $n = 10$, 3 mice) of current pulse stimulation. ***D***, Distribution of event duration evoked by double NMDA pulse (black circles, $n = 5$, 3 mice) and by single NMDA pulse in the absence (green, $n = 11$, 3 mice) and in the presence (cyan, $n = 5$, 3 mice) of evoked Pv interneuron firing activity. In each experiment, single NMDA pulses without light stimulation were performed at least twice as in the representative experiment reported in ***B***. All data points are normalized to the mean duration of double NMDA pulse-evoked ictal events. ***E***, Paired distribution of ictal onset delay measured from local field potential recorded at the focus ($n = 5$, 3 mice). *$p < 0.05$. **$p < 0.01$.

NMDA pulse ($n = 20$ ictals, 7 mice) was also significantly faster than that evoked by double NMDA pulses ($n = 14$ ictals, 7 mice, $p = 0.00023$, t test; Fig. 3*E*; see Materials and Methods). These latter observations suggest that, upon light stimulation, the neuronal network of the focus more readily respond to the ictogenic stimulus. We then performed some experiments restricting illumination to a smaller area by using a 50-μm-diameter optical fiber. Under these conditions, a single NMDA pulse coupled with the optogenetic stimulation also successfully evoked an ictal event ($n = 3$ ictals, 2 mice; Fig. 3*G*,*H*). Moving the optical fiber to a region distant ~1 mm from the focus failed to elicit an ictal event ($n = 3$ single NMDA pulses, 2 mice; Fig. 3*I*), indicating that the optogenetic stimulation needs to recruit Pv interneurons at the focus to significantly lower ictal event threshold. A contribution to the prompt response of the neuronal network to NMDA stimulation could potentially derive from an impairment of inhibition, possibly due to a depolarization block of Pv interneurons that, at the focus, are overstimulated by the synergic action of NMDA and light pulses. This possibility was ruled out by juxtasomal recordings of firing activity from Pv interneurons at the focus. These recordings revealed that light pulses applied during the NMDA stimulation did not cause a depolarization block in any of the cells studied ($n = 13$, 2 mice; mean distance from the NMDA pipette tip, 210.2 ± 1.24 μm), rather inducing in these cells an intense firing, which showed unchanged mean action potential frequency before and during NMDA stimulation (mean ± SEM, 67.7 ± 5.27 Hz before and 67.8 ± 7.72 Hz during NMDA stimulation). Because each cortical Pv interneuron is synaptically connected to hundreds of nearby pyramidal neurons (Wang et al., 2002; Packer and Yuste, 2011) and local optical stimulation of Pv cells is effective in decreasing the focal seizure threshold, we hypothesized that the activity of a single interneuron might be enough to mediate this phenomenon. To address this question, we activated individual Pv interneurons using G42 mice, which express GFP in a subpopulation of Pv interneurons (Chattopadhyaya et al., 2004). After patching GFP-positive cells that were classified as FS interneurons (Fig. 4*A*), we applied a single NMDA pulse that, as expected, failed to evoke an ictal event and only evoked a short-lasting change in the local field potential trace and a transient firing discharge in the Pv interneuron ($n = 11$ single NMDA pulses, 3 mice; Fig. 4*B*, left, right). We then applied a sequence of depolarizing current pulses (1 s steps at 0.5 Hz for 60 s) that triggered in the Pv interneuron a sustained, rhythmic firing discharge. Under these conditions, a single NMDA pulse evoked an ictal event as revealed by the local field potential and the intracellular recordings (Fig. 4*B*, middle) in five out of ten single NMDA pulses ($n = 10$, 3 mice; Fig. 4*C*). As observed in the previous optogenetic experiments (see Fig. 3*C*), the duration of the ictal events ($n = 5$, 3 mice) was strikingly longer than the duration of the field potential change evoked by single NMDA pulses in the absence of single-cell stimulation ($n = 11$ single NMDA pulses, 3 mice, $p = 0.0027$, t test; Fig. 4*D*). The duration of these ictal events was comparable with the duration of the ictal events evoked by double NMDA pulses in the same experiments ($n = 5$ ictals, 3 mice, $p = 0.73$, t test; Fig. 5*D*). Furthermore, the latency of ictal event onset after single NMDA pulses paired with individual Pv cell stimulation was also significantly shorter than that of the events elicited by double NMDA pulses ($n = 5$ ictals, 3 mice, $p = 0.042$, paired t test; Fig. 4*E*). This reduction was similar, although less marked, to what observed in optogenetic experiments (Fig. 3*D*).

Together, these results demonstrate that rhythmic Pv interneuron activity at the epileptogenic focus, obtained either through wide field optogenetic stimulation or depolarizing cur-

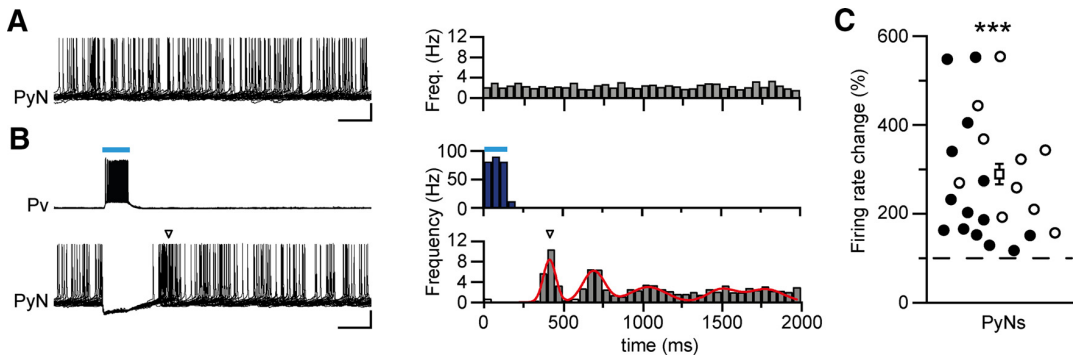

Figure 5. Optogenetic activation of Pv interneurons induce postinhibitory rebound spiking in pyramidal neurons. ***A***, ***B***, Representative simultaneous current-clamp recordings from a pyramidal neuron, depolarized to action potential threshold by steady-state current injection, and a Pv interneuron in the absence (***A***, left panel) and presence of pulsed light stimulation at 0.5 Hz (***B***, left panels). Recordings were performed in the presence of 4-AP and 0.5 mM Mg^{2+}. Histograms of the relative firing rate as a function of time, calculated over 50 ms time bins, obtained by the analysis of 300 consecutive sweeps (***A***, ***B***, right panels). Open arrowheads indicate the main spike clustering. Red line indicates the multipeak fitting of the firing rate over time (reduced $\chi^2 = 0.99$). Calibration: 200 ms, 20 mV. ***C***, Distribution of normalized firing rate changes during rebound spiking both in basal conditions (empty circles, $n = 10$) and in the presence of 4-AP (full circles, $n = 14$). The mean value of both datasets is represented by the empty square (284 ± 28.1%, $n = 24$ cells, 14 slices, 6 mice). ***$p < 0.001$ (Wilcoxon signed-rank test).

rent pulses applied to individual cells, contributes to lower the threshold for ictogenesis and turns a subthreshold stimulus into a reliable ictogenic trigger.

Optogenetic activation of Pv interneurons induces postinhibitory rebound spiking and promotes coordinated firing in pyramidal neurons

Activation of GABAergic interneuron inhibitory signals may enhance seizure generation by synchronizing neural excitatory networks (for review, see Avoli and de Curtis, 2011). We therefore tested whether Pv interneuron activation enhances coordinated firing in pyramidal neurons. To answer this question, we first performed current-clamp recordings from ChR2-expressing Pv interneuron-pyramidal neuron pairs during 0.5 Hz light pulse stimulation (Fig. 5). Whereas Pv interneurons were activated by blue light pulses, tonic spiking of the pyramidal cell (induced by holding the cell at depolarized potential; Fig. 5*A*) was largely suppressed (Fig. 5*B*). Moreover, both in the presence ($n = 14$ cells, 6 mice; Fig. 5*B*) and in the absence of 4-AP ($n = 10$ cells, 6 mice), pyramidal neurons also exhibited marked postinhibitory rebound spiking after the end of the light stimulus and successive spike clusterings. This rebound spiking period was accompanied by a significant increase in the firing rate in 24 of the 35 pyramidal neurons recorded. On average, during the rebound, a threefold increase of the firing rate was observed in these neurons ($n = 24$ cells, 6 mice, $p = 1.19E-7$, Wilcoxon signed-rank test; Fig. 5*C*). In paired recordings from pyramidal neurons, we then explored the hypothesis that the spike clustering during the rebound period caused by the rhythmic Pv interneuron activation could increase the degree of synchronization in pyramidal neurons (Fig. 6A_1,A_2). Under control conditions, two neighboring pyramidal neurons (mean distance, 52.6 ± 11.05 μm, 7 pairs, 5 mice) generated action potentials that fell randomly within the 2 s window (Fig. 6A_1,B_1), as also shown by the probability distribution (Fig. 6C_1, red and green traces). To evaluate the degree of correlation between the two spike trains, we computed the NN distance between the spikes from the two neurons. The cumulative distribution of all NN distances is shown by the red curve (observed spikes) in Figure 6D_1. Next, we shuffled the spike timing of one neuron and recomputed the NN distances (Fig. 6B_1,C_1, randomized PyN1). When spikes were shuffled, we found that the cumulative distribution of NN distances (blue curve, randomized spikes) was not significantly different from the distribution of observed spikes (red curve) demonstrating that the spiking of the two pyramidal neurons was not correlated ($n = 230$ spikes, $p = 0.96$, Kolmogorov–Smirnov test; Fig. 6D_1). During blue light illumination delivered to activate Pv cells, we observed the suppression of firing and a rebound spiking in both neurons immediately after the light stimulus (Fig. 6A_2). We generated a spike train by shuffling the spikes in the nonsilenced window (randomized PyN1; Fig. 6B_2,C_2). The comparison of the cumulative distributions of the NN distances of the observed spikes (red trace) and randomized spikes (blue trace) showed that the randomized spikes had a wider distribution with respect to that of the recorded spikes, indicating that after light pulses the spikes of the two neurons tended to group together ($n = 447$ spikes, $p = 0.015$, Kolmogorov–Smirnov test; Fig. 6D_2). This effect is quantified in Figure 6*E* where the NN distance distributions for the observed (red curve) and the randomized spike train (blue curve) are reported. The difference between the two distributions (gray trace) indicates that Pv interneurons induced in pyramidal neurons an excess of synchronous spikes in a time window of 500 ms after release of inhibition. Similar results were obtained in the absence of 4-AP and the increase in synchrony for all pairs, both in 4-AP and in basal conditions, is reported in Figure 6*F* ($n = 7$ pairs, 5 mice, $p = 0.0054$, paired *t* test).

These windows of enhanced synchrony generated in the pyramidal neuron network by the rhythmic inhibition of Pv interneurons may be at the basis of the ictogenic effect induced by light pulse stimulation at the epileptogenic focus. If this were the case, we would expect the ictal events to initiate after the recovery from inhibition, and not during the firing suppression period (354 ± 19.0 ms, $n = 24$, 6 mice) in pyramidal neurons, as measured in each cell by the minimal time between the onset of the light pulse and the first recorded action potential. Consistent with this prediction, we found that all ictal events ($n = 35$, 19 mice), with one exception (representing 2.86% of all ictal events, opposed to an expected 17.7%), initiated during these windows of enhanced synchronous excitation in pyramidal neurons (Fig. 6*G*). Furthermore, the distribution of the ictal event onset probability exhibited a peak that coincides with the rebound peak in the mean spiking probability distribution of pyramidal neurons (Fig. 6*H*).

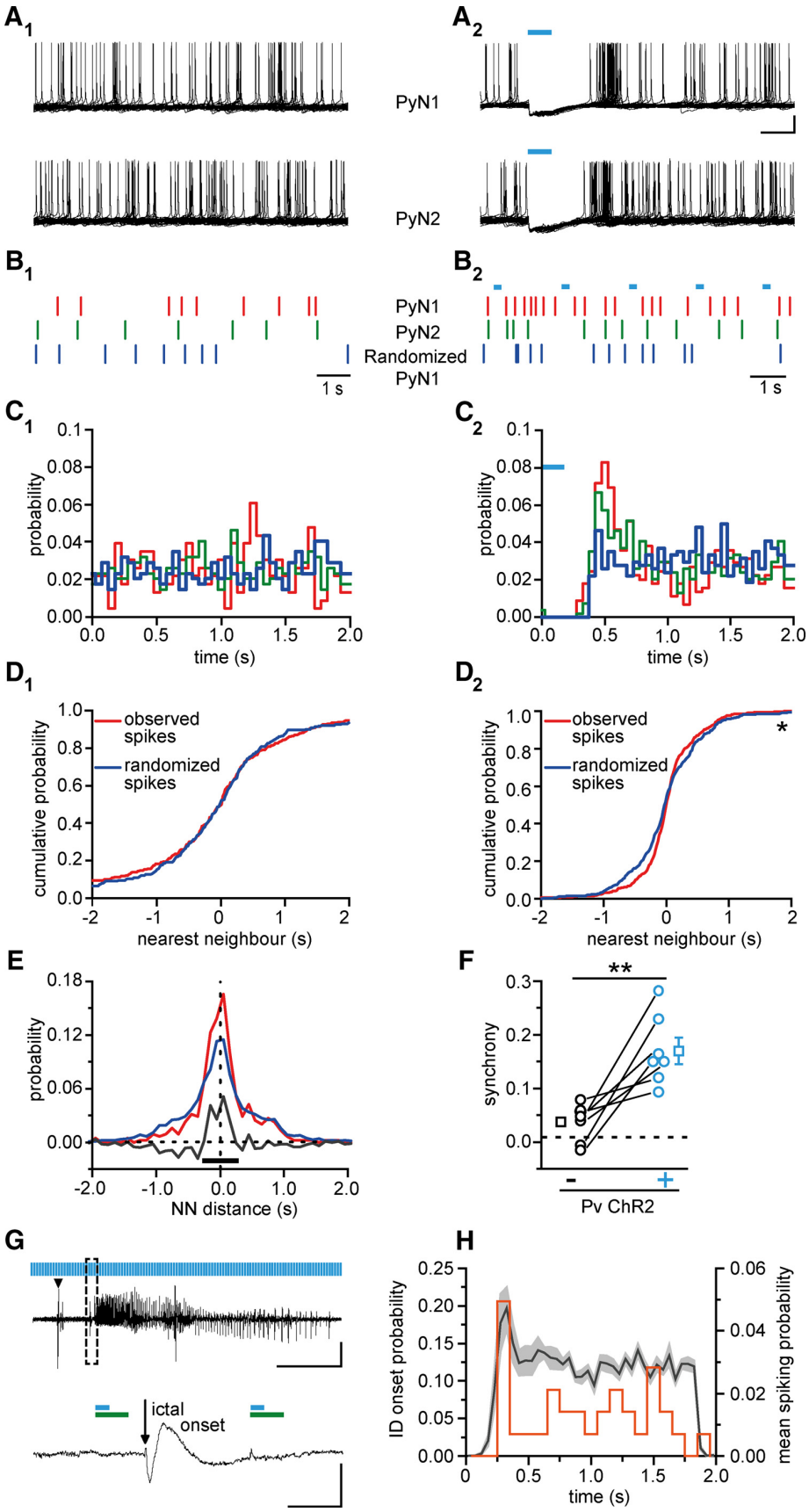
A1
A2
PyN1
PyN2
B1
B2
PyN1
PyN2
Randomized
PyN1
1 s
1 s
C1
C2
probability
time (s)
D1
D2
observed spikes
randomized spikes
cumulative probability
nearest neighbour (s)
*
E
probability
NN distance (s)
F
**
synchrony
Pv ChR2
G
ictal onset
H
ID onset probability
mean spiking probability
time (s)

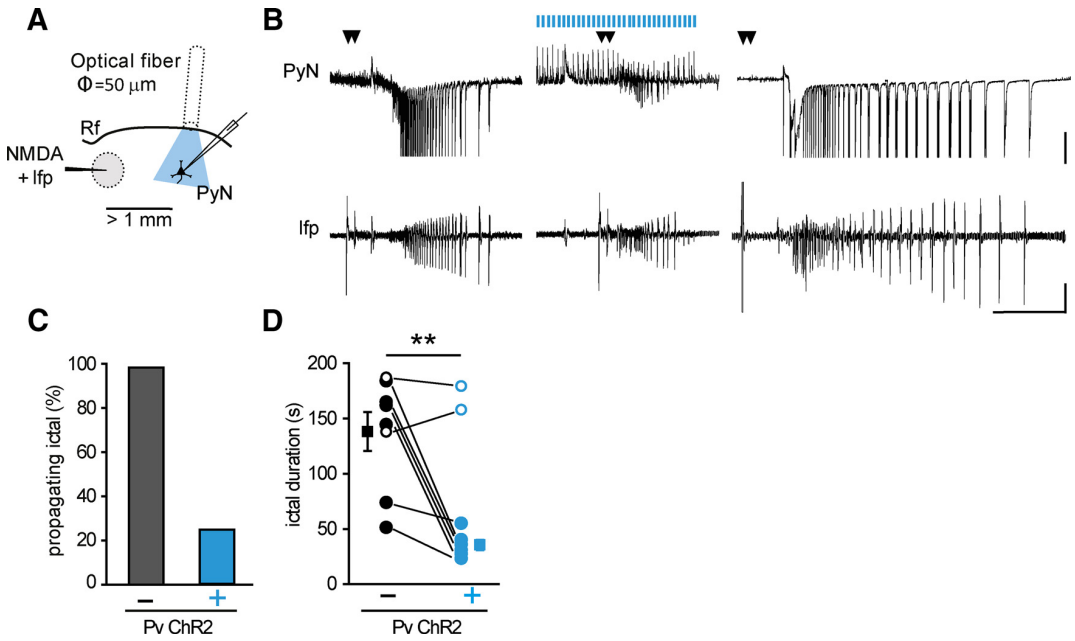

Figure 7. Optogenetic activation of Pv interneurons distant from the focus blocks ictal event propagation and shortens ictal event duration at the focus. ***A***, Schematic of the experiment. ***B***, Representative voltage-clamp recordings ($V_h = -50$ mV) from a pyramidal neuron located >1 mm from the focus and simultaneous local field potential recordings at the focus in the absence (left and right) and in the presence (middle) of light stimulation starting 60 s before the double NMDA pulse. Calibration: 40 s, 0.01 mV, 500 pA. ***C***, Percentage of propagating ictal events in the absence ($n = 14$, 3 mice) and in the presence of light stimulation ($n = 8$, 3 mice). ***D***, Paired distribution of ictal event duration evoked by double NMDA pulses in the absence (empty and full black circles, $n = 8$, 3 mice) and in the presence (empty and full cyan circles, $n = 8$, 3 mice) of light stimulation, as measured from local field potentials recorded at the focus. The duration of the two ictal events that were not blocked by local optogenetic activation of Pv interneurons was not reduced. Mean values of black and cyan full circles are represented by full squares. Paired sample *t* test was performed on the values obtained from the six successful experiments (3 mice). $^{**}p < 0.01$.

Activation of Pv interneurons in regions distant from the focus blocks the propagation and shortens the duration of ictal events

We next investigated the role of Pv interneurons in the regulation of ictal event propagation. To this aim, we specifically stimulated Pv interneurons in the propagating region by positioning the optical fiber (50 μm diameter) at ~1 mm from the focus (Fig. 7*A*). In the presence of Pv interneuron stimulation, the recruitment of the pyramidal neuron into the propagating ictal event was prevented in six of eight double NMDA pulses ($n = 8$, 3 mice), whereas in the absence of Pv interneuron stimulation, a double NMDA pulse evoked an ictal event that always recruited the pyramidal neuron ($n = 14$ double NMDA pulses, 3 mice; Fig. 7*B*,*C*). Interestingly, in the six experiments in which the recruitment of the pyramidal neuron was prevented (Fig. 7*D*, cyan closed circles), ictal event duration at the focus was reduced to 33 ± 4% of paired controls ($n = 6$ ictal events, 3 mice, $p = 0.009$, paired *t* test; Fig. 7*D*). In the two unsuccessful experiments (Fig. 7*D*, open cyan circles), ictal event duration at the focus was not affected.

Given that the activation of single Pv interneurons is sufficient to mimic the effect of optogenetic Pv interneuron activation at the focus (Fig. 4), we tested the hypothesis that activation of a single Pv interneuron is also sufficient to block the recruitment of neighboring pyramidal neurons into the propagating ictal event. The progression of ictal events was monitored by current-clamp recordings from GFP-positive Pv FS interneurons in slices from G42 mice and, in a subset of experiments, also by simultaneous Ca^{2+} imaging from neurons loaded with the Ca^{2+} indicator Rhod-2 AM. As reported previously (Trevelyan et al., 2006; Cammarota et al., 2013), spatially distinct clusters of neurons were recruited into the propagating ictal event at different times (Fig. 8*A*, red and blue spots, *B*, red and blue traces). Notably, the recruitment of the second cluster of neurons (Fig. 8*A*,*B*, blue traces and spots), occurred shortly after firing impairment of the Pv interneuron (Fig. 8*B*, black trace). We then applied a sequence of 1 s intracellular depolarizing current pulses at 0.5 Hz that evoked in the patched Pv interneuron a firing discharge similar to that in-

←

Figure 6. Optogenetic activation of Pv interneurons promotes synchronous firing in pyramidal neurons. ***A*$_1$**, ***A*$_2$**, Spike trains recorded in 2-s-long sweeps from two neighboring pyramidal neurons in the absence (***A*$_1$**) and in the presence (***A*$_2$**) of light pulse stimulation at 0.5 Hz. Cyan bars represent 150 ms light pulses. The rhythmic activation of Pv interneurons causes a temporal modulation of spikes in both pyramidal neurons. Calibration: 200 ms, 20 mV. ***B*$_1$**, ***B*$_2$**, Raster plots showing the spike timing of the two pyramidal neurons (red and green bars) and a randomized trial (blue bars). ***C*$_1$**, ***C*$_2$**, Probability distribution in the 2 s period in the absence (***C*$_1$**) and in the presence (***C*$_2$**) of rhythmic optogenetic activation of Pv interneurons. ***D*$_1$**, ***D*$_2$**, For each spike produced by the pyramidal neuron 2 (PyN2), the distance from the closest spike produced by PyN1 was computed. The observed cumulative distribution of the nearest neighbor distances is plotted in red ($n = 230$ spikes). The distribution was computed again after randomization of the spike train of PyN1 (blue trace, $n = 230$ spikes). In the presence of optogenetic stimulation (***D*$_2$**), the difference between the observed cumulative distribution and the cumulative distribution obtained after randomization is statistically significant ($n = 447$ spikes, $^{*}p < 0.05$, Kolomogorov–Smirnov test). ***E***, The integral of the difference between observed and simulated distributions has been computed in an interval centered ~0, returning a measure of the synchronization between the two pyramidal neurons. ***F***, Summary report for the increase in pyramidal neuron synchrony induced by Pv interneuron activation ($n = 7$ pairs, 5 mice) in the presence (black circles) and in the absence (cyan circles) of pulsed light stimulation both in basal ACSF and 4-AP. $^{**}p < 0.01$. ***G***, Representative local field potential recording of an NMDA-evoked ictal event in the presence of light pulse stimulation. The ictal event onset between two light pulses is shown at enlarged scales. Green bars represent the firing suppression period in pyramidal neurons induced by light stimulation of ChR2-expressing Pv interneurons (cyan bars, 150 ms at 0.5 Hz). Calibration: 40 s, 0.01 mV; inset, 500 ms, 0.01 mV. ***H***, Distribution of both the ictal onset probability (orange line, $n = 31$ ictal events in 100 ms time bins, 17 mice) and the pyramidal neuron mean spiking probability in 4-AP (light gray represents SEM; $n = 24$ cells, 6 mice; 50 ms time bins) as a function of time during pulsed light stimulation of Pv interneurons. The 0 value is set as the end of the light stimulus.

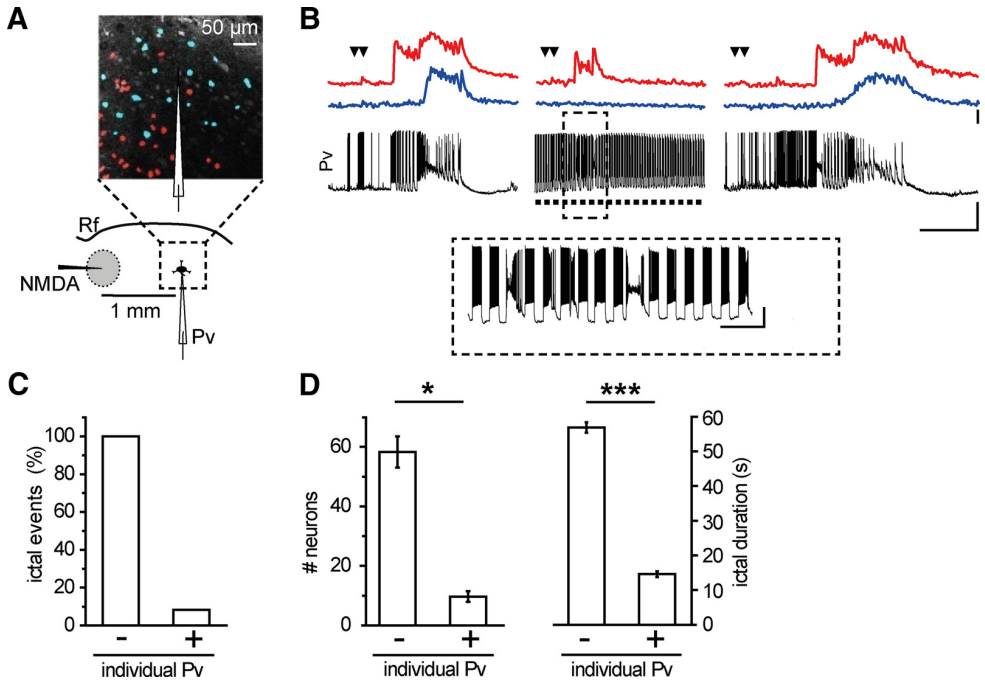

Figure 8. Individual Pv interneuron activation in penumbra regions blocks ictal event propagation. ***A***, Schematic of the experiment and differential interference contrast image illustrating the neuronal clusters progressively recruited into the ictal event in Ca^{2+} imaging experiments. ***B***, Representative single current-clamp recordings from a Pv interneuron and simultaneous mean Ca^{2+} signal from two neuronal clusters (red and blue traces; soma position of these neurons is reported in ***A*** according to their different time of recruitment into the propagating ictal event. Steps of current were repeatedly injected to evoke firing activity (inset) that prevented the occurrence of a full ictal event. Calibration: 40 s, $\Delta F/F_0$ 40%, 40 mV; inset, 5 s, 20 mV. ***C***, Bar histogram of the percentage of NMDA evoked ictal events without (−, $n = 23$, 8 mice) or during (+, $n = 12$, 8 mice) stimulation of individual Pv interneurons. ***D***, Bar histograms reporting the number of recruited neurons (left) and ictal event duration (right) measured in red neuron Ca^{2+} signals, in the absence and in the presence of current pulse stimulation of Pv interneurons ($n = 3$ ictal events, 2 mice). $^*p < 0.05$. $^{***}p < 0.001$.

duced by the optogenetic stimulation, starting 30 s before the double NMDA pulse. Under these conditions, and in all but one of the performed experiments ($n = 12$ double NMDA pulses, 8 mice; Fig. 8*C*), the firing impairment in the patched Pv interneuron was prevented (Fig. 8*B*, middle, inset). As a consequence, only part of the neurons that belong to the first cluster (Fig. 8*B*, red trace) closer to the focus, but not neurons of the second cluster (Fig. 8*B*, blue traces) surrounding the patched Pv interneuron, were recruited into the ictal event. In the presence of Pv interneuron stimulation, the mean number of neurons recruited into the propagating ictal event was significantly reduced with respect to controls ($n = 3$ double NMDA pulses, 2 mice, $p = 0.02$, paired *t* test; Fig. 8*D*). The recruited neurons exhibited a drastic shortening of the ictal event, as measured from the Ca^{2+} signal change ($n = 29$ neurons; Fig. 8*D*) with respect to controls ($n = 175$ neurons, 3 ictals, 2 mice, $p = 1.95E\text{-}60$, *t* test; Fig. 8*D*). The shortening of ictal events was similar to that observed in the optogenetic experiments where ictal event duration at the focus was significantly reduced after the propagation was blocked by optogenetic Pv interneuron activation (Fig. 7*D*).

The afterdischarges travel backwards to the focus and affect ictal event duration

What process can underlie the ictal event shortening at the focus following Pv interneuron stimulation in the propagating region? The ictal event wave front generates new sources of the afterdischarges as it advances across the cortex (Trevelyan et al., 2007a). If the afterdischarges emerging from recently recruited territories travel back with respect to that of the propagating ictal event, as it was described for spontaneous ictal events in slices of occipital cortex (Trevelyan et al., 2007a), they could sustain and prolong the clonic phase of the ictal event. To address this hypothesis, we analyzed the timing of the afterdischarges in voltage-clamp paired recordings from two pyramidal neurons located at different distances from the focus (Fig. 9*A*). We found that the ictal event wavefront propagated first to the neuron closer to the focus (Fig. 9*B*, top) and then to the more distant neuron (Fig. 9*B*, bottom). During the clonic phase, however, the afterdischarges that initially propagated in the same direction as the ictal event wavefront changed direction (Fig. 9*C*). As revealed by the cross-correlation diagram, after the switch in direction, all the afterdischarges propagated toward the original site of ictal event generation (Fig. 9 *B*, *C*, bottom). Similar results were obtained in four ictal events from three pyramidal neuron pairs (3 mice; Fig. 9*D*; see Materials and Methods).

Discussion

Using a temporal cortex slice model, we investigated the contribution of Pv-expressing GABAergic interneurons to the different stages that characterize a focal seizure-like ictal discharge. Our results show that, at the epileptogenic focus, a rhythmic activity in Pv interneurons, induced by optogenetic stimulation or current pulses to individual cells, enhances the generation of focal ictal events, whereas in regions distant from the focus the same interneuron activity blocks ictal event spread.

It is widely recognized that the role of GABAergic interneurons on brain networks goes far beyond the general depressant inhibitory action originally described (Freund and Katona, 2007; Bonifazi et al., 2009; Hu et al., 2014; Somogyi et al., 2014). Regarding epilepsy, data favoring either anticonvulsant or procon-

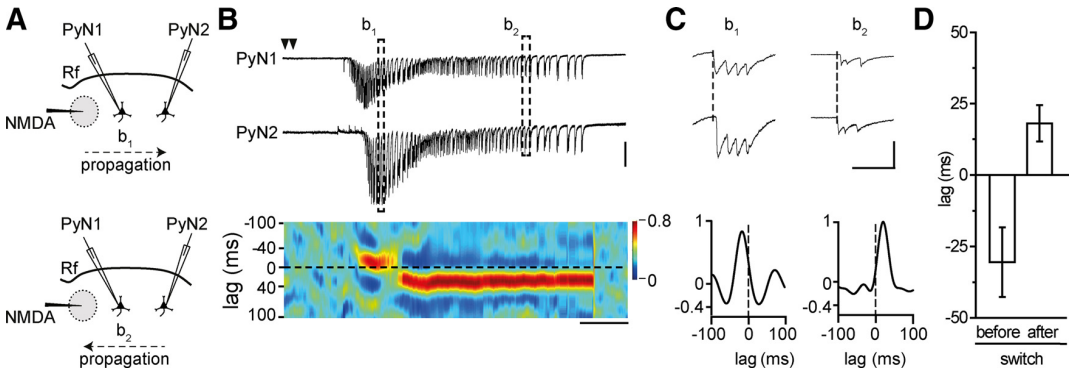

Figure 9. Afterdischarges invert their propagation direction during ictal events. ***A***, Schematic of the experiment also illustrating the switch in the direction of ictal propagation. ***B***, Representative traces of a dual voltage-clamp ($V_h = -50$ mV) recording from two pyramidal neurons 1 mm apart and pseudocolor plot of the cross-correlation (see Materials and Methods) during a focal ictal event showing the switch in the afterdischarge direction ($n = 4$, 3 mice). Calibration: 10 s, 500 pA. ***C***, Two afterdischarges at enlarged time scale with cross-correlation diagrams of the relative bin. Calibration: 200 ms, 200 pA. ***D***, Mean lag before and after the switch in the afterdischarge direction ($n = 4$, 3 mice).

vulsant role are reported. Indeed, although an effective control of seizure propagation by feedforward inhibition was described previously (Prince and Wilder, 1967; Schwartz and Bonhoeffer, 2001; Trevelyan et al., 2006, 2007b; Schevon et al., 2012; Cammarota et al., 2013), increased GABAergic inhibitory signals were reported to favor, under certain conditions, seizure initiation (Avoli et al., 1996; Cossart et al., 2005; Derchansky et al., 2008; Gnatkovsky et al., 2008; Mann and Mody, 2008; Avoli and de Curtis, 2011; Grasse et al., 2013; Jiruska et al., 2013). Recent optogenetic studies also lead to conflicting views on the role of inhibition in epilepsy. In seizure models *in vivo* (Krook-Magnuson et al., 2013; Paz et al., 2013), optogenetic activation of GABAergic interneurons was found to suppress ongoing epileptiform activities, whereas in other models *in vitro* optogenetic activation of Pv interneurons and, although less efficiently, somatostatin interneurons enhanced spontaneous ictal events (Shiri et al., 2014; Yekhlef et al., 2014). Our study reconciles these conflicting views by revealing that, in the same model of epileptiform activity, Pv interneurons play a dual opposing role, either favoring the generation or opposing the propagation of ictal events. The ultimate nature of their action appears to be determined by the spatial and temporal relationship between their rhythmic inhibitory activity and the emergent network dynamics that at the focus generate an ictal event and in distant regions govern ictal event propagation.

We found that an optogenetic activation of Pv interneurons at the focus fails to block NMDA-evoked ictal events. The same stimulation initiated a few seconds after the onset of epileptiform activity also failed to interrupt ongoing ictal events and significantly prolonged their duration. Previous optogenetic studies in hippocampal slices revealed that coactivation of several interneuron subclasses impacts epileptiform activity by prolonging the interval between successive interictal-like events more effectively than activation of Pv or somatostatin interneurons alone (Ledri et al., 2014). It cannot therefore be excluded that a similar approach could also affect the generation of NMDA-evoked ictal events.

We also found that a subthreshold stimulus for ictal event generation became suprathreshold if coupled with optogenetic Pv interneuron activation. Intracellular current pulses to individual Pv interneurons also favored ictal event generation, demonstrating that this effect is independent on the tool used to activate Pv interneurons (optogenetics vs electrophysiology) and that single-cell activation is sufficient to mediate this phenomenon.

To explain this result, we hypothesized that at the focus an enhanced coordinated spiking in pyramidal neurons contributes to ictal event initiation. In this framework, and consistent with previous studies (Cobb et al., 1995; Stark et al., 2013), we observed that the rhythmic inhibition originating from Pv interneurons was followed by a postinhibitory rebound spiking that boosted excitation and drove coordinated activity in pyramidal neurons. We suggest that these windows of enhanced coordinated firing contribute to the increased local circuit excitability that, at the focus, initiates an ictal discharge in response to subthreshold excitation. In accordance with this view, NMDA-evoked ictal events were generated in these time windows, immediately after the firing suppression period induced in pyramidal neurons by Pv interneuron activation. These observations render unlikely that GABAergic signaling by Pv interneurons favored ictal event generation by directly depolarizing pyramidal neurons. Because of intracellular Cl^- accumulation in pyramidal neurons upon intense interneuron activity (Fujiwara-Tsukamoto et al., 2004; Rivera et al., 2004), GABA signaling may become excitatory (Staley et al., 1995; Kaila et al., 1997), contributing to both seizure onset (Pathak et al., 2007) and afterdischarge generation (Ellender et al., 2014). If this were the case, however, ictal events are expected to initiate in coincidence with the Pv interneuron-mediated GABAergic inhibition onto pyramidal neurons and not during the rebound spiking that follows the recovery from inhibition, as we observed.

Our results also showed that, when an ictal event was evoked at the focus, its propagation was arrested by increasing inhibition in the propagating region through either an optogenetic stimulation restricted to Pv interneurons of this region or intracellular current pulse to individual interneurons. This finding is consistent with previous *in vivo* observations revealing that optogenetic GABAergic interneuron activation can suppress ongoing epileptiform activities (Krook-Magnuson et al., 2013; Paz et al., 2013; Ledri et al., 2014). Indeed, the epileptogenic focus could not be precisely identified in these studies. Therefore, the optogenetic stimulation most likely did not include the Pv interneurons at the focus and it arrested ictal event propagation, in accordance with our study.

The cellular events that underlined the block of ictal event propagation might involve the impact in propagating regions of two different patterns of network activity: the successive waves of excitation of the propagating ictal discharge and the rhythmic inhibition generated locally by Pv interneurons. It is noteworthy that the same rhythmic activity induced by current pulses in in-

dividual Pv interneurons that in propagating regions blocked the ictal discharge at the focus enhanced ictal event generation. This result may reflect the reduced connectivity in brain slices. However, it cannot be excluded that a similar action can be also exerted in the intact brain given that inhibition provided by a single cortical Pv interneuron can be extended to hundreds of synaptically connected pyramidal neurons (Wang et al., 2002; Packer and Yuste, 2011).

The potential of Pv interneurons to interrupt ictal event propagation is further supported by results from our Ca^{2+} imaging experiments. We observed that, upon activation of intense rhythmic firing in individual Pv interneurons, neurons surrounding the stimulated Pv interneurons were not recruited into propagating ictal discharge. However, neurons that were closer to the focal area were still recruited, but they exhibited a drastic ictal discharge shortening similar to that observed after ictal spread was blocked by optogenetic Pv interneuron activation in the propagating region. A possible cellular event that may account for ictal event shortening at the focus comes from afterdischarge analysis in pair recordings from pyramidal neurons at different distances from the focus. Obtained data suggest that the reduced ictal event duration could be a direct consequence of ictal event propagation block that prevented newly generated afterdischarges to travel backwards to the original focus. Notably, the afterdischarges showed only one switch in the direction of propagation suggesting that ictal events propagated unidirectionally from the site of NMDA application (in proximity to the rhinal fissure) across the temporal cortex. Consistent with this view, afterdischarges in spontaneous ictal events, probably arising from multiple foci, have been reported to frequently switch the direction of propagation (Trevelyan et al., 2007a). Given the limits of brain slice preparations, these results need to be validated in the living brain. However, they suggest that halting seizure propagation in patients may result in seizure shortening in the entire neural network, including the foci. This may represent a promising tool to prevent neurological damages frequently associated with long-lasting seizures.

We identified the action of Pv interneurons in a brain slice model in which the distinct dynamics of ictal event initiation and propagation could be investigated separately. This preparation has known limitations with respect to the living brain state, such as reduced long-range axonal connections and the removal of cortico-thalamo-cortical projections. It should also be noted that the local NMDA excitation represents an experimental tool that we used to drive normal networks to ictal events. Caution is, therefore, warranted before extrapolating our data to the epileptic brain. Nevertheless, it must be also underlined that NMDA-induced ictal events were similar to those arising spontaneously from unpredictable foci. Most importantly, our cortical slice model of focal ictal events allows experiments that can be hardly performed in the living brain. For example, the optogenetic stimulation restricted to Pv interneurons of the focus that we performed in our model is unfeasible in currently available *in vivo* models of seizures where seizure initiation site is not identifiable in advance.

In conclusion, the functional dichotomy of Pv interneurons that we here describe extends our understanding of the cellular mechanisms that in local circuits control the generation and the propagation of focal epileptiform discharges. Results obtained validate the efficacy of an optogenetic activation of Pv interneurons in opposing seizure propagation, but, in parallel, they also show that GABAergic inhibition can enhance seizure generation by promoting synchronized network activity. The promising use of optogenetics in seizure control (Tye and Deisseroth, 2012; Kokaia et al., 2013) must therefore be carefully weighted to avoid its potential negative consequences.

References

Anderson WW, Lewis DV, Swartzwelder HS, Wilson WA (1986) Magnesium-free medium activates seizure-like events in the rat hippocampal slice. Brain Res 398:215–219. CrossRef Medline

Avoli M, de Curtis M (2011) GABAergic synchronization in the limbic system and its role in the generation of epileptiform activity. Prog Neurobiol 95:104–132. CrossRef Medline

Avoli M, Barbarosie M, Lücke A, Nagao T, Lopantsev V, Köhling R (1996) Synchronous GABA-mediated potentials and epileptiform discharges in the rat limbic system in vitro. J Neurosci 16:3912–3924. Medline

Bartos M, Vida I, Jonas P (2007) Synaptic mechanisms of synchronized gamma oscillations in inhibitory interneuron networks. Nat Rev Neurosci 8:45–56. CrossRef Medline

Bonifazi P, Goldin M, Picardo MA, Jorquera I, Cattani A, Bianconi G, Represa A, Ben-Ari Y, Cossart R (2009) GABAergic hub neurons orchestrate synchrony in developing hippocampal networks. Science 326:1419–1424. CrossRef Medline

Buzsáki G, Wang XJ (2012) Mechanisms of gamma oscillations. Annu Rev Neurosci 35:203–225. CrossRef Medline

Cammarota M, Losi G, Chiavegato A, Zonta M, Carmignoto G (2013) Fast spiking interneuron control of seizure propagation in a cortical slice model of focal epilepsy. J Physiol 591:807–822. CrossRef Medline

Chattopadhyaya B, Di Cristo G, Higashiyama H, Knott GW, Kuhlman SJ, Welker E, Huang ZJ (2004) Experience and activity-dependent maturation of perisomatic GABAergic innervation in primary visual cortex during a postnatal critical period. J Neurosci 24:9598–9611. CrossRef Medline

Cobb SR, Buhl EH, Halasy K, Paulsen O, Somogyi P (1995) Synchronization of neuronal activity in hippocampus by individual GABAergic interneurons. Nature 378:75–78. CrossRef Medline

Connors BW (1984) Initiation of synchronized neuronal bursting in neocortex. Nature 310:685–687. CrossRef Medline

Cossart R, Bernard C, Ben-Ari Y (2005) Multiple facets of GABAergic neurons and synapses: multiple fates of GABA signalling in epilepsies. Trends Neurosci 28:108–115. CrossRef Medline

Derchansky M, Jahromi SS, Mamani M, Shin DS, Sik A, Carlen PL (2008) Transition to seizures in the isolated immature mouse hippocampus: a switch from dominant phasic inhibition to dominant phasic excitation. J Physiol 586:477–494. CrossRef Medline

Dugué GP, Dumoulin A, Triller A, Dieudonné S (2005) Target-dependent use of co-released inhibitory transmitters at central synapses. J Neurosci 25:6490–6498. CrossRef Medline

Ellender TJ, Raimondo JV, Irkle A, Lamsa KP, Akerman CJ (2014) Excitatory effects of parvalbumin-expressing interneurons maintain hippocampal epileptiform activity via synchronous afterdischarges. J Neurosci 34:15208–15222. CrossRef Medline

Freund TF, Katona I (2007) Perisomatic inhibition. Neuron 56:33–42. CrossRef Medline

Fujiwara-Tsukamoto Y, Isomura Y, Kaneda K, Takada M (2004) Synaptic interactions between pyramidal cells and interneurone subtypes during seizure-like activity in the rat hippocampus. J Physiol 557:961–979. CrossRef Medline

Gnatkovsky V, Librizzi L, Trombin F, de Curtis M (2008) Fast activity at seizure onset is mediated by inhibitory circuits in the entorhinal cortex in vitro. Ann Neurol 64:674–686. CrossRef Medline

Gómez-Gonzalo M, Losi G, Chiavegato A, Zonta M, Cammarota M, Brondi M, Vetri F, Uva L, Pozzan T, de Curtis M, Ratto GM, Carmignoto G (2010) An excitatory loop with astrocytes contributes to drive neurons to seizure threshold. PLoS Biol 8:e1000352. CrossRef Medline

Grasse DW, Karunakaran S, Moxon KA (2013) Neuronal synchrony and the transition to spontaneous seizures. Exp Neurol 248:72–84. CrossRef Medline

Gutnick MJ, Connors BW, Prince DA (1982) Mechanisms of neocortical epileptogenesis *in vitro*. J Neurophysiol 48:1321–1335. Medline

Hu H, Gan J, Jonas P (2014) Interneurons. Fast-spiking, parvalbumin^{+} GABAergic interneurons: from cellular design to microcircuit function. Science 345:1255–1263. CrossRef Medline

Jiruska P, de Curtis M, Jefferys JG, Schevon CA, Schiff SJ, Schindler K (2013)

Synchronization and desynchronization in epilepsy: controversies and hypotheses. J Physiol 591:787–797. CrossRef Medline

Kaila K, Lamsa K, Smirnov S, Taira T, Voipio J (1997) Long-lasting GABA-mediated depolarization evoked by high-frequency stimulation in pyramidal neurons of rat hippocampal slice is attributable to a network-driven, bicarbonate-dependent K^+ transient. J Neurosci 17:7662–7672. Medline

Kepecs A, Fishell G (2014) Interneuron cell types are fit to function. Nature 505:318–326. CrossRef Medline

Kokaia M, Andersson M, Ledri M (2013) An optogenetic approach in epilepsy. Neuropharmacology 69:89–95. CrossRef Medline

Kovács R, Kardos J, Heinemann U, Kann O (2005) Mitochondrial calcium ion and membrane potential transients follow the pattern of epileptiform discharges in hippocampal slice cultures. J Neurosci 25:4260–4269. CrossRef Medline

Krook-Magnuson E, Armstrong C, Oijala M, Soltesz I (2013) On-demand optogenetic control of spontaneous seizures in temporal lobe epilepsy. Nat Commun 4:1376. CrossRef Medline

Ledri M, Madsen MG, Nikitidou L, Kirik D, Kokaia M (2014) Global optogenetic activation of inhibitory interneurons during epileptiform activity. J Neurosci 34:3364–3377. CrossRef Medline

Levy RB, Reyes AD (2012) Spatial profile of excitatory and inhibitory synaptic connectivity in mouse primary auditory cortex. J Neurosci 32:5609–5619. CrossRef Medline

Losi G, Cammarota M, Chiavegato A, Gómez-Gonzalo M, Carmignoto G (2010) A new experimental model of focal seizures in the entorhinal cortex. Epilepsia 51:1493–1502. CrossRef Medline

Mann EO, Mody I (2008) The multifaceted role of inhibition in epilepsy: seizure-genesis through excessive GABAergic inhibition in autosomal dominant nocturnal frontal lobe epilepsy. Curr Opin Neurol 21:155–160. CrossRef Medline

Markram H, Toledo-Rodriguez M, Wang Y, Gupta A, Silberberg G, Wu C (2004) Interneurons of the neocortical inhibitory system. Nat Rev Neurosci 5:793–807. CrossRef Medline

Miles R, Wong RK (1983) Single neurones can initiate synchronized population discharge in the hippocampus. Nature 306:371–373. CrossRef Medline

Monyer H, Markram H (2004) Interneuron Diversity series: molecular and genetic tools to study GABAergic interneuron diversity and function. Trends Neurosci 27:90–97. CrossRef Medline

Packer AM, Yuste R (2011) Dense, unspecific connectivity of neocortical parvalbumin-positive interneurons: a canonical microcircuit for inhibition? J Neurosci 31:13260–13271. CrossRef Medline

Pathak HR, Weissinger F, Terunuma M, Carlson GC, Hsu FC, Moss SJ, Coulter DA (2007) Disrupted dentate granule cell chloride regulation enhances synaptic excitability during development of temporal lobe epilepsy. J Neurosci 27:14012–14022. CrossRef Medline

Paz JT, Davidson TJ, Frechette ES, Delord B, Parada I, Peng K, Deisseroth K, Huguenard JR (2013) Closed-loop optogenetic control of thalamus as a tool for interrupting seizures after cortical injury. Nat Neurosci 16:64–70. CrossRef Medline

Prince DA, Wilder BJ (1967) Control mechanisms in cortical epileptogenic foci: "surround" inhibition. Arch Neurol 16:194–202. CrossRef Medline

Rivera C, Voipio J, Thomas-Crusells J, Li H, Emri Z, Sipilä S, Payne JA, Minichiello L, Saarma M, Kaila K (2004) Mechanism of activity-dependent downregulation of the neuron-specific K-Cl cotransporter KCC2. J Neurosci 24:4683–4691. CrossRef Medline

Schevon CA, Weiss SA, McKhann G Jr, Goodman RR, Yuste R, Emerson RG, Trevelyan AJ (2012) Evidence of an inhibitory restraint of seizure activity in humans. Nat Commun 3:1060. CrossRef Medline

Schiff ML, Reyes AD (2012) Characterization of thalamocortical responses of regular-spiking and fast-spiking neurons of the mouse auditory cortex in vitro and in silico. J Neurophysiol 107:1476–1488. CrossRef Medline

Schwartz TH, Bonhoeffer T (2001) In vivo optical mapping of epileptic foci and surround inhibition in ferret cerebral cortex. Nat Med 7:1063–1067. CrossRef Medline

Shiri Z, Manseau F, Levesque M, Williams S, Avoli M (2014) Interneuron activity leads to initiation of low-voltage fast-onset seizures. Ann Neurol. Advance online publication. Retrieved Dec. 27, 2014. doi: 10.1002/ana.24342. CrossRef Medline

Somogyi P, Katona L, Klausberger T, Lasztóczi B, Viney TJ (2014) Temporal redistribution of inhibition over neuronal subcellular domains underlies state-dependent rhythmic change of excitability in the hippocampus. Philos Trans R Soc Lond B Biol Sci 369:20120518. CrossRef Medline

Staley KJ, Soldo BL, Proctor WR (1995) Ionic mechanisms of neuronal excitation by inhibitory GABAA receptors. Science 269:977–981. CrossRef Medline

Stark E, Eichler R, Roux L, Fujisawa S, Rotstein HG, Buzsáki G (2013) Inhibition-induced theta resonance in cortical circuits. Neuron 80:1263–1276. CrossRef Medline

Trevelyan AJ, Sussillo D, Watson BO, Yuste R (2006) Modular propagation of epileptiform activity: evidence for an inhibitory veto in neocortex. J Neurosci 26:12447–12455. CrossRef Medline

Trevelyan AJ, Baldeweg T, van Drongelen W, Yuste R, Whittington M (2007a) The source of afterdischarge activity in neocortical tonic-clonic epilepsy. J Neurosci 27:13513–13519. CrossRef Medline

Trevelyan AJ, Sussillo D, Yuste R (2007b) Feedforward inhibition contributes to the control of epileptiform propagation speed. J Neurosci 27:3383–3387. CrossRef Medline

Tye KM, Deisseroth K (2012) Optogenetic investigation of neural circuits underlying brain disease in animal models. Nat Rev Neurosci 13:251–266. CrossRef Medline

Wang Y, Gupta A, Toledo-Rodriguez M, Wu CZ, Markram H (2002) Anatomical, physiological, molecular and circuit properties of nest basket cells in the developing somatosensory cortex. Cereb Cortex 12:395–410. CrossRef Medline

Yekhlef L, Breschi GL, Lagostena L, Russo G, Taverna S (2014) Selective activation of parvalbumin- or somatostatin-expressing interneurons triggers epileptic seizure-like activity in the mouse medial entorhinal cortex. J Neurophysiol. Advance online publication. Retrieved Dec. 10, 2014. doi: 10.1152/jn.00841.2014. CrossRef Medline

3.3 APPENDIX A:

Optogenetic activation of Parvalbumin interneurons maintains focal epileptiform activity via synchronous afterdischarges

Iacopo Marcon, Michele Sessolo, Gabriele Losi, Letizia Mariotti, Serena Bovetti, Tommaso Fellin and Giorgio Carmignoto

A rhythmic optogenetic activation of Pv interneurons initiated after ictal onset can significantly prolong the duration of epileptiform events [155]. To gain insights into the mechanism at the basis of this unexpected event, we decided to carefully analyze the clonic phase pattern of the prolonged ictal discharges. Interestingly, we found that a large number of afterdischarges initiated immediately after the onset of a light pulse (Fig 1B), as indicated by the analysis of the latency between light pulses and afterdischarge onsets (Fig 1C-D). The degree of synchronization between the afterdischarge and the light pulse increased progressively along with the development of the ictal clonic phase (Fig 1E-F), and towards the end of the epileptiform event almost every light pulse is rapidly followed by an afterdischarge

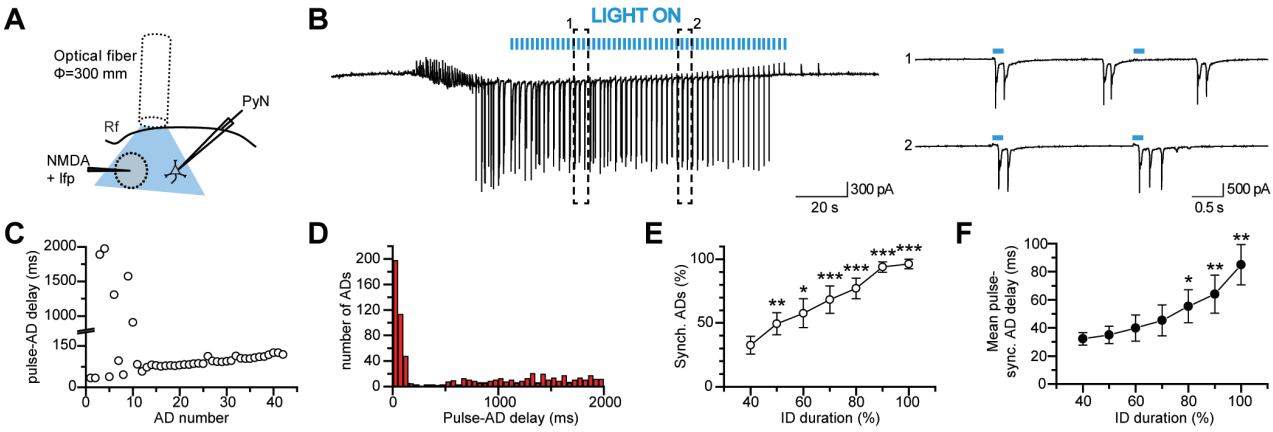

Figure 1. Rhythmic optogenetic activation of Pv interneuron at the epileptogenic focus synchronizes afterdischarges (A) Schematic of the experimental configuration. (B) Voltage-clamp recording from a PyN (Vh = - 50 mV) located 400 μm from the epileptogenic focus. (C) Delays between the onset of the light pulse and that of the following AD, as a function of the progressive AD number, from 30% to 100% of ictal duration represented above. (D) number of ADs as a function of pulse-AD delay obtained from 9 ictals (670 ADs, nine mice). (E) Mean percentage of synchronized ADs (within 150 ms after light pulse onset) during ictal discharge development (n=9, nine mice). (F) Mean delay between the onset of the light pulse and that of the synchronized AD as a function of the ictal duration (n = 9, nine mice). Paired t-test was applied with respect to the first mean value.

(Fig. 1E).

The mean distribution of the time interval between two successive afterdischarges in the clonic phase of several ictal events during rhythmic optogenetic stimulation of Pv cells revealed a large peak at 2 s, corresponding to the 0.5 Hz of the light pulses, and a smaller peak at 4 s (Fig. 2). These peaks are absent in the distribution of the

afterdischarge time intervals from control ictal events where pulsed light stimulation was absent (Fig. 2).

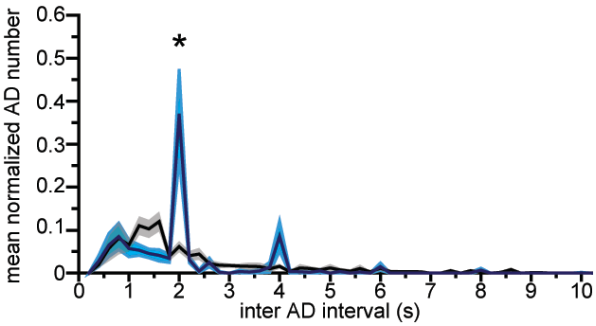

Figure 2 Pulsed light activation of Pv interneurons at 0.5 Hz controls afterdischarge frequency. Mean normalized AD number represented as a function of inter AD interval in presence (cyan line: n = 663 AD intervals, 9 ictal events, nine mice) and in absence (black line: n = 709 AD intervals, 11 ictal events, eleven mice) of light pulse stimulation (time bins, 200 ms). Shaded areas represent standar error over the mean (black and blue

To further analyze the synchronizing effect on the afterdischarges of Pv interneuron stimulation, we computed the average power spectrum of the voltage recordings from pyramidal neurons in the presence and in the absence of light stimulation. Since we observed that syncrhronization increases along with the progression of the clonic phase, we analyzed two time windows of 30 s, at the beginning and at the end of the clonic phase. This analysis revealed a clear peak at 0.5 Hz and relative armonics in the power spectrum computed from the last part of ictal events in the presence of light stimulation, confirming the synchronization of the afterdischarges with light pulses (Fig 3). Notably, these peaks are absent in the power spectrum of ictal events in the absence of light stimulation (Fig 3).

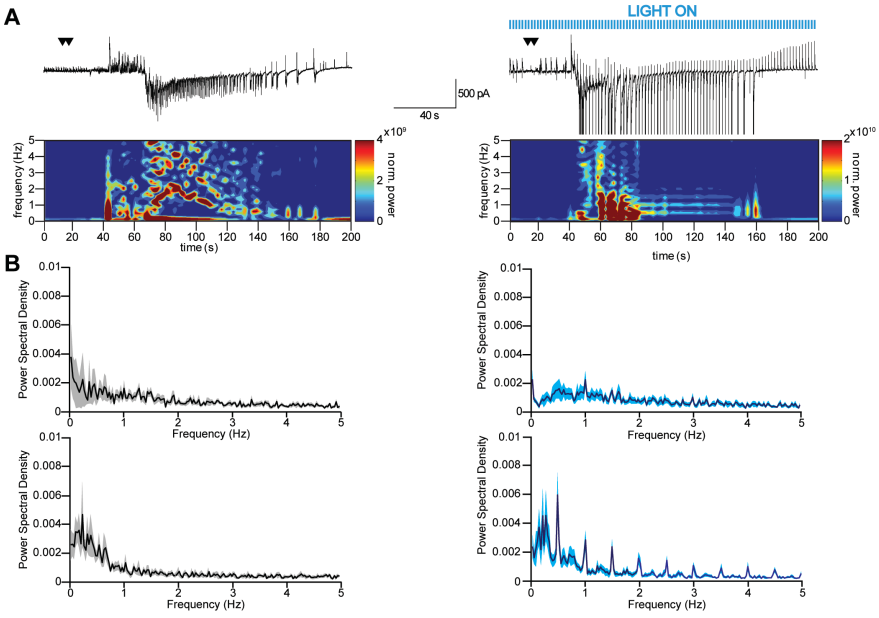

Figure 3 Optogenetic Pv interneuron activation at 0.5Hz generate a 0.5 Hz frequency band and relative harmonics during the ictal event. (A) Normalized power spectrograms computed by estimating the power spectrum in consecutive 5 s bins of ictal events represented above. (B) Average normalized power spectral density (PSD) computed over 30 s of the initial part (first and second panel) and terminal part (third and fourth panel) of ictal events recorded in voltage clamp from PyNs. (n=7, seven mice). In black are represented PSD of ictal discharges in absence of light pulse stimulation, while in blue are represented PSD of ictal discharges in the presence of 0.5 Hz Pv interneurons photostimulation. Shaded areas represent standar error over the mean (s.e.m.).

Discussion

We report here that a rhythmic optogenetic activation of Pv interneurons at 0.5 Hz synchronizes the afterdischarges in the clonic phase during NMDA-evoked ictal events. This synchronizing effect of Pv interneurons may account for the increased duration of ictal events that we observed. Therefore, we propose the hypothesis that Pv interneuron activity can set the timing for afterdischarge generation and that through this action they can contribute to prolong the clonic phase of the seizure. In support of this hypothesis, spontaneous and light-evoked afterdischarges within a given experiment were observed to exhibit similar patterns. Our hypothesis is in line with the evidence from another group demonstrating that Pv interneurons can maintain epileptiform activity in the hippocampus by synchronizing the afterdischarges [108]. This effect, according to the authors, is caused by an excitatory GABAergic transmission that results from a transient collapse of the chloride (Cl^-) reversal potential in pyramidal neurons caused by the epileptiform activity. Indeed, when Pv interneurons where optogenetically silenced during the clonic phase, the frequency of the afterdischarges significantly decreased.

Additional methods

The quantification of the synchronizing effect of Pv interneuron stimulation at 0.5 Hz on afterdischarges was determined by measuring the delay between the onset of each afterdischarge and the light pulse from the 30% to 100% of ictal length. Power spectral density of voltage-clamp traces were computed using the fast fourier transform (FFT) algorithm in Matlab. Electrophysiological data were subsampled at 100 Hz and mean subtracted before frequency analysis.

OXFORD UNIVERSITY PRESS | Cerebral Cortex

Unaltered network activity and interneuronal firing during spontaneous cortical dynamics in vivo in a mouse model of Severe Myoclonic Epilepsy of Infancy

Journal:	*Cerebral Cortex*
Manuscript ID	Draft
Manuscript Type:	Original Articles
Date Submitted by the Author:	n/a

Complete List of Authors:	De Stasi, Angela; Istituto Italiano di Tecnologia, Neuroscience and Brain Technologies Farisello, Pasqualina; Istituto Italiano di Tecnologia, Neuroscience and Brain Technologies Marcon, Iacopo; National Research Council (CNR), Neuroscience Institute; University of Padova, Department of Biomedical Sciences Cavallari, Stefano; Istituto Italiano di Tecnologia, Neuroscience and Brain Technologies Forli, Angelo; Istituto Italiano di Tecnologia, Neuroscience and Brain Technologies Vecchia, Dania; Istituto Italiano di Tecnologia, Neuroscience and Brain Technologies Losi, Gabriele; National Research Council (CNR), Neuroscience Institute Mantegazza, Massimo; IPMC, CNRS UMR7275 and University of Nice-Sophia Antipolis, Neuroscience Panzeri, Stefano; Italian Institute of Technology, Department of Robotics, Brain and Cognitive Sciences Carmignoto, Giorgio; CNR Institute of Neuroscience, University of Padova; Giorgio Carmignoto, Giorgio Carmignoto Bacci, Alberto; ICM–Institut du Cerveau et de la Moelle épinière, Neuroscience Fellin, Tomaso; Italian Institute of Technology, Dept Neuroscience and Brain Technologies
Keywords:	Dravet syndrome, NaV1.1, parvalbumin-positive interneurons, somatostatin-positive interneurons, somatosensory cortex

Unaltered network activity and interneuronal firing during spontaneous cortical dynamics *in vivo* in a mouse model of Severe Myoclonic Epilepsy of Infancy

Abbreviated title: *In vivo network and cellular dynamics in SMEI*

Angela Michela De Stasi[1,2#], Pasqualina Farisello[1,3#], Iacopo Marcon[4], Stefano Cavallari[2,5], Angelo Forli[1,2], Dania Vecchia[1,2], Gabriele Losi[4], Massimo Mantegazza[6], Stefano Panzeri[2,5], Giorgio Carmignoto[4], Alberto Bacci[3,7*], Tommaso Fellin[1,2*]

[1] Optical Approaches to Brain Function Laboratory, Istituto Italiano di Tecnologia, Genova, Italy.
[2] Neural Coding Laboratory, Istituto Italiano di Tecnologia, Genova, Italy.
[3] Fondazione EBRI "Rita Levi-Montalcini", Roma, Italy.
[4] CNR Neuroscience Institute and University of Padova, Padova, Italy.
[5] Neural Computation Laboratory, Istituto Italiano di Tecnologia, Rovereto, Italy.
[6] IPMC, CNRS UMR7275 and University of Nice-Sophia Antipolis, Valbonne, France.
[7] Sorbonne Universités UPMC Paris 06, UMR S 112, Inserm U 1127, CNRS UMR 7225 and ICM–Institut du Cerveau et de la Moelle épinière, Paris France.

[#] Equal contribution

[*] Corresponding authors: Tommaso Fellin, Optical Approaches to Brain Function Laboratory and Neural Coding Laboratory, Istituto Italiano di Tecnologia, Via Morego 30, 16163 Genova, Italy, tel: +39 010 71781549, fax:+39 010 71781230, email: tommaso.fellin@iit.it. Alberto Bacci, ICM - Institut du Cerveau et de la Moelle épinière, Paris, France, tel: +33 (0)1 5727 4062, email: alberto.bacci@icm-institute.org

Keywords: Dravet syndrome, $Na_V1.1$, parvalbumin-positive interneurons, somatostatin-positive interneurons, somatosensory cortex.

Abstract

Severe Myoclonic Epilepsy of Infancy (SMEI) is associated with loss of function of the *SCN1A* gene encoding the $Na_V1.1$ sodium channel isoform. Previous studies in *Scn1a*$^{-/+}$ mice during the pre-epileptic period reported selective reduction in interneuron excitability and proposed this as the main pathological mechanism underlying SMEI. Yet, the functional consequences of this interneuronal dysfunction at the circuit level *in vivo* are unknown. Here we investigated whether *Scn1a*$^{-/+}$ mice showed alterations of cortical network function. We found that various forms of spontaneous network activity were similar in *Scn1a*$^{-/+}$ during the pre-epileptic period compared to WT *in vivo*. Importantly, in brain slices from *Scn1a*$^{-/+}$ mice, the excitability of parvalbumin- (PV) and somatostatin- (SST) interneurons was reduced, epileptiform activity propagated more rapidly and complex synaptic changes were observed. However *in vivo*, optogenetic reduction of firing in PV- or SST- cells in WT mice failed to mimic the *Scn1a*$^{-/+}$ phenotype, and juxtasomal recordings from identified PV- and SST-interneurons showed unaffected interneuronal firing during spontaneous cortical dynamics in *Scn1a*$^{-/+}$ compared to WT. These results demonstrate that interneuronal hypoexcitability is not observed in *Scn1a*$^{-/+}$ mice during spontaneous activities *in vivo* and suggest that additional mechanisms may contribute to homeostatic rearrangements and the pathogenesis of SMEI.

Introduction

Severe Myoclonic Epilepsy of Infancy (SMEI), or Dravet syndrome, is a rare epileptic encephalopathy, characterized by severe intractable seizures, ataxia, autistic-like deficits, cognitive disorders and premature death (Dravet 2000;Dravet et al. 2005). Many drugs are ineffective in the treatment of SMEI and currently no cure is available. Mutations in the *SCN1A* gene, coding for the alpha subunit of the voltage-gated sodium channels $Na_V1.1$, were identified in approximately 70% of SMEI patients (Meisler and Kearney 2005), with most mutations leading to a haploinsufficiency and loss of channel

function (Claes et al. 2001;Ohmori et al. 2002). Importantly, a mouse model generated by disrupting one allele of the *Scn1a* gene (*Scn1a*$^{-/+}$ mouse) recapitulates many aspects of the human pathology, including an initial asymptomatic period followed by the appearance of temperature-induced seizures, spontaneous seizures and sporadic death after the third postnatal week (Yu et al. 2006). Several studies investigated the pathogenic mechanisms leading to SMEI, focusing mainly on the early cellular dysfunctions that occur in the epileptogenic period. During the initial asymptomatic period, pyramidal neurons showed no differences in the voltage dependence of activation and inactivation of sodium channels in *Scn1a*$^{-/+}$ mice (Yu et al. 2006). Remarkably, however, both in cortical structures and cerebellum, GABAergic inhibitory interneurons exhibited a significant decrease in voltage-dependent sodium current, leading to reduced firing (Yu et al. 2006). These data agree with immunohistological evidence suggesting preferential expression of $Na_V1.1$ in interneurons (Ogiwara et al. 2007). Therefore, understanding how functional alterations of the $Na_V1.1$ channel are reflected in cortical network changes during the pre-epileptic period is fundamental to identify possible therapeutic avenues before the onset of this devastating disease.

In cortical structures, GABAergic interneurons are remarkably heterogeneous (Ascoli et al. 2008;DeFelipe et al. 2013): different interneuron types inhibit specific compartments of principal neurons, resulting in a highly specialized division of labor, governing all forms of cortical activity (Isaacson and Scanziani 2011). Accordingly, malfunctioning of specific GABAergic circuits often results in neurological and psychiatric symptoms (Le and Monyer 2013;Marin 2012;Lewis et al. 2011), such as those shown in SMEI patients (Dravet et al. 2005). In *Scn1a*$^{-/+}$ mice the excitability of both parvalbumin- (PV) and somatostatin- (SST) positive cells is reduced (Tai et al. 2014), suggesting that an altered excitability is shared among different interneuron subtypes. Moreover, selective disruption of

the *Scn1a* gene in PV-positive (Dutton et al. 2011) or SST-positive (Rubinstein et al. 2015) cells increased susceptibility to thermally-induced seizures.

Based on these findings, it was proposed that, during the epileptogenic period, reduced excitability of specific subclasses of interneurons represents the main cellular mechanism leading to SMEI. Given the crucial role of interneurons in sculpting cortical activity (Isaacson and Scanziani 2011), disruption of interneuron excitability is expected to result in major network alterations. However, cellular studies on *Scn1a* mutant mice were performed in brain slices, which, although allowing in-depth analyses of excitability and synaptic properties at single-cell level, are devoid of the constant intense activity typical of the living brain. Thus, the functional consequences of *Scn1a* deletion and of interneuron dysfunction on neuronal networks *in vivo* are still unknown.

To address this issue, we combined *in vivo* electrophysiological recordings, optogenetics and two-photon guided juxtasomal recordings with patch-clamp recordings from genetically-identified interneurons in brain slices from *Scn1a*$^{-/+}$ mice, focusing on the pre-epileptic period. Surprisingly, we found that spontaneous cortical dynamics were largely unchanged in anesthetized and awake *Scn1a*$^{-/+}$ animals compared to controls *in vivo*. Patch-clamp recordings in cortical slices confirmed PV- and SST-interneurons' reduced excitability upon current injections, and altered synaptic activity. However, these deficits were not paralleled by altered interneuronal firing during *in vivo* network activity. Importantly, acute and reversible reduction of PV- and SST-positive cell firing in control mice, invariably resulted in enhanced network activity. These findings suggest that reduced interneuronal excitability in *Scn1a*$^{-/+}$ animals is not the only alteration occurring during the pre-epileptic period and that additional mechanisms may play a role in homeostatic rearrangements and in the genesis of SMEI.

Materials and methods

Experiments involving animals were carried out in accordance with the guidelines established by the European Community Council Directive and approved by the National Council on Animal Care of the Italian Ministry of Health.

Animals

A mixed background line of mice (C57BL6:CD1) carrying a *SCN1A* gene ablation was used as in (Yu et al. 2006;Liautard et al. 2013). To disrupt the *SCN1A* gene, a replacement-type construct was targeted to the last coding exon (Yu et al. 2006;Liautard et al. 2013). Heterozygous mice and wild-type littermates (males or females) were selected for experiments. Age of mice was between postnatal day 16 to 18 (P16-P18), except for experiments displayed in figure 4 that were performed on P15-P18 mice. To identify PV- and SST-positive interneurons, the mouse line *Gt(ROSA)26Sortm14(CAG-tdTomato)Hze*/J (here called simply "Tomato"), that carries the floxed Td-Tomato sequence under the ubiquitous promoter ROSA26, was crossed with the *Pvalbtm1(cre)Arbr*/J (called "PV-Cre") mouse line, that expresses the Cre enzyme under the parvalbumin promoter or with the *Ssttm 2.1(c re)Zjh* /J (named "SST-Cre") that expresses the Cre enzyme under the somatostatin promoter, respectively. Double transgenic animals *Gt(ROSA)26Sortm14(CAG-tdTomato)Hze*/J / *Pvalbtm1(cre)A rbr*/Ja (named "PV-Tomato") and *Gt(ROSA)26Sortm14(CAG-tdTomato)Hze*/J / *Ssttm 2.1(cre)Zjh* /J ("SST-Tomato") were subsequently crossed with a $Na_V1.1$-KO heterozygous mouse to achieve the triple transgenic mice, WT-PV-Tomato or *Scn1a*$^{-/+}$-PV-Tomato, and WT-SST-Tomato or *Scn1a*$^{-/+}$-SST-Tomato, respectively. *Gt(ROSA)26Sortm14(CAG-tdTomato)Hze*/J (stock #007908), *Pvalbtm1(cre)Arbr*/J (stock #008069) and *Ssttm 2.1(cre)Zjh* /J (stock #13044) mouse lines were purchased from the Jackson Laboratory (JacksonLab, Bar Harbor, Maine).

In vivo Local Field Potential and Multi-Unit activity recording

Mice were anesthetized with 15% urethane (1,8 g / kg in physiological solution) and placed on a stereotaxic apparatus. The body temperature was constantly monitored and kept at 37 °C with a heating blanket. To ensure a deep and constant level of anesthesia, heartbeat, vibrissae movements, eyelid reflex, responses to tail and toe pinching were frequently controlled before and during the surgery. In some experiments, respiration rate and oxygen saturation were controlled by a pulseoxymeter (MouseOx, Starr Life Sciences Corp., Oakmont, PA). A local lidocaine injection was performed over the cranial area of interest and, after a few minutes, a longitudinal incision was performed to expose the skull. A small cranial window (< 1 mm) was opened at coordinates (0 mm bregma, 3.5 mm lateral to sagittal sinus), roughly corresponding to the somatosensory area of the cortex, while keeping the surface of the brain moist with the normal HEPES-buffered artificial cerebrospinal fluid (aCSF). The dura was carefully removed using a metal needle. For awake head-restrained recordings, mice were anesthetized with ketamine/xylazine (Ketaset, 100 mg / ml / Rompun 20 mg / ml; 10 ml / g body weight). Surgery was performed as described for the anesthetized condition, with the only difference that small metal plaque was sealed on the mouse head to ensure better mechanical stability. Mice were kept at controlled body temperature until awakening.

To record LFP and MUA signals bipolar custom-built tungsten electrodes (FHC Inc., Bowdoin, ME, distance between the tips ~ 300-350 µm, impedance 0,1 MOhm at 1 kHz) were inserted in the cortex. Electrical signals were acquired in the 0.1 – 5000 Hz band, amplified via an AM-amplifier (AM-system, Carlsborg, WA) and digitized at 25-50 kHz using a Digidata 1440 interface and PClamp software (Molecular Device, Sunnyvale, CA).

Slice preparation and patch-clamp recording

Animals were deeply anesthetized with urethane (1,8 g / kg) or Zoletil (40 mg / kg) and decapitated. The brain was quickly removed and immersed in the cold (4°C) "cutting solution" containing (in mM): 125 NaCl, 2.5 KCl, 1.25 NaH_2PO_4, 25 $NaHCO_3$, 2 $MgCl_2$, 1 $CaCl_2$, 25 glucose, 2 Na-pyruvate, 3 Myo-inositol and 0.4 ascorbic acid (pH 7.4, 95% O_2 / 5% CO_2). Coronal slices (300 µm thick) of neocortex were prepared with a vibratome (VT1000S, Leica Microsystems, GmbH, Wetzlar, Germany), incubated in cutting solution at 34°C for 30 min and then at room temperature for additional 30 minutes before transfer to the recording chamber. For experiments shown in Fig. 4 after dissection, the brain was transferred to ice-cold standard ACSF, sACSF (in mM 125 NaCl, 2.5 KCl, 2 $CaCl_2$, 1 $MgCl_2$, 25 glucose, pH 7.4 with 95% O2 / 5% CO_2). 350 µm-thick slices were cut in the solution described in (Dugue et al. 2005). Slices were then first transferred for 1 min in a 95% O_2 and 5% CO_2 saturated solution containing (in mM): 225 D-mannitol, 2.5 KCl, 1.25 NaH_2PO_4, 26 $NaHCO_3$, 25 glucose, 0.8 $CaCl_2$, 8 $MgCl_2$, 2 kynurenic acid with 95% O_2 / 5% CO_2, then transferred in sACSF at 30 °C for 20 min, and finally maintained at room temperature.

Recordings in Fig. 3, 5C, 6C, 7 and 8 were performed at 30-32 °C using an inline solution heater and a temperature controller (TC-344B, Warner Instruments, Hamden, CT, USA), while continuously perfusing the slices with aCSF bubbled with 95%O2 / 5% CO2 (pH 7.4). The aCSF contained (in mM): 125 NaCl, 2.5 KCl, 1.25 NaH_2PO_4, 25 $NaHCO_3$, 2 $MgCl_2$, 2 $CaCl_2$, 25 glucose. For experiments in Fig. 4, brain slices were continuously perfused at high rate with the following solution (in mM): NaCl, 120; KCl, 3.2; KH2PO4, 1; $NaHCO_3$, 26; $MgCl_2$, 0.5; $CaCl_2$, 2; glucose, 10; at pH 7.4 (with 95% O_2 / 5% CO_2).

Patch-clamp, whole-cell recordings in Fig. 3, 7, 8 were performed in the infragranular layers of the neocortex of WT and *Scn1a*$^{-/+}$ mice. Pyramidal neurons were visually identified using infrared video microscopy and characterized by large somata and pia-oriented apical dendrites. PV- and SST-positive interneurons were identified using Tomato fluorescence in triple transgenic mice (see previous section describing animals). To record spontaneous excitatory postsynaptic currents (sEPSCs, Fig. 7), glass electrodes (2.5 – 4 MOhm resistance) were filled with intracellular solution containing (in mM): 124 K-gluconate, 9 KCl, 10 Hepes, 1 EGTA, 2 $MgCl_2$, 4 MgATP, 0.3 Na_3GTP, pH adjusted to 7.2 with KOH, 280 – 300 mOsm. The estimated E_{Cl} was -60 mV based on the Nernst equation. sEPSC were recorded at an holding potential of -60 mV and were blocked by D-(-)-2-Amino-5-phosphonopentanoic acid (D-APV,50 µM) and 6,7-Dinitroquinoxaline-2,3-dione disodium salt (DNQX., 10 µM). All drugs were purchased from Tocris Bioscience (Bristol, UK). To record spontaneous inhibitory postsynaptic currents (sIPSCs, Fig. 8) and autaptic activity, electrodes were filled with intracellular solution containing (in mM): 70 K-gluconate, 70 KCl, 10 Hepes, 1 EGTA, 2 $MgCl_2$, 4 MgATP, 0.3 Na_3GTP, pH adjusted to 7.2 with KOH, 280 – 300 mOsm. This solution generates an inhibitory GABAergic inward current, because the Nernst equation predicts an E_{Cl} about -16 mV and recordings were performed at the holding potential of -70 mV. D-APV (50 µM) and DNQX (10 µM) were added to the aCSF during experiments to block excitatory neurotransmission. All recorded IPSCs were blocked by the $GABA_A$ receptor antagonist gabazine (12.5 µM). Both intracellular solutions were used to record membrane excitability (Fig. 3). Access resistance was monitored throughout the recordings and was typically < 20-25 MOhm. For experiments displayed in Fig. 4, the intracellular pipette solution was (in mM): K-gluconate, 145; $MgCl_2$, 2; EGTA, 0.5; Na_2ATP, 2; Na_3GTP, 0.2; HEPES, 10; to pH 7.2 with KOH, osmolarity, 305 – 315 mOsm. For experiments displayed in Fig. 5C, 6C, the intracellular pipette solution was (in mM): K-gluconate, 140; $MgCl_2$, 1; NaCl, 8; Na_2ATP, 2; Na_3GTP, 0.5; HEPES, 10; phosphocreatine, 10; to pH 7.2 with KOH, osmolarity, 295 – 310 mOsm. Data were not corrected for

the liquid junction potential. Signals were amplified and filtered using a Multiclamp 700B patch-clamp amplifier (Molecular Device, Sunnyvale, CA). Data were digitized at 50 kHz with a Digidata 1440 and PClamp software (Molecular Device, Sunnyvale, CA).

Ictal event generation

Ictal event induction experiments were performed in the presence of 4-AP (50-100 μM) or in the presence of 0 Mg^{2+} containing extracellular solution. A pressure ejection unit (PDES, NPI Electronics, Tamm, Germany) was used to apply a single or double pulse to the NMDA (1 mM, Sigma Aldrich, Milano, Italy)-containing pipettes with a 3 s interval, a pressure of 4–10 psi, and a duration of 200-600 ms. The NMDA-containing pipette was positioned in vicinity of the rhinal fissure. The epileptogenic focus was defined as the region up to 300 μm from the pipette tip where neurons were directly activated by NMDA (Gomez-Gonzalo et al. 2010), while the ictal propagating region is the region distant at least 400 μm from the NMDA-containing pipette tip. All pyramidal neurons recorded were at a distance of 1 mm from the NMDA-containing pipette tip.

Virus injection

Stereotaxic injection of AAVflex.CBA.Arch-GFP.WPRE.SV40 (Penn Vector Core, Philadelphia, PA) was performed in the cortex of PV-Cre and SST-Cre mice at P0 (P0 was considered as the day of birth). Pups were deeply anesthetized by hypothermia and immobilized on a customized stereotaxic apparatus. A small skin incision was performed along midline and viruses were injected with a glass micropipette in the somatosensory area of the cortex. Stereotaxic coordinates for injections were: 0 mm bregma, 1.5 mm lateral to sagittal sinus, and 0.25-0.3 mm depth. Approximately 200-300 nl of virus was slowly delivered into the brain for each animal. At the end the injection, the pipette was slowly

withdrawn, the skin carefully sutured, and the pups quickly warmed and revitalized under a heating infrared lamp. Electrophysiological experiments were performed at 3-4 weeks after the injection.

Optogenetic stimulation

Optical stimulation of Arch was achieved using a 594 nm solid-state laser source (Cobolt, Vretenvägen, Sweden). The laser was controlled by a command voltage, via an analog signal using an acousto-optic modulator (Gooch & Housego, USA). Light pulses were delivered to the brain through an optical fiber (200 µm diameter, amsTechnologies, Milan, Italy) which was located as close as possible to the surface of the brain slice (Fig. 5C and 6C) or to the surface of the brain (Fig. 5D-E and Fig. 6D-E). For combined electrophysiological and optogenetic experiments *in vivo*, the fiber was placed parallel to the recording bipolar electrode to minimize optical artifacts (Cardin et al. 2010). To gradually modulate the effect of the optogenetic perturbation on the firing properties of interneurons, light intensity was titrated through the use of neutral density filters (placed in the optical path between the laser source and the fiber optic) and ranged between ~ 3 and 30 mW (measured at the fiber tip). Light pulse duration was 500 milliseconds in all experiments displayed in figures 5-6.

Two-photon targeted juxtasomal recording

A laser scanning Ultima scanhead (Bruker Italia, Milan, Italy) coupled with an Ultra II Cameleon laser source (Coherent Italy, Milan, Italy) was used to monitor Tomato fluorescence using 720 nm light wavelength. Animal preparation was performed as described previously but without removing the dura. Electrophysiological juxtasomal recordings were performed with borosilicate glass pipettes (2 mm outer diameter, 3 – 7 MOhm resistance in brain tissue) which were filled with extracellular solution containing: NaCl 127 mM, KCl 3.2 mM, $CaCl_2$ 2mM, $MgCl_2$ 1mM, Hepes 10 mM, and Alexa Fluor 488, pH 7.4. Pipettes were initially lowered through the pia applying a positive pressure (250 mbar)

until the depth of interest (150-300 µm) was reached. At this point, a lower positive pressure (25 mbar) was applied. Based on the fluorescence image of Tomato-positive cells and of Alexa Fluor 488, the pipette was slowly moved towards the target cell. When a contact between the pipette and the fluorescent cell was achieved, the positive pressure was released and a dim negative pressure was applied to facilitate the formation of the juxtasomal recording configuration (resistance 40-400 MOhm). Electrical signals were amplified by an ELC-01X amplifier (npi electronic, Tamm, Germany), digitized by an ITC-18 interface (InstruTECH Corporation, Port Washington, NY) and acquired using Patchmaster (HEKA Elektronik, Lambrecht, Germany).

Immunohistochemistry and confocal image acquisition

Under deep urethane anesthesia, animals were transcardially perfused using 0.01 M PBS pH 7.4, followed by 4% paraformaldehyde (PFA) in PBS. Brains were subsequently removed, post fixed for six hours in PFA, incubated in a 30% sucrose PBS solution for cryoprotection and finally cut with a cryostat (Leica Microsystems Italia, Milan, Italy) in coronal slices of 40 µm thickness. Floating slices from fluorescent tissue (Fig. 2) were collected, mounted on glass slides using Vectashield (Vector Laboratories, Peterborough, UK) or [1,4-diazobicyclo-(2,2,2)octane] (DABCO)-based antifade mounting medium and coverslipped. For immunofluorescence staining (Fig. 2, 5A-B and 6A-B) floating sections were incubated for at least 24 hours at 4ºC in primary antibody diluted in 5% NGS in 0.3 % Triton-X 100 in PBS. After washing in PBS, the slices were incubated in 0.3 % Triton-X 100 in PBS for 2 hours at room temperature in the appropriate secondary antibody. Some sections were then stained with Hoechst for 30 min at room temperature, and mounted on glass slides using DABCO-based antifade mounting medium. Primary antibodies used were: anti-GABA (1:1000, rabbit, Sigma A2052); anti-Somatostatin (1:100, rat, Millipore MAB354); anti-Parvalbumin (1: 1000, mouse, Sigma P3088). Secondary antibodies used were: Alexa 488 (1:800, goat anti-rabbit, Invitrogen A11034);

Alexa 647 (1:800, goat anti-rabbit, Invitrogen A21245); Alexa 647 (1:800 goat anti-mouse, Invitrogen A21236).

Data analysis

Analysis of LFP and MUA signals was performed using customized Matlab code (Matlab, Natick, MA). For LFP analysis, extracellular potentials were down-sampled (1 kHz) and low-pass filtered (cut-off frequency, 100 Hz). A power spectrum was generated for each recorded animal using a hamming window (window length: 4096 points, 50% overlap) on recording traces of ~ 5-10 minutes duration. Power spectra were normalized to the total signal power in the 0.1-100 Hz interval. In the normalized spectra, power values corresponding to different frequency bands (0.5-1 Hz, slow oscillations; 2-4 Hz, delta oscillations; 4-8 Hz, theta oscillations; 8-14 Hz, alpha-spindles; 30-90 Hz, gamma oscillations) were calculated for both WT and *Scn1a*$^{-/+}$ mice. For MUA analysis, extracellular signals were high-pass filtered (cut-off frequency, 300 Hz) and thresholded according to a value set five times the standard deviation of the baseline signal (baseline). The baseline was chosen as a time window of > 0.5 s where no extracellular spikes occurred. Spontaneous down- to up-state transitions were identified as the time point in which the signal crossed the threshold. Up- to down-state transitions were identified as the time points in which the MUA signal crossed the threshold and remained below the threshold for longer than 100 ms. Up- and down-state durations were calculated from the time of the down-to-up and the up-to-down transitions. Up-states shorter than 10 ms were not considered true up-states. Spikes were identified using a first-derivative spike-sorting algorithm.

In Fig. 4 the recruitment of principal neurons into propagating ictal events was marked by the transition from the predominant inhibitory to the predominant excitatory phase (t_{IE}), which was defined as the timing in which the ratio between the inhibition and the excitation index was for the first time less than

0.1. Inhibition and excitation indices were calculated, respectively, as the part of the positive and the negative component of the time derivative of the trace which exceeded five times the mean standard deviation evaluated during the baseline (Cammarota et al. 2013). Ictal event duration in voltage-clamp recordings was calculated from the t_{IE} to the end of the last afterdischarge recorded with an instant frequency higher than 0.1 Hz.

For the optogenetic experiments (Fig. 5D-E and 6D-E), three temporal windows were considered: 100 ms before the light stimulation, 500 ms during the laser stimulus, and 100 ms after the light illumination. At least 6 sweeps for each experiment were analyzed. The spectral content of the LFP signal was quantified by calculating the short-time Fourier transform over a moving Hamming window of 100 ms. Power values were normalized to the total power in the "pre" period.

For experiments in figure 9-10, to obtain the spike train we first applied a high-pass filter to the mean-subtracted juxtasomal signal (Kaiser filter with zero phase-lag and 0.5 Hz bandwidth, small passband ripple, 0.05 dB, and high stopband attenuation, 60 dB, cut-off frequency, 100 Hz). We then used a detection threshold. Depending on the noise level, the threshold varied across cells resulting in a mean value for PV-positive and SST-positive cells of 7.3 and 9.4 times the standard deviation of the filtered juxtasomal signal, respectively. The inter-spike-interval (ISI, Fig. 9D and 10D) was defined as the time interval between two consecutive APs, while the coefficient of variations of the ISI (CV_{ISI}) was defined as the ratio of the standard deviation to the mean of the ISI distribution.

In brain slice experiments, the average frequency of APs (Fig. 3B, D, F) was calculated for increasing depolarizing current injections (50 pA step, 600 ms duration). The input resistance (R_{in}, table 1) was calculated from hyperpolarizing current injections; AP threshold was measured at the inflection point

of rising phase of the AP; AP amplitude was measured between the threshold and the AP peak; AP duration was measured at half height between threshold and peak; the AP rise time was calculated as the difference between the time occurrence of the AP threshold and the time of the AP maximum positive peak; the AP after-hyperpolarization (AHP) amplitude was computed between the threshold and the minimum negative peak of the AP; AHP duration was calculated between the time of occurrence of the AP threshold and the time of occurrence of the minimal AP peak. Autaptic currents were elicited in the voltage-clamp configuration by a short voltage depolarization (from a holding potential of -70 to 0 mV, 0.3 - 1.0 ms duration) as in (Bacci and Huguenard 2006). Autaptic currents were blocked by application of gabazine (12.5 μM) and their amplitude was measured at the peak. In combined electrophysiological and optogenetic experiments (Fig. 5C and 6C), the frequency of APs was calculated in a time window of 350 ms before and after the light stimulus and in a time window of 500 ms during light stimulation. Detection of spontaneous excitatory and inhibitory postsynaptic currents (sEPSCs and sIPSCs) was performed with Minianalysis (Synaptosoft Inc., Fort Lee, NJ) using a threshold criterion, setting the threshold at three times the standard deviation of the baseline noise. Detected events were visually inspected and artifactual events removed. The median of the distribution of amplitudes and inter-event-intervals (IEIs) for both sEPSCs and sIPSCs was calculated for each recorded cell. Mean values provided in the result section were calculated by averaging the medians across cells. Offline analysis was carried out with Clampfit 10.2, application of pClamp 10.2 (Molecular Device, Sunnyvale, CA), MiniAnalysis (Synaptosoft, Decatur, GA) and Origin 8.6 (OriginLab Corporation, Northampton, MA).

Statistics

Values are expressed as mean ± SEM. To evaluate normality, a Kolmogorov-Smirnov normality test was run on each experimental sample. When comparing two populations of data, Student's *t*-test was

used to calculate statistical significance in case of Gaussian distribution, otherwise the non-parametric Mann-Whitney test was used. This choice reflects the standard practice in statistics (Box et al. 2005) to use the parametric test (that has more statistical power) whenever the appropriate conditions are applicable, and to use a more general, but less statistically sensitive, test when the conditions for applying the parametric test are not met. When multiple populations of data were compared, one- or two-way ANOVA with Bonferroni *post hoc* tests were used in case of Gaussian distribution. The non-parametric Friedman with Dunn *post hoc* test was used in Fig. 5D, 6C, 6D. The Kolmogorov-Smirnov test for experiments in figure 9C, 9E, 10B, 10D. All tests were two-sided.

Results

Cortical network activities in WT and Scn1a$^{-/+}$ mice in vivo

We performed extracellular Local Field Potential (LFP) and Multi-Unit Activity (MUA) recordings in the deep regions (~ 700 µm) of the neocortex of urethane-anesthetized WT and heterozygous *Scn1a*$^{-/+}$ mice during the pre-epileptic period (P16-P18, Fig. 1). Under this type of anesthesia, neocortical circuits are spontaneously active (Crunelli and Hughes 2010). A main component of these intrinsic activities is the slow oscillation (Metherate et al. 1992;Steriade et al. 1993a;Steriade et al. 1993c;Steriade et al. 1993b). This rhythm is observed both at the level of individual cells (Steriade et al. 1993c;Petersen et al. 2003b), and mass signals (Steriade et al. 1993a). During the slow oscillation neurons alternate between an up-state, characterized by elevated firing, and a down-state, characterized by neuronal silence (Steriade et al. 1993a;Steriade 2006). As expected, spontaneous network activity in WT and heterozygous *Scn1a*$^{-/+}$ mice was dominated by this rhythmic activity (Fig. 1B). LFP recordings were quantified by calculating the signal power in different frequency bands (see Materials and Methods) and comparison between WT and *Scn1a*$^{-/+}$ mice was performed (Fig. 1C). *Scn1a*$^{-/+}$ mice

displayed no significant change in the power of slow (frequency interval: 0.5-1 Hz), delta (2-4 Hz), theta (4-8 Hz), alpha/spindles (8-14 Hz) and gamma (30-90 Hz) oscillations compared to the WT controls. Average normalized power values: 0.36 ± 0.02 *vs* 0.36 ± 0.02 (p = 0.75, Mann-Whitney test) for the 0.5-1 Hz interval for WT and *Scn1a*$^{-/+}$ mice, respectively; 0.08 ± 0.01 *vs* 0.07± 0.01 (p = 0.48, Mann-Whitney test) for the 2-4 Hz interval; 0.035 ± 0.005 *vs* 0.027 ± 0.003 (p = 0.54, Mann-Whitney test) for the 4-8 Hz interval; 0.019± 0.003 *vs* 0.014 ± 0.002 (p = 0.42, Mann-Whitney test) for the 8-14 Hz interval; 0.011 ± 0.002 *vs* 0.008 ± 0.001 (p = 0.63, Mann-Whitney test) for the 30-90 Hz interval. N = 18 animals for WT, N = 17 animals for *Scn1a*$^{-/+}$ mice. We further quantified spontaneous network dynamics by analyzing the MUA signal, which mainly reflected the supra-threshold activity of neurons (Logothetis 2003), and we found no significant differences of spike activity between the two genotypes. Average values of up-state parameters were: up-state frequency, 0.91 ± 0.08 Hz *vs* 0.93 ± 0.06 Hz (p = 0.8, unpaired Student's *t*-test) for WT and *Scn1a*$^{-/+}$ mice; average up-state duration, 0.29 ± 0.04 s *vs* 0.23 ± 0.02 s (p = 0.18 , unpaired Student's *t*-test) for WT and *Scn1a*$^{-/+}$ mice; average down-state duration: 1.09 ± 0.26 s *vs* 0.97 ± 0.12 s (p = 0.90, Mann-Whitney test) for WT and *Scn1a*$^{-/+}$ mice; average number of spikes per up-state: 45 ± 9 *vs* 31 ± 6 (p = 0.30, Mann-Whitney test) for WT and *Scn1a*$^{-/+}$ mice. WT, N = 17; *Scn1a*$^{-/+}$, N = 19.

Given the heterogeneity in cortical circuits across different tissue depth (Adesnik and Scanziani 2010;Beltramo et al. 2013;Feldmeyer 2012), we asked whether disrupting the *Scn1a* gene could have different effects on deep *vs* more superficial cortical regions. To tackle this question, we repeated the extracellular recordings described previously at ~ 300 μm depth. Besides a small, but significant, decrease in the average power of oscillations in the delta (2-4 Hz) and theta (4-8 Hz) frequency band, the LFP signal was largely unaffected in superficial cortical areas in *Scn1a*$^{-/+}$ mice compared to

controls, as observed in deeper regions (Fig. 1B-C). Average normalized power values: 0.30 ± 0.02 *vs* 0.33 ± 0.02 (p = 0.22, Mann-Whitney test) for the 0.5-1 Hz interval for WT and *Scn1a*$^{-/+}$ mice, respectively; 0.11 ± 0.01 *vs* 0.08 ± 0.01 (p = 0.004, Mann-Whitney test) for the 2-4 Hz interval; 0.06 ± 0.01 *vs* 0.04 ± 0.01 (p = 0.02, Mann-Whitney test) for the 4-8 Hz interval; 0.05 ± 0.01 *vs* 0.04 ± 0.01 (p = 0.13, Mann-Whitney test) for the 8-14 Hz interval; 0.029 ± 0.004 *vs* 0.020 ± 0.004 (p = 0.14, Mann-Whitney test) for the 30-90 Hz interval. N = 18 animals for WT, N = 16 animals for *Scn1a*$^{-/+}$ mice. Analysis of the MUA signal in recordings performed at ~ 300 microns depth confirmed unaltered up-state frequency, up-state duration, down-state duration and number of spikes per up-state in *Scn1a*$^{-/+}$ compared to WT mice. Average up-state frequency: 0.74 ± 0.07 Hz *vs* 0.62 ± 0.05 Hz (p = 0.13, Mann-Whitney test) for WT and *Scn1a*$^{-/+}$ mice; average values of up-state duration: 0.22 ± 0.03 s *vs* 0.20 ± 0.01 s (p = 0.95, Mann-Whitney test); average values of down-state duration: 1.48 ± 0.30 s *vs* 1.60 ± 0.15 s (p = 0.08, Mann-Whitney test); average number of spikes per up-state: 25 ± 6 *vs* 21 ± 3 (p = 0.99, Mann-Whitney test). WT, N = 17; *Scn1a*$^{-/+}$, N = 18.

Since urethane has diffuse effects on both inhibitory and excitatory neurotransmission (Petersen et al. 2003a;Dombeck et al. 2007), anesthesia could potentially mask the effect of disrupting the *Scn1a* gene by inducing abnormal circuits dynamics. To address this concern, we repeated the experiments displayed in Fig. 1B-C in awake, head-restrained mice placing the metal electrodes initially in deep cortical regions (~ 700 μm). As shown in Fig. 1D-E, under these experimental conditions network activities were different from those observed under urethane anesthesia (Fig. 1B-C). The LFP was dominated by small amplitude, high frequency oscillations that were in contrast with the large amplitude, low frequency oscillations observed in the anesthetized condition. However, similarly to the anesthetized condition, no significant differences were detected in the LFP signal in *Scn1a*$^{-/+}$ mice

compared to controls. Average normalized power values: 0.19 ± 0.02 *vs* 0.17 ± 0.01 (p = 0.36, unpaired Student's *t*-test) for the 2-4 Hz interval for WT and *Scn1a*$^{-/+}$ mice, respectively; 0.095 ± 0.008 *vs* 0.097 ± 0.007 (p = 0.84, unpaired Student's *t*-test) for the 4-8 Hz interval; 0.052 ± 0.004 *vs* 0.052 ± 0.005 (p = 0.95, unpaired Student's *t*-test) for the 8-14 Hz interval; 0.027 ± 0.004 *vs* 0.023 ± 0.001 (p = 0.37, unpaired Student's *t*-test) for the 30-90 Hz interval. N = 15 animals for both WT and *Scn1a*$^{-/+}$ mice. The lower frequency band (0.5-1 Hz) was excluded in this analysis because of the larger movement artifacts in the awake compared to the anesthetized animal preparation, which mainly affected the lower frequency band (< 1Hz). Recordings in more superficial cortical regions (~ 300 μm depth) confirmed no significant difference in the signal power in any frequency band that was analyzed in *Scn1a*$^{-/+}$ mice compared to controls. Average normalized power values: 0.15 ± 0.02 *vs* 0.14 ± 0.02 (p = 0.58, unpaired Student's *t*-test) for the 2-4 Hz interval for WT and *Scn1a*$^{-/+}$ mice, respectively; 0.08 ± 0.01 *vs* 0.08 ± 0.01 (p = 0.97, unpaired Student's *t*-test) for the 4-8 Hz interval; 0.06 ± 0.01 *vs* 0.06 ± 0.01 (p = 0.98, unpaired Student's *t*-test) for the 8-14 Hz interval; 0.027 ± 0.004 *vs* 0.028 ± 0.005 (p = 0.88, unpaired Student's *t*-test) for the 30-90 Hz interval. N = 15 animals for both WT and *Scn1a*$^{-/+}$ mice.

Decreased excitability of specific classes of interneurons in brain slices from Scn1a$^{-/+}$ *mice*

Previous studies pointed to the dysfunction in interneuronal excitability as the main cellular alteration leading to SMEI (Yu et al. 2006;Ogiwara et al. 2007;Cheah et al. 2012;Han et al. 2012). Given that interneuronal firing tightly controls the output of principal cells (Isaacson and Scanziani 2011;Sohal et al. 2009;Cardin et al. 2009;Freund and Katona 2007), it is somewhat surprising to observe no difference in spontaneous network activities in *Scn1a*$^{-/+}$ mice *in vivo* (Fig. 1). We thus decided to directly measure the excitability of interneurons in our experimental model, focusing on two main

subpopulations: PV- and SST-expressing cells, which account for ~ 70% of the total interneuronal population in the cortex (Rudy et al. 2011). To identify PV- and SST-positive interneurons in WT and *Scn1a*$^{-/+}$ mice, we generated triple transgenic animals expressing the red fluorescent protein Td-Tomato (Tomato) specifically in these cellular subtypes (Fig. 2). Floxed Tomato mice were crossed with either the PV-Cre mouse line that expressed the Cre enzyme under the PV promoter, or with the SST-Cre line that expressed the Cre enzyme under the SST promoter. Heterozygous double transgenic animals were then crossed with *Scn1a*$^{-/+}$ mice to achieve WT-PV-Tomato (Fig. 2A-B) or *Scn1a*$^{-/+}$-PV-Tomato (Fig. 2C-D) and WT-SST-Tomato (Fig. 2E-F) or *Scn1a*$^{-/+}$-SST-Tomato (Fig. 2G-H) mice, respectively. These animals were then used for patch-clamp experiments in slices (Fig. 3) from the somatosensory cortex at P16-P18 (the same cortical region and the same time interval used for *in vivo* recordings). We first performed recordings from pyramidal neurons which were visually identified with differential interference contrast. All recorded cells had a regular firing discharge pattern (Fig. 3A) and a main apical dendrite, which was visible under the microscope, all features that are typical of pyramidal cortical neurons (Contreras 2004). In current-clamp configuration, we recorded the membrane potential response to hyperpolarizing and depolarizing current injections. The average frequency of action potentials (APs) discharged at a given current injection was similar between WT and *Scn1a*$^{-/+}$ mice (Fig. 3B, interaction, $p > 0.99$, two-way repeated measures ANOVA with Bonferroni *post hoc* test, N = 27 cells for both WT and *Scn1a*$^{-/+}$), as were the biophysical properties of recorded neurons (Table 1). We then recorded from Tomato-positive neurons in WT-PV-Tomato and *Scn1a*$^{-/+}$-PV-Tomato transgenic mice (Fig. 3C). In WT-PV-Tomato (simply called WT in Fig. 3C-D), fluorescent cells displayed the typical features of fast spiking PV-positive interneurons (Ascoli et al. 2008;DeFelipe et al. 2013), including high frequency of AP firing, small adaptation and low input resistance (Fig. 3C, table 1). However, in *Scn1a*$^{-/+}$-PV-Tomato mice (simply called *Scn1a*$^{-/+}$ in Fig. 3C-D) the discharge pattern of fluorescent cells was deeply affected compared to WT controls. Cells displayed a delayed or

stuttering fast-spiking behavior, which resulted in decreased average frequency of AP firing upon current injections (Fig. 3C-D, interaction, $p < 1E\text{-}5$, two-way repeated measures ANOVA with Bonferroni *post hoc* test, N = 21 and 28 cells for WT and *Scn1a*$^{-/+}$, respectively). We finally performed recordings from Tomato-positive neurons in WT-SST-Tomato transgenic mice. We found that fluorescent cells displayed substantial adaptation in their AP firing, higher input resistance and longer spikes compared to fluorescent cells in PV-Tomato animals (Fig. 3E, table 1), all features that are typical of SST cells. In *Scn1a*$^{-/+}$-SST-Tomato mice, fluorescent cells had similar electrophysiological properties, although the average frequency of APs discharged upon current injection was significantly decreased for higher values of current injections in cells from these mice compared to controls (Fig. 3E-F, interaction, $p < 1E\text{-}5$, two-way repeated measures ANOVA with Bonferroni *post hoc* test, N = 25 and 28 cells for WT and *Scn1a*$^{-/+}$, respectively).

Faster propagation of focal ictal discharges in slices from Scn1a$^{-/+}$ *mice.*

The decrease in interneuronal firing of inhibitory cells observed in *Scn1a*$^{-/+}$ mice may alter the propensity to generate epileptiform activity. To test this possibility, we probed cortical networks of WT and *Scn1a*$^{-/+}$ mice with local applications of NMDA (Fig. 4) that resulted in generation and propagation of focal seizure-like, ictal discharges (Losi et al. 2010;Gomez-Gonzalo et al. 2010). NMDA was initially applied in the presence of the proconvulsant 4-aminopyridine (4-AP) (Losi et al. 2010;Gomez-Gonzalo et al. 2010). By using patch-clamp recordings from pyramidal neurons, we monitored the ictal discharge propagation at 1 mm from the focal area (the NMDA application site). We found that, in slices from *Scn1a*$^{-/+}$ mice, local NMDA applications evoked in pyramidal neurons long-lasting ictal events characterized by the typical tonic/clonic transition phase that had similar duration as the ictal events evoked in cortical slices from WT mice (Fig. 4A, average ictal duration, 78 ± 8 s *vs* 74 ± 10 s; N = 38 events from 12 *Scn1a*$^{-/+}$ mice and N = 24 events from 11 WT mice; $p = 0.72$, unpaired Student's *t*-

test). However, ictal events recorded in *Scn1a*$^{-/+}$ mice occurred after the NMDA pulse application with a delay significantly shorter than in WT mice (Fig. 4C, left histogram, p = 2.7E-5, Mann-Whitney test and Fig. 4D). We repeated similar experiments in a different model of ictal generation, in which we applied the NMDA pulses while perfusing the slice with a nominally Mg^{2+} free extracellular solution (0 Mg^{2+}). Also under these experimental conditions, the onset of the ictal event in the pyramidal neurons distant from the focus occurred with a shorter delay in *Scn1a*$^{-/+}$ mice with respect to WT controls (Fig. 4C, right histogram, p = 0.023, unpaired Student's *t*-test.). Consistent with this shorter delay, the number of the pre-ictal inhibitory barrages, which are evoked in pyramidal neurons mainly by parvalbumin-expressing fast spiking interneurons (Cammarota et al. 2013), was reduced in *Scn1a*$^{-/+}$ with respect to WT mice (5 ± 1 *vs* 11 ± 1, N = 17 ictal events from 4 *Scn1a*$^{-/+}$ mice and N = 17 ictal events from 5 WT mice; p = 2.5E-3, unpaired Student's *t*-test).

Acute inhibition of PV- and SST-positive interneurons fails to mimic the Scn1a$^{-/+}$ *phenotype*

I*n vivo* experiments in both anesthetized and awake animals showed no major changes in spontaneous network activities in *Scn1a*$^{-/+}$ mice (Fig. 1). These *in vivo* results seem difficult to interpret in light of the significant cell-specific dysfunction observed in slice recordings (Fig. 3). One possibility is that a reduction in the excitability of PV- and SST-interneurons *in vivo* does not significantly alter spontaneous, non-epileptic network dynamics. To test this hypothesis directly, we acutely decreased the firing activities of PV- and SST-positive interneurons *in vivo* using inhibitory optogenetic manipulations and light titration (see Materials and Methods). We expressed the inhibitory opsin Archaerhodopsin (Arch) specifically in PV- or SST-positive interneurons by injecting adeno-associated viruses carrying a double-floxed Arch sequence in PV-Cre (Fig. 5) or SST-Cre (Fig. 6) WT animals, respectively. Immunohistological analysis confirmed that the majority of opsin-positive cells stained for GABA both in PV-Cre (Fig. 5B) and SST-Cre (Fig. 6B) animals. Moreover, using intracellular

patch-clamp recordings in brain slices, we confirmed that illumination with yellow light (λ = 594 nm) significantly reduced AP firing in both PV-Cre (Fig. 5C, p = 0.022, one-way repeated measures ANOVA test with Bonferroni *post hoc* test) and SST-Cre (Fig. 6C, p = 2.3E-5, Friedman test with Dunn's *post hoc* test) injected animals.

We then investigated the effect of acutely reducing AP firing in PV- and SST-positive cells on spontaneous network dynamics by combining extracellular recordings with optogenetic photoinhibition in awake head-restrained mice. We delivered pulses of yellow light (stimulus duration of 500 ms) to the cortical surface through an optical fiber. In injected PV-Cre and SST-Cre animals, yellow light illumination reliably affected ongoing cortical activities. In all injected PV-Cre mice (N = 11), light illumination led to large alterations in the LFP that started after light onset and ended at light cessation (Fig. 5D, top). The power of most LFP frequencies increased as shown in the corresponding spectrogram (Fig. 5D, bottom), especially in the gamma band (Fig. 5E, p < 1E-4, Friedman test with Dunn's Multiple Comparison test). In animals expressing Arch in SST-positive interneurons, yellow light illumination also caused a change in the ongoing circuit activities recorded with the LFP. High frequency oscillations were significantly increased upon yellow light illumination (Fig. 6D-E, p = 3E-4, Friedman test with Dunn's Multiple Comparison test). At the end of the light stimulation, a period of low oscillatory activity was observed (Fig. 6D). This latter finding is compatible with the rebound firing activity that characterizes a subpopulation of SST-positive cells following membrane hyperpolarization (Ascoli et al. 2008;DeFelipe et al. 2013).

Synaptic changes in Scn1a$^{-/+}$ mice

Optogenetic experiments described previously (Fig. 5-6) demonstrate that acute silencing of PV- or SST-positive interneurons did not mimic the phenotype of *Scn1a*$^{-/+}$ mice, suggesting that, besides

reduced excitability of interneurons, additional mechanisms may come into play and account for the unaltered network activity observed *in vivo* (Fig. 1). One possibility is that interneuronal dysfunction is counterbalanced by changes in synaptic properties. To address this hypothesis, we investigated excitatory and inhibitory synaptic currents in cortical slices from WT and *Scn1a*$^{-/+}$ animals. We first recorded spontaneous excitatory postsynaptic currents (sEPSCs) from pyramidal (Fig. 7A-B), PV-positive (Fig. 7C-D) and SST-positive (Fig. 7E-F) cells. We found that the amplitude of sEPSCs was significantly increased in pyramidal cells (Fig. 7B, left panel; average amplitude: 10.7 ± 0.6 pA *vs* 8.2 ± 0.4 pA for N = 10 cells in *Scn1a*$^{-/+}$ mice and N = 7 cells in WT mice, respectively, p = 9.9E-3, unpaired Student's *t*-test), while sEPSC amplitude was unchanged in PV-positive cells (Fig. 7D, left panel; average amplitude: 18.5 ± 0.7 pA *vs* 16.2 ± 1.1 pA, p = 0.10, unpaired Student's *t*-test, N = 7 cells for both *Scn1a*$^{-/+}$ and WT) and SST-positive interneurons (Fig. 7F, left panel; average amplitude: 13.8 ± 3.2 pA *vs* 12.2 ± 1.7 pA, p = 0.94, Mann-Whitney test, N = 6 cells for both *Scn1a*$^{-/+}$ and WT). The Inter-Event Interval (IEI) of sEPSCs was not significantly different in pyramidal cells (Fig. 7B, right panel; average IEI: 0.14 ± 0.04 s *vs* 0.19 ± 0.04 s in N = 10 cells in *Scn1a*$^{-/+}$ mice and N = 7 cells in WT mice, respectively, p = 0.11, Mann-Whitney test), PV-positive cells (Fig. 7D, right panel; average IEI: 0.050 ± 0.010 s *vs* 0.029 ± 0.003 s, p = 0.08, unpaired Student's *t*-test, N = 7 cells for both *Scn1a*$^{-/+}$ and WT) and SST-positive cells (Fig. 7F, right panel; average IEI: 0.17 ± 0.02 s *vs* 0.17 ± 0.05 s, p = 0.98, unpaired Student's *t*-test, N = 6 cells for both *Scn1a*$^{-/+}$ and WT). We then recorded spontaneous inhibitory postsynaptic currents (sIPSCs, Fig. 8) and found that their amplitude was significantly increased in PV-positive cells (Fig. 8D, left panel; average amplitude: 34.5 ± 4.6 pA *vs* 21.0 ± 2.5 pA for N = 8 cells in *Scn1a*$^{-/+}$ mice and N = 8 cells in WT animals, respectively, p = 0.02, unpaired Student's *t*-test), while it was unchanged in pyramidal neurons (Fig. 8B, left panel; average amplitude: 17.5 ± 1.8 pA *vs* 17.6 ± 1.6 pA, p = 0.97, unpaired Student's *t*-test, N = 8 cells for both *Scn1a*$^{-/+}$ and WT) and SST-positive cells (Fig. 8F, left panel; average amplitude: 15.6 ± 1.1 pA *vs* 13.6

± 1.2 pA, p = 0.24, unpaired Student's *t*-test, N = 8 cells for both *Scn1a*$^{-/+}$ and WT). The IEI of sIPSCs was unaffected in pyramidal neurons (Fig. 8B, right panel; average IEI: 0.17 ± 0.04 s *vs* 0.17 ± 0.03 s for N = 8 cells in *Scn1a*$^{-/+}$ mice and N = 8 cells in WT animals, respectively, p = 0.96, unpaired Student's *t*-test), PV-positive cells (Fig. 8D, right panel; average IEI: 0.15 ± 0.03 s *vs* 0.16 ± 0.04 s, p = 0.88, unpaired Student's *t*-test, N = 8 cells for both *Scn1a*$^{-/+}$ and WT) and SST-positive cells (Fig. 8F, right panel; average IEI: 0.38 ± 0.06 s *vs* 0.38 ± 0.06 s, p = 0.95, unpaired Student's *t*-test, N = 8 cells for both *Scn1a*$^{-/+}$ and WT). Moreover, the amplitude of GABAergic autaptic currents onto PV-positive interneurons was also significantly increased in slices from *Scn1a*$^{-/+}$ mice compared to controls (data not shown; average amplitude of autaptic GABAergic current: 475 ± 99 pA *vs* 211 ± 97 pA, p = 0.02, Mann-Whitney test, N = 15 for *Scn1a*$^{-/+}$ mice and N = 14 for WT, respectively).

Spontaneous firing activities of individual interneurons in vivo

The decreased firing rate in interneurons upon somatic current injections that we observed in slices from *Scn1a*$^{-/+}$ mice (Fig. 3) is larger for higher values of current injections, especially in SST-positive interneurons (Fig. 3F). It is important to understand whether these changes in interneuronal excitability are also detected in the intact brain, where cells are driven to fire by physiological synaptic currents. To this aim, we recorded the firing of individual, genetically identified interneurons *in vivo* during spontaneous network activities. We first targeted PV-positive neurons. We performed two-photon-guided juxtasomal recordings in anesthetized WT-PV-Tomato (simply called WT in Fig. 9) and *Scn1a*$^{-/+}$-PV-Tomato (called *Scn1a*$^{-/+}$). Using two-photon microscopy, we visualized individual Tomato-positive cells and recorded their firing activity in juxtasomal configuration (Fig. 9B). Fig. 9C displays the distributions of average firing rates in all the recorded cells in WT (left) and *Scn1a*$^{-/+}$ (right) mice, which were not significantly different (p = 0.16, N = 15 WT and N = 14 *Scn1a*$^{-/+}$ animals, Kolmogorov-Smirnov test). The average distributions of inter-spike intervals (ISI, Fig. 9D, interaction

ISI bin-transgene p = 0.16, N = 32 WT and N = 34 *Scn1a*$^{-/+}$ animals, two-way repeated measures ANOVA) and the distributions of the coefficient of variation of the ISI (CV_{ISI}, Fig. 9E, p = 0.15, N = 15 WT and N = 14 *Scn1a*$^{-/+}$ animals, Kolmogorov-Smirnov test) were also not significantly different between WT and *Scn1a*$^{-/+}$.

We then recorded from SST-positive interneurons (Fig. 10). The distributions of average firing rates in all the recorded cells in WT and *Scn1a*$^{-/+}$ mice were not significantly different (Fig. 10B, p = 0.97, N = 12 WT and N = 11 *Scn1a*$^{-/+}$ animals, Kolmogorov-Smirnov test). The average ISI distributions (Fig. 10C, interaction ISI bin-transgene p = 0.96, N = 27 WT and N = 21 *Scn1a*$^{-/+}$ animals, two-way repeated measures ANOVA) and the distributions of CV_{ISI} (Fig. 10D, p = 0.22, N = 12 WT and N = 11 *Scn1a*$^{-/+}$ animals, Kolmogorov-Smirnov test) were also unaffected in *Scn1a*$^{-/+}$ compared to WT controls, confirming no major changes in interneuronal firing during spontaneous activity *in vivo*.

Discussion

Identifying early dysfunctions of neuronal networks before the onset of the symptoms of SMEI is fundamental to develop a therapeutic approach of this intractable disease. Here, we have investigated the activity of cortical microcircuits at the network and cellular level during the pre-epileptic period in *Scn1a*$^{-/+}$ mice, a widespread experimental model of SMEI. To our knowledge this is the first analysis of single-cell firing during *in vivo* network activity in a mouse model of SMEI.

Unaltered spontaneous network dynamics in Scn1a$^{-/+}$ *mice in vivo*

In our *in vivo* experiments, we found that spontaneous cortical dynamics over a large frequency range, including gamma oscillations, were largely similar in *Scn1a*$^{-/+}$ mice compared to WT controls (Fig. 1). Most importantly, this finding was independent from the depth of the cortical recording (see Results)

and it was confirmed in both anesthetized (Fig. 1B-C) and awake, head-restrained (Fig. 1D-E) mice. These results suggest that no major alterations in local network activities are observed throughout the neocortex during the pre-epileptic period in *Scn1a*$^{-/+}$ animals. This surprising finding is at odds with previously published data reporting strongly decreased excitability of interneurons in *Scn1a*$^{-/+}$ mice (Ogiwara et al. 2007;Yu et al. 2006;Cheah et al. 2012;Han et al. 2012;Tai et al. 2014). Indeed, these interneuronal deficits were proposed to be the major pathophysiological mechanism of SMEI. Moreover, the markedly altered firing of inhibitory interneurons was expected to produce other prominent global cortical effects, given the crucial role of inhibitory circuits in controlling cortical network dynamics (Isaacson and Scanziani 2011), including oscillations in the beta-gamma frequency band (Sohal et al. 2009;Cardin et al. 2009;Uhlhaas and Singer 2010;Hu et al. 2014).

Interneuronal hypoexcitability and synaptic changes in cortical slices from Scn1a$^{-/+}$ *mice*

To correctly interpret our results in light of previous work, we directly measured cellular firing properties in slice preparation in our experimental model (Fig. 3). We have examined three key elements of the cortical circuitry: the excitatory principal neurons and two major classes of inhibitory cells, perisomatic-targeting PV-positive basket cells and dendrite-targeting SST-expressing interneurons. We found that the biophysical properties and the excitability of principal neurons were not significantly affected (Fig. 3A-B), while a decreased efficacy in AP generation upon depolarizing current injections was observed in PV-positive (Fig. 3C-D) and SST-positive (Fig. 3E-F) neurons. Although hypoexcitability was observed in both PV- and SST-positive interneurons, PV-positive cells displayed a pronounced reduction in firing over a wide range of current injections. In contrast SST-positive cells displayed reduced excitability only for larger values of current injection. These data are in large agreement with previous reports demonstrating that, in acutely isolated cells and brain slices, the excitability of interneurons, but not that of pyramidal cells, is decreased in *Scn1a*$^{-/+}$ mice (Ogiwara et

al. 2007;Yu et al. 2006;Cheah et al. 2012;Han et al. 2012). These results also confirm that, in brain slices, interneuronal dysfunction is observed in different classes of inhibitory cells (PV- and SST-positive)(Tai et al. 2014).

In brain slices, we further investigated the effect of the *Scn1a* gene deletion on synaptic currents. We recorded spontaneous excitatory and inhibitory synaptic currents (sEPSCs and sIPSCs, respectively) in principal cells (Fig. 7A-B, 8A-B), PV-positive (Fig. 7C-D, 8C-D) and SST-positive (Fig. 7E-F, 8E-F) interneurons. The largest effects that we observed were an increase in the amplitude of sEPCS in principal cells (Fig. 7B, left panel) and an increase in the amplitude of sIPSCs in PV-positive cells (Fig. 8D, left panel). Interestingly, a prominent source of inhibition of PV-positive cells, autaptic self-inhibition (Bacci and Huguenard 2006;Deleuze et al. 2014), was also significantly increased in *Scn1a*$^{-/+}$ mice (see Results section). We did not observe changes in the IEI of sEPSCs and sIPSCs under our experimental conditions (Fig. 7B, D, F and Fig. 8B, D, F), in contrast to what previously reported in this (Yu et al. 2006;Ogiwara et al. 2007;Cheah et al. 2012;Han et al. 2012) and other models of $Na_V1.1$ channelopathies (Hedrich et al. 2014;Gu et al. 2014;Tsai et al. 2015). Differences in the recorded cell type, brain area and animal age could account for these discrepancies. Taken together, our results suggest that altered functionality of Nav1.1 channels leads to homeostatic synaptic changes, which affect the excitatory and inhibitory synaptic weight differently in distinct elements of the cortical microcircuit. Overall, the most prominent effect is a stronger synaptic inhibition of interneurons, especially PV-positive cells. If exacerbated during development, this specific alteration of inhibition on PV-positive cells could lead to a disinhibitory mechanism that could favor the outbreak of epileptic seizures during the onset of the disease. In support of this view, epileptiform events were found to propagate faster in slices from *Scn1a*$^{-/+}$ mice compared to controls (Fig. 4).

Extrapolating in vivo cellular and network dynamics from slice experiments

Slice recordings point to interneuronal dysfunction and potential circuit disinhibition as the main alterations occurring in the pre-epileptic period in the cortex of *Scn1a*$^{-/+}$ mice (Fig. 3, 7, 8). Based on these findings, major changes would be expected at the network level in the intact brain. In contrast, our *in vivo* recordings (Fig. 1) demonstrated unaltered spontaneous network dynamics in both anesthetized and awake mice. How to reconcile these apparent conflicting results? Can we directly compare *in vitro* with *in vivo* results? In other words, how far can we extrapolate *in vitro* results to the *in vivo* condition? First, it is important to remind that the firing activity of cortical cells *in vivo* is largely triggered by incoming synaptic inputs and not by artificial current injections. These inputs are driven by ongoing circuit activities (Petersen et al. 2003b;Sachidhanandam et al. 2013;Harris and Mrsic-Flogel 2013) that involve and are sustained by the activity of a huge number of cells and much larger number of synaptic connections. For example, recurrent spontaneous activities observed in the cortex during anesthesia (the so called slow oscillations) are observed in virtually all cortical neurons (Steriade et al. 1993a;Steriade et al. 1993c;Steriade et al. 1993b), spread as traveling waves over millimeters of cortical tissue (Massimini et al. 2004) and are strongly influenced by synaptically-connected areas, such as the contralateral cortex (Mohajerani et al. 2010) or the thalamus (David et al. 2013;Sheroziya and Timofeev 2014). Second, in brain slices many of these local and long-range synaptic connections are inevitably severed, thus preventing the recurrent excitatory drive (Crunelli and Hughes 2010) and potentially fundamental neuromodulatory effects (Carracedo et al. 2013;Marder 2012) that can deeply influence cellular spiking activity and network dynamics. Third, intracellular recordings in brain slices sample the activity of a limited number of cells and synaptic connections, numbers that are orders of magnitude smaller than the thousands of cells and synapses involved in the regulation of *in vivo* circuit dynamics. This massive undersampling, together with the aforementioned limitations of the *in vitro* preparation, suggest that it might not always be straightforward to precisely

predict the outcome of a given genetic manipulation on network function *in vivo* based exclusively on slice recordings.

Unaltered interneuronal firing during spontaneous cortical dynamics in Scn1a$^{-/+}$ mice in vivo

In the attempt to explain our contrasting *in vitro* and *in vivo* results, we directly measured interneuronal firing activity *in vivo* during spontaneous network dynamics. Surprisingly, we found that both PV- and SST-positive interneurons displayed similar firing rate, inter spike time interval and coefficient of variation in *Scn1a*$^{-/+}$ mice with respect to controls (Fig. 9-10). These findings agree with the unaltered network dynamics that we observed *in vivo* with LFP and MUA recordings (Fig. 1), but contrast with the marked reduction in excitability that we observed in brain slices (Fig. 3C-F). Various mechanisms may explain these different results. For example, PV- and SST-positive cells in Scna1a$^{-/+}$ mice fire less spikes in response to prolonged depolarizing current injections (Fig. 3), and this effect is stronger at stimuli that elicit high frequency firing in control mice, especially for SST-positive interneurons (Fig. 3F). This suggests that in *Scn1a*$^{-/+}$ mice interneurons may behave normally, at frequencies below a certain threshold, but they might lose their ability to fire at higher frequency, e.g. during epileptic discharges. Indeed, previous reports indicated that fast-spiking cortical interneurons *in vivo* can fire at up to 800 Hz during seizure activity (Timofeev et al. 2002), and this could play a role in controlling seizure propagation (Cammarota et al. 2013). It is therefore possible that during the spontaneous activity in the asymptomatic pre-epileptic period, interneurons are not forced to fire at those high frequencies and thus no phenotype is visible at the network level. If the network is challenged with a strong stimulus (e.g. a local NMDA application) network abnormalities become visible. Experiments in figure 4 are in line with this hypothesis. However, it should also be noted that in our recordings of spontaneous activity PV- and SST-positive interneurons *in vivo* fire with an instantaneous frequency up to 160 Hz and 80 Hz (Fig. 9D, 10C). At these rates, significant dysfunctions are already observed in

brain slice experiments (Fig. 3D, F). Nevertheless, few APs are discharged with high instantaneous frequencies across cells: 10-15 % in PV-positive cells with instantaneous frequency > 50 Hz (Fig. 9D, inset) and 1-3 % in SST-positive cells with instantaneous frequency with > 50 Hz (Fig. 10C, inset).

An alternative possibility is that compensatory mechanisms may mask the dysfunction of GABAergic cell excitability observed in slices from *Scn1a*$^{-/+}$ mice. For example, homeostatic changes at the synaptic (Turrigiano and Nelson 2004) or circuit (Marder 2011) level may counteract interneuronal hypofunction and result in unaltered network activity. Synaptic alterations are indeed observed in *Scn1a*$^{-/+}$ mice (Tai et al. 2014;Liautard et al. 2013) both at the level of inhibitory and excitatory synapses (Fig. 7-8). However, the mechanisms underlying the cell-type specific changes of excitatory and inhibitory synaptic transmission in *Scn1a*$^{-/+}$ mice described here remain to be elucidated. As described above the most prominent effects are stronger synaptic excitation of principal neurons (Fig. 7B, left panel) and stronger synaptic inhibition of PV-positive interneurons (Fig. 8D, left panel) which would, however, predict increased network hyperexcitability and disinhibition rather than compensation. In any case, for the reasons explained previously it is difficult to predict the impact of these changes on network activities *in vivo*. In this regard, it is interesting to note that optogenetic reduction of AP firing in both PV- and SST-positive interneurons in awake WT mice resulted in large changes in network activities. These data demonstrate that acute reduction of the excitability in both interneuronal subtypes elicits strong network effects, suggesting that interneuronal dysfunction may not be the only alteration present during the pre-epileptic period in *Scn1a*$^{-/+}$ mice and that potential additional cellular mechanisms may come into play. For example, homeostatic rearrangements may counteract the effect of the mutation in the pre-epileptic period, but might not be sufficient to block the development of seizures in the epileptic period. This is consistent with the resistance of induction of ictal activity with application of 4-AP in the pre-epileptic period (Yu et al. 2006;Liautard et al. 2013).

In summary, in this study we investigated the cellular and network abnormalities arising in the pre-epileptic period in a mouse model of SMEI. We confirmed that interneuronal dysfunction in excitability is observed in brain slices upon current injections. However, we surprisingly found that network dynamics and interneuronal spiking were normal in the intact brain during ongoing activities, suggesting that additional cellular and network mechanisms may play a fundamental role in the pathogenesis of SMEI. These results contribute to unravel the basic mechanisms of SMEI pathogenesis and may represent an important step forward to the identification of new cellular targets for the pharmacological treatment of this intractable form of human epilepsy.

Acknowledgments

We thank S. Zucca for help with two-photon guided juxtasomal recordings, G. D'Urso for help with immunohistochemical experiments, confocal image acquisition, maintenance of the mouse colony, and E. Boyden for AAVflex.CBA.Arch-GFP.WPRE.SV40 (Addgene 22222). This work was supported by grants from Telethon-Italy (GGP10138) to TF, AB and GC; the Istituto Italiano di Tecnologia, European Research Council (ERC, NEURO-PATTERNS), FP7-Health (DESIRE), San Paolo "Programma in Neuroscienze" and MIUR FIRB (RBAP11X42L) to TF; the Institut du Cerveau et de la Moelle épinière (Paris), Giovanni Armenise-Harvard Foundation: Career Development Award, European Research Council (ERC) under the European Community's 7th Framework Programmme (FP7/2007-2013)/ERC grant agreement No 200808), "Investissements d'avenir" ANR-10-IAIHU-06, and ANR Programme Blanc (ANR-13-BSV4-0015-01) to AB.

Contributions

AMDS, AF performed in vivo recordings. PF performed intracellular recordings in brain slices. IM and GL recorded and analyzed ictal events. DV performed optogenetic experiments in brain slices. AMDS, PF, IM, SC, SP, DV and GL performed analysis. MM provided tools and reagents. AB and TF conceived and coordinated the project. GC, AB and TF wrote the paper. All authors commented upon and approved the final version of the manuscript.

References

1. Adesnik H, Scanziani M. 2010. Lateral competition for cortical space by layer-specific horizontal circuits. Nature 464:1155-1160.
2. Ascoli GA, et al. 2008. Petilla terminology: nomenclature of features of GABAergic interneurons of the cerebral cortex. Nat Rev Neurosci 9:557-568.
3. Bacci A, Huguenard JR. 2006. Enhancement of spike-timing precision by autaptic transmission in neocortical inhibitory interneurons. Neuron 49:119-130.
4. Beltramo R, D'Urso G, Dal MM, Farisello P, Bovetti S, Clovis Y, Lassi G, Tucci V, De Pietri TD, Fellin T. 2013. Layer-specific excitatory circuits differentially control recurrent network dynamics in the neocortex. Nat Neurosci 16:227-234.
5. Box GEP, Hunter JS, Hunter WG. 2005. Statistics for Experimenters: Design, Innovation, and Discovery. Wiley.
6. Cammarota M, Losi G, Chiavegato A, Zonta M, Carmignoto G. 2013. Fast spiking interneuron control of seizure propagation in a cortical slice model of focal epilepsy. J Physiol 591:807-822.
7. Cardin JA, Carlen M, Meletis K, Knoblich U, Zhang F, Deisseroth K, Tsai LH, Moore CI. 2009. Driving fast-spiking cells induces gamma rhythm and controls sensory responses. Nature 459:663-667.
8. Cardin JA, Carlen M, Meletis K, Knoblich U, Zhang F, Deisseroth K, Tsai LH, Moore CI. 2010. Targeted optogenetic stimulation and recording of neurons in vivo using cell-type-specific expression of Channelrhodopsin-2. Nat Protoc 5:247-254.
9. Carracedo LM, Kjeldsen H, Cunnington L, Jenkins A, Schofield I, Cunningham MO, Davies CH, Traub RD, Whittington MA. 2013. A neocortical delta rhythm facilitates reciprocal interlaminar interactions via nested theta rhythms. J Neurosci 33:10750-10761.

10. Cheah CS, Yu FH, Westenbroek RE, Kalume FK, Oakley JC, Potter GB, Rubenstein JL, Catterall WA. 2012. Specific deletion of NaV1.1 sodium channels in inhibitory interneurons causes seizures and premature death in a mouse model of Dravet syndrome. Proc Natl Acad Sci U S A 109:14646-14651.
11. Claes L, Del-Favero J, Ceulemans B, Lagae L, Van BC, De JP. 2001. De novo mutations in the sodium-channel gene SCN1A cause severe myoclonic epilepsy of infancy. Am J Hum Genet 68:1327-1332.
12. Contreras D. 2004. Electrophysiological classes of neocortical neurons. Neural Netw 17:633-646.
13. Crunelli V, Hughes SW. 2010. The slow (<1 Hz) rhythm of non-REM sleep: a dialogue between three cardinal oscillators. Nat Neurosci 13:9-17.
14. David F, Schmiedt JT, Taylor HL, Orban G, Di GG, Uebele VN, Renger JJ, Lambert RC, Leresche N, Crunelli V. 2013. Essential thalamic contribution to slow waves of natural sleep. J Neurosci 33:19599-19610.
15. DeFelipe J, et al. 2013. New insights into the classification and nomenclature of cortical GABAergic interneurons. Nat Rev Neurosci 14:202-216.
16. Deleuze C, Pazienti A, Bacci A. 2014. Autaptic self-inhibition of cortical GABAergic neurons: synaptic narcissism or useful introspection? Curr Opin Neurobiol 26:64-71.
17. Dombeck DA, Khabbaz AN, Collman F, Adelman TL, Tank DW. 2007. Imaging large-scale neural activity with cellular resolution in awake, mobile mice. Neuron 56:43-57.
18. Dravet C. 2000. Severe myoclonic epilepsy in infants and its related syndromes. Epilepsia 41 Suppl 9:7.
19. Dravet C, Bureau M, Oguni H, Fukuyama Y, Cokar O. 2005. Severe myoclonic epilepsy in infancy: Dravet syndrome. Adv Neurol 95:71-102.

20. Dugue GP, Dumoulin A, Triller A, Dieudonne S. 2005. Target-dependent use of co-released inhibitory transmitters at central synapses. J Neurosci 25:6490-6498.

21. Dutton SB, Sawyer NT, Kalume F, Jumbo-Lucioni P, Borges K, Catterall WA, Escayg A. 2011. Protective effect of the ketogenic diet in Scn1a mutant mice. Epilepsia 52:2050-2056.

22. Feldmeyer D. 2012. Excitatory neuronal connectivity in the barrel cortex. Front Neuroanat 6:24.

23. Freund TF, Katona I. 2007. Perisomatic inhibition. Neuron 56:33-42.

24. Gomez-Gonzalo M, Losi G, Chiavegato A, Zonta M, Cammarota M, Brondi M, Vetri F, Uva L, Pozzan T, de CM, Ratto GM, Carmignoto G. 2010. An excitatory loop with astrocytes contributes to drive neurons to seizure threshold. PLoS Biol 8:e1000352.

25. Gu F, Hazra A, Aulakh A, Ziburkus J. 2014. Purinergic control of hippocampal circuit hyperexcitability in Dravet syndrome. Epilepsia 55:245-255.

26. Han S, Tai C, Westenbroek RE, Yu FH, Cheah CS, Potter GB, Rubenstein JL, Scheuer T, de la Iglesia HO, Catterall WA. 2012. Autistic-like behaviour in Scn1a+/- mice and rescue by enhanced GABA-mediated neurotransmission. Nature 489:385-390.

27. Harris KD, Mrsic-Flogel TD. 2013. Cortical connectivity and sensory coding. Nature 503:51-58.

28. Hedrich UB, Liautard C, Kirschenbaum D, Pofahl M, Lavigne J, Liu Y, Theiss S, Slotta J, Escayg A, Dihne M, Beck H, Mantegazza M, Lerche H. 2014. Impaired action potential initiation in GABAergic interneurons causes hyperexcitable networks in an epileptic mouse model carrying a human Na(V)1.1 mutation. J Neurosci 34:14874-14889.

29. Hu H, Gan J, Jonas P. 2014. Interneurons. Fast-spiking, parvalbumin(+) GABAergic interneurons: from cellular design to microcircuit function. Science 345:1255263.

30. Isaacson JS, Scanziani M. 2011. How inhibition shapes cortical activity. Neuron 72:231-243.

31. Le MC, Monyer H. 2013. GABAergic interneurons shape the functional maturation of the cortex. Neuron 77:388-405.

32. Lewis DA, Fish KN, Arion D, Gonzalez-Burgos G. 2011. Perisomatic inhibition and cortical circuit dysfunction in schizophrenia. Curr Opin Neurobiol 21:866-872.

33. Liautard C, Scalmani P, Carriero G, de CM, Franceschetti S, Mantegazza M. 2013. Hippocampal hyperexcitability and specific epileptiform activity in a mouse model of Dravet syndrome. Epilepsia 54:1251-1261.

34. Logothetis NK. 2003. The underpinnings of the BOLD functional magnetic resonance imaging signal. J Neurosci 23:3963-3971.

35. Losi G, Cammarota M, Chiavegato A, Gomez-Gonzalo M, Carmignoto G. 2010. A new experimental model of focal seizures in the entorhinal cortex. Epilepsia 51:1493-1502.

36. Marder E. 2011. Variability, compensation, and modulation in neurons and circuits. Proc Natl Acad Sci U S A 108 Suppl 3:15542-15548.

37. Marder E. 2012. Neuromodulation of neuronal circuits: back to the future. Neuron 76:1-11.

38. Marin O. 2012. Interneuron dysfunction in psychiatric disorders. Nat Rev Neurosci 13:107-120.

39. Massimini M, Huber R, Ferrarelli F, Hill S, Tononi G. 2004. The sleep slow oscillation as a traveling wave. J Neurosci 24:6862-6870.

40. Meisler MH, Kearney JA. 2005. Sodium channel mutations in epilepsy and other neurological disorders. J Clin Invest 115:2010-2017.

41. Metherate R, Cox CL, Ashe JH. 1992. Cellular bases of neocortical activation: modulation of neural oscillations by the nucleus basalis and endogenous acetylcholine. J Neurosci 12:4701-4711.

42. Mohajerani MH, McVea DA, Fingas M, Murphy TH. 2010. Mirrored bilateral slow-wave cortical activity within local circuits revealed by fast bihemispheric voltage-sensitive dye imaging in anesthetized and awake mice. J Neurosci 30:3745-3751.

43. Ogiwara I, Miyamoto H, Morita N, Atapour N, Mazaki E, Inoue I, Takeuchi T, Itohara S, Yanagawa Y, Obata K, Furuichi T, Hensch TK, Yamakawa K. 2007. Nav1.1 localizes to axons of parvalbumin-positive inhibitory interneurons: a circuit basis for epileptic seizures in mice carrying an Scn1a gene mutation. J Neurosci 27:5903-5914.

44. Ohmori I, Ouchida M, Ohtsuka Y, Oka E, Shimizu K. 2002. Significant correlation of the SCN1A mutations and severe myoclonic epilepsy in infancy. Biochem Biophys Res Commun 295:17-23.

45. Petersen CC, Grinvald A, Sakmann B. 2003a. Spatiotemporal dynamics of sensory responses in layer 2/3 of rat barrel cortex measured in vivo by voltage-sensitive dye imaging combined with whole-cell voltage recordings and neuron reconstructions. J Neurosci 23:1298-1309.

46. Petersen CCH, Hahn TTG, Mehta M, Grinvald A, Sakmann B. 2003b. Interaction of sensory responses with spontaneous depolarization in layer 2/3 barrel cortex. Proc Natl Acad Sci USA 100:13638-13643.

47. Rubinstein M, Han S, Tai C, Westenbroek RE, Hunker A, Scheuer T, Catterall WA. 2015. Dissecting the phenotypes of Dravet syndrome by gene deletion. Brain.

48. Rudy B, Fishell G, Lee S, Hjerling-Leffler J. 2011. Three groups of interneurons account for nearly 100% of neocortical GABAergic neurons. Dev Neurobiol 71:45-61.

49. Sachidhanandam S, Sreenivasan V, Kyriakatos A, Kremer Y, Petersen CC. 2013. Membrane potential correlates of sensory perception in mouse barrel cortex. Nat Neurosci 16:1671-1677.

50. Sheroziya M, Timofeev I. 2014. Global intracellular slow-wave dynamics of the thalamocortical system. J Neurosci 34:8875-8893.

51. Sohal VS, Zhang F, Yizhar O, Deisseroth K. 2009. Parvalbumin neurons and gamma rhythms enhance cortical circuit performance. Nature 459:698-702.

52. Steriade M. 2006. Grouping of brain rhythms in corticothalamic systems. Neuroscience 137:1087-1106.

53. Steriade M, Contreras D, Dossi RC, Nunez A. 1993a. The Slow (Less-Than-1 Hz) Oscillation in Reticular Thalamic and Thalamocortical Neurons - Scenario of Sleep Rhythm Generation in Interacting Thalamic and Neocortical Networks. J Neurosci 13:3284-3299.

54. Steriade M, Nunez A, Amzica F. 1993b. A Novel Slow (Less-Than-1 Hz) Oscillation of Neocortical Neurons In-Vivo - Depolarizing and Hyperpolarizing Components. J Neurosci 13:3252-3265.

55. Steriade M, Nunez A, Amzica F. 1993c. Intracellular Analysis of Relations Between the Slow (Less-Than-1 Hz) Neocortical Oscillation and Other Sleep Rhythms of the Electroencephalogram. J Neurosci 13:3266-3283.

56. Tai C, Abe Y, Westenbroek RE, Scheuer T, Catterall WA. 2014. Impaired excitability of somatostatin- and parvalbumin-expressing cortical interneurons in a mouse model of Dravet syndrome. Proc Natl Acad Sci U S A 111:E3139-E3148.

57. Timofeev I, Grenier F, Steriade M. 2002. The role of chloride-dependent inhibition and the activity of fast-spiking neurons during cortical spike-wave electrographic seizures. Neuroscience 114:1115-1132.

58. Tsai MS, Lee ML, Chang CY, Fan HH, Yu IS, Chen YT, You JY, Chen CY, Chang FC, Hsiao JH, Khorkova O, Liou HH, Yanagawa Y, Lee LJ, Lin SW. 2015. Functional and structural deficits of the dentate gyrus network coincide with emerging spontaneous seizures in an Scn1a mutant Dravet Syndrome model during development. Neurobiol Dis 77:35-48.

59. Turrigiano GG, Nelson SB. 2004. Homeostatic plasticity in the developing nervous system. Nat Rev Neurosci 5:97-107.

60. Uhlhaas PJ, Singer W. 2010. Abnormal neural oscillations and synchrony in schizophrenia. Nat Rev Neurosci 11:100-113.

61. Yu FH, Mantegazza M, Westenbroek RE, Robbins CA, Kalume F, Burton KA, Spain WJ, McKnight GS, Scheuer T, Catterall WA. 2006. Reduced sodium current in GABAergic interneurons in a mouse model of severe myoclonic epilepsy in infancy. Nat Neurosci 9:1142-1149.

Table 1

	Principal cells		PV-positive cells		SST-pos. cells	
	WT N = 27 cells	***Scn1a*$^{-/+}$** N = 27 cells	**WT** N = 21 cells	***Scn1a*$^{-/+}$** N = 28 cells	**WT** N = 25 cells	***Scn1a*$^{-/+}$** N = 28 cells
R_{in} (MΩ)	103 ± 9	107 ± 9	109 ± 8	86 ± 5*	208 ± 16	195 ± 14
AP amplitude (mV)	84 ± 2	85 ± 1	66 ± 2	63 ± 2	72 ± 2	71 ± 2
AP duration (ms)	1.04 ± 0.05	1.09 ± 0.04	0.36 ± 0.01	0.39 ± 0.01	0.65 ± 0.02	0.79 ± 0.04**
AP risetime (ms)	0.59 ± 0.03	0.59 ± 0.02	0.37 ± 0.01	0.40 ± 0.01*	0.56 ± 0.02	0.63 ± 0.02**
AP threshold (mV)	-42.6 ± 0.7	-42.0 ± 0.8	-41.7 ± 1.1	-42.4 ± 0.9	-42.1 ± 0.8	-42.5 ± 0.7
AHP ampl. (mV)	-11.6 ± 0.7	-11.6 ± 0.8	-21.4 ± 0.7	-18.7 ± 0.9*	-14.9 ± 1.1	-14.8 ± 1.0
AHP duration (ms)	47.6 ± 5.3	68.9 ± 14.8	1.00 ± 0.06	1.02 ± 0.05	2.47 ± 0.11	2.91 ± 0.17*

Table 1. Biophysical properties of recorded neurons. Statistical significance was evaluated with unpaired Student's t-test. *, $p < 0.05$; **, $p < 0.01$; ***, $p < 0.001$.

Figure 1

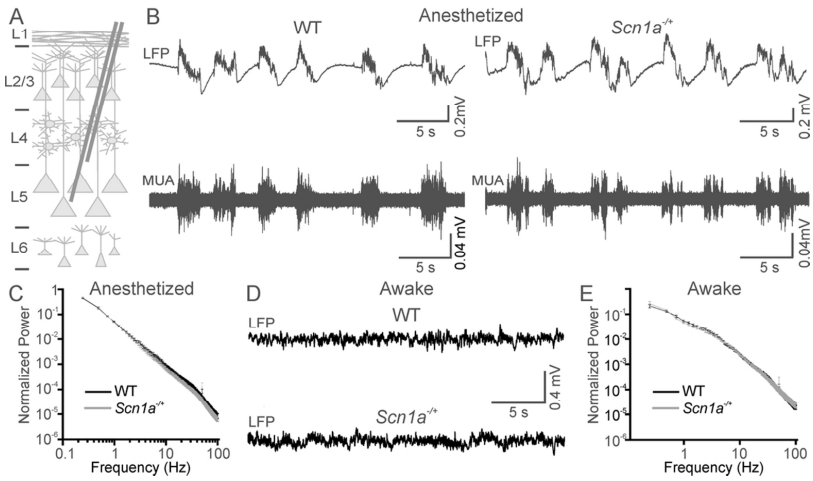

Figure 1. Cortical network dynamics in wild type (WT) and Scn1a-/+ mice in vivo. A) Schematic representation of experimental configuration. Recording electrodes were placed at ~ 700 μm depth. B) Representative traces of Local Field Potential (LFP, top traces) and Multi-Unit Activity (MUA, bottom traces) activity in anesthetized WT (left) and Scn1a-/+ (right) mice during spontaneous activity. C) Average normalized LFP power spectra for WT (N = 18) and Scn1a-/+ mice (N = 17). D) Representative traces of LFP in awake head-restrained WT (top) and Scn1a-/+ (bottom) mice showing spontaneous activity. E) Average normalized LFP power spectra in awake, head-restrained mice. WT, N = 15; Scn1a-/+ mice, N = 15.
100x65mm (300 x 300 DPI)

Figure 2

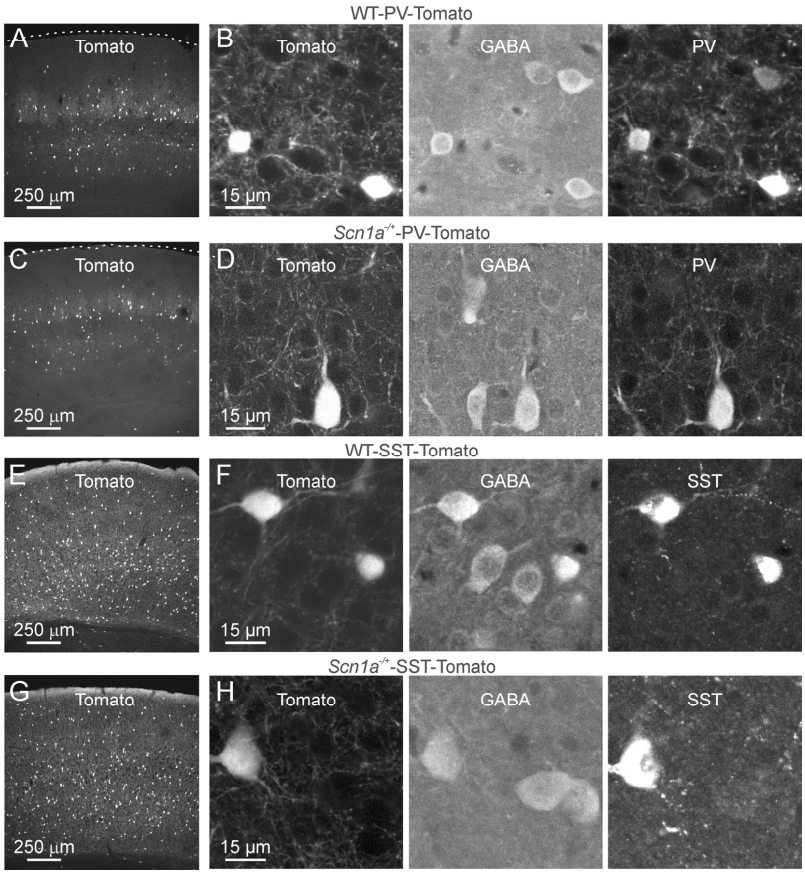

Figure 2. Identification of genetically-specified subclasses of interneurons in WT and Scn1a-/+ mice. A) Confocal image showing Tomato fluorescence in a section from the cortex of a WT-PV-Tomato mouse. B) A zoom in of two Tomato-positive cells is shown in the leftmost panel. The section shown in (B) was stained against GABA (middle panel) and PV (rightmost panel). C-D) Same as in A-B for Scn1a-/+-PV-Tomato. E-F) Same as in A-B for WT-SST-Tomato. G-H) Same as in A-B for Scn1a-/+-SST-Tomato.
141x160mm (300 x 300 DPI)

Figure 3

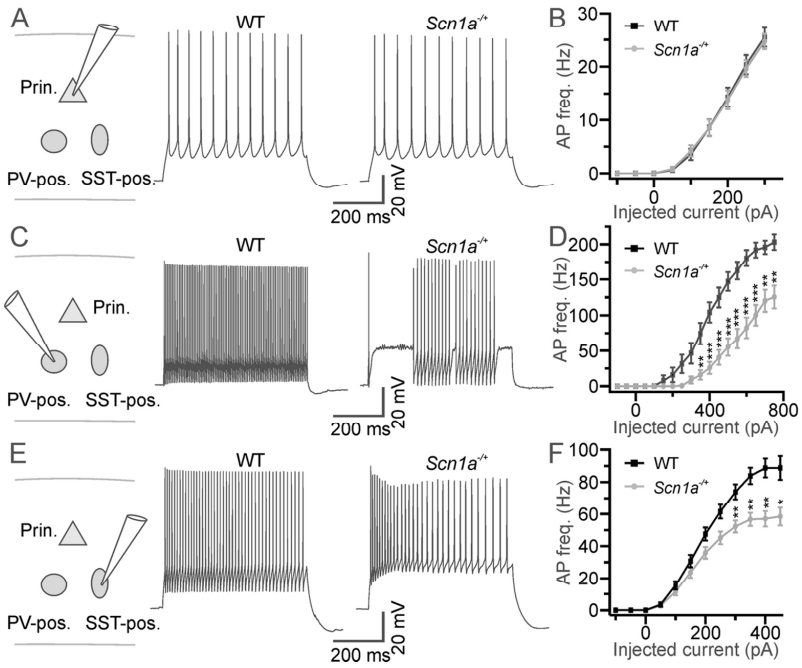

Figure 3. Cell type-specific dysfunction of excitability in brain slices from Scn1a-/+ mice. A) Left: schematic of the experimental configuration. Prin., principal neuron; PV-pos., parvalbumin-positive interneuron; SST-pos., somatostatin-positive interneuron. Right: representative current-clamp recordings from pyramidal neurons recorded from WT (left) and Scn1a-/+ (right) mice in cortical slice. B) Average frequency of action potential (AP) firing in principal neurons as a function of injected current for WT (N = 27 cells, black) and Scn1a-/+ (N = 27 cells, grey). C) Representative current-clamp recordings from Tomato-positive interneurons recorded in cortical slices from a WT-PV-Tomato (WT, left) and a Scn1a-/+ -PV-Tomato (Scn1a-/+, right) mouse. D) Average frequency of AP firing as a function of injected current for fluorescent cells recorded in WT-PV-Tomato mice (N = 21, black) and Scn1a-/+-PV-Tomato mice (N = 28, grey). The asterisks indicate significance at each value of current injection evaluated with the Bonferroni post hoc test. *, $p < 0.05$; **, $p < 0.01$; ***, $p < 0.001$. E) Representative current-clamp recordings from Tomato-positive cells recorded in cortical slices from WT-SST-Tomato (left) and Scn1a-/+ -SST-Tomato (right) animals. F) Average frequency of AP firing as a function of injected current for cells recorded in WT-SST-Tomato animals (N = 25, black) and Scn1a-/+ -SST-Tomato animals (N = 28, grey).
109x98mm (300 x 300 DPI)

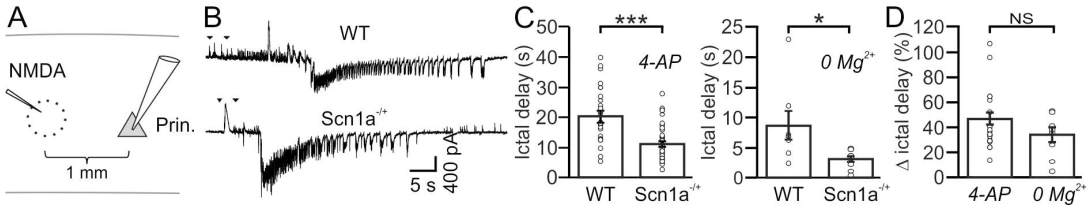

Figure 4. Faster propagation of focal ictal discharges in slices from Scn1a-/+ mice. A) Schematic of the experimental configuration for the generation of focal ictal discharges. B) Representative voltage-clamp recordings at -50 mV of an NMDA-induced ictal event in a pyramidal neuron 1 mm away from the NMDA application site in a WT (top) and a Scn1a-/+ (bottom) mouse. C) Left: average delays of ictal onset in pyramidal neurons from WT (N = 24 ictal events from 11 mice) and Scn1a-/+ (N = 38 ictal events from 12 mice) animals in the presence of 4-AP. Right: average delays of ictal onset in pyramidal neurons from WT (N = 8 ictal events from 2 mice) and Scn1a-/+ (N = 9 ictal events from 2 mice) animals in low Mg2+ (0 Mg2+). D) Average values of ictal onset delay normalized to control in 4-AP (N = 38 ictal events from 12 mice) and low Mg2+ (N = 9 ictal events from 2 mice).
37x8mm (300 x 300 DPI)

Figure 5

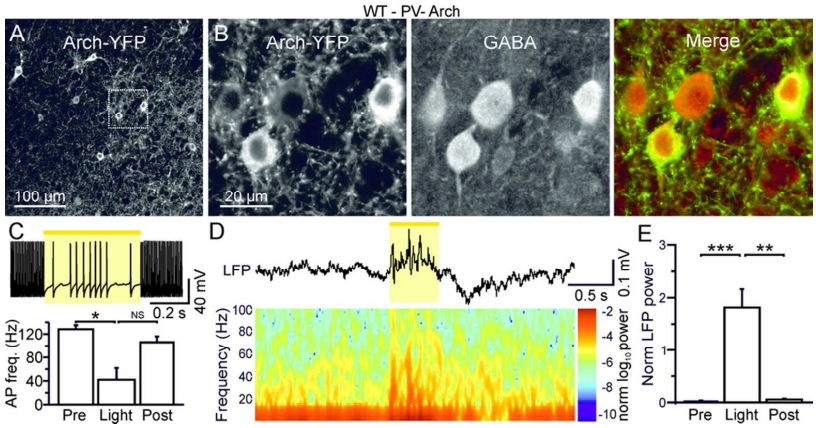

Figure 5. Acute optogenetic reduction of firing in PV-positive cells affects ongoing network dynamics in vivo. A) Confocal image of cortical section from a WT-PV-Cre animal which was injected with AAV transducing Arch-YFP. B) A zoom in of two Arch-YFP-positive cells (leftmost panel) is shown. The same section shown in (B) was stained for GABA (middle panel). The merge of the two images is shown in the rightmost panel. C) Top: slice recording displaying membrane potential response to yellow light pulse in a representative Arch-positive neuron. AP discharge was elicited in the recorded neuron by current injection (600 pA). Bottom: Histogram displaying the average AP frequency before (pre), during (stim) and after (post) light stimulation in N = 4 recorded cells. D) Representative LFP trace (top) and corresponding spectrogram (bottom) showing the effect of yellow light illumination on spontaneous cortical activity in awake, head-restrained WT-PV-Cre animals which were injected with AAVs carrying a doublefloxed Arch sequence. E) Average values of normalized LFP power before (pre), during (stim) and after (post) light stimulation (N = 11 mice). LFP power was calculated in the spectral range 30-90 Hz.
85x49mm (300 x 300 DPI)

Figure 6

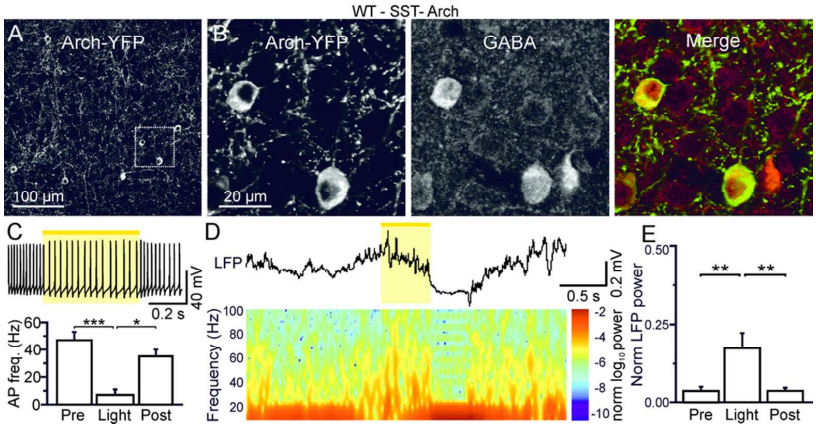

Figure 6. Acute optogenetic reduction of firing in SST-positive cells affects ongoing network dynamics in vivo. A) Confocal image of cortical section from a WT-SST-Cre animal which was injected with AAV transducing Arch-YFP. B) A zoom in of two Arch-YFP-positive cells (leftmost panel) is shown. The same section shown in (B) was stained for GABA (middle panel). The merge of the two images is shown in the rightmost panel. C) Top: slice recording displaying membrane potential response to yellow light pulse in a representative Arch-positive neuron. AP discharge was elicited in the recorded neuron by current injection (300 pA). Bottom: Histogram displaying the average AP frequency before (pre), during (stim) and after (post) light stimulation in N = 12 recorded cells. D) Representative LFP trace (top) and corresponding spectrogram (bottom) showing the effect of yellow light illumination on spontaneous cortical activity in awake, head-restrained WT-SST-Cre animals which were injected with AAVs carrying a doublefloxed Arch sequence. E) Average values of normalized LFP power before (pre), during (stim) and after (post) light stimulation (N = 9 mice). LFP power was calculated in the spectral range 30-90 Hz.
85x49mm (300 x 300 DPI)

Figure 7

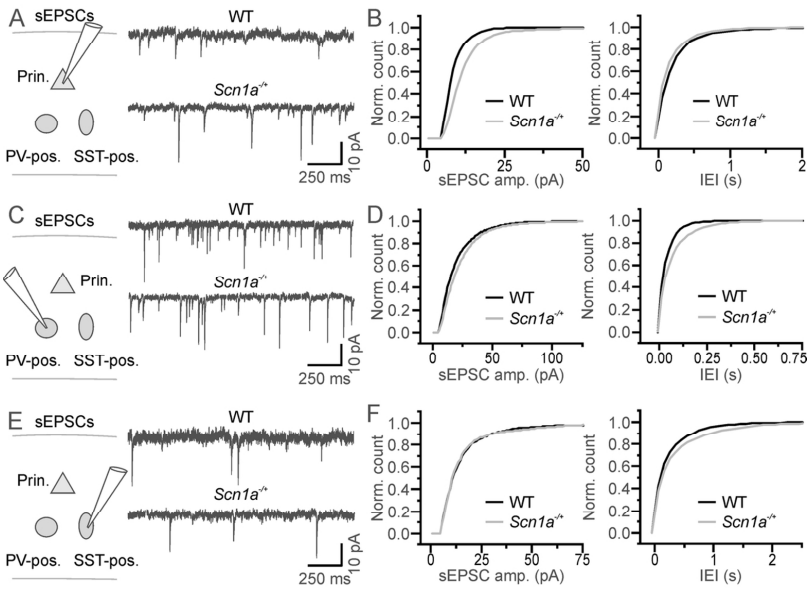

Figure 7. Cell type-specific changes in spontaneous excitatory postsynaptic currents in brain slices from Scn1a-/+ mice. A) Left: schematic of the experimental configuration. Recordings were performed from principal cortical neurons. Right: spontaneous excitatory postsynaptic currents (sEPSCs) in slices from WT (top) and Scn1a-/+ (bottom) animals recorded from principal neurons. B) Cumulative distribution of the amplitude (left) and frequency (right) of sEPSCs recorded from WT (N = 7 cells) and Scn1a-/+ (N = 10 cells). C-D) and E-F) same as in A-B) for sEPSCs recorded from PV-positive (WT, N = 7 cells; Scn1a-/+, N = 7 cells) and SST-positive (WT, N = 6 cells; Scn1a-/+, N = 6 cells) interneurons, respectively.
110x86mm (300 x 300 DPI)

Figure 8

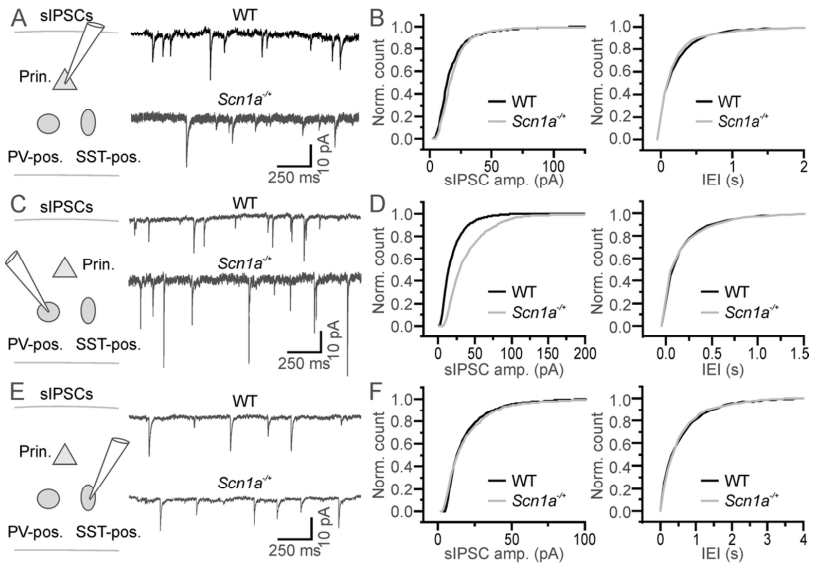

Figure 8. Cell type-specific changes in spontaneous inhibitory postsynaptic currents in brain slices from Scn1a-/+ mice. A) Left: schematic of the experimental configuration. Recordings were performed from principal cortical neurons. Right: spontaneous inhibitory postsynaptic currents (sIPSCs) in slices from WT (top) and Scn1a-/+ (bottom) animals recorded from principal neurons. B) Cumulative distribution of the amplitude (left) and frequency (right) of sIPSCs recorded from WT (N = 8 cells) and Scn1a-/+ (N = 8 cells). C-D) and E-F) same as in A-B) for sIPSCs recorded from PV-positive (WT, N = 8 cells; Scn1a-/+, N = 8 cells) and SST-positive (WT, N = 8 cells; Scn1a-/+, N = 8 cells) interneurons, respectively.
106x80mm (300 x 300 DPI)

Figure 9

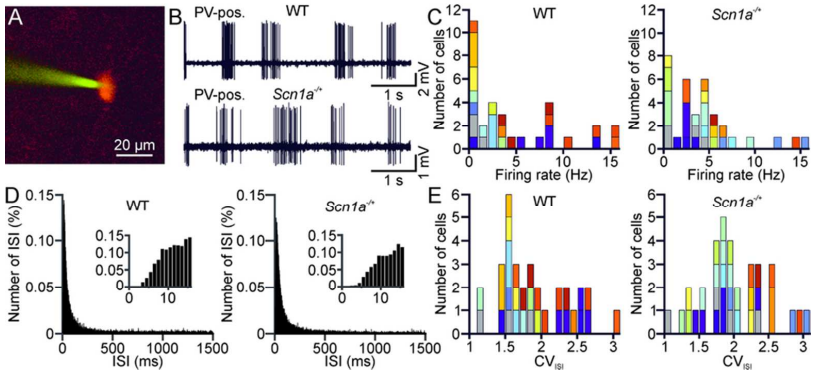

Figure 9. Two-photon guided juxtasomal recordings from PV-positive interneurons in vivo. A) Two-photon image showing a Tomato-positive (red signal) layer II interneuron in an anesthetized WT - PV-Cre mouse which was crossed with a Tomato reporter mouse line. Under visual control, a glass pipette filled with Alexa 488 (green signal) is lowered within the cortical tissue until a juxtasomal recording is obtained with a genetically-identified cell. B) Juxtasomal recording from a Tomato-positive cell in a WT (top) and Scn1a-/+ (bottom) mouse. C) Distribution of the average firing rate of recorded cells in WT (left, N = 32 cells from 15 different animals) and Scn1a-/+ (right, N = 34 cells from 14 different animals). Cells recorded from the same animal are displayed with the same color code. D) Average (over cells) distribution of the inter spike interval (ISI) in WT (left) and Scn1a-/+ (right) for the same set of recordings analyzed in C. Bin, 1 ms. The distributions are shown at an expanded time scale in the insets. E) Distribution of the coefficient of variation of the inter spike intervals (CVISI) in WT (left) and Scn1a-/+ (right). Same color code as in panel C.
78x39mm (300 x 300 DPI)

Figure 10

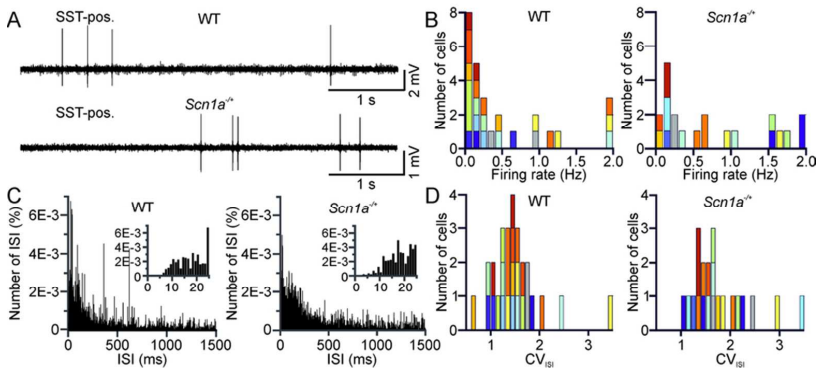

Figure 10. Two-photon guided juxtasomal recordings from SST-positive interneurons in vivo. A) Juxtasomal recording from a Tomato- and SST-positive cell in anesthetized WT (top) and Scn1a-/+ (bottom) mice. B) Distribution of the average firing rate of recorded cells in WT (left, N = 27 cells from 12 different animals) and Scn1a-/+ (right, N = 21 cells from 11 different animals). The color code indicates cells recorded in different animals. C) Average (over cells) distribution of the inter spike interval (ISI) in WT (left) and Scn1a-/+ (right) for the same set of recordings analyzed in B. Bin, 1 ms. The distributions are shown at an expanded time scale in the insets. D) Distribution of the coefficient of variation of the inter spike intervals (CVISI) in WT (left) and Scn1a-/+ (right). Same color code as in panel C.
79x39mm (300 x 300 DPI)

3.5 APPENDIX B:

GABAergic tonic current is reduced in *Scn1a*$^{+/-}$ mice

Iacopo Marcon, Gabriele Losi and Giorgio Carmignoto

The experiments reported in De Stasi et. al. revealed a faster propagation of focal epileptiform activity in brain slices from *Scn1a*$^{+/-}$ mice with respect to WT mice. This experimental observation hints at a defective feedforward inhibition that may originate from an impairment of Pv interneuron firing discharges. However, the analysis of the pre-ictal inhibitory barrages that are commonly observed in principal neurons ahead of propagating seizures and that represent a hallmark of the feedforward inhibition generated by Pv interneurons [4], failed to highlight any differences of the inhibitory signals in principal neurons from *Scn1a*$^{+/-}$ and WT mice in terms of both amplitude and overall charge transferred. To explain this unexpected finding, we hypothesized that a compensatory mechanism may exist in *Scn1a*$^{+/-}$ mice that involves a decrease in the GABAergic tonic inhibition on pyramidal cells. Indeed, a reduced level of tonic inhibition could result in a reduced intracellular chloride concentration in these cells that, in turn, enhances the driving force for chloride entry at inhibitory synapses. An enhancement in the chloride driving force might compensate for a defective inhibitory transmission at Pv interneuron-pyramidal neuron synapses. To address this hypothesis, we performed experiments that used Picrotoxin (PTX), a selective $GABA_A$ receptor blocker, to isolate the GABAergic tonic current in layer V pyramidal neurons from temporal cortex slices. We found that in *Scn1a*$^{+/-}$ mice the GABAergic tonic current is significantly reduced with respect to WT littermate controls (Fig. 1, 62.11 ± 12.54 vs 108.25 ± 21.67pA, unpaired t-test, p = 0.042).

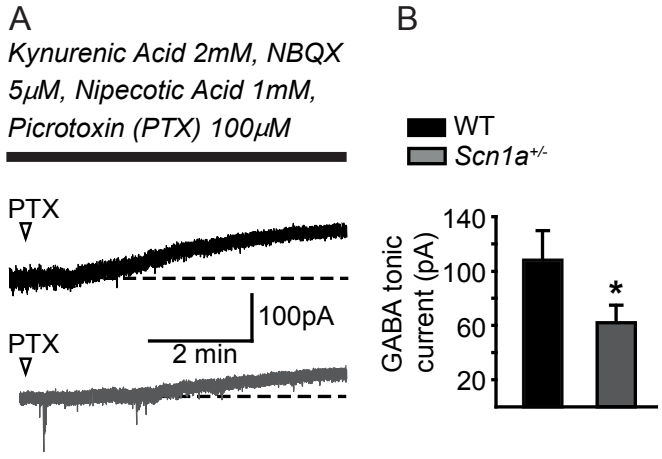

Figure 1. GABAergic tonic current is reduced in *Scn1a*$^{+/-}$ mice.

(A) Representative voltage-clamp recordings at -60 mV of pyramidal neurons in temporal cortex slices from WT (black) and *Scn1a*$^{+/-}$ (grey) mice in the presence of Kynurenic acid, NBQX, Nipecotic acid and Picrotoxin (PTX). (B) Quantification of the GABAergic tonic current density in pyramidal neurons from WT (black, n = 9 cells, 3 mice) and *Scn1a*$^{+/-}$ (grey, n = 11 cells, 4 mice) mice. * = $p < 0.05$

RESEARCH ARTICLE

The Inhibitory Neurotransmitter GABA Evokes Long-Lasting Ca^{2+} Oscillations in Cortical Astrocytes

Letizia Mariotti, Gabriele Losi, Michele Sessolo, Iacopo Marcon, and Giorgio Carmignoto

Studies over the last decade provided evidence that in a dynamic interaction with neurons glial cell astrocytes contribut to fundamental phenomena in the brain. Most of the knowledge on this derives, however, from studies monitoring the astrocyte Ca^{2+} response to glutamate. Whether astrocytes can similarly respond to other neurotransmitters, including the inhibitory neurotransmitter GABA, is relatively unexplored. By using confocal and two photon laser-scanning microscopy the astrocyte response to GABA in the mouse somatosensory and temporal cortex was studied. In slices from developing (P15-20) and adult (P30-60) mice, it was found that in a subpopulation of astrocytes GABA evoked somatic Ca^{2+} oscillations. This response was mediated by $GABA_B$ receptors and involved both $G_{i/o}$ protein and inositol 1,4,5-trisphosphate (IP_3) signalling pathways. *In vivo* experiments from young adult mice, revealed that also cortical astrocytes in the living brain exibit $GABA_B$ receptor-mediated Ca^{2+} elevations. At all astrocytic processes tested, local GABA or Baclofen brief applications induced long-lasting Ca^{2+} oscillations, suggesting that all astrocytes have the potential to respond to GABA. Finally, in patch-clamp recordings it was found that Ca^{2+} oscillations induced by Baclofen evoked astrocytic glutamate release and slow inward currents (SICs) in pyramidal cells from wild type but not $IP_3R2^{-/-}$ mice, in which astrocytic $GABA_B$ receptor-mediated Ca^{2+} elevations are impaired. These data suggest that cortical astrocytes in the mouse brain can sense the activity of GABAergic interneurons and through their specific recruitment contribut to the distinct role played on the cortical network by the different subsets of GABAergic interneurons.

GLIA 2015;00:000–000

Key words: GABAB receptor, calcium, somatosensory cortex, temporal cortex

Introduction

Over the last decade the glial cell astrocytes, beyond their broad control of brain tissue homeostasis and metabolism, have been recognized to regulate neuronal network activities (Araque et al., 2001; Carmignoto, 2000; Halassa et al., 2007; Haydon and Carmignoto, 2006; Perea et al., 2009; Volterra and Meldolesi, 2005). Indeed, astrocytes can modulate synaptic transmission and contribute to important phenomena in brain function thanks to a dynamic interaction with neurons that is finely regulated in time and space (Araque et al., 2014). It is now clear that astrocytes respond to the excitatory neurotransmitter glutamate with Ca^{2+} elevations mediated by metabotropic glutamate receptors (mGluR) and in response to this activation release various gliotransmitters, including glutamate, ATP, and D-serine that can exert multiple actions on neuronal communication, the nature of which depends on the specific type of targeted neuronal receptor and circuit. For example, astrocyte-derived glutamate can potentiate excitatory synaptic transmission through activation of presynaptic mGluR or N-methyl-D-aspartate (NMDA) receptors (Jourdain et al., 2007; Navarrete and Araque, 2010; Navarrete et al., 2012), but it can also favor neuronal synchronies by inducing slow inward currents mediated by postsynaptic NMDA receptors (D'Ascenzo et al., 2007;

View this article online at wileyonlinelibrary.com. DOI: 10.1002/glia.22933

Published online Month 00, 2015 in Wiley Online Library (wileyonlinelibrary.com). Received July 20, 2015, Accepted for publication Sep 28, 2015.

Address correspondence to Giorgio Carmignoto; via U.Bassi 58/b, 35121 Padova, Italy. E-mail: gcarmi@bio.unipd.it

From the Neuroscience Institute, National Research Council (CNR) and Department of Biomedical Sciences, University of Padova, via U.Bassi 58/B, Padova, 35121, Italy

L. Mariotti and G. Losi contributed equally to this work.

Fellin et al., 2004; Pirttimaki et al., 2013). Whether astrocytes can similarly respond to other neurotransmitters such as GABA is relatively unexplored and of great importance (for reviews, see Losi et al., 2014; Velez-Fort et al., 2011). Indeed, although depending on a minority of all cortical neurons, GABAergic signaling plays fundamental roles in the brain as it governs the excitability of principal neurons and dynamically controls network activity across the brain, generating cortical oscillations and participating in signal integration and synaptic plasticity (Bartos et al., 2007; Cardin et al., 2009; Klausberger et al., 2003; Petersen and Crochet, 2013; Sohal et al., 2009; Stark et al., 2013; Varga et al., 2012). It is worth underline that studies in brain slices revealed that hippocampal astrocytes respond to exogenous GABA with Ca^{2+} elevations mediated by both $GABA_A$ and $GABA_B$ receptors (Meier et al., 2008), whereas astrocytes from the olfactory bulb exhibit Ca^{2+} elevations that appear to be mediated exclusively by GABA transporters (Kozlov et al., 2006). In the present study, we characterize the response of astrocytes to GABAergic signals in different cortical areas by using single and two-photon laser-scanning microscopy for Ca^{2+} imaging and patch-clamp recordings in both brain slice and *in vivo* preparations. A recruitment of astrocytes by GABAergic signals may have functional consequences different or complementary to the highly specialized roles that the different interneuron classes have in the regulation of the brain circuit activity.

Materials and Methods

Animals

All procedures were conducted in accordance with the Italian and European Communities Council Directive on Animal Care and were approved by the Italian Ministry of Health. We used C57BL/6J mice (both sexes) at postnatal days 15–20 (P15–20; young) and P35–60 (adults). We also used $IP_3R2^{-/-}$ mice (Li et al., 2005) and mice obtained by crossing GCaMP3 (B6;129S-*Gt(ROSA)26-Sortm38(CAG-GCaMP3)Hzel*J) and GLAST-CreERT2 mice (Mori et al., 2006). The expression of GCaMP3 was tamoxifen-inducible. Tamoxifen (SIGMA Aldrich, Milano, IT) was dissolved in corn oil (20 mg/mL stock solution) and injected intraperitoneally (1 mg/day) twice in young mice (P7–10) and for 5 days in adult (P30–35) mice. Mice were analyzed 10 days after the last tamoxifen-injection.

Brain Slice Preparation

Coronal slices of 350 μm containing somatosensory (SSCx) or temporal cortex (TeCx) were obtained from mice at postnatal days P15–20 and P30–60. Animals were anaesthetized with Zoletil (40 mg/kg, Virbac, Cedex, France) and Xilazyne (40 mg/kg, BIO98 srl, Barcelona, Spain) and the brain was removed and transferred into an ice-cold solution (ACSF, in mM: 125 NaCl, 2.5 KCl, 2 $CaCl_2$, 1 $MgCl_2$, 25 glucose, pH 7.4 with 95% O_2, and 5% CO_2). Coronal slices were cut with a vibratome (Leica Vibratome VT1000S Mannheim, Germany) in the solution described in Dugue et al. (2005). Slices were transferred for 1 minute in a solution at room temperature containing (in mM): 225 D-mannitol, 2.5 KCl, 1.25 NaH_2PO_4, 26 $NaHCO_3$, 25 glucose, 0.8 $CaCl_2$, 8 $MgCl_2$, 2 kynurenic acid with 95% O_2, and 5% CO_2. Slices were transferred in ACSF at 30°C for 20 minutes and then maintained at room temperature for the entire experiment.

Dye Loading

Brain slices were kept in ACSF with Sulforhodamine 101 (SR-101) (0.2 μM, Sigma Aldrich, Milano, Italy) at 30°C for 15 minutes to selectively stain astrocytes (Nimmerjahn et al., 2004) and then loaded for 15 minutes at 31°C with the Ca^{2+} sensitive dyes Fluo-4 AM (10 μM; Life Technologies, Monza, Italy). Loading mix containing sulfinpyrazone (200 μM, Sigma Aldrich, Milano, Italy), pluronic F-127 (0.12%, Sigma Aldrich, Milano, Italy), and kynurenic acid (1 mM, Sigma Aldrich, Milano, Italy) and was constantly bubbled with 95% O_2 and 5% CO_2.

Drug Applications

Drugs applied with bath perfusion were (in μM): GABA 200 (Tocris, Bristol, United Kingdom); Baclofen 20–50 (BAC; Tocris, Bristol, United Kingdom); SCH50911 20–50 (Tocris, Bristol, United Kingdom), CGP52432 2.5 (Abicam Biomedicals, United Kingdom), Muscimol 100 (MUS; Tocris, Bristol, United Kingdom), Picrotoxin 100 (PTX; SIGMA Aldrich, Milano, Italy), DHPG 20-50 (Tocris, Bristol, United Kingdom), D-AP5 50 (Abicam Biomedicals, United Kingdom), Tetrodotoxin 0.5–1 (TTX; Abcam, Cambridge, United Kingdom). A pressure ejection unit (PDES, NPI Electronics, Tamm, Germany) connected to a glass pipette (tip diameter 2–3 μm) containing GABA or BAC (both at 500 μM) was used for local drug applications (pressure 3 psi; duration 200 ÷ 600 ms). Pertussis toxin (PerTx; SIGMA Aldrich, Milano, Italy) was dissolved in ACSF (7.5 μg/mL) and slices were incubated for 3–5 hours.

Brain Slice Imaging Experiments

Slice imaging experiments were conducted with a confocal laser scanning microscope TCS-SP5-RS (Leica Microsystems, GmbH, Wetzlar, Germany) equipped with two lasers tuned at 488 nm and 550 nm or with a two photon laser scanning microscope Multiphoton Imaging System (Scientifica Ltd., Uckfield, East Sussex, United Kingdom) equipped with a pulsed infrared laser (Chameleon Ultra 2, Coherent, Santa Clara, CA) tuned at 780 or 910 nm. Power at sample was controlled in the range 5–10 mW. The excitation wavelengths used were: 488 or 780 nm for Fluo-4 AM and 488 or 910 nm for GCaMP3 for single or two photon excitation, respectively. Images were acquired at a resolution of 512 × 512 with at 1–2 Hz frame rate. Imaging was performed in cortical layers II–III and V and conducted at maximum for 1 hour with 1–2 minutes recording sessions every 5 minutes.

In Vivo Imaging Experiments

Mice were anaesthetized with an intraperitoneal injection of urethane ethylcarbamate (1.5 g/kg body weight, 10%; SIGMA Aldrich, Milano, Italy) solved in saline solution. Animal pinch withdrawal and eyelid reflex were tested to assay the depth of anesthesia. Dexamethasone sodium phosphate (2 mg/kg body weight, MSD,

Boxmeer, Netherlands) was injected intramuscularly to reduce cortical stress response during surgery and prevent cerebral oedema. Dextran TRITC (20 μL; Sigma Aldrich, Milan, Italy) was injected in caudal vein to selectively mark blood vessel. Body temperature was maintained at 37°C with a feedback-regulated heating pad. We monitored the respiration rate, heart rate and core body temperature throughout the experiment. The mouse was head-fixed and a craniotomy of 2–3 mm in diameter was drilled over the SSCx (AP 2.5 mm from bregma; ML 3.3 mm). The dura was carefully removed and the craniotomy was immediately covered with a coverslip with a hole. Warm HEPES-buffered artificial cerebrospinal fluid (ACSF, in mM: NaCl, 125; KCl, 5; glucose, 10; HEPES, 10; $MgSO_4$ 2; and $CaCl_2$, 2; at [pH 7.4]) filled the chamber to prevent desiccation and maintain ionic balance. To perform topical application of BAC, a borosilicate micropipette (Sutter instruments 1–2 μm tip diameter) was positioned over the hole on the coverslip. Imaging was performed with a two-photon microscope (Ultima IV, Prairie Technology now Bruker, USA) at 910 nm with a Chameleon 2 laser (see above). Imaging was performed at a resolution of 512 × 512 pixels in superficial layers (50–150 μm below the cortical surface) and acquired at 1–2 Hz. Imaging session lasted up to 2 hours with 1–2 minutes recording sessions every 5 minutes.

Electrophysiological Recordings

Brain slices were continuously perfused in a submerged chamber at a rate of 3–4 mL/min with (in mM): NaCl, 120; KCl, 2.5; NaH_2PO4, 1; $NaHCO_3$, 26; $MgCl_2$, 1; $CaCl_2$, 2; glucose, 10; at pH 7.4 (with 5% CO_2/95% O_2). Single and dual cell recordings were performed in voltage-clamp and current-clamp configuration using a multiclamp-700B amplifier (Molecular Devices, Foster City, CA) under the same microscopes as for slice imaging (see above). Signals were filtered at 1 kHz and sampled at 10 kHz with a Digidata 1440s interface and pClamp10 software (Molecular Devices, Foster City, CA). Typical pipette resistance was 3–4 MΩ. Access resistance was monitored throughout the recordings and was typically less than 25 MΩ. Whole-cell intracellular pipette solution was (in mM): K-gluconate, 145; $MgCl_2$, 5; EGTA, 0.5; Na_2ATP, 2; Na_2GTP, 0.2; HEPES, 10; to pH 7.2 with KOH, osmolarity, 280 ÷ 290 mOsm (calculated liquid junction potential: −14 mV). Pyramidal cells were identified on the basis of their distinct morphology and their response to hyperpolarizing and depolarizing 750 ms current steps. We selected only neurons showing a firing discharge with no spike amplitude accommodation (except for the second action potential in some cells), small after hyperpolarization and low steady-state frequency (15 ÷ 23 Hz with 200 pA current injection). SICs were recorded in Mg^{2+} free solution in presence of TTX, 1 μM (Abcam, Cambridge, UK) at a holding potential of −70 mV.

Data Analysis and Statistics

Data analysis was performed with Clampfit 10, Origin 8.0 (Microcal Software), Microsoft Office, ImageJ (NIH) and MATLAB 7.6.0 R2008A (Mathworks, Natick, MA). For imaging experiments, image sequences were aligned and processed with ImageJ and MATLAB. Region of interests (ROIs) were manually drawn around cellular body and processes using the red channel from the SR-101 signal. All pixels within each ROI were averaged to give a single time course $F(t)$. The Ca^{2+} signal for each ROIs was computed as $\Delta F/F_0 = (F(t) - F_0)/(F_0 - \text{background})$, where F_0 is the baseline fluorescence level obtained by averaging the fluorescence recorded during baseline activity. Peaks in the fluorescence were considered significant event when exceeding three standard deviation of the signal measured in baseline conditions. In electrophysiological experiments, inward currents with rise time (10%–90%) slower than 10 ms and amplitude greater than 20 pA were classified as SICs. The relative frequency of SICs was measured in the 5 minutes post pressure pulse applications (average of 1–3 applications, repeated every 5 minutes) then divided by each cell's control calculated in the period before BAC application (5 ÷ 25 minutes). For the analysis of other SICs parameters (rise, decay, duration, peak amplitude, and charge transferred) two minutes following BAC applications were considered.

According to data normal distribution we performed two-tailed Student's *t*-test for the percentage of active astrocytes and SIC frequency. Otherwise we used Wilcoxon test for Ca^{2+} peak frequency and Mann–Whitney test for SICs area, rise, decay, duration, and peak amplitude. Results were considered statistically significant when $^{*}P < 0.05$, $^{**}P < 0.01$, $^{***}P < 0.001$. All results are presented as mean ± s.e.m.

Results

Cortical Astrocytes Exhibit $GABA_B$ Receptor-Mediated Ca^{2+} Oscillations in Response to the Inhibitory Neurotransmitter GABA

We studied the response of astrocytes to GABA in slice preparations from the SSCx of young mice (P15–20) after incubation with the selective astrocytic marker SR-101 and the Ca^{2+} fluorescent indicator Fluo-4 AM (Fig. 1A,B). The Ca^{2+}-mediated fluorescence changes in astrocytes were recorded upon bath perfusion with GABA in the presence of TTX to block neuronal activity. At resting conditions a small fraction of astrocytes exhibited spontaneous Ca^{2+} transients at low frequency (Fig. 1D). Upon GABA applications, a significant number of cortical astrocytes showed a sustained Ca^{2+} response characterized by repetitive Ca^{2+} peaks (Fig. 1C1–3, D). To dissect out the GABA receptor involved in the astrocytic response, we next tested the effect of selective $GABA_A$ and $GABA_B$ receptor agonists and antagonists. We found that GABA-evoked Ca^{2+} responses in astrocytes were fundamentally unchanged in the presence of the selective $GABA_A$ receptor blocker PTX (Fig. 1C2, D), whereas both the frequency of Ca^{2+} oscillations and the number of active astrocytes were drastically reduced when GABA was applied in the presence of selective $GABA_B$ receptor antagonists (CGP 52432 and SCH 50911, Fig. 1C3, D). Consistent with a $GABA_B$ receptor-mediated response, the selective $GABA_A$ receptor agonist MUS failed to activate astrocytes (Fig. 1D). Conversely, the selective $GABA_B$ receptor agonist BAC induced Ca^{2+} elevations in astrocytes that were similar to those evoked by GABA (Fig. 1C4, D). Comparable results were also

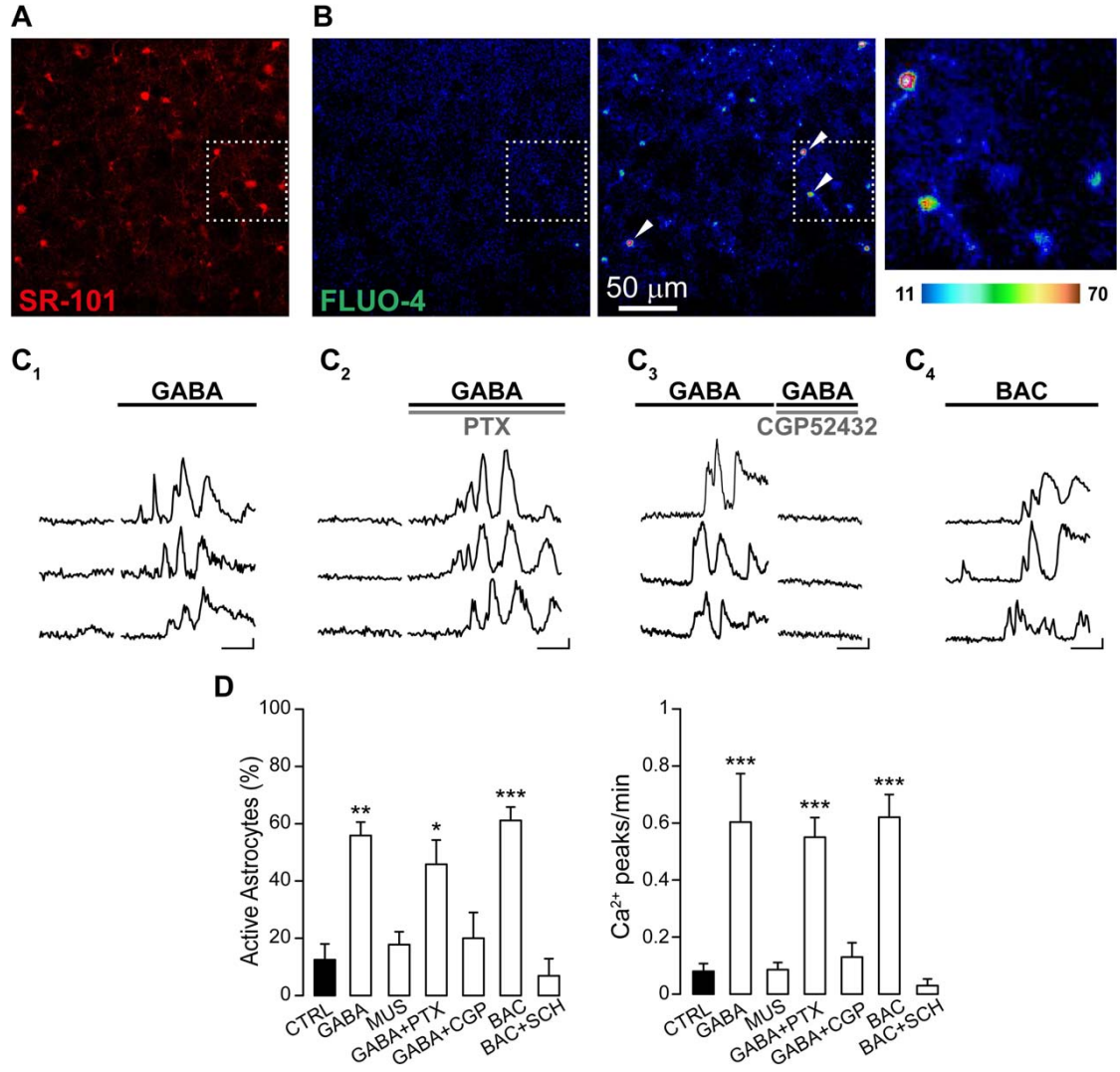

FIGURE 1: GABA activates somatic Ca^{2+} transients in astrocytes via $GABA_B$ receptor. (A) Red-fluorescent SR-101 selective labelling of astrocytes from SSCx. (B) Pseudo-colored images from FLUO-4 AM fluorescence signal acquired before (left) and after GABA applications in the presence of PTX (middle). The *white square* indicates the magnification with four astrocytic soma showing Ca^{2+} increases (right). Images are a maximal intensity projection of 35 frames. ($C_{1\text{-}4}$) Fluorescence signals over time from three astrocytes (indicated in B by *arrowheads*) in basal conditions and after perfusion with GABA (C_1), GABA and PTX (C_2), GABA and CGP 52432 (C_3) or BAC (C_4), respectively (scale bars: 50% $\Delta F/F_0$, 50 s). (D) Histograms showing the percentage of active astrocytes and the Ca^{2+} events frequency in different experimental conditions: GABA (76 astrocytes, 4 experiments; for percentage $P = 0.002$; for frequency $P = 1.97\ e^{-9}$), MUS (112 astrocytes, 5 experiments; for percentage $P = 0.644$; for frequency $P = 0.793$), GABA in presence of PTX (125 astrocytes, 5 experiments; for percentage $P = 0.015$; for frequency $P = 1.98\ e^{-9}$), GABA in presence of CGP 52432 (117 astrocytes, 9 experiments; for percentage $P = 0.451$, for frequency $P = 0.433$), BAC (99 astrocytes, 6 experiments; for percentage $P = 3.654\ e^{-5}$; for frequency $P = 2.24\ e^{-15}$), BAC in presence of SCH 50911 (112 astrocytes, 4 experiments; for percentage $P = 0.761$, for frequency $P = 0.500$).

obtained in slices from the TeCx where BAC evoked Ca^{2+} responses in 47.9% ± 12.1% of the astrocytes monitored (94 astrocytes, 4 experiments), suggesting that astrocyte responsiveness to GABA may be conserved in different neocortical regions. As in the SSCx, the astrocytic response in the TeCx was also prevented by the $GABA_B$ receptor antagonists SCH 50911 (data not shown).

$GABA_B$ receptor-Mediated Ca^{2+} Elevations in Astrocytes Depend on Activation of Both $G_{i/O}$ Protein and IP_3 Signaling

To clarify the cellular mechanism of $GABA_B$ receptor-mediated Ca^{2+} transients in astrocytes, we first tested the involvement of $G_{i/o}$ protein activation, because neuronal $GABA_B$ receptors are coupled to this subset of G-proteins

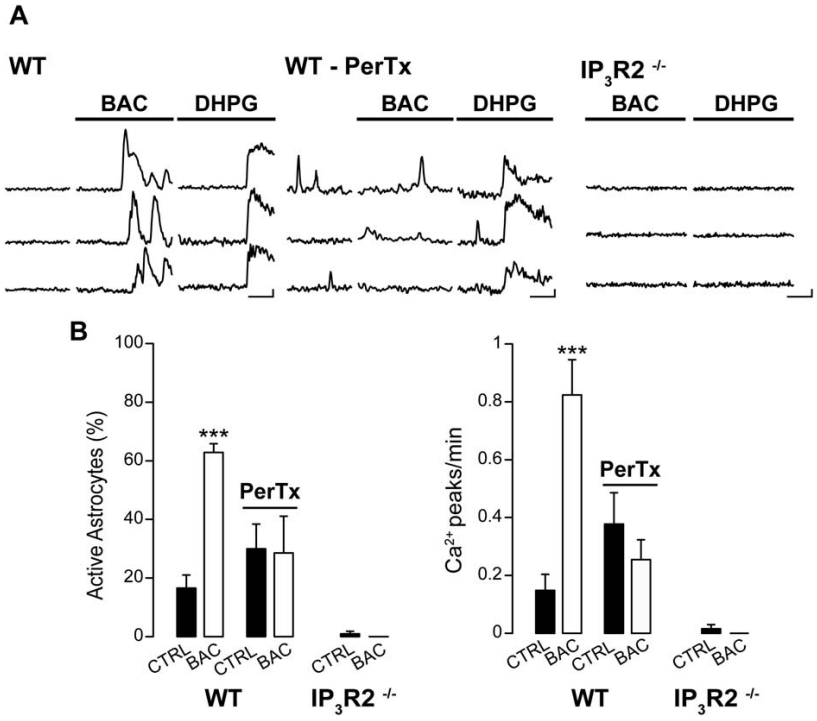

FIGURE 2: Astrocyte $GABA_BR$ activation recruits $G_{i/o}$ protein and IP_3 intracellular cascade. (A) Ca^{2+} signal changes from three representative astrocytes in response to BAC in control conditions (WT), after $G_{i/o}$ protein block by PerTx (WT-PerTx) and in transgenic mice lacking astrocytic inositol-1,4,5-trisphosphate ($IP_3R2^{-/-}$) signaling. As a control, we used DHPG that evoked Ca^{2+} increases in slices from WT, but not in $IP_3R2^{-/-}$ mice (scale bars: 50% $\Delta F/F_0$, 50 s). (B) Histograms showing the percentage of active astrocytes and the frequency of Ca^{2+} events per minute upon BAC applications, both in presence and in absence of PerTx (54 astrocytes in control conditions vs. 53 astrocytes treated with PerTx; 5 experiments; CTRL: for percentage $P = 0.00012$, for frequency $P = 1.19\ e^{-7,}$ PerTX: for percentage $P = 0.931$, for frequency $P = 0.185$) and in $IP_3R2^{-/-}$ mice (90 astrocytes, 7 experiments; for percentage $P = 0.337$, for frequency $P = 1$). In presence of PerTx, BAC failed to evoke astrocytic Ca^{2+} elevations.

(Bettler et al., 2004). Slices loaded with Fluo-4 AM and the selective astrocytic marker SR-101 were incubated with the $G_{i/o}$ blocker PerTx. We found that PerTx occluded in astrocytes the BAC-induced Ca^{2+} events, but not those evoked by DHPG, an agonist of the metabotropic glutamate receptor 1 and 5 associated with Gq-protein and IP_3 intracellular

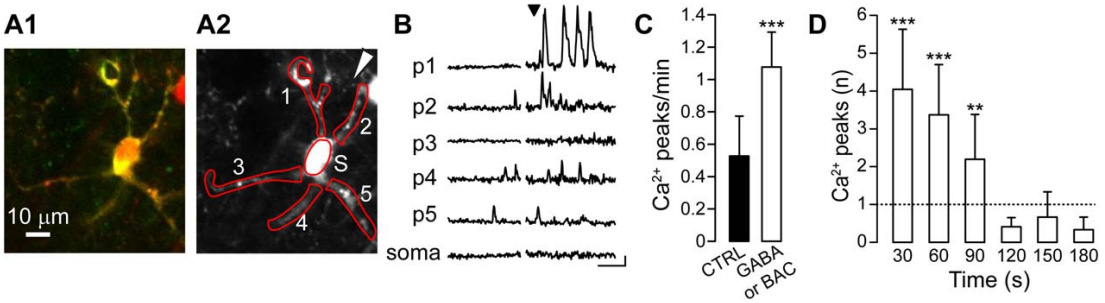

FIGURE 3: GABA activates long lasting Ca^{2+} transients in astrocytic processes. (A_1) Two-photon Ca^{2+} imaging of an astrocyte expressing the genetically encoded Ca^{2+} indicator $GCaMP_3$ and loaded with SR-101. Merged picture in which GCaMP3 and SR-101 positive astrocyte appear in yellow. (A_2) Mean intensity projection from SR-101 signal. Red ROIs highlight five primary processes and the soma, white arrowhead indicates the position of the pipette. (B) Ca^{2+} traces before and after local BAC applications (*black arrowhead*) from the five processes in A_2 (1–5) and from the soma (s; scale bars: 20% $\Delta F/F_0$, 50 s). (C) Histograms of Ca^{2+} peak frequency before and after GABA or BAC applications (pooled data, 89 primary processes from 16 astrocytes, 9 experiments; for frequency $P = 2.85\ e^{-6}$). (D) Mean number of Ca^{2+} peaks at different times after the brief GABA or BAC applications. The number was normalized to the mean value of Ca^{2+} oscillations observed in basal conditions and represented by the grey dotted line. Each period corresponds to a bin of 30 s (for 30 s, $P = 8.08\ e^{-6}$; for 60 s, $P = 3.82\ e^{-6}$; for 90, $P = 0.009$).

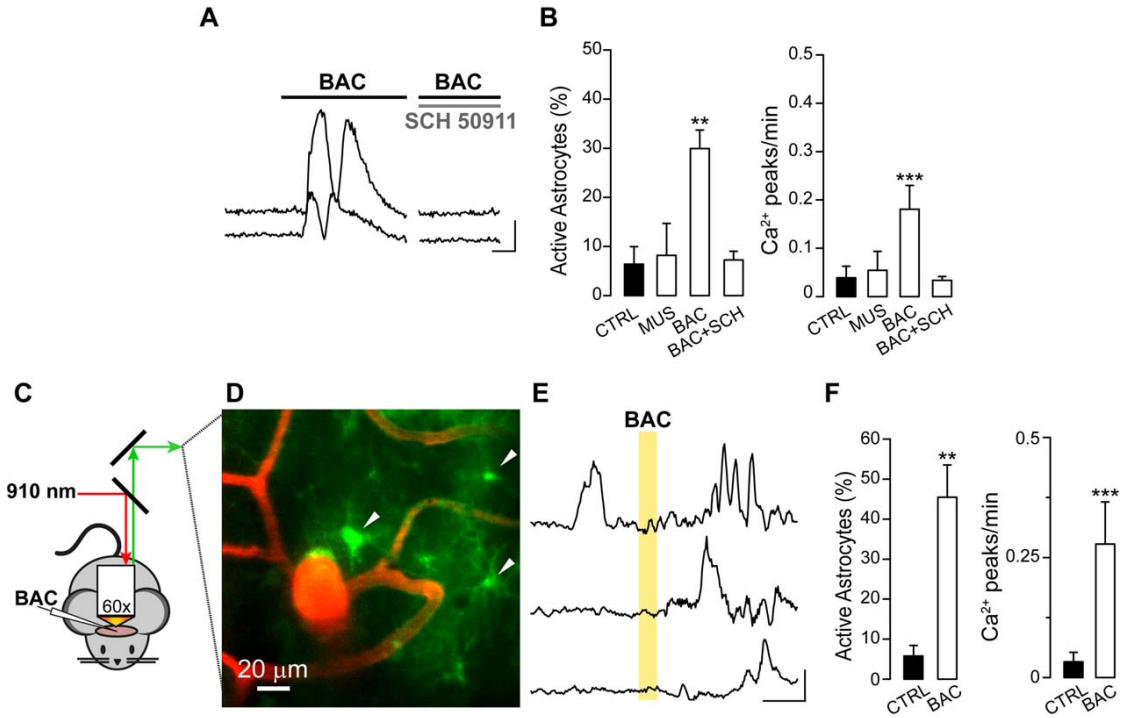

FIGURE 4: Local BAC applications trigger astrocyte Ca^{2+} transients in GCaMP3 adult mice. (A,B) Experiments in brain slices. (A) Fluorescence signals over time from two representative astrocytes acquired in basal conditions and after application of BAC alone or BAC with SCH 50911 (scale bars: 50% $\Delta F/F_0$, 50 s). (B) Histograms showing the percentage of active astrocytes and the Ca^{2+} event frequency in different experimental conditions: MUS (48 astrocytes, 4 experiments; for percentage $P = 0.915$, for frequency $P = 1$), BAC (92 astrocytes, 6 experiments; for percentage $P = 0.004$, for frequency $P = 1.51e^{-5}$), SCH 50911 (30 astrocytes, 2 experiments; for percentage $P = 0.151$, for frequency $P = 1$). (C–F) Experiments in anaesthetized mice. (C) Schematic representation of the two-photon *in vivo* set up. The excitation wavelength 910 nm excites both Dextran-TRITC and GCaMP3. (D) Maximal projection of blood vessels filled with Dextran-TRITC and astrocytes expressing GCaMP3 in layer I/II of SSCx (right). *White arrowheads* indicate three representative astrocytes soma. (E) Ca^{2+} traces before and after a BAC application. *Yellow area* marks the local BAC application (scale bars: 20% $\Delta F/F_0$, 50 s). (F) Summarizing histograms showing the percentage of active astrocytes and the Ca^{2+} events frequency in control conditions and after BAC applications (72 astrocytes, 4 animals; for percentage $P = 0.003$, for frequency $P = 9.61\ e^{-7}$).

signalling pathway (Fig. 2A, B), indicating that $G_{i/o}$-protein activation is necessary for BAC-induced Ca^{2+} elevations (Fig. 2A). We then evaluated whether the IP_3 pathway could also be involved by using SSCx and TeCx slices obtained from IP_3 receptor type 2-deficient mice ($IP_3R2^{-/-}$). The expression of this receptor in the brain is confined mainly, if not exclusively, to astrocytes in which it mediates the release of Ca^{2+} from endoplasmic reticulum (Hertle and Yeckel, 2007; Holtzclaw et al., 2002; Sharp et al., 1999). We first confirmed that the intracellular somatic Ca^{2+} elevations mediated by IP_3 signaling pathway are impaired in these mice, applying DHPG that failed to evoke any Ca^{2+} response (Fig. 2A). We next observed that astrocytes from these slice preparations also failed to respond to BAC (Fig. 2A, B) suggesting that beside $G_{i/o}$-protein, in astrocytes $GABA_B$-receptor mediated Ca^{2+} signal changes in response to GABA depend also on IP_3 intracellular cascade.

The Response of Astrocytic Processes to GABA is Composed of Sustained Ca^{2+} Oscillations

To further characterize the response to GABAergic signals at the level of astrocytic processes, we imaged Ca^{2+} signal dynamics in SSCx slices obtained from mice expressing the genetically encoded Ca^{2+} indicator GCaMP3 selectively in astrocytes (GCaMP3::GLAST-CreERT2 mice, see "Materials and Methods" sections). After loading slices with SR-101, we quantified the number of cells positive for both SR-101 and GCaMP3 (Fig. 3A1). We found that 74.8% ± 5.6% of 116 SR-101 labeled astrocytes (8 experiments) also expressed GCaMP3. Most importantly, all GCaMP3-expressing cells were marked by SR-101 confirming their astrocytic identity. We then used brief pressure pulses (200–500 ms duration, 2–3 PSI) to apply BAC or GABA from a glass micropipette located 10–20 µm from the processes of interest (Fig. 3A2). We found that a single, brief $GABA_B$ receptor agonist

application induced repetitive Ca^{2+} peaks in processes that outlasted the stimulus duration for at least 90 seconds (Fig. 3B–D). Notably, GABA was regularly effective in inducing Ca^{2+} elevations at the level of the processes whereas the response to GABA bath applications at the level of the soma was observed only in a subpopulation of astrocytes.

The $GABA_B$ Receptor Evoked Response in SSCx Astrocytes is Conserved in the Living Brain of Adult Mice

We next asked whether the astrocyte response to $GABA_B$ receptor activation that we observed in cortical slices from young mice is maintained in adulthood. We found that in slices obtained from adult GCaMP3::GLAST-CreERT2 mice ($30 < P < 60$), BAC triggered Ca^{2+} transients similar to those observed in astrocytes from young mice, although the number of responsive astrocytes was lower with respect to that in slices from young animals (Fig. 4A, B; compare with Fig. 1). Also in adult slices, MUS failed to activate astrocytes (Fig. 4B) while the $GABA_B$ receptor antagonist SCH 50911 largely suppressed the astrocytic Ca^{2+} response to BAC (Fig. 4A, B).

To validate the results obtained in brain slice preparations, we performed two-photon Ca^{2+} imaging in the living brain of P30–60 anaesthetized GCaMP3 mice (Fig. 4C, D). We found that a large number of astrocytes from layer I/II of the primary SSCx responded to BAC applied to cortical surface with repetitive Ca^{2+} elevations (Fig. 4E, F).

GABA-Activated Astrocytes Release Glutamate That Evokes Pyramidal Neuron Firing Activity

We next investigated whether and how GABA-activated astrocytes signal back to neurons. In SSCx slices from young mice (P15–20), we performed single and dual cell patch-clamp recordings from pyramidal neurons in SSCx slices in the presence of TTX (1 μM) and nominally Mg^{2+} free solution to favor NMDA receptors activation. Under these conditions, we recorded low frequency glutamatergic SICs that we know to be due to spontaneous release of glutamate from astrocytes (Fellin et al., 2004). To avoid a sustained activation of neuronal $GABA_B$ receptors by bath applied BAC, we used local BAC pressure pulse applications (400–600 ms, 5–7 PSI). This stimulation evoked a hyperpolarizing current mediated by neuronal postsynaptic $GABA_B$ receptors in neurons located less than 100 μm from the BAC pipette tip (Fig. 5A, range 80 ÷ 150 μm; mean duration, 54 ± 9 s; $n = 10$ neurons). BAC applications also induced long-lasting Ca^{2+} oscillations in astrocytes (Fig. 3) and SICs in neurons with a frequency that remained increased with respect to control for 2 minutes after BAC applications (Fig. 5A, B). Spontaneous and BAC-induced SICs, in the 2 minutes following the application, had similar slow kinetics (rise 10%–90%: 94 ± 13 ms, $n = 60$, before and 90 ± 13 ms, $n = 38$, after BAC, $P = 0.897$; decay 90%–10%: 339 ± 46 ms, $n = 56$, before and 358 ± 54 ms, $n = 33$, after BAC, $P = 0.340$; duration: 0.78 ± 0.10 s, $n = 60$, before and 0.70 ± 0.10s; $n = 40$, after BAC, $P = 0.935$; 18 experiments), area (Fig. 5C) and peak amplitude (-75 ± 7 pA, $n = 59$ before and -101 ± 14 pA, $n = 40$, $P = 0.145$,; see also Fig. 5F). Similarly to what observed with other stimuli also BAC-induced SICs were mediated by NMDA receptors being strongly reduced by D-AP5 (50 μM; Fig. 5A, E; peak -28 ± 12 pA, $P = 0.0001$; $n = 9$, 5 experiments).

To assess whether BAC-evoked SICs depend on astrocytic Ca^{2+} elevations, we performed patch-clamp experiments in slices from $IP_3R2^{-/-}$ mice in which G-protein coupled Ca^{2+} elevations are impaired in astrocytes, as reported above (Fig. 2A). We found that in slices from $IP_3R2^{-/-}$ mice, BAC failed to increase SIC frequency in pyramidal neurons (Fig. 5C, E; 13 experiments). These data indicate that the increased SIC frequency observed in neurons upon BAC challenge is mediated by IP_3-mediated Ca^{2+} elevations in astrocytes.

In diverse brain regions including cortex, hippocampus and nucleus accumbens (D'Ascenzo et al., 2007; Fellin et al., 2004), pair recording experiments revealed that SICs can occur with a high degree of synchrony in contiguous pyramidal neurons. We thus tested whether BAC-evoked SICs could also occur synchronously in neighboring pyramidal neurons. To this aim, we performed patch-clamp recordings from pairs of adjacent pyramidal neurons (Fig. 5B; <100 μm apart) and found that after BAC application 8 out of 20 SICs recorded were synchronous (range 4 ÷ 74 ms from 2 paired recordings). Next, to assess the possibility that SICs could induce action potential firing in pyramidal cells, we first divided the amplitude of all SICs recorded to each cell's rheobase current. We found that SICs above rheobase were 58% in control and 67% following BAC applications (Fig. 5F). Finally, in dynamic clamp experiments we injected SICs in pyramidal neurons of increasing amplitude and duration in the absence of TTX. We found that 100 pA SIC evoked 1 to 2 action potentials in 3 out of 9 cells tested, while larger events evoked intense firing activity in all cells tested (Fig. 5G; 3.4 ± 0.4 and 11.4 ± 1.1 action potentials with SICs of 131 pA, $n = 9$, and 285 pA, $n = 8$, respectively).

Discussion

In the present study we provide evidence that a similar subpopulation of astrocytes from two cortical regions of the mouse brain, that is, the SSCx and the TeCx, responds to GABA with intracellular Ca^{2+} increases which depend on activation of both $GABA_B$ receptors and IP_3 intracellular signaling. These Ca^{2+} elevations have a marked tendency to oscillate for prolonged periods even after brief $GABA_B$ receptor activations and induce in astrocytes the release of the gliotransmitter

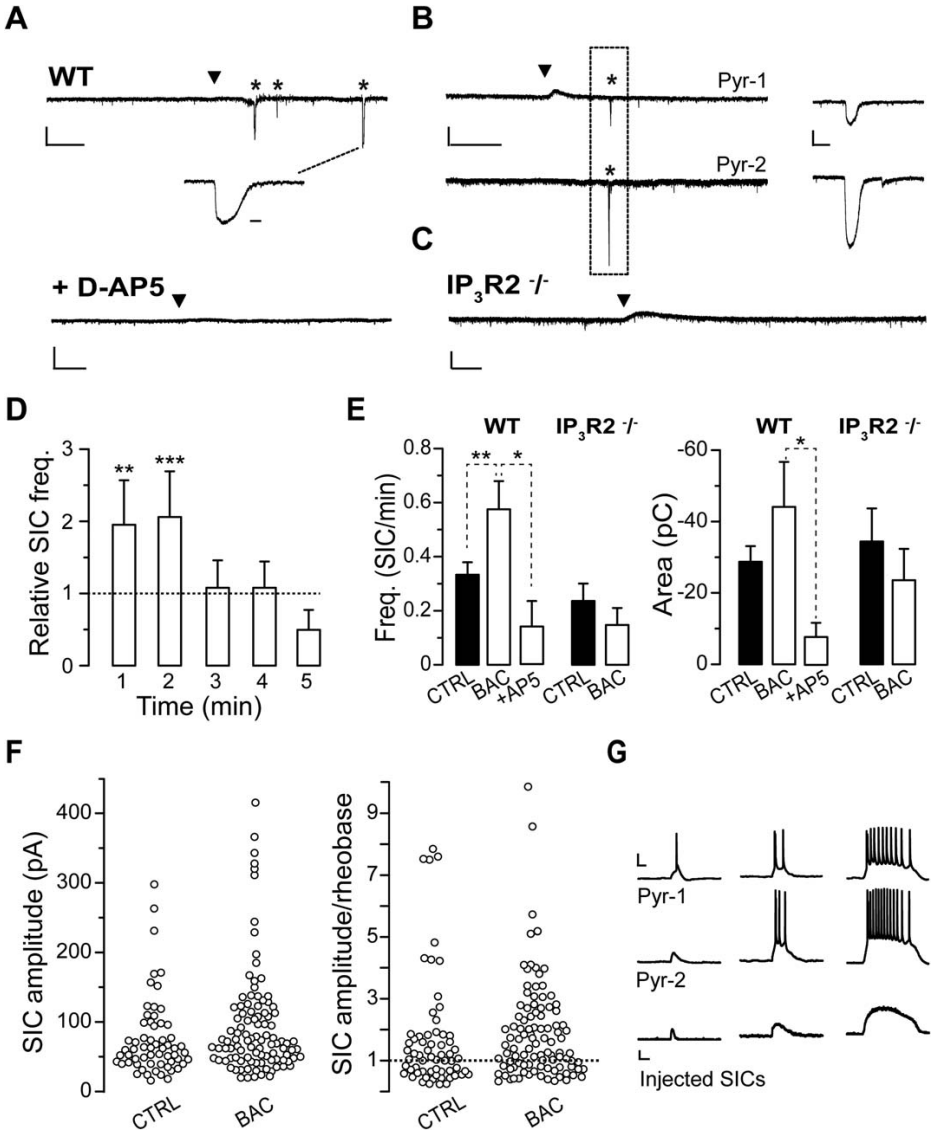

FIGURE 5: GABA-activated astrocytes evoke SICs in pyramidal neurons. (A–C) Representative whole cell currents from single pyramidal neurons (A) or a pair (C) of adjacent pyramidal neurons (90 μm apart; Pyr-1 and −2) showing the occurrence of SICs (*asterisks*) after a BAC local application (*black arrowheads*) to layer V SSCx in a WT mouse and the absence of SICs upon a similar BAC application in presence of D-AP5 (A) and in $IP_3R2^{-/-}$ mice (C). (Scale bars: For single recordings: 1 minute, 100 pA; enlarged SIC: 500 ms; for paired recording and D-AP5: 20 s, 100 pA and 2 s for the enlarged SIC. **(D)** The relative SIC frequency is significantly increased for 2 minutes following BAC application (see Methods; $n = 21$ cells, $P = 0.006$ and 0.001, for first and second minute, respectively). **(E)** Summary of SIC mean frequency and area before and after (2 minutes) local BAC applications in WT and $IP_3R2^{-/-}$ mice. (Frequency: for WT, $n = 21$ cells, $P = 0.010$; in presence of D-AP5, $P = 0.028$, $n = 5$ cells; for $IP_3R2^{-/-}$ mice, $n = 13$ cells; $P = 0.367$; Area: for WT mice, $n = 60$ SICs for control and 38 after BAC; $P = 0.407$; in presence of D-AP5, $P = 0.050$, $n = 9$ SICs; for $IP_3R2^{-/-}$ mice, $n = 30$ and 9 SICs for control and after BAC, respectively, $P = 0.536$). **(F)** Distribution of all SIC peak amplitude recorded before and after BAC applications (**left**) and ratio of each SIC peak amplitude to the action potential threshold (rheobase) in each cell (**right**). **(G)** Examples of membrane potential recordings (upper and middle traces) from two different pyramidal neurons (Pyr-1 and −2) during the injection of SICs of increasing size (lower traces, peak amplitudes of 100, 131, and 285 pA) show the occurrence of action potentials during SICs.

glutamate which evokes synchronous NMDAR-mediated depolarizing events in pyramidal neurons. Such a functional response of astrocytes to the inhibitory neurotransmitter GABA suggests that the recruitment of astrocytes may accompany the activity of the different classes of interneurons in the brain and have functional consequences on local network excitability.

Previous studies in cultured astrocytes (Nilsson et al., 1993) and hippocampal slices from young rats (Meier et al., 2008) described GABA-induced Ca^{2+} elevations in astrocytes that were mediated by both $GABA_A$ and $GABA_B$ receptors, while others reported in hippocampal astrocytes Ca^{2+} responses exclusively mediated by $GABA_B$ receptors (Kang et al., 1998; Serrano et al., 2006). Activation of $GABA_A$ receptors in astrocytes may lead to a membrane depolarization and increase the intracellular Ca^{2+} in these cells through voltage-operated calcium channel (VOCC) activation. In our experiments, however, we never observed astrocytic Ca^{2+} elevations upon a selective activation of the $GABA_A$ receptor. This discrepancy may possibly be ascribed to the different area, that is, cortex versus hippocampus, or species used, that is, mouse versus rats. Notably, however, while in cultures astrocytes can express VOCCs (Parpura et al., 2011; Verkhratsky et al., 2012; Verkhratsky and Steinhauser, 2000) and cells undergoing reactive astrogliosis in status epilepticus can exhibit measurable L- and P/Q channel activity (Westenbroek et al., 1998), whether astrocytes *in situ* express VOCCs remains unclear (Carmignoto et al., 1998). An additional mechanism that can indirectly favor astrocytic Ca^{2+} elevations in response to GABA has been revealed in slices from the developing olfactory bulb. There, an intense activity of the GABA transporters (GATs) is observed to cause a Na^+ overloading in the astrocytes which then leads to Ca^{2+} elevations due to an inverse operation of the Na^+/Ca^{2+} exchanger (Doengi et al., 2009). The fact that in our experiments GABA-mediated responses in astrocytes were abolished by $GABA_B$ receptor selective antagonists argues against a possible involvement of GATs in cortical astrocyte response to GABA.

In rat hippocampal astrocytes, a developmental profile of $GABA_B$ receptor-mediated astrocytic responses, with a peak between P11 and P15 and a marked decline after P21, has been described (Meier et al., 2008). In slices from young adult mice we found that the percentage of GABA-responsive astrocytes was only slightly reduced with respect to that observed in slices from P15–20 mice. In addition and most importantly, in specific *in vivo* experiments in anaesthetized adult GCaMP3 mice, we observed prompt Ca^{2+} elevations in layer I/II astrocytes of the SSCx in response to the $GABA_B$ receptor agonist BAC. All in all, our results provide evidence that from the early development to adulthood, neocortical astrocytes maintain their potential to respond to GABA with Ca^{2+} elevations and that their response is fundamentally mediated by $GABA_B$ receptor activation.

An additional observation that we describe here regards the mechanism at the basis of the astrocyte Ca^{2+} response to GABA. We reveal that the astrocytic response is sensitive to the $G_{i/o}$ blocker PerTx. We also reveal that in slices obtained from $IP_3R2^{-/-}$ mice $GABA_B$-mediated Ca^{2+} responses are also abolished which suggests an involvement of both signaling, that is, the $G_{i/o}$ protein and the IP_3-mediated intracellular pathway, in astrocytic GABA-induced Ca^{2+} elevations. The full intracellular cascade at the basis of the $GABA_B$ receptor-mediated intracellular Ca^{2+} increases remains, however, unclear. In general, astrocytic Ca^{2+} oscillations result from the activation of the G_q-coupled metabotropic receptor and IP_3 intracellular signaling cascade. It is possible that also $G_{i/o}$ protein signalling converges on the IP_3-signaling pathway. Indeed, it has been shown that activation of $G_{\beta/\gamma}$ complex can lead to stimulation of PLC_β1-3 (Pierce et al., 2002) or directly of IP_3 formation (Zeng et al., 2003). Alternatively, a specific interaction between $G_{i/o}$ and G_q protein could occur and mediate IP_3R2-dependent astrocytic responses. Notwithstanding these possible hypotheses, additional studies are necessary to fully elucidate the intracellular mechanism of the GABA-mediated Ca^{2+} response in astrocytes.

Elevations in the intracellular Ca^{2+} in response to GABA were observed not only at the level of the soma, but also at astrocytic processes that are, in principle, closer than the soma to GABAergic axon terminals. Consistent with the expression of $GABA_B$ receptors at these sites, in slices from GCaMP3::GLAST-CreERT2 mice we observed Ca^{2+} oscillations at these astrocytic processes upon a single, brief stimulation with GABA or BAC applied locally through a glass pipette. This response at the processes was observed even in absence of Ca^{2+} increases at the soma, and although they were induced by a brief stimulation, they were sustained for about two minutes, largely outlasting stimulus duration. These results suggest that, similarly to glutamate-mediated Ca^{2+} elevations, GABA-mediated Ca^{2+} elevations at the processes can be integrated by the astrocytes into a more global response that eventually includes the soma.

We found that GABA-activated astrocytes release glutamate which triggers in pyramidal cells NMDA receptor-mediated SICs. We also found that these events in the virtual absence of extracellular Mg^{2+} induce an intense action potential firing in these cells. In the presence of physiological extracellular Mg^{2+} SIC amplitude is, however, reduced (Fellin et al., 2004). Therefore, under physiological conditions only large amplitude SICs may induce a membrane depolarization in pyramidal cells sufficient to reach action potential threshold. Consistent with the sustained Ca^{2+} oscillations induced in astrocytes by GABA, SICs occurred for a few minutes, outlasting the time of GABA agonist applications. Notably, our data revealed that in slices from $IP_3R2^{-/-}$ mice $GABA_B$ receptor stimulation failed to evoke both Ca^{2+} elevations in astrocytes and SICs in pyramidal neurons, further validating the astrocytic origin and the Ca^{2+} dependency of GABA-evoked SICs. In line with previous observations from different brain regions (Angulo et al., 2004; Bardoni et al., 2010;

Cavelier and Attwell, 2005; D'Ascenzo et al., 2007; Fellin et al., 2004; Gomez-Gonzalo et al., 2010; Nestor et al., 2007; Pirttimaki et al., 2013; Reyes-Haro et al., 2010; Shigetomi et al., 2008), SICs were demonstrated to be mediated by NMDA receptors and to occur synchronously in adjacent pyramidal neurons. These observations suggest that astrocytes in response to a brief stimulation with the inhibitory neurotransmitter GABA, signal back to local circuits and by enhancing synchronized activity in pyramidal neurons turn a local transient inhibition into a delayed excitation.

In conclusion, in the present study we show that astrocytes from two different neocortical regions committed to different brain functions, that is, the SSCx and the TeCx of the mouse, have the potential to sense synaptic GABA and to respond to this signal with oscillatory Ca^{2+} transients and glutamate release that can affect local network activities. Our observations urge for additional studies that could specifically explore whether and how astrocytes are recruited by the different classes of GABAergic interneurons.

Acknowledgment

Grant sponsor: Telethon Italy; Grant number: GGP12265; Grant sponsor: Fondazione Cariparo; Grant sponsor: National Research Council Aging Project; Grant sponsor: Fondo Per gli Investimenti della Ricerca di Base; Grant number: RBAP11X42L.

We thank Alfonso Araque and Tommaso Fellin for the generous gift of $IP_3R2^{-/-}$ and GLAST-CreERT2 mice, respectively. We also thank Angela Chiavegato for help with *in vivo* procedures; Alessandra Tessari and Micaela Zonta for excellent technical support.

References

Angulo MC, Kozlov AS, Charpak S, Audinat E. 2004. Glutamate released from glial cells synchronizes neuronal activity in the hippocampus. J Neurosci 24:6920–6927.

Araque A, Carmignoto G, Haydon PG. 2001. Dynamic signaling between astrocytes and neurons. Annu Rev Physiol 63:795–813.

Araque A, Carmignoto G, Haydon PG, Oliet SH, Robitaille R, Volterra A. 2014. Gliotransmitters travel in time and space. Neuron 81:728–739.

Bardoni R, Ghirri A, Zonta M, Betelli C, Vitale G, Ruggieri V, Sandrini M, Carmignoto G. 2010. Glutamate-mediated astrocyte-to-neuron signalling in the rat dorsal horn. J Physiol 588(Pt 5):831−846.

Bartos M, Vida I, Jonas P. 2007. Synaptic mechanisms of synchronized gamma oscillations in inhibitory interneuron networks. Nat Rev Neurosci 8:45–56.

Bettler B, Kaupmann K, Mosbacher J, Gassmann M. 2004. Molecular structure and physiological functions of $GABA_B$ receptors. Physiol Rev 84: 835–867.

Cardin JA, Carlen M, Meletis K, Knoblich U, Zhang F, Deisseroth K, Tsai LH, Moore CI. 2009. Driving fast-spiking cells induces gamma rhythm and controls sensory responses. Nature 459:663–667.

Carmignoto G. 2000. Reciprocal communication systems between astrocytes and neurones. Prog Neurobiol 62:561–581.

Carmignoto G, Pasti L, Pozzan T. 1998. On the role of voltage-dependent calcium channels in calcium signaling of astrocytes in situ. J Neurosci 18: 4637–4645.

Cavelier P, Attwell D. 2005. Tonic release of glutamate by a DIDS-sensitive mechanism in rat hippocampal slices. J Physiol 564(Pt 2):397–410.

D'Ascenzo M, Fellin T, Terunuma M, Revilla-Sanchez R, Meaney DF, Auberson YP, Moss SJ, Haydon PG. 2007. mGluR5 stimulates gliotransmission in the nucleus accumbens. Proc Natl Acad Sci USA 104:1995–2000.

Doengi M, Hirnet D, Coulon P, Pape HC, Deitmer JW, Lohr C. 2009. GABA uptake-dependent Ca^{2+} signaling in developing olfactory bulb astrocytes. Proc Natl Acad Sci USA 106:17570–17575.

Dugue GP, Dumoulin A, Triller A, Dieudonne S. 2005. Target-dependent use of co-released inhibitory transmitters at central synapses. J Neurosci 25: 6490–6498.

Fellin T, Pascual O, Gobbo S, Pozzan T, Haydon PG, Carmignoto G. 2004. Neuronal synchrony mediated by astrocytic glutamate through activation of extrasynaptic NMDA receptors. Neuron 43:729–743.

Gomez-Gonzalo M, Losi G, Chiavegato A, Zonta M, Cammarota M, Brondi M, Vetri F, Uva L, Pozzan T de Curtis M, Ratto GM, Carmignoto G. 2010. An excitatory loop with astrocytes contributes to drive neurons to seizure threshold. PLoS Biol 8:e1000352.

Halassa MM, Fellin T, Haydon PG. 2007. The tripartite synapse: Roles for gliotransmission in health and disease. Trends Mol Med 13:54–63.

Haydon PG, Carmignoto G. 2006. Astrocyte control of synaptic transmission and neurovascular coupling. Physiol Rev 86:1009–1031.

Hertle DN, Yeckel MF. 2007. Distribution of inositol-1,4,5-trisphosphate receptor isotypes and ryanodine receptor isotypes during maturation of the rat hippocampus. Neuroscience 150:625–638.

Holtzclaw LA, Pandhit S, Bare DJ, Mignery GA, Russell JT. 2002. Astrocytes in adult rat brain express type 2 inositol 1,4,5-trisphosphate receptors. Glia 39:69–84.

Jourdain P, Bergersen LH, Bhaukaurally K, Bezzi P, Santello M, Domercq M, Matute C, Tonello F, Gundersen V, Volterra A. 2007. Glutamate exocytosis from astrocytes controls synaptic strength. Nat Neurosci 10:331–339.

Kang J, Jiang L, Goldman SA, Nedergaard M. 1998. Astrocyte-mediated potentiation of inhibitory synaptic transmission. Nat Neurosci 1:683–692.

Klausberger T, Magill PJ, Marton LF, Roberts JD, Cobden PM, Buzsaki G, Somogyi P. 2003. Brain-state- and cell-type-specific firing of hippocampal interneurons in vivo. Nature 421:844−848.

Kozlov AS, Angulo MC, Audinat E, Charpak S. 2006. Target cell-specific modulation of neuronal activity by astrocytes. Proc Natl Acad Sci USA 103:10058–10063.

Li X, Zima AV, Sheikh F, Blatter LA, Chen J. 2005. Endothelin-1-induced arrhythmogenic Ca^{2+} signaling is abolished in atrial myocytes of inositol-1,4,5-trisphosphate(IP_3)-receptor type 2-deficient mice. Circ Res 96:1274–1281.

Losi G, Mariotti L, Carmignoto G. 2014. GABAergic interneuron to astrocyte signalling: A neglected form of cell communication in the brain. Philos Trans R Soc Lond B Biol Sci 369:20130609.

Meier SD, Kafitz KW, Rose CR. 2008. Developmental profile and mechanisms of GABA-induced calcium signaling in hippocampal astrocytes. Glia 56:1127–1137.

Mori T, Tanaka K, Buffo A, Wurst W, Kuhn R, Gotz M. 2006. Inducible gene deletion in astroglia and radial glia–a valuable tool for functional and lineage analysis. Glia 54:21–34.

Navarrete M, Araque A. 2010. Endocannabinoids potentiate synaptic transmission through stimulation of astrocytes. Neuron 68:113–126.

Navarrete M, Perea G, de Sevilla DF, Gomez-Gonzalo M, Nunez A, Martin ED, Araque A. 2012. Astrocytes mediate in vivo cholinergic-induced synaptic plasticity. PLoS Biol 10:e1001259.

Nestor MW, Mok LP, Tulapurkar ME, Thompson SM. 2007. Plasticity of neuron-glial interactions mediated by astrocytic EphARs. J Neurosci 27: 12817–12828.

Nilsson M, Eriksson PS, Ronnback L, Hansson E. 1993. GABA induces Ca^{2+} transients in astrocytes. Neuroscience 54:605–614.

Nimmerjahn A, Kirchhoff F, Kerr JN, Helmchen F. 2004. Sulforhodamine 101 as a specific marker of astroglia in the neocortex in vivo. Nat Methods 1:31–37.

Parpura V, Grubisic V, Verkhratsky A. 2011. Ca^{2+} sources for the exocytotic release of glutamate from astrocytes. Biochim Biophys Acta 1813:984–991.

Perea G, Navarrete M, Araque A. 2009. Tripartite synapses: Astrocytes process and control synaptic information. Trends Neurosci 32:421–431.

Petersen CC, Crochet S. 2013. Synaptic computation and sensory processing in neocortical layer 2/3. Neuron 78:28–48.

Pierce KL, Premont RT, Lefkowitz RJ. 2002. Seven-transmembrane receptors. Nat Rev Mol Cell Biol 3:639–650.

Pirttimaki TM, Codadu NK, Awni A, Pratik P, Nagel DA, Hill EJ, Dineley KT, Parri HR. 2013. 7 Nicotinic receptor-mediated astrocytic gliotransmitter release: Aβ effects in a preclinical Alzheimer's mouse model. PLoS One 8: e81828.

Reyes-Haro D, Muller J, Boresch M, Pivneva T, Benedetti B, Scheller A, Nolte C, Kettenmann H. 2010. Neuron-astrocyte interactions in the medial nucleus of the trapezoid body. J Gen Physiol 135:583–594.

Serrano A, Haddjeri N, Lacaille JC, Robitaille R. 2006. GABAergic network activation of glial cells underlies hippocampal heterosynaptic depression. J Neurosci 26:5370–5382.

Sharp AH, Nucifora FC, Jr., Blondel O, Sheppard CA, Zhang C, Snyder SH, Russell JT, Ryugo DK, Ross CA. 1999. Differential cellular expression of isoforms of inositol 1,4,5-triphosphate receptors in neurons and glia in brain. J Comp Neur 406:207–220.

Shigetomi E, Bowser DN, Sofroniew MV, Khakh BS. 2008. Two forms of astrocyte calcium excitabilty have distinct effects on NMDA receptor-mediated slow inward currents in pyramidal neurons. J Neurosci 28:6659–6663.

Sohal VS, Zhang F, Yizhar O, Deisseroth K. 2009. Parvalbumin neurons and gamma rhythms enhance cortical circuit performance. Nature 459: 698–702.

Stark E, Eichler R, Roux L, Fujisawa S, Rotstein HG, Buzsaki G. 2013. Inhibition-induced theta resonance in cortical circuits. Neuron 80:1263–1276.

Varga C, Golshani P, Soltesz I. 2012. Frequency-invariant temporal ordering of interneuronal discharges during hippocampal oscillations in awake mice. Proc Natl Acad Sci USA 109:E2726–E2734.

Velez-Fort M, Audinat E, Angulo MC. 2011. Central role of GABA in neuron-glia interactions. Neuroscientist 18:237–250.

Verkhratsky A, Rodriguez JJ, Parpura V. 2012. Calcium signalling in astroglia. Mol Cell Endocrinol 353:45–56.

Verkhratsky A, Steinhauser C. 2000. Ion channels in glial cells. Brain Res Brain Res Rev 32:380–412.

Volterra A, Meldolesi J. 2005. Astrocytes, from brain glue to communication elements: The revolution continues. Nat Rev Neurosci 6:626–640.

Westenbroek RE, Bausch SB, Lin RC, Franck JE, Noebels JL, Catterall WA. 1998. Upregulation of L-type Ca^{2+} channels in reactive astrocytes after brain injury, hypomyelination, and ischemia. J Neurosci 18:2321–2334.

Zeng W, Mak DO, Li Q, Shin DM, Foskett JK, Muallem S. 2003. A new mode of Ca^{2+} signaling by G protein-coupled receptors: Gating of IP_3 receptor Ca^{2+} release channels by Gβγ. Curr Biol 13:872–876.

BIBLIOGRAPHY

1. Kandel, E.R., et al., *Principles of Neural Science*. Fifth ed, ed. McGraw-Hill. Vol. 1. 2013, United States of America: McGraw-Hill. 1760.
2. Krook-Magnuson, E., et al., *On-demand optogenetic control of spontaneous seizures in temporal lobe epilepsy.* Nature Communications, 2013. **4**: p. 1376.
3. Losi, G., M. Cammarota, and G. Carmignoto, *The role of astroglia in the epileptic brain.* Frontiers in Pharmacology, 2012. **3**: p. 132.
4. Cammarota, M., et al., *Fast spiking interneuron control of seizure propagation in a cortical slice model of focal epilepsy.* The Journal of Physiology, 2013. **591**(Pt 4): p. 807-22.
5. Harris, K.D. and T.D. Mrsic-Flogel, *Cortical connectivity and sensory coding.* Nature, 2013. **503**(7474): p. 51-8.
6. McCormick, D.A. and D. Contreras, *On the cellular and network bases of epileptic seizures.* Annu Rev Physiol, 2001. **63**: p. 815-46.
7. Zhang, F., et al., *Circuit-breakers: optical technologies for probing neural signals and systems.* Nat Rev Neurosci, 2007. **8**(8): p. 577-81.
8. Kerr, J.N., et al., *Spatial organization of neuronal population responses in layer 2/3 of rat barrel cortex.* The Journal of Neuroscience, 2007. **27**(48): p. 13316-28.
9. Petersen, C.C., *The functional organization of the barrel cortex.* Neuron, 2007. **56**(2): p. 339-355.
10. Isaacson, J.S. and M. Scanziani, *How inhibition shapes cortical activity.* Neuron, 2011. **72**(2): p. 231-43.
11. Blaesse, P., et al., *Cation-chloride cotransporters and neuronal function.* Neuron, 2009. **61**(6): p. 820-838.
12. Luscher, C., et al., *G protein-coupled inwardly rectifying K+ channels (GIRKs) mediate postsynaptic but not presynaptic transmitter actions in hippocampal neurons.* Neuron, 1997. **19**(3): p. 687-695.
13. Isaacson, J.S., J.M. Solis, and R.A. Nicoll, *Local and diffuse synaptic actions of GABA in the hippocampus.* Neuron, 1993. **10**(2): p. 165-175.
14. Silberberg, G. and H. Markram, *Disynaptic inhibition between neocortical pyramidal cells mediated by Martinotti cells.* Neuron, 2007. **53**(5): p. 735-46.

15. Kapfer, C., et al., *Supralinear increase of recurrent inhibition during sparse activity in the somatosensory cortex.* Nature Neuroscience, 2007. **10**(6): p. 743-53.
16. Andersen, P., J.C. Eccles, and Y. Loyning, *Recurrent inhibition in the hippocampus with identification of the inhibitory cell and its synapses.* Nature, 1963(198): p. 540-542.
17. Hu, H., J. Gan, and P. Jonas, *Interneurons. Fast-spiking, parvalbumin^{+} GABAergic interneurons: from cellular design to microcircuit function.* Science, 2014. **345**(6196): p. 1255263.
18. Buzsaki, G., *Feed-forward inhibition in the hippocampal formation.* Progress in Neurobiology, 1984. **22**(2): p. 131-153.
19. Pouille, F. and M. Scanziani, *Enforcement of temporal fidelity in pyramidal cells by somatic feed-forward inhibition.* Science, 2001. **293**(5532): p. 1159-63.
20. Anderson, J.S., M. Carandini, and D. Ferster, *Orientation tuning of input conductance, excitation, and inhibition in cat primary visual cortex.* Journal of Neurophysiology, 2000. **84**(2): p. 909-26.
21. Sanchez-Vives, M.V., et al., *Inhibitory modulation of cortical up states.*
. Journal of Neurophysiology, 2010. **104**(3): p. 1314-1324.
22. Ascoli, G.A., et al., *Petilla terminology: nomenclature of features of GABAergic interneurons of the cerebral cortex.* Nature Reviews. Neuroscience, 2008. **9**(7): p. 557-68.
23. Rudy, B., et al., *Three groups of interneurons account for nearly 100% of neocortical GABAergic neurons.* Developmental Neurobiology, 2011. **71**(1): p. 45-61.
24. Klausberger, T. and P. Somogyi, *Neuronal diversity and temporal dynamics: the unity of hippocampal circuit operations.* Science, 2008. **321**(5885): p. 53-7.
25. Cauli, B., et al., *Classification of fusiform neocortical interneurons based on unsupervised clustering.* Proc Natl Acad Sci U S A., 2000. **97**(11): p. 6144-6149.
26. Kawaguchi, Y. and Y. Kubota, *Physiological and morphological identification of somatostatin- or vasoactive intestinal polypeptide-containing cells among GABAergic cell subtypes in rat frontal cortex.* The Journal of Neuroscience, 1996. **16**(8): p. 2701-15.

27. Pfeffer, C.K., et al., *Inhibition of inhibition in visual cortex: the logic of connections between molecularly distinct interneurons.* Nature Neuroscience, 2013. **16**(8): p. 1068-76.
28. Xu, H., et al., *Neocortical somatostatin-expressing GABAergic interneurons disinhibit the thalamorecipient layer 4.* Neuron, 2013. **77**(1): p. 155-67.
29. Gentet, L.J., et al., *Unique functional properties of somatostatin-expressing GABAergic neurons in mouse barrel cortex.* Nature Neuroscience, 2012. **15**(4): p. 607-12.
30. Kawaguchi, Y. and Y. Kubota, *GABAergic cell subtypes and their synaptic connections in rat frontal cortex.* Cerebral Cortex, 1997. **7**(6): p. 476-86.
31. Connors, B.W. and M.J. Gutnick, *Intrinsic firing patterns of diverse neocortical neurons.* Trends Neurosci, 1990. **13**(3): p. 99-104.
32. Cauli, B., et al., *Molecular and physiological diversity of cortical nonpyramidal cells.* The Journal of Neuroscience, 1997. **17**(10): p. 3894-906.
33. Markram, H., et al., *Interneurons of the neocortical inhibitory system.* Nature Reviews. Neuroscience, 2004. **5**(10): p. 793-807.
34. Cardin, J.A., et al., *Driving fast-spiking cells induces gamma rhythm and controls sensory responses.* Nature, 2009. **459**(7247): p. 663-7.
35. Stark, E., et al., *Inhibition-induced theta resonance in cortical circuits.* Neuron, 2013. **80**(5): p. 1263-76.
36. Letzkus, J.J., et al., *A disinhibitory microcircuit for associative fear learning in the auditory cortex.* Nature, 2011. **480**(7377): p. 331-5.
37. World Health Organization, *Epilepsy.* Fact sheet N°999, 2015.
38. Noebel, J.L., et al., *Jasper's Basic Mechanisms of the Epilepsies.* 2012.
39. Kostopoulos, G.K., *Involvement of the thalamocortical system in epileptic loss of consciousness.* Epilepsia, 2001. **42 Suppl 3**: p. 13-9.
40. Chang, B.S. and D.H. Lowenstein, *Epilepsy.* N Engl J Med, 2003. **349**(13): p. 1257-66.
41. Steinlein, O.K., et al., *A missense mutation in the neuronal nicotinic acetylcholine receptor alpha 4 subunit is associated with autosomal dominant nocturnal frontal lobe epilepsy.* Nat Genet, 1995. **11**(2): p. 201-3.
42. Escayg, A., et al., *Mutations of SCN1A, encoding a neuronal sodium channel, in two families with GEFS+2.* Nat Genet, 2000. **24**(4): p. 343-5.

43. Lossin, C., et al., *Molecular basis of an inherited epilepsy.* Neuron, 2002. **34**(6): p. 877-84.
44. Barela, A.J., et al., *An epilepsy mutation in the sodium channel SCN1A that decreases channel excitability.* J Neurosci, 2006. **26**(10): p. 2714-23.
45. Kahlig, K.M., S.N. Misra, and A.L. George, Jr., *Impaired inactivation gate stabilization predicts increased persistent current for an epilepsy-associated SCN1A mutation.* J Neurosci, 2006. **26**(43): p. 10958-66.
46. Dravet, C., M. Bureau, and P. Genton, *Benign myoclonic epilepsy of infancy: electroclinical symptomatology and differential diagnosis from the other types of generalized epilepsy of infancy*, in *The Benign Localized and Generalized Epilepsies in Early Childhood*, R. Degen and F.E. Dreifuss, Editors. 1992, Elsevier Science: Amsterdam. p. 131-135.
47. Ogiwara, I., et al., *$Na_V1.1$ localizes to axons of parvalbumin-positive inhibitory interneurons: a circuit basis for epileptic seizures in mice carrying an Scn1a gene mutation.* The Journal of Neuroscience, 2007. **27**(22): p. 5903-14.
48. Yu, F.H., et al., *Reduced sodium current in GABAergic interneurons in a mouse model of severe myoclonic epilepsy in infancy.* Nature Neuroscience, 2006. **9**(9): p. 1142-9.
49. Oakley, J.C., et al., *Temperature- and age-dependent seizures in a mouse model of severe myoclonic epilepsy in infancy.* Proceedings of the National Academy of Sciences of the United States of America, 2009. **106**(10): p. 3994-9.
50. Kalume, F., et al., *Reduced sodium current in Purkinje neurons from $Na_V1.1$ mutant mice: implications for ataxia in severe myoclonic epilepsy in infancy.* The Journal of Neuroscience, 2007. **27**(41): p. 11065-74.
51. Pitkänen, A., P.A. Schwartzkroin, and S.L. Moshé, *Models of Seizures and Epilepsy*. 2006, Amsterdam: Elsevier.
52. Stanton, P.K., et al., *Epileptiform activity induced by lowering extracellular $[Mg^{2+}]$ in combined hippocampal-entorhinal cortex slices: modulation by receptors for norepinephrine and N-methyl-D-aspartate.* Epilepsy Research, 1987. **1**(1): p. 53-62.
53. Jefferys, J.G., *Experimental neurobiology of epilepsies.* Curr Opin Neurol, 1994. **7**(2): p. 113-22.

54. Matsumoto, H. and C.A. Marsan, *Cortical Cellular Phenomena in Experimental Epilepsy: Ictal Manifestations.* Exp Neurol, 1964. **9**: p. 305-26.
55. de Curtis, M. and G. Avanzini, *Interictal spikes in focal epileptogenesis.* Progress in Neurobiology, 2001. **63**(5): p. 541-67.
56. Jones, R.S. and J.D. Lambert, *Synchronous discharges in the rat entorhinal cortex in vitro: site of initiation and the role of excitatory amino acid receptors.* Neuroscience, 1990. **34**(3): p. 657-70.
57. Szente, M. and A. Baranyi, *Mechanism of aminopyridine-induced ictal seizure activity in the cat neocortex.* Brain Res, 1987. **413**(2): p. 368-73.
58. Miles, R. and R.K. Wong, *Single neurones can initiate synchronized population discharge in the hippocampus.* Nature, 1983. **306**(5941): p. 371-3.
59. Miles, R. and R.K. Wong, *Excitatory synaptic interactions between CA3 neurones in the guinea-pig hippocampus.* J Physiol, 1986. **373**: p. 397-418.
60. Traub, R.D., J.G. Jefferys, and R. Miles, *Analysis of the propagation of disinhibition-induced after-discharges along the guinea-pig hippocampal slice in vitro.* The Journal of Physiology, 1993. **472**: p. 267-87.
61. Connors, B.W., *Initiation of synchronized neuronal bursting in neocortex.* Nature, 1984. **310**(5979): p. 685-7.
62. Traub, R.D., J.G. Jefferys, and M.A. Whittington, *Enhanced NMDA conductance can account for epileptiform activity induced by low Mg2+ in the rat hippocampal slice.* The Journal of Physiology, 1994. **478 Pt 3**: p. 379-93.
63. Azouz, R., M.S. Jensen, and Y. Yaari, *Ionic basis of spike after-depolarization and burst generation in adult rat hippocampal CA1 pyramidal cells.* The Journal of Physiology, 1996. **492**(Pt 1): p. 211-23.
64. Truccolo, W., et al., *Single-neuron dynamics in human focal epilepsy.* Nature Neuroscience, 2011. **14**(5): p. 635-41.
65. Schevon, C.A., et al., *Evidence of an inhibitory restraint of seizure activity in humans.* Nature Communications, 2012. **3**: p. 1060.
66. Avoli, M., et al., *Network and pharmacological mechanisms leading to epileptiform synchronization in the limbic system in vitro.* Progress in Neurobiology, 2002. **68**(3): p. 167-207.
67. Pare, D., M. deCurtis, and R. Llinas, *Role of the hippocampal-entorhinal loop in temporal lobe epilepsy: extra- and intracellular study in the isolated guinea pig brain in vitro.* The Journal of Neuroscience, 1992. **12**(5): p. 1867-81.

68. McNamara, J.O., *Emerging insights into the genesis of epilepsy.* Nature, 1999. **399**(6738 Suppl): p. A15-22.
69. McNamara, J.O., Y.Z. Huang, and A.S. Leonard, *Molecular signaling mechanisms underlying epileptogenesis.* Science's STKE: Signal Transduction Knowledge Environment, 2006. **2006**(356): p. re12.
70. Pinto, D.J., et al., *Initiation, propagation, and termination of epileptiform activity in rodent neocortex in vitro involve distinct mechanisms.* The Journal of Neuroscience, 2005. **25**(36): p. 8131-40.
71. Cossart, R., C. Bernard, and Y. Ben-Ari, *Multiple facets of GABAergic neurons and synapses: multiple fates of GABA signalling in epilepsies.* Trends in Neurosciences, 2005. **28**(2): p. 108-15.
72. Avoli, M., et al., *Pharmacology and electrophysiology of a synchronous GABA-mediated potential in the human neocortex.* Neuroscience, 1994. **62**(3): p. 655-66.
73. Kohling, R., et al., *Ictal epileptiform activity is facilitated by hippocampal GABAA receptor-mediated oscillations.* J Neurosci, 2000. **20**(18): p. 6820-9.
74. Avoli, M., et al., *Synchronous GABA-mediated potentials and epileptiform discharges in the rat limbic system in vitro.* The Journal of Neuroscience, 1996. **16**(12): p. 3912-24.
75. Avoli, M. and M. de Curtis, *GABAergic synchronization in the limbic system and its role in the generation of epileptiform activity.* Progress in Neurobiology, 2011. **95**(2): p. 104-32.
76. D'Antuono, M., et al., *$GABA_A$ receptor-dependent synchronization leads to ictogenesis in the human dysplastic cortex.* Brain, 2004. **127**(Pt 7): p. 1626-40.
77. Cobb, S.R., et al., *Synchronization of neuronal activity in hippocampus by individual GABAergic interneurons.* Nature, 1995. **378**(6552): p. 75-8.
78. Bartos, M., I. Vida, and P. Jonas, *Synaptic mechanisms of synchronized gamma oscillations in inhibitory interneuron networks.* Nature Reviews. Neuroscience, 2007. **8**(1): p. 45-56.
79. Buzsáki, G. and X.J. Wang, *Mechanisms of gamma oscillations.* Annual Review of Neuroscience, 2012. **35**: p. 203-25.
80. Mizuseki, K., et al., *Theta oscillations provide temporal windows for local circuit computation in the entorhinal-hippocampal loop.* Neuron, 2009. **64**(2): p. 267-80.

81. Shiri, Z., et al., *Interneuron Activity Leads to Initiation of Low-Voltage Fast-Onset Seizures.* Annals of Neurology, 2014.
82. Yekhlef, L., et al., *Selective activation of parvalbumin- or somatostatin-expressing interneurons triggers epileptic seizure-like activity in the mouse medial entorhinal cortex.* Journal of Neurophysiology, 2014: p. jn 00841 2014.
83. Kaila, K., et al., *GABA actions and ionic plasticity in epilepsy.* Current Opinion in Neurobiology, 2013. **26C**: p. 34-41.
84. Jefferys, J.G., *Basic mechanisms of focal epilepsies.* Experimental Physiology, 1990. **75**(2): p. 127-62.
85. Prince, D.A. and B.J. Wilder, *Control mechanisms in cortical epileptogenic foci. "Surround" inhibition.* Archives of Neurology, 1967. **16**(2): p. 194-202.
86. Schwartz, T.H. and T. Bonhoeffer, *In vivo optical mapping of epileptic foci and surround inhibition in ferret cerebral cortex.* Nature Medicine, 2001. **7**(9): p. 1063-7.
87. Prince, D.A. and K. Jacobs, *Inhibitory function in two models of chronic epileptogenesis.* Epilepsy Res, 1998. **32**(1-2): p. 83-92.
88. Lieb, J.P., et al., *A comparison of EEG seizure patterns recorded with surface and depth electrodes in patients with temporal lobe epilepsy.* Epilepsia, 1976. **17**(2): p. 137-60.
89. Gnatkovsky, V., et al., *Fast activity at seizure onset is mediated by inhibitory circuits in the entorhinal cortex in vitro.* Annals of Neurology, 2008. **64**(6): p. 674-86.
90. Uva, L., M. Avoli, and M. de Curtis, *Synchronous $GABA_A$-receptor-dependent potentials in limbic areas of the in-vitro isolated adult guinea pig brain.* European Journal of Neuroscience, 2009. **29**(5): p. 911-20.
91. Boido, D., et al., *Network dynamics during the progression of seizure-like events in the hippocampal-parahippocampal regions.* Cereb Cortex, 2014. **24**(1): p. 163-73.
92. Trombin, F., V. Gnatkovsky, and M. de Curtis, *Changes in action potential features during focal seizure discharges in the entorhinal cortex of the in vitro isolated guinea pig brain.* Journal of Neurophysiology, 2011. **106**(3): p. 1411-23.

93. Derchansky, M., et al., *Transition to seizures in the isolated immature mouse hippocampus: a switch from dominant phasic inhibition to dominant phasic excitation.* The Journal of Physiology, 2008. **586**(2): p. 477-94.
94. Ziburkus, J., et al., *Interneuron and pyramidal cell interplay during in vitro seizure-like events.* Journal of Neurophysiology, 2006. **95**(6): p. 3948-54.
95. Wong, B.Y. and D.A. Prince, *The lateral spread of ictal discharges in neocortical brain slices.* Epilepsy Res, 1990. **7**(1): p. 29-39.
96. Ohara, S., et al., *Propagation of tonic posturing in supplementary motor area (SMA) seizures.* Epilepsy Res, 2004. **62**(2-3): p. 179-87.
97. Trevelyan, A.J., et al., *Modular propagation of epileptiform activity: evidence for an inhibitory veto in neocortex.* The Journal of Neuroscience, 2006. **26**(48): p. 12447-55.
98. Trevelyan, A.J., D. Sussillo, and R. Yuste, *Feedforward inhibition contributes to the control of epileptiform propagation speed.* The Journal of Neuroscience, 2007. **27**(13): p. 3383-7.
99. Dreier, J.P. and U. Heinemann, *Late low magnesium-induced epileptiform activity in rat entorhinal cortex slices becomes insensitive to the anticonvulsant valproic acid.* Neurosci Lett, 1990. **119**(1): p. 68-70.
100. Bekkers, J.M. and C.F. Stevens, *Presynaptic mechanism for long-term potentiation in the hippocampus.* Nature, 1990. **346**(6286): p. 724-9.
101. Whittington, M.A., R.D. Traub, and J.G. Jefferys, *Erosion of inhibition contributes to the progression of low magnesium bursts in rat hippocampal slices.* The Journal of Physiology, 1995. **486 (Pt 3)**: p. 723-34.
102. Pfeiffer, M., et al., *Effects of gamma-aminobutyric acid (GABA) agonists and GABA uptake inhibitors on pharmacosensitive and pharmacoresistant epileptiform activity in vitro.* Br J Pharmacol, 1996. **119**(3): p. 569-77.
103. Naylor, D.E., H. Liu, and C.G. Wasterlain, *Trafficking of $GABA_A$ receptors, loss of inhibition, and a mechanism for pharmacoresistance in status epilepticus.* The Journal of Neuroscience, 2005. **25**(34): p. 7724-33.
104. Dinocourt, C., et al., *Loss of interneurons innervating pyramidal cell dendrites and axon initial segments in the CA1 region of the hippocampus following pilocarpine-induced seizures.* J Comp Neurol, 2003. **459**(4): p. 407-25.
105. Raimondo, J.V., et al., *Ion dynamics during seizures.* Front Cell Neurosci, 2015. **9**: p. 419.

106. Losi, G., et al., *A brain slice experimental model to study the generation and the propagation of focally-induced epileptiform activity.* Journal of Neuroscience Methods, 2015.
107. Tai, C., et al., *Impaired excitability of somatostatin- and parvalbumin-expressing cortical interneurons in a mouse model of Dravet syndrome.* Proceedings of the National Academy of Sciences of the United States of America, 2014. **111**(30): p. E3139-48.
108. Ellender, T.J., et al., *Excitatory effects of parvalbumin-expressing interneurons maintain hippocampal epileptiform activity via synchronous afterdischarges.* The Journal of Neuroscience, 2014. **34**(46): p. 15208-22.
109. Trevelyan, A.J., et al., *The source of afterdischarge activity in neocortical tonic-clonic epilepsy.* The Journal of Neuroscience, 2007. **27**(49): p. 13513-9.
110. Rogawski, M.A. and W. Loscher, *The neurobiology of antiepileptic drugs.* Nature Reviews. Neuroscience, 2004. **5**(7): p. 553-64.
111. Duncan, R., et al., *Ictal single photon emission computed tomography in occipital lobe seizures.* Epilepsia, 1997. **38**(7): p. 839-43.
112. Fisher, R., et al., *Electrical stimulation of the anterior nucleus of thalamus for treatment of refractory epilepsy.* Epilepsia, 2010. **51**(5): p. 899-908.
113. Morrell, M.J. and R.N.S.S.i.E.S. Group, *Responsive cortical stimulation for the treatment of medically intractable partial epilepsy.* Neurology, 2011. **77**(13): p. 1295-304.
114. Paz, J.T. and J.R. Huguenard, *Microcircuits and their interactions in epilepsy: is the focus out of focus?* Nature Neuroscience, 2015. **18**(3): p. 351-9.
115. Boyden, E.S., et al., *Millisecond-timescale, genetically targeted optical control of neural activity.* Nat Neurosci, 2005. **8**(9): p. 1263-8.
116. Deisseroth, K., *Optogenetics: 10 years of microbial opsins in neuroscience.* Nat Neurosci, 2015. **18**(9): p. 1213-25.
117. Tye, K.M. and K. Deisseroth, *Optogenetic investigation of neural circuits underlying brain disease in animal models.* Nature Reviews. Neuroscience, 2012. **13**(4): p. 251-66.
118. Zhang, F., et al., *Optogenetic interrogation of neural circuits: technology for probing mammalian brain structures.* Nat Protoc, 2010. **5**(3): p. 439-56.
119. Davidson, B.L. and X.O. Breakefield, *Viral vectors for gene delivery to the nervous system.* Nat Rev Neurosci, 2003. **4**(5): p. 353-64.

120. Ledri, M., et al., *Global Optogenetic Activation of Inhibitory Interneurons during Epileptiform Activity.* The Journal of Neuroscience, 2014. **34**(9): p. 3364-77.
121. Paz, J.T., et al., *Closed-loop optogenetic control of thalamus as a tool for interrupting seizures after cortical injury.* Nature Neuroscience, 2013. **16**(1): p. 64-70.
122. Barres, B.A., *The mystery and magic of glia: a perspective on their roles in health and disease.* Neuron, 2008. **60**(3): p. 430-40.
123. Carmignoto, G. and M. Gomez-Gonzalo, *The contribution of astrocyte signalling to neurovascular coupling.* Brain Research Reviews, 2010. **63**(1-2): p. 138-48.
124. Perea, G., M. Navarrete, and A. Araque, *Tripartite synapses: astrocytes process and control synaptic information.* Trends in Neurosciences, 2009. **32**(8): p. 421-31.
125. Halassa, M.M., T. Fellin, and P.G. Haydon, *The tripartite synapse: roles for gliotransmission in health and disease.* Trends in Molecular Medicine, 2007. **13**(2): p. 54-63.
126. Araque, A., et al., *Gliotransmitters Travel in Time and Space.* Neuron, 2014. **81**(4): p. 728-739.
127. Haydon, P.G. and G. Carmignoto, *Astrocyte control of synaptic transmission and neurovascular coupling.* Physiological Reviews, 2006. **86**(3): p. 1009-31.
128. Zhang, Q., et al., *Synaptotagmin IV regulates glial glutamate release.* Proceedings of the National Academy of Sciences of the United States of America, 2004. **101**(25): p. 9441-9446.
129. Woo, D.H., et al., *TREK-1 and Best1 channels mediate fast and slow glutamate release in astrocytes upon GPCR activation.* Cell, 2012. **151**(1): p. 25-40.
130. Maragakis, N.J. and J.D. Rothstein, *Mechanisms of Disease: astrocytes in neurodegenerative disease.* Nature Clinical Practice. Neurology, 2006. **2**(12): p. 679-89.
131. Seifert, G., K. Schilling, and C. Steinhauser, *Astrocyte dysfunction in neurological disorders: a molecular perspective.* Nature Reviews. Neuroscience, 2006. **7**(3): p. 194-206.
132. Blackburn, D., et al., *Astrocyte function and role in motor neuron disease: a future therapeutic target?* Glia, 2009. **57**(12): p. 1251-64.

133. Hamby, M.E. and M.V. Sofroniew, *Reactive astrocytes as therapeutic targets for CNS disorders.* Neurotherapeutics, 2010. **7**(4): p. 494-506.
134. McKhann, G.M., 2nd, et al., *Intraoperative hippocampal electrocorticography to predict the extent of hippocampal resection in temporal lobe epilepsy surgery.* Journal of Neurosurgery, 2000. **93**(1): p. 44-52.
135. Kofuji, P. and E.A. Newman, *Potassium buffering in the central nervous system.* Neuroscience, 2004. **129**(4): p. 1045-56.
136. Li, L., V. Head, and L.C. Timpe, *Identification of an inward rectifier potassium channel gene expressed in mouse cortical astrocytes.* Glia, 2001. **33**(1): p. 57-71.
137. Seifert, G., et al., *Analysis of astroglial K^+ channel expression in the developing hippocampus reveals a predominant role of the Kir4.1 subunit.* The Journal of Neuroscience, 2009. **29**(23): p. 7474-88.
138. Olsen, M.L. and H. Sontheimer, *Functional implications for Kir4.1 channels in glial biology: from K^+ buffering to cell differentiation.* Journal of Neurochemistry, 2008. **107**(3): p. 589-601.
139. Lenzen, K.P., et al., *Supportive evidence for an allelic association of the human KCNJ10 potassium channel gene with idiopathic generalized epilepsy.* Epilepsy Research, 2005. **63**(2-3): p. 113-8.
140. Inyushin, M., et al., *Potassium channel activity and glutamate uptake are impaired in astrocytes of seizure-susceptible DBA/2 mice.* Epilepsia, 2010. **51**(9): p. 1707-13.
141. Tanaka, K., et al., *Epilepsy and exacerbation of brain injury in mice lacking the glutamate transporter GLT-1.* Science, 1997. **276**(5319): p. 1699-702.
142. Cavus, I., et al., *Extracellular metabolites in the cortex and hippocampus of epileptic patients.* Annals of Neurology, 2005. **57**(2): p. 226-35.
143. Seifert, G., G. Carmignoto, and C. Steinhauser, *Astrocyte dysfunction in epilepsy.* Brain Research Reviews, 2010. **63**(1-2): p. 212-21.
144. Eid, T., et al., *Loss of glutamine synthetase in the human epileptogenic hippocampus: possible mechanism for raised extracellular glutamate in mesial temporal lobe epilepsy.* Lancet, 2004. **363**(9402): p. 28-37.
145. Fellin, T., et al., *Neuronal synchrony mediated by astrocytic glutamate through activation of extrasynaptic NMDA receptors.* Neuron, 2004. **43**(5): p. 729-743.

146. Angulo, M.C., et al., *Glutamate released from glial cells synchronizes neuronal activity in the hippocampus.* The Journal of Neuroscience, 2004. **24**(31): p. 6920-6927.
147. Tian, G.-F., et al., *An astrocytic basis of epilepsy.* Nature Medicine, 2005. **11**(9): p. 973-81.
148. Wetherington, J., G. Serrano, and R. Dingledine, *Astrocytes in the epileptic brain.* Neuron, 2008. **58**(2): p. 168-78.
149. Gomez-Gonzalo, M., et al., *An excitatory loop with astrocytes contributes to drive neurons to seizure threshold.* PLoS Biology, 2010. **8**(4): p. e1000352.
150. Fraser, D.D., et al., *$GABA_A$/benzodiazepine receptors in acutely isolated hippocampal astrocytes.* The Journal of Neuroscience, 1995. **15**(4): p. 2720-32.
151. Kang, J., et al., *Astrocyte-mediated potentiation of inhibitory synaptic transmission.* Nature Neuroscience, 1998. **1**(8): p. 683-692.
152. Steinhauser, C., R. Jabs, and H. Kettenmann, *Properties of GABA and glutamate responses in identified glial cells of the mouse hippocampal slice.* Hippocampus, 1994. **4**(1): p. 19-35.
153. Egawa, K., et al., *Cl^- homeodynamics in gap-junction-coupled astrocytic networks on activation of GABAergic synapses.* The Journal of Physiology, 2013. **591**(Pt 16): p. 3901-17.
154. Serrano, A., et al., *GABAergic network activation of glial cells underlies hippocampal heterosynaptic depression.* The Journal of Neuroscience, 2006. **26**(20): p. 5370-82.
155. Sessolo, M., et al., *Parvalbumin-Positive Inhibitory Interneurons Oppose Propagation But Favor Generation of Focal Epileptiform Activity.* The Journal of Neuroscience, 2015. **35**(26): p. 9544-57.